Immune Regulation in Human Filariasis

Dissertation

zur

Erlangung eines Doktorgrades (Dr. rer. nat.)

der

Mathematisch-Naturwissenschaftlichen Fakultät

der

Rheinischen Friedrich-Wilhelms-Universität Bonn

vorgelegt von **Kathrin Arndts**

aus Trier

Bonn 2012

Angefertigt mit Genehmigung der Mathematisch-Naturwissenschaftlichen Fakultät der Rheinischen Friedrich-Wilhelms-Universität Bonn

1. Gutachter: Prof. Dr. med. Achim Hörauf
2. Gutachter: Prof. Dr. rer. nat. Waldemar Kolanus

Tag der Promotion: 07.12.2012
Erscheinungsjahr: 2013

Summary

Vector transmitted diseases such as the tropical helminth infections onchocerciasis and lymphatic filariasis (LF) affect more than 150 million people worldwide and are both considered major public health concerns. In order to guarantee the fulfillment of their complex lifecycle, adult filarial nematodes release millions of microfilariae (MF), which are engulfed by mosquito vectors and the current strategy to eliminate filarial infections focuses upon interrupting this transmission through annual mass drug administration (MDA). Nevertheless, repeated rounds of drug intake are needed to interrupt the lifecycle and gathering information about immunological processes could reveal alternative approaches in order to break transmission. Filariasis results in different pathological outcomes ranging from asymptomatic individuals to patients with severe pathology. Recently, a subgroup of asymptomatic latently infected patients has become apparent in LF; these individuals are amicrofilaremic despite chronic infection. With regards to immunological aspects, this subgroup has been neglected so far even though they are of special interest since they represent a roadblock in terms of parasite transmission. Moreover, immunological facets of asymptomatic microfilaremic (patent) individuals have been intensively described in the literature but usually in comparison to patients suffering from severe pathology. In onchocerciasis, most patients are patently infected and are characterized by weak or even absent inflammation. Interestingly, however, some infected individuals who lack severe pathology are amicrofilaremic and is considered to be a result of repeated MDA. Therefore, the present thesis aimed at analyzing the immune responses of a large cohort of LF or onchocerciasis infected individuals characterized by the absence or presence of MF. In addition, the signaling pathway of interleukin 10 (IL-10) was investigated since it is known from the literature that this immunosuppressive cytokine is a key player during filariasis. Results from infected individuals were compared with those from infection-free volunteers from the same endemic areas. In cases of infection with LF, immune profiles were also determined following the administration of different treatment regimes. Within this thesis it was shown that amicrofilaremic individuals could be characterized by lower parasite burden but increased immune responses with regards to their cytokine and antigen-specific immunoglobulin levels. In contrast, the presence of worm offspring was associated with a down-regulation of these immune responses but was not sufficient to induce the same immunomodulation in cells from non-endemic healthy blood donors in *in vitro* experiments. Moreover, analyzing gene expression profiles of regulatory, $CD4^+$ and $CD8^+$ T cell populations from individuals with patent and latent LF infection strengthened the observation that both groups of individuals cannot only be separated due to the presence or absence of MF *per se* but also due to differences in their immune profiles. These data provide novel insights into possible mechanisms which either actively hinder the release of MF from adult worms or their migration to the periphery in amicrofilaremic infected patients. Further research into these aspects may broaden the range of strategies currently employed to reduce transmission and in turn eliminate filariasis.

Zusammenfassung

Vektorübertragene Erkrankungen wie die tropischen Helmintheninfektionen Onchozerkose und Lymphatische Filariose (LF) beeinträchtigen weltweit mehr als 150 Millionen Menschen und werden daher als schwerwiegende Gesundheitsprobleme eingestuft. Während ihres komplexen Lebenszyklus scheiden adulte Filarien Millionen von Mikrofilarien (MF) aus, welche von Mücken aufgenommen werden. Die derzeitige Strategie zur Eliminierung von Filarieninfektionen konzentriert sich auf eine Unterbrechung der Transmission durch jährliche Massentherapiebehandlungen. Allerdings sind zur Unterbindung des Lebenszyklus mehrfache Wiederholungen dieser Behandlung notwendig, daher könnten zusätzliche Informationen über die immunologischen Prozesse während der Infektion alternative Ansätze zur Unterbrechung der Transmission ermöglichen. Filariosen haben verschiedene pathologische Ausprägungen, die von asymptomatischen Individuen bis hin zu Patienten mit schwerer Pathologie reichen können. Innerhalb der LF Patienten wurde vor kurzem eine weitere Subgruppe von asymptomatischen, latent infizierten Individuen erkennbar; diese Individuen sind trotz einer chronischen Infektion MF^-. Obwohl diese Subgruppe von Patienten eine Sackgasse im Hinblick auf die Transmission des Parasiten darstellt, wurden sie bisher in Bezug auf eine detaillierte immunologische Analyse vernachlässigt. Ferner wurden die immunologischen Facetten der asymptomatischen, MF^+ (patenten) Individuen bereits intensiv in der Literatur beschrieben, jedoch meist im Vergleich zu Patienten mit schwerer Pathologie. Die meisten Onchozerkose Patienten weisen eine patente Infektion auf und sind durch eine schwache oder eine fehlende Entzündungsreaktion gekennzeichnet. Interessanterweise gibt es allerdings auch MF^- Individuen ohne schwerwiegende Pathologie, was auf eine wiederholte Massentherapiebehandlungen zurückzuführen sein könnte. Das Ziel der vorliegenden Arbeit war es, die Immunantworten einer großen Kohorte von Patienten zu analysieren, die eine Onchozerkose oder LF Infektion aufweisen und durch die An- oder Abwesenheit von MF charakterisiert sind. Zusätzlich wurde der Signalweg des Zytokins Interleukin-10 (IL-10) untersucht, da bereits aus der Literatur bekannt ist, dass IL-10 eine Schlüsselrolle bei Filarieninfektionen spielt. Die Ergebnisse der infizierten Individuen wurden mit denen von gesunden Freiwilligen aus den gleichen Endemiegebieten verglichen. Im Falle der Infektion mit LF wurden zusätzlich die Immunprofile nach einer Behandlung der Patienten mit verschiedenen Therapien bestimmt. In der vorliegenden Doktorarbeit konnte gezeigt werden, dass MF^- Patienten eine niedrigere Parasitenlast sowie eine verstärkte Immunantwort im Hinblick auf ihre Zytokinfreisetzung und ihre antigen-spezifischen Immunglobulinproduktion aufweisen. Im Gegensatz dazu war in MF^+ Individuen die Präsenz des Wurmnachwuchses mit einer verminderten Immunantwort assoziiert; allerdings war diese nicht ausreichend, um die gleiche Immunmodulation in Zellen von gesunden Blutspendern in *in vitro* Experimenten zu induzieren. Des Weiteren untermauerte die Analyse der Genexpressionsprofile von regulatorischen, $CD4^+$ und $CD8^+$ T-Zellen von MF^+ und MF^- LF infizierten Individuen die *in vitro* Beobachtung, dass beide Gruppen von Patienten nicht nur aufgrund der An- oder Abwesenheit der MF *per se* zu unterscheiden sind, sondern auch aufgrund der Unterschiede bezüglich ihres immunologischen Profils. Diese Daten bieten neue Einblicke in die möglichen Mechanismen, welche innerhalb der infizierten MF^- Patienten entweder direkt eine Freisetzung der MF aus adulten Würmern oder deren Migration in die Peripherie verhindern. Eine weitere Erforschung dieser Aspekte könnte das Spektrum der derzeitig verwendeten Strategien zur Reduktion der Transmission erweitern und somit langfristig zur Eliminierung von Filariosen beitragen.

List of abbreviations

AAM	alternatively activated macrophages
αCD3	anti CD3
αCD28	anti CD28
ADCC	antibody-dependent cell-mediated cytotoxicity
ADLA	acute dermatolymphangioadenitis
AFL	acute filarial lymphangitis
Ag	antigen
ALB	albendazole
ANOVA	analysis of variance
AP	alkaline phosphatase
APC	allophycocyanine
APCs	antigen presenting cells
APOC	African Programme of Onchocerciasis Control
APS	ammonium persulfate
aRNA	amplified antisense ribonucleic acid
B.m. extract	*Brugia malayi* extract
BSA	bovine serum albumin
bp	base pairs
CBA	cytometric bead array
CD	cluster of differentiation
cDNA	complementary desoxyribonucleic acid
CFA	circulating filarial antigen
DC	dendritic cell
DEC	diethylcarbamazine
DMSO	dimethyl sulfoxide
DNA	desoxyribonuclein acid
DTT	dithiothreitol
EDTA	ethylene diaminetetraacetic acid
ELISA	enzyme linked immunosorbent assay
EN	endemic normal
FACS	fluorescence activated cell scanning/sorting
FCS	fetal calf serum
FDS	filarial dance sign
FITC	fluoresceine isothiocyanate
Foxp3	forkhead box protein 3
fw	forward
GEO	generalized onchocerciasis
GITR	glucocorticoid-induced tumor necrosis factor receptor
GITR-L	glucocorticoid-induced tumor necrosis factor receptor ligand

GPELF	Global Programme to Eliminate Lymphatic Filariasis
HRP	horseradish peroxidase
Ig	immunoglobulin
IL	interleukin
IL-10R	interleukin-10 receptor
IFN-γ	interferon gamma
IVM	ivermectin
Jak	janus kinase
L3	third stage larvae
LF	lymphatic filariasis
LPS	lipopolysaccharide
L.s. extract	*Litomosoides sigmodontis* extract
MACS	magnetic activated cell sorting
MDA	mass drug administration
MF	microfilariae
µg	microgram
mg	milligram
MHC	major histocompatibility complex
ml	mililiter
mM	millimolar
mRNA	messenger RNA
MSP	merozoite surface protein
ng	nanogram
nTreg	natural occurring regulatory T cells
OD	optical density
O.v. extract	*Onchocerca volvulus* extract
PAGE	polyacrylamide gel electrophoresis
PBMCs	peripheral blood mononuclear cells
PBS	phosphate buffered saline solution
PBST	phosphate buffered saline solution tween
PCR	polymerase chain reaction
PE	phycoerythrin
PFA	paraformaldehyde
pg	picogram
PI	putatively immune
PMSF	phenylmethanesulfonyl fluoride
PPD	purified protein derivative of Mycobacterium
RNA	ribonucleic acid
rpm	rounds per minute
RT	room temperature
rv	reverse

SB	specific buffy-coat
SDS	sodium dodecyl sulfate
STAT	signal transducer and activator of transcription
TBE	tris/borate/EDTA
TEMED	tetramethyl ethylene diamine
TGF-β	transforming growth factor beta
Th1	type 1 helper T cell
Th2	type 2 helper T cell
Th17	type 17 helper T cell
TLR	Toll-like receptor
TMB	tetramethylbenzidine
TNF	tumor necrosis factor
TPE	tropical pulmonary eosinophilia
Treg	regulatory T cells
Tyk	tyrosine kinase
VEGF	vascular endothelial growth factor
VEGF-R	vascular endothelial growth factor receptor
WHO	world health organisation

Table of contents

1. Introduction

A unique aspect of filarial nematodes is the dwelling of the endosymbiotic *Wolbachia*. This relationship further complicates the deciphering of already complex immune responses. The following section provides an overview of current knowledge surrounding the filarial manifestations termed onchocerciasis and lymphatic filariasis (LF). In addition to epidemiological and current treatment regimes the chapter also includes a comprehensive summary of the immunological aspects touching on both innate and adaptive responses. In part, these data provided the basis for the studies conducted in the following chapters which determined the immune profiles of differentially infected patients.

1.1. Onchocerciasis

1.1.1 Parasite biology and epidemiology

Onchocerciasis is a chronic helminth disease caused by the tissue-invading filariae *Onchocerca volvulus* (*O. volvulus*) which is transmitted by blood-feeding black flies of the genus *Simulium*. Onchocerciasis is endemic in 34 countries and more than 37 million people are infected [1]. The infection is most abundant in Africa (more than 99% of cases), but there are also small foci in Southern and Central America (figure 1.1). Approximately 90 million people are at risk of infection with *O. volvulus* which can lead to debilitating skin disease like dermatitis and ocular inflammation which can ultimately end in blindness [2].

Figure 1.1. Global distribution of *Onchocerca volvulus*. Depicted are African countries with endemic onchocerciasis (left part) and endemic foci in Latin America (right part). Countries participating in the former Onchocerciasis Control Program region are shown in green and those participating in the African Program for Onchocerciasis Control are depicted in yellow. Adapted from http://www.mectizan.org/onchocerciasis-maps.

The highest rates of infection and disease manifestations are found in communities adjacent to rivers, hence the designation “river blindness” [1], which is the world’s fourth leading cause of preventable blindness. In general, onchocerciasis contributes to higher mortality and economic loss making it a major public health concern as well as a social stigmatism [3, 4].

Onchocerca filariae have to fulfil a five-stage life cycle which begins with the transmission of infective third stage larvae (L3) from the small obligate vector of the genus *Simulium*, which breeds close to fast-flowing rivers (figure 1.2). Since the flight range of these vectors is approximately 12 km, transmission areas are localized to this radius around the breeding sites [3]. The transmitted larvae moult twice in the host and develop over a year into white thread-like adult worms, that live coiled in subcutaneous or deeper tissues forming characteristic fibrous nodules (onchocercomas) [3, 5]. These onchocercomas are defined as capsules of connective skin tissue in which several parasites are aggregated [6]. In contrast to the sessile females which are 30–80 cm in length, the ten times shorter adult males do not induce the formation of nodules but travel within the subcutaneous tissue, entering and leaving the nodules to inseminate a number of resident females, which then start to produce their offspring (first stage larvae, also called microfilariae, MF). On average, a nodule houses 2-50 female worms, but only 1-10 males [7]. Filariae have an average life of 10-15 years and the number of females in any one infected may range from 1 to over 60.

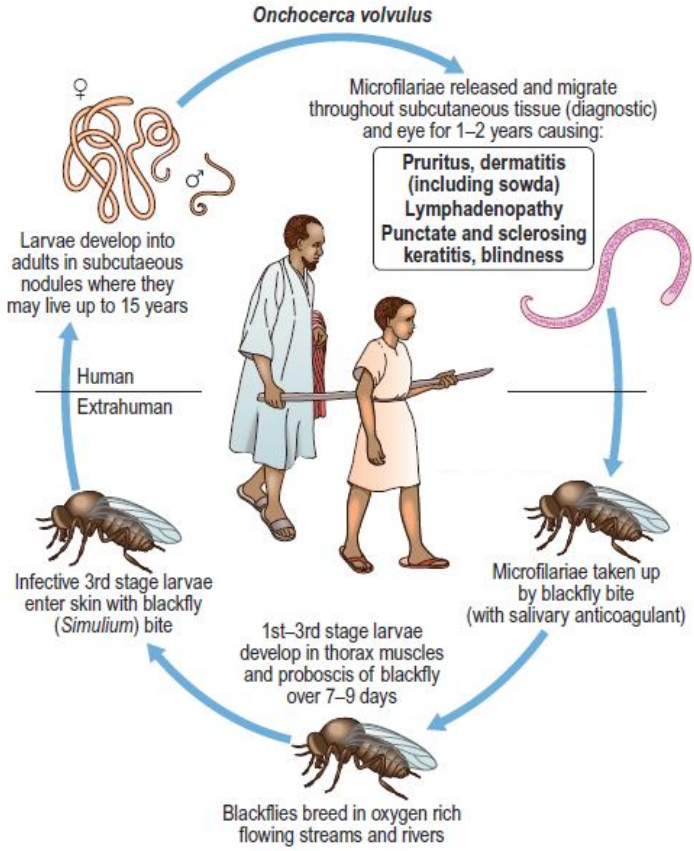

Figure 1.2. Life cycle of *Onchocerca volvulus*. Adapted from [3].

Fertilized female worms are able to release 1,000 to 3,000 MF per day resulting in an enormous reproductive capacity of the worms [7]. These offspring migrate to the skin and other tissues where they can live for up to 18 months until they are engulfed by their vectors during a blood meal [8, 9]. Inside their intermediate host they undergo another two moulting steps over 10-12 days before reaching the infectious L3 stage.

1.1.2 Pathology of Onchocerciasis

In general, given that the principle of parasitism is long-term coexistence, it is actually advantageous for both the host and parasite to avoid pro-inflammatory immune responses. Therefore, any arising pathology in the host may be viewed as a failure of appropriate anti-inflammatory mechanisms [10]. In the case of *O. volvulus,* the long-term persistence of the parasite indicates that it has evolved highly adapted mechanisms of immune evasion [7]. Nevertheless, the spectrum of disease manifestations in infected individuals is quite varied and the diversity of clinical responses is thought to reflect the intensity and type of immune response to the parasite itself or to the parasite's products [1, 11]. Adult filarial worms are not considered strong inducers of inflammation. Therefore, the appearance of pathology is generally linked to migrating MF or more precisely to reactions to degraded or moribund MF in the skin or in the eye. Even subcutaneous nodules, consisting of host immune cells and tissues trigger few or no clinical symptoms [3, 12]. The most severe disease manifestation is actually elicited by the death of MF passing through the cornea [12, 13]. During their migration, MF may invade the conjunctiva, cornea and the posterior regions of the eye. Increasing numbers of degenerating MF can induce the release of multiple somatic antigens that in turn provoke inflammatory responses of resident cells due to a breakdown of the immune privilege, which normally prevents inflammation [7]. Around dead MF punctate keratitis (inflammation of the cornea, figure 1.3) can develop and permanent exposure can lead to iridocyclitis (inflammation of the iris) which results in permanent visual impairment or in its most severe form blindness [1].

Figure 1.3. Pathology of *Onchocerca volvulus*. Left and middle picture show typical dermatitis and the right image depicts a sclerosing keratitis. Adapted from [3] and from [14].

Nowadays, loss of sight induced by O*. volvulus* is rarely found; however, affected individuals show a broad range of other clinical manifestations. Studies on human onchocerciasis tend to classify patients into three groups: 1) asymptomatic individuals, persons with so called generalized onchocerciasis or GEO who have palpable nodules in their skin; 2) patients with severe pathology (termed hyperreactive form or sowda) and 3) putative immune individuals (PI, also termed endemic normals or EN) who never develop any signs of parasitemia or clinical onchocerciasis, despite their lifelong exposure to the parasite [5]. The majority of infected individuals in endemic areas belong to the asymptomatic form of onchocerciasis. These individuals are hyporesponsive and tolerate high loads of MF [11]. Although they do not kill viable MF, they can mount strong immune responses towards damaged adult worms or MF [7, 10]. Between the two polar forms (hypo- and hyperreactive form) there is a variety of individuals presenting intermediate symptoms, including those with primary infections, who are able to kill MF, but present a low degree of hyporesponsiveness [9]. Interestingly, there is evidence for a further group of hyporesponsive individuals who are are also MF^- probably as a result of repeated rounds of treatment intake or increased vector control. This phenomenon is designated as post-patent, occult or expiring infection [15, 16]. In contrast to hyporesponsiveness, hyperreactivity on the other hand appears seldomly [2]. If pathology arises, it is principally located at the skin, since the skin contains masses of MF [5, 7]. Skin pathology is characterized by rashes, lesions and troublesome itching (figure 1.3). Furthermore, affected individuals can suffer from disfiguring skin disease lesions and in association, the intense psychosocial implications of chronic pruritus. Induction of these symptoms results from the destruction of cutaneous MF by strong local and systemic immune responses. If the dermal reaction is not limited, it can be accompanied by depigmentation (“leopard skin”) as well as by loss of skin elasticity and structure, resulting in signs of premature skin ageing (e.g. “lizard skin” or “hanging groin”). A further type of hyperreactivity in the skin is the so called sowda form, which is defined by severe chronic papular dermatitis and hyperpigmentation which appears unilaterally [7]. Occurrence of the sowda form is focused in certain geographically regions (it is most common in Yemen and Sudan) and moreover it has been correlated with specific genetic polymorphisms [3, 17]. Interestingly, individuals affected by hyperreactivity are characterized by low numbers of parasites (less than 10 MF per mg of skin or the absence of worm offspring). The low numbers of adult worms are further linked with lower frequencies of nodules and increased immune responses, particularly of type 2 helper (Th2) T cells [1, 7, 9].

1.1.3 Immune responses during infection with *Onchocerca volvulus*

One of the most interesting aspects for immunologists is the question how adult worms manage to be tolerated for up to 15 years in the human body and produce 5 to 10 million MF

during this time [18]. Nevertheless, there is a broad range of immune responses in infected individuals which in part reflects the diverse disease manifestations.

Helminth infections are associated with humoral or Th2 responses and it is believed that Th2 immunity actually evolved in response to such infections in order to counterbalance classical cell mediated Th1 responses which certainly damage worms, but also cause collateral damage to host tissue [19, 20]. Therefore, the Th2 response has some sort of "protective" function in terms of avoiding severe pathology. Previous studies have assigned the cytokines interleukin (IL)-3, IL-4, IL-5, IL-9, IL-10 and IL-13 and the antibody isotypes immunoglobulin (Ig)G1, IgG4 and IgE to these Th2 responses. Nowadays, IL-10 is allocated to regulatory immune responses [21] whereas IL-9 belongs to a further subgroup of T cells, namely Th9 cells whose function and specific transcription factor are not known so far [22].

Patients with the generalized form of the disease tolerate high loads of MF, however they are characterized by mild or moderate skin dermatitis [7]. Peripheral blood mononuclear cells (PBMCs) of these individuals produce low levels of the hallmark Th1 cytokine interferon (IFN)-gamma and show no or weak parasite-specific proliferative immune cell responses when re-stimulated with *O. volvulus* extract [3, 23, 24]. Thus, it was previously thought that these patients have elevated Th2 immune responses [13, 15], but today it is known that in GEO patients immunomodulatory mechanisms exist that limit and control Th2 immune responses in order to prevent damaging effects [25, 26]. These effects are probably mediated by adult female worms in order to protect their offspring and to establish long-lasting parasitic infections [18, 25, 27]. Due to the fact that there is a calculated turnover of 1,000-3,000 MF per day from each female worm in patent GEO individuals, down-regulation of proliferation responses and suppression of pro-inflammatory cytokines seems to be an essential step to avoid extensive immune responses that could damage both host and parasite [24]. To add an additional level of complication, in *O. volvulus*, all individual worms and all life cycle stages contain an intracellular bacterial symbiont (*Wolbachia*, see section 1.3) that is essential for worm fertility and survival. These bacteria were shown to induce pro-inflammatory innate responses via Toll-like receptors (TLR), specialized pattern-recognition receptors (PRRs), which detect conserved structures of pathogens [28]. Since host inflammatory responses to MF and *Wolbachia* are thought to be the driving force behind onchocercal keratitis and dermatitis [5], adverse immune reactions induced by *Wolbachia* have to be counterbalanced in order to guarantee the worm's survival. It is hypothesized that consistently increasing the exposure of the host's immune system to worm antigen results in hyporesponsiveness, which in turn results in unresponsiveness to bystander antigens [25]. For example, *in vitro* experiments demonstrated that the amount of skin MF was negatively associated with the levels of secreted Th2 cytokines of PBMCs from onchocerciasis patients

stimulated with *O. volvulus* extract [29] whereas the magnitude of Th2 responses augments with increasing severity of pathology but this is not strictly correlated [5].

Studies have elucidated several mechanisms and cell types that are thought to play a role in modulating immune responses in asymptomatic filarial infected individuals. Amongst them are regulatory T cells (Tregs), alternatively activated macrophages (AAMs), regulation of TLR that sense *Wolbachia* and anti-inflammatory cytokines like transforming growth factor beta (TGF-β) and IL-10 [18, 30-33]. During the last years, Tregs expressing the transcription factor forkhead box P3 (Foxp3) have become a central focus of attention because they are indispensable for immunological unresponsiveness to self-antigens and in suppressing excessive immune responses deleterious to the host [34]. They are a subpopulation of helper $CD4^+$ T cells and are able to suppress overly active Th1 and Th2 cells. Unlike Th1, Th2 and Th17 T cells, which all mediate pro-inflammatory effects and activate further T- and B-cell populations, regulatory T cells inhibit pro-inflammatory immune responses by eliciting anti-inflammatory signals via cell to cell contact through glucocorticoid-induced tumour-necrosis factor receptor-related protein (GITR) or cytotoxic T lymphocyte antigen 4 (CTLA-4) or via the secretion of regulatory cytokines (like IL-10 and TGF-β). Multiple studies have implicated an important function of Tregs during helminth infection. For example, it was shown that the majority of T cell clones generated from onchocercomas of GEO individuals had a suppressive profile and moreover immunohistochemistry revealed the local presence of Tregs inside nodules [9, 18].

Alongside Tregs, AAMs also play an important role during filarial infections. In contrast to conventional macrophages, which mediate pro-inflammatory immune reactions, AAMs are characterized by their diminished immune response to TLR stimuli and by reduced expression of the genes associated with in antigen presentation and processing. Upon activation they induce less pro-inflammatory cytokines but more TGF-β and in general they seem to block Th1 immune responses. Moreover, they can contribute to wound healing which is important during filarial infections since the penetrating parasites can cause extensive damage as they pass through tissue, releasing proteolytic enzymes that injure cells and tissue [34-38]. In accordance with these effects, AAMs are found to be up-regulated in asymptomatic patients infected with the closely related filariae *W. bancrofti* and they could probably account for the diminished parasite antigen-specific T cell responses seen in these individuals [31]. Moreover, macrophages with an alternative activation phenotype were also found in onchocercomas of hyporeactive individuals [32].

As mentioned above, TLRs belong to PRRs and recognize conserved structures derived from microbes. Murine models of ocular onchocerciasis have linked the induction of corneal pathology with the triggering of TLR2 and TLR4 [39, 40]. Human studies revealed that LF infected MF^+ patients expressed decreased baseline levels of TLRs on their B and T cells

compared to uninfected controls. B cells and also monocytes of these infected persons were both characterized by decreased expression of TLRs following stimulation with the helminth antigen and diminished cytokine secretion following TLR stimulation compared to uninfected individuals [33, 36]. In contrast, LF patients suffering from severe pathology were shown to express higher levels of TLR indicating that TLR expression is associated with disease manifestations [41, 42]. These data provide evidence that parasites also induce regulation of TLR expression in order to evade detrimental immune responses, albeit only for infections with LF so far.

TGF-β is a highly conserved regulatory cytokine with pleiotropic effects on cell proliferation, differentiation, migration, and survival and appears to play a role in multiple biological processes including development, carcinogenesis, fibrosis, wound healing, and immune responses [43]. Its function includes the reduction of inflammation, immunosuppression, regulation of cell proliferation, differentiation and migration, and regulation of extracellular matrix production [44]. The involvement of TGF-β during filarial infections stemmed from studies which demonstrated that there were increased levels of TGF-β in the onchocercomas of hyporeactive patients which could theoretically suppress defensive Th2 responses and counterbalance immunopathology. In contrast, levels of TGF-β are decreased in hyperreactive individuals [9]. Interestingly, it was also demonstrated that levels of this cytokine increased with the onset of MF production and with worm burden *per se* [32]. Immunohistology of nodules also demonstrated that numerous cell types release TGF-β including T cells, plasma/B cells, macrophages, mast cells, fibrocytes and vascular endothelial cells [32] and as mentioned above it can also be secreted by AAMs [37]. Generation of antigen-specific regulatory T cell clones (Tr1) from onchocercomas showed that these cells induce peripheral tolerance through the production of TGF-β [18] although neutralization of TGF-β enhanced but did not completely restore proliferation in re-stimulation assays with PBMCs from GEO individuals [24]. Further studies demonstrated that filariae also possess *tgf-β* genes and produce TGF-β homologues that may contribute to the maintenance of the physiological integrity of worm tissues [45]. All these results emphasize a key role of TGF-β during onchocerciasis although they also indicate the involvement of additional suppressive mechanisms.

IL-10 is another generally known immunosuppressive cytokine that can limit potential tissue damage caused by inflammation and can inhibit both innate and adaptive immune responses. This cytokine is produced by various cells of the innate and adaptive immune system, including dendritic cells, macrophages, mast cells, natural killer (NK) cells, eosinophils, neutrophils, $CD4^+$ and $CD8^+$ T cells, and B cells. Signal transducer and transcription activator 3 (STAT3) is the key downstream transcription factor used by IL-10 [46]. The IL-10 receptor (IL-10R) is composed of two different chains (IL-10R1 and IL-10R2)

and upon IL-10 binding to the IL-10R complex, the IL-10/IL-10R1 interaction changes the cytokine conformation allowing the association of IL-10R2 (see figure 1.4). Subsequently, two members of the Janus kinase family are activated namely Janus kinase 1 (Jak1) and Tyrosine kinase 2 (Tyk2), presumably by cross-phosphorylation of two tyrosine residues (Tyr 446 and Tyr 496) on the intracellular domain of the IL-10 receptor 1 (IL-10R1). These phosphorylated tyrosines mediate the direct interaction of STAT3 via their SH2 domain to the IL-10 receptor complex. Additionally, STAT1 and, in certain cell types, STAT5 molecules are activated in IL-10-treated cells. These transcription factors build homo- and heterodimers that migrate into the cell nucleus and bind to the STAT binding elements of various promoters in order to induce transcription of the corresponding genes [21, 47]. The important role of IL-10 during filarial infections was demonstrated in several studies. For example, it was shown that neutralization of IL-10 during *in vitro* experiments restored the proliferative capacity of PBMCs from hyporeactive patients [24, 48]. In addition, $CD4^+$ T cell clones from nodules of GEO individuals were shown to be strong producers of IL-10 [18]. Furthermore, IL-10 is associated with the induction of IgG4 indicating that IL-10 influences both cellular and humoral immune responses [49]. For example, *in vitro* generated regulatory T cell clones that preferentially induce IgG4 by B cells were inhibited in their IgG4 production if IL-10 was

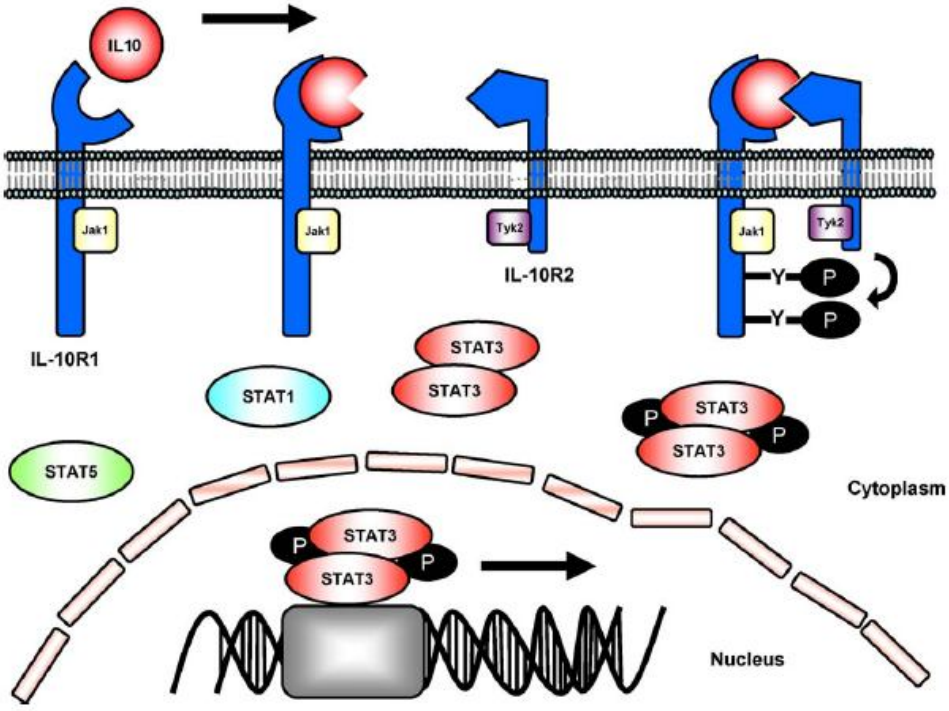

Figure 1.4. IL-10 signaling pathway. IL-10 binds first to IL-10R1. This interaction leads to a conformation change of the cytokine creating a binding site for IL-10R2. The close proximity of both receptor components leads to the reciprocal activation of the receptor-associated Jak1 and Tyk2. Following the tyrosine phosphorylation of the cytoplasmatic part of IL-10R1, STAT3 molecules are bound and phosphorylated by the Janus kinases. Additionally, STAT1 and, STAT5 molecules are activated. STAT homo- or heterodimers immigrate into the nucleus where they bind to the STAT binding elements of various promoters in order to induce transcription of the corresponding genes. Adapted from [21].

blocked. Interestingly, the same effect was observed, if the interaction between GITR and its ligand were blocked [50]. In general, hyporeactive GEO individuals are characterized by high IgG4 production [49, 51]. IgG4 is a poor inducer of antibody-dependent cell-mediated cytotoxicity (ADCC) since it does not fix the complement system and binds rather weakly to effector cell Fc receptors [51, 52]. However, IgG4 can compete with IgE for antigenic binding sites and has a higher affinity than IgE [53] thereby preventing the host from pro-inflammatory immune responses by saturating IgE receptors and preventing the bridging of *O. volvulus* specific IgE which avoids mast cell degranulation [7]. Thus, induction of IgG4 is believed to represent one of the major mechanisms used by filarial parasites to evade destruction by their host's immune system [54]. In line with these facts, staining of onchocercomas of GEO individuals revealed an increase of IgG4 producing plasma cells compared to the hyperreactive form of the infection [9]. In conclusion, individuals with the GEO form are characterized by strong immune regulatory mechanisms which prevent the attack of live MF in order to protect host and parasite.

In contrast to the hyporeactive form of onchocerciasis, mechanisms inducing tolerance are considered damaged or inhibited in hyperreactive individuals. Interestingly, this form of the disease clusters in families and is associated with distinct gene variants [17]. Affected individuals are further defined by strong Th2 cytokine responses and eosinophilia [17]. Eosinophils are known to attack filarial larvae through the release of cytotoxic cationic proteins as well as mediators like oxygen radicals thereby also damaging host cells. Many of the eosinophil-specific mediators act directly on mast cells and aggravate inflammation [43]. Indeed, eosinophils can be found around the few live or disintegrating MF in hyperreactive patients [7]. Moreover, analysis of the onchocercomas from hyperreactive individuals revealed that they contain massive infiltration of lymphocytes (like plasma cells), eosinophils, neutrophils, macrophages and mast cells in contrast to nodules of GEO individuals which are characterized by moderate inflammation [13, 55]. In addition, it could be shown in immunohistochemical stainings that hyperreactive individuals have less TGF-β in their nodules than GEO patients which could induce immunosuppression [9]. Concerning the humoral immune response, it has also been described that hyperreactive patients are characterized by high levels of IgE but interestingly, also increased levels of IgG1 and IgG3 in their sera [5]. Immunohistochemical stainings of the nodules confirmed the presence of increased amounts of IgG1 and IgE producing plasma cells [9]. In conclusion, hyperreactive individuals obviously have the capacity to kill MF, but this is associated with severe pro-inflammatory responses.

In the third group, consisting of naturally resistant or putatively immune persons, individuals show a different immunological profile composed of a strong mix of Th1 and Th2 responses which is mainly characterized by the production of IFN-γ and IL-5 [13]. This increased

Th1/Th2 immune response prevents the development of patent infections, in contrast to individuals with the generalized form of onchocerciasis. It could be shown that PBMCs from PI individuals secrete more cytokines upon re-stimulation with a larval antigen or adult worm antigen than GEO patients [13, 15, 24, 56, 57]. Moreover, PBMCs from PI individuals show higher proliferative activity and they secrete less IL-10 than those from hyporeactive individuals [15, 58]. Furthermore, it is known that the levels of Fc receptor- and complement-binding IgG3-type antibodies are higher in PI individuals compared to those of GEO individuals [13] and in general they have higher levels of circulating antigen-specific IgG1 and IgG3. Both are regarded as being possibly protective since they are involved in antibody-dependent cellular cytotoxicity reactions against filarial larvae [59].

1.2 Lymphatic filariasis

1.2.1 Parasite biology and epidemiology

Lymphatic filariasis is a major neglected tropical disease that causes acute and chronic morbidity. It is spread across 81 countries and 120 million people are infected (see figure 1.5) with a third of the latter seriously incapacitated and disfigured by the disease [60]. In addition, an estimated 1.34 billion people live in areas where filariasis is endemic and are at risk of infection [61, 62]. Approximately 65% of infected individuals live in South-East Asia,

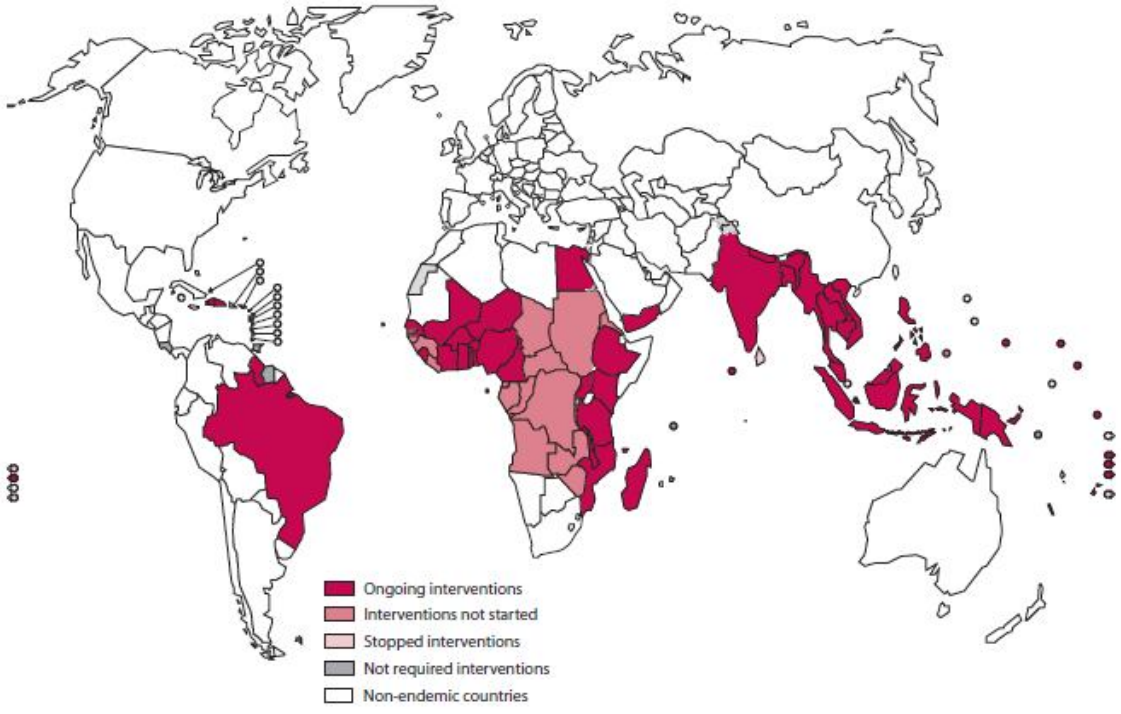

Figure 1.5. Global distribution of LF and status of mass drug administration. Adapted from [61].

30% in Africa and the remainder in other tropical areas [http://www.who.int/mediacentre/factsheets/fs102/en/index.html]. Lymphatic filariasis is prevalent in both urban and rural areas, but the majority of cases occur among the poor. Mortality is uncommon but the morbidity associated with this infection can be considerable and lifelong [63] since individuals suffer from severe functional impairment that ranges from loss of working time to completely giving up an occupation [64]. The consequential socioeconomic impact has therefore designated this infection a major public health concern. Lymphatic filariasis is provoked by infection with the threadlike nematodes *Wuchereria bancrofti, Brugia malayi* or *Brugia timori* which are transmitted by anopheline and culicine mosquitoes. More than 90% of infections are caused by *W. bancrofti* [65]. The infective L3 enter the host during the blood meal of the vector and migrate through the lymphatics (figure 1.6). The L3 moult into L4 and finally into sexual dimorphic adult worms [66], which exist for up to 8 years in their hosts. The site of adult worm parasitism is in dilated nests within the lymphatic vessels which are most commonly found in the extremities and male genitalia. Here, inseminated females start to produce millions of MF which are 200-250 μm in length and circulate in periodical patterns in the blood to coincide with the vector's feeding habits [1]. During another blood meal these MF can be ingested again by the vector mosquito.

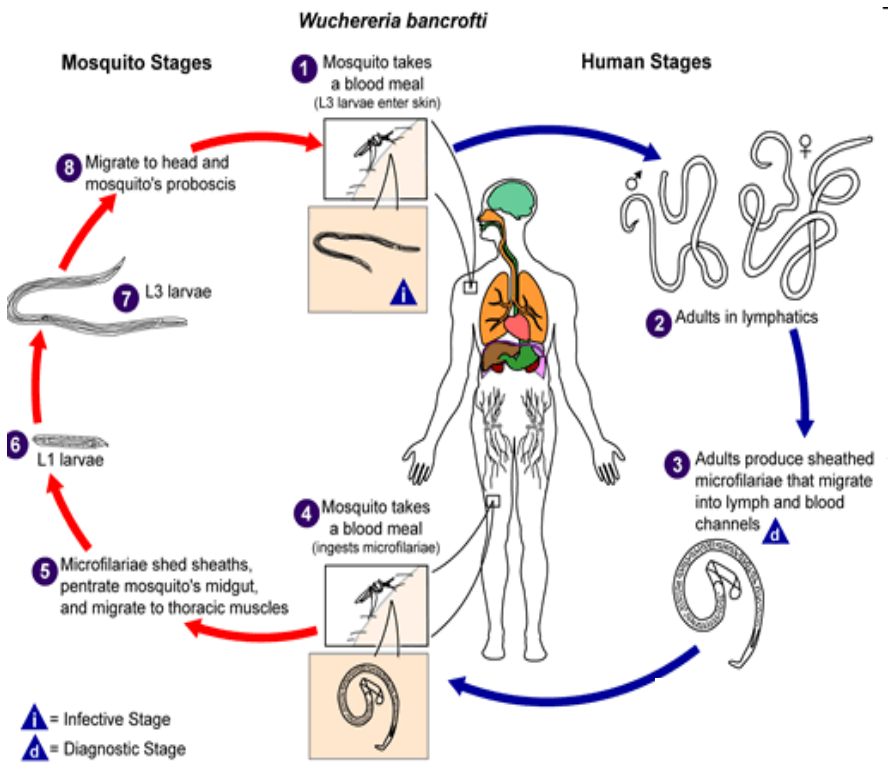

Figure 1.6. Life cycle of *W. bancrofti*. Adapted from http://www.dpd.cdc.gov/dpdx.

1.2.2 Pathology of lymphatic filariasis

Lymphatic filariasis is a chronic and persistent disease that endures over many years. Comparable to infections with *O. volvulus* the majority of infected individuals elicit very few signs of disease [67], but in general the spectrum of clinical presentations found among individuals in endemic regions of LF is extremely broad.

The most common clinical manifestation, the asymptomatic (patent) form, is associated with high levels of MF and circulating filarial antigen but with absence of obvious pathology [68]. These patients serve as the reservoir for continued transmission of the parasite. In contrast, individuals with severe pathology have few or no MF but vigorous specific immune responses [69]. In addition to the asymptomatic and symptomatic form, the disease can be further divided into acute (or early) and chronic phases but of course it has proven difficult to focus on acute or early infections because the time of infection cannot be easily ascertained [70]. Furthermore, some individuals remain free of infections despite lifelong exposure to the parasites; these individuals are referred to as EN.

In the early phase of infection there are two different acute manifestations of LF: acute filarial lymphangitis (AFL) and acute dermatolymphangioadenitis (ADLA) [71]. The former one is induced by the death of the filarial worms and may end in hydrocele formation (accumulation of lymph fluid in the tunica vaginalis, occurs only in bancroftian filariasis, figure 1.7) whereas ADLA is not induced by the worm *per se* but is associated with bacterial infections that may induce lymphedema (accumulation of lymph fluid in the legs, scrotum, breasts and arms, figure 1.7) [72, 73]. However, in contrast to onchocerciasis, pathology in LF is mainly caused by the adult stage of the worm [2]. There is almost no immune reaction to adult worms as long as they are alive but inflammation does occur when adult worms die; either drug-induced or spontaneously resulting in local necrosis around the parasite [74, 75]. Dead parasites are then either completely absorbed or partially calcified. Inside the affected tissues they provoke changes that induce dilation of the lymphatics and thickening of the lymphatic vessel wall as well as fibrosis and lymphatic obstruction [1, 70, 76]. Granuloma formation, defined as infiltration of plasma cells, eosinophils, neutrophils and macrophages, has also been demonstrated in and around these infected vessels by histological stainings [70]. If these induced immune reactions are not limited (see below) they can lead to different irreversible clinical manifestations such as lymphedema which may progress to the most severe disease form, called elephantiasis (non reversible edema, with skin thickening and nodular or warty excrescences), to urogenital disorders or to hydroceles [77]. These individuals are often referred to as chronic pathology (CP) patients. In fact, the occurrence of lymphedema and hydrocele is not mutually exclusive and both are characterized by dilation of the lymphatic vessels and extravasation of fluid from the vessels into the surrounding tissues. The enlargement of the lymph vessels results in less efficient lymph flow which in the

Figure 1.7. Aspects of severe pathology elicited by LF infection. Left picture shows severe lymphedema in the right leg whereas the right picture depicts an example of hydrocele. Adapted from [78] and from http://www.dolf.wustl.edu.

legs is always orientated against gravity. In contrast to hydrocele patients, lymphedema affected individuals become more vulnerable to opportunistic microorganisms that may enter the lymphatics through smaller wounds; these little injuries would be usually unnoticed in people without lymphatic disease [74]. Besides these secondary bacterial or fungal infections, other studies have provided evidence that pathology is a genetic trait since its development is seen in clusters of families and several distinct polymorphisms have been identified. Moreover, genetic traits have also been correlated with parasite burden and the susceptibility to infection *per se* [44, 74, 79].

A further rare form of pathology, that is present in less than 1% of all LF infected individuals, is the so called tropical pulmonary eosinophilia (TPE) [80]. This type of illness reflects an immunological hyperresponsiveness of the host. Affected patients suffer from cough, fever, and hepatosplenomegaly [81]. They are characterized by the absence of MF in the bloodstream because the worm offspring is rapidly opsonized with anti-microfilarial antibodies and finally cleared in the pulmonary vasculature. Trapped MF degenerate and release antigenic components that trigger local inflammatory processes with accumulation and activation of eosinophils in the lungs. Consequently, asthmatic symptoms are induced as a result of pulmonary allergic responses mediated by specific IgE antibodies directed against the MF [76, 80, 82].

1.2.3 Immune responses during infection with lymphatic filariasis

The immune system of individuals living in endemic areas of LF is permanently exposed to incoming larvae, dying adult worms and degenerating embryos released from fecund adult female worms and to the endosymbiotic *Wolbachia* (see section 1.3). All these factors lead to low-level but constant triggering of innate and adaptive immune cascades and it seems that

the frequency and intensity of the host's response is related to the degree of clinical disease and pathology [2, 74, 83].

Responses of affected individuals can be pinpointed to the phase of infection since there are stage specific reactions to antigens from larvae, MF and adult worms. Antigens of these distinct stages stimulate the release of diverse patterns of cytokines and therefore immune responses are different in the acute and chronic phase [84]. For example, *in vitro* studies have demonstrated that antigenic extracts of MF influence dendritic cell (DC) characteristics during their differentiation process. Indeed, alteration of DC function by MF resulted in less efficient activation of T cells and modified cytokine release [85]. In addition, live MF have been shown to induce apoptosis in immature DCs; this diminishes their capacity to function appropriately which in turn has significant consequences on the activation of $CD4^+$ T cells [86]. In association, live L3 decrease the capacity of epidermal Langerhans cells to stimulate $CD4^+$ T cells and another report revealed that they rather induced Th1 dominated responses in T cells from uninfected persons in the presence of antigen presenting cells [87, 88]. Studies with patients suffering from AFL have demonstrated that they have significantly increased levels of TNF in their sera compared to microfilaremic individuals or those with chronic pathology. The level of this pro-inflammatory cytokine has been correlated to the severity of the acute disease [70, 89].

However, the majority of the previous studies focused on comparing microfilaremic individuals versus CP patients because these two groups represent the major poles of infection. Down-regulation of proliferation in response to parasite-specific antigen stimulation is a hallmark of patent infection, although the ability to respond to non-parasite antigens and mitogens is equivalent to those observed in asymptomatic MF^+ individuals and those with chronic lymphatic pathology [90]. This T cell hyporesponsiveness is further reflected by the decreased production of IFN-γ and IL-2 from cells of infected individuals with no clinical signs of disease [91]. King *et al* demonstrated an association of this down-regulated immune response in asymptomatic individuals with a lower frequency of parasite-specific T and B cells of microfilaremic individuals compared to CP patients [92]. Besides the down-regulated Th1 immune responses, asymptomatic microfilaremic patients have earlier been characterized by dominant Th2 immune responses (typified by increased levels of IL-4 and IL-5) [70] but nowadays increased Treg responses (high levels of immunosuppressive cytokines like IL-10 and increased Foxp3-positive T cells) are associated with patent infections [1]. In fact, PBMCs from patent individuals spontaneously secrete higher levels of IL-10 compared to individuals with chronic pathology. Furthermore, IL-10 production by PBMCs in response to parasite antigens was also found to be significantly increased in asymptomatic MF^+ individuals than in individuals with lymphatic pathology. In contrast, IL-10 production to non parasite antigens was equivalent in the two groups [90, 93]. Use of

blocking antibodies against IL-10 reversed the lack of proliferation in PBMCs from microfilaremic patients. The same effect was seen using anti-TGF-β antibodies, although to a lesser degree but caused no enhanced responses by T cells of CP individuals [94]. All these mechanisms are thought to be driven by the helminth in order to evade host defenses and ensure survival [67, 83, 94, 95]. Therefore, LF patients with elevated levels of regulatory responses and an altered balance between Th1 and Th2 cytokines are thought to tolerate higher parasite burdens and show low pathological symptoms. In contrast, individuals with few or no parasites and deliberating pathology mount strong filarial-specific immune responses [67, 96]. Patients with severe pathology also display stronger Th1 immune responses (IL-6 and IL-8) or even increased Th17 responses when compared to microfilaremic individuals [41, 95, 97, 98]. These pro-inflammatory cytokines and their receptors are associated with the induction of vascular endothelial growth factors (VEGFs) [99, 100] which have been shown in previous studies to be linked with lymphangiogenesis and vascular permeability [78]. In fact, investigations revealed that a single nuclear polymorphism in VEGF-A is significantly higher in hydrocele patients than in microfilaremic or lymphedema individuals [79]. Interestingly, patients suffering from severe pathology also have different single nucleotide polymorphisms (SNPs) for TGF-β than asymptomatic individuals indicating that genetic traits are also responsible for these overt reactions [44].

Furthermore, the immunosuppression of the microfilaremic patients is characterized by higher IgG4 production in comparison to individuals with severe pathology, which is in line with patients infected with the generalized form of onchocerciasis (see section 1.1.3). It is described that an active LF infection promotes the production of IgG4 and limits the levels of IgE in contrast to severe pathology where the development of pathology is associated with higher IgE:IgG4 ratios [101]. In fact, the proportion of the parasite specific IgE differs in the various clinical states of LF: the highest levels are found in patients with TPE and the lowest in those with asymptomatic microfilaremia [102]. Previous studies have revealed that CP individuals are characterized by increased levels of filarial-specific IgG1 antibodies but no significant differences were seen in IgG2 or IgG3 levels compared to the microfilaremic patients [59, 103]. Therefore, the induction of IgG4 in the asymptomatic individuals seems to represent one major mechanism used by filarial parasites to evade destruction by their host's immune system [54].

In EN, the immune responses are comparable to those of the putatively immune individuals found in onchocerciasis areas. Thus, these subjects remain free of demonstrable filarial infection and do not present any of the immune traits found in either acute or chronic filarial disease manifestations [104]. PBMCs of EN proliferate significantly more in response to the specific antigen and moreover they secrete higher levels of IL-2 and IFN-γ compared to the microfilaremic and amicrofilaremic patients [105]. Furthermore these individuals contain

higher levels of IgG1 and IgG2, but decreased levels of IgG4 in their sera compared to MF^+ patients [106].

1.3 *Wolbachia*

Lymphatic filariasis and onchocerciasis causing helminths live in mutual symbiosis with *Wolbachia* endobacteria, which belong to the order Rickettsiales. In contrast to most arthropod-*Wolbachia* associations, where *Wolbachia* have parasitic habits, the endosymbiosis of *W. bancrofti*, *B. malayi*, *B. timori* and *O. volvulus* with *Wolbachia* is obligate, implying an indispensable role of the endobacteria for fertility, reproduction, larval moulting and the survival of the helminths [7, 107, 108]. These bacteria can be detected in all development stages, they are restricted to the hypodermis and reproductive tissues of the female worm, including the oocytes (see figure 1.8) and they are transmitted transovarially from one worm generation to the next [7, 109].

Previous observations have associated the presence of this endobacteria with the induction of pathogenesis since it could be shown that *Wolbachia*, released from larvae or adults, are potent inducers of innate inflammation. Murine and human *in vitro* studies have confirmed that these endosymbiotic bacteria lead to classic activation of macrophages and promote recruitment and activation of neutrophils thereby triggering pro-inflammatory cytokines, such as TNF, IL-1β and IL-6, and nitric oxide mainly via the TLR2 pathway [5, 12, 28, 39, 74, 110-112]. Furthermore, it was shown that these pro-inflammatory cytokines could in turn mediate the upregulation of VEGFs which are associated with the development of pathology [78]. Recent research has also focused on the unique relationship since the residing endosymbionts are also a target for anthelmintic therapy and the application of antibiotics (tetracyclines) has been shown to efficiently deplete *Wolbachia* and in turn cause worm death (see section 1.5). Indeed, depletion of *Wolbachia* with doxycycline was actually shown to improve pathology and decrease levels of VEGFs [78].

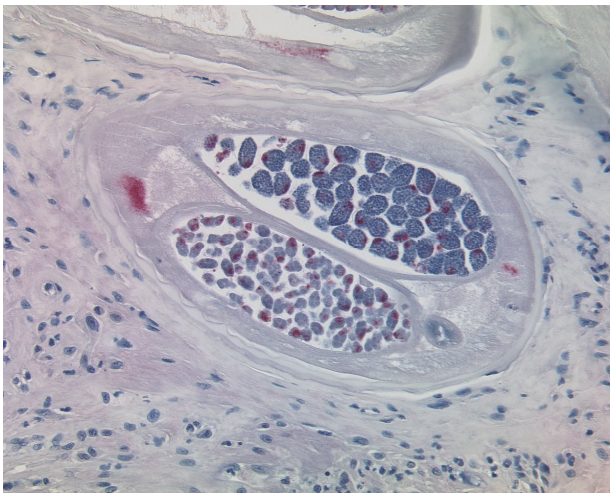

Figure 1.8. A female *O. volvulus* worm with *Wolbachia* endosymbionts. Depicted is a transverse section through a female *O. volvulus* worm with *Wolbachia* stained in red using antibodies against *Wolbachia* surface protein. Courtesy of Dr. Sabine Specht.

1.4 Diagnosis of onchocerciasis and lymphatic filariasis

The traditional way to diagnose infection with the parasite *O. volvulus* is the palpation of nodules. In patients from Latin America, the parasite is transmitted by the vector *Simulium ochraceum*. These mosquitoes typically bite the upper region of the patient; therefore, nodules are often located on the head and upper body. In contrast, in African individuals nodules are mostly found over the hips, over the sacral bone and lower limbs, but also on the thorax and near the knee because the vector *Simulium damnosum* bites the lower parts of the body [3]. In order to detect MF, small skin biopsies are taken with a corneoscleral punch. These small biopsies (also called skin snips) are restricted to the upper dermis and thus should not reach blood capillaries since contamination of a skin snip with blood may result in detection of other blood-borne MF species [3]. Motile MF migrate out of the small biopsies and can be counted under a dissecting microscope [113]. In general, skin snips are a common tool to identify an established infection in patently infected individuals [1].

Diagnosis of LF traditionally relies on the determination of blood circulating MF. In order to identify asymptomatic LF, nocturnal venous blood is checked for the presence of MF using membrane filters to enrich the worm offspring [114]. The detection of MF has been essential for diagnosing the disease but this method is limited to patent infections. Therefore, other tests have been developed such as a specific enzyme linked immunosorbent assay (ELISA), or the rapid card test that measures circulating filarial antigen (CFA), which are released from adult worms and can be detected in plasma samples of *W. bancrofti* infected individuals [115-117]. In contrast to the diagnosis of *O. volvulus* and to infections with *Brugia* worms it is possible to identify cryptic or latent infections with *W. bancrofti* using these tests. Besides the determination of latent infection, the CFA even allows the identification of individuals with low parasitemia which could occur, for example, after treatment with microfilaricidal drugs. The CFA tests have revealed that there are roughly equal proportions of MF^+ and MF^- individuals and due to the lack of pathology, the latter group has remained largely undetected and excluded from many former studies [117].

An additional diagnostic parameter for *W. bancrofti* infection is the visualization of active nematodes via ultrasonography since adult worms show characteristic pattern of movements within the lymphatic vessels of the scrotum of male patients. This is termed filarial dance sign (FDS) [118, 119]. In patients infected with *B. malayi* ultrasonic imaging of adult filaria is of limited use because these worm nests are not stable over time and are not localized in distinct parts of the body [120, 121], thus, worm nests will be detected only in a fraction of patients. However, with these tools it is now possible to differentiate in bancroftian filariasis between patent and latent infected individuals and in addition, confirm the prevalence of live nematodes. Although these methods are not applicable for brugian infections serology

assays can be performed by analyzing brugia-specific immunoglobulins in ELISAs [101, 122].

1.5 Treatment of onchocerciasis and lymphatic filariasis

There remains no vaccine against helminth infections. Thus, besides vector control, chemotherapy is the method of choice to eliminate the disease [123]. In the last two decades, diethylcarbamazine (DEC), ivermectin (IVM) and albendazole (ALB) have been used for successful mass drug administration (MDA) against filarial infections. These standard drugs are used in order to interrupt transmission with a consequent reduction in the burden of infection and to diminish morbidity [2].

The mode of functioning of DEC is not completely understood but it is known that this drug results in the sequestration of MF and their final destruction by the immune system. Murine and human *in vitro* studies suggest that DEC blocks the cyclooxygenase pathway in parasites which leads to death of MF [2, 124]. Ivermectin is a well tolerated macrocyclic lactone which acts by hyperpolarization of parasitic glutamate-sensitive channels thereby preventing neuronal transmission resulting in muscle paralysis [125, 126]. In contrast to DEC, IVM treatment does not induce local destruction of MF. Recently, IVM was shown to decrease the amount of proteins released by the excretory/secretory vesicles of MF preventing the secretion of immunomodulatory molecules by the worm offspring which usually block the host's immune response [123]. Finally, ALB is a broad-spectrum anthelmintic drug against flatworms, nematodes and cestodes that inhibits the polymerization of worm β-tubulin and microtubule formation [127].

In order to treat LF, DEC or IVM each in combination with ALB, are used by the global programme to eliminate lymphatic filariasis (GPELF). Given as a single dose DEC is effective in reducing acute and chronic cases of microfilaraemia for at least one year, and this is the basis of MDA in areas without co-endemic onchocerciasis. Diethylcarbamazine cannot be used in endemic regions of the latter since its administration causes MF death and leads to irreversible local ocular damage [128] therefore, in onchocerciasis endemic areas IVM is used in combination with ALB in order to treat LF. In the case of onchocerciasis infections, IVM is the sole drug given annually or biannually by the African Programme of Onchocerciasis Control (APOC) and the Onchocerciasis Elimination Programme for the Americas (OEPA) [1, 60, 129-131].

Although DEC, IVM and ALB have been successfully used in the past to kill MF, these drugs show no (in case of IVM in *O. volvulus* infections) or only moderate (valid for ALB in LF) macrofilaricidal effects [132]. That is, they do not kill adult worms which would in essence eliminate the infection. Therefore, repeated rounds of treatment have been given in order to break transmission. For success, such treatment would need to occur for many years at least

as long as adult worms are alive which can exceed 15 years in onchocerciasis and 8 years in LF. Long-term treatment however has severe drawbacks since there is evidence for drug resistance [133]. In addition, treatment with IVM or DEC causes microfilarial death, resulting in adverse reactions like fever, headache, dizziness, myalgia, arthralgia and lymph node enlargement because *Wolbachia* are released into the blood where they induce pro-inflammatory immune responses [134].

As mentioned above, *Wolbachia* are essential for worm survival. This unique relationship has provided an alternative avenue for chemotherapeutic treatment since it is known that tetracyclines are effective against these *Rickettsia*-like bacteria [7, 135]. Previous animal studies demonstrated that depletion of *Wolbachia* by tetracycline leads to degeneration and sterility of adult worms [109, 135, 136]. Furthermore, in contrast to the mainly microfilaricidal drugs mentioned above, therapy with tetracycline antibiotics directly targets the *Wolbachia* leading to the inhibition of worm development, embryogenesis, fertility and viability [135, 137]. These anti-wolbachial effects of doxycycline have been addressed in several field studies and have demonstrated that treatment regimes of 3-8 weeks leads to elimination of MF, sterile female filariae and worm death indicating macrofilaricidal effects as well [78, 137-142]. However, since doxycycline is contraindicated for children below 9 years, pregnant or breastfeeding women, and in general not practical for MDA because of huge logistical challenges and the length of required treatment regimes, there is still the need for new effective drugs with macrofilaricidal activity and long-lasting suppression of embryo production [62]. Nevertheless, doxycycline is considered an effective tool for individual drug treatment.

The further registered antibiotic rifampicin has also shown promising activity in experimental trials with mice [143] and was therefore investigated in human pilot studies where it could be demonstrated that rifampicin lead to significant reduction of *Wolbachia* loads, albeit less efficient than doxycycline [144]. Although rifampicin (like doxycycline) is clearly not feasible for MDA it may be useful for the individual treatment of children since it can be taken by children under the age of 9 years. An additional study was conducted in order to test if the combination of doxycycline and rifampicin would increase the beneficial effects on filariae infected individuals. This pilot study demonstrated a moderate macrofilaricidal activity [129] but still there is the urgent need to develop improved micro- and macrofilaricidal drugs in order to reduce the amount of filarial infected individuals and to break transmission.

1.6 Aims and objectives

Collectively, the tropical helminth infections LF and onchocerciasis affect more than 150 million people worldwide and are considered major public health concerns [1]. Whilst perusing the literature it became clear that several results with regards to immunological responses could not be compared since these analyses have mainly focused on the assessment of MF^+ individuals compared to CP patients or of EN compared to one of these two groups. Indeed, the determination of any immunological differences in LF infected asymptomatic MF^+ or MF^- patients has so far been neglected. A reason for such disregard so far, at least in *W. bancrofti* infections, has been the fact that the number of latently infected individuals was underestimated because they were not detected with former diagnostic tools. However, the application of new diagnostic tests has revealed that the percentages of *W. bancrofti* infected latent and patent individuals are almost equally distributed. MF^- infected individuals represent a dead end in terms of transmission and moreover, it remained unclear how these patients maintain their latent phenotype. That is, whether host mechanisms actively prevent MF from reaching the peripheral blood (in LF) or the skin (onchocerciasis). Further research into these aspects may broaden the range of strategies currently employed to reduce transmission and in turn eliminate filariasis. With respect to onchocerciasis, the present study was also able to investigate the profiles of MF^+ and MF^- individuals even though the latter is not the normal situation. Here, the lack of MF relates perhaps to the number of rounds of MDA which is mainly microfilaricidal.

Therefore, the main aim of this thesis was the characterisation of immunological aspects of asymptomatic LF and onchocerciasis infected individuals. These aspects included the assessment of immunological profiles following re-stimulation of isolated PBMCs with filarial or bystander antigens and the prevalence of filarial-specific Ig subclasses. Moreover, elucidating mechanisms inducing protective Igs (e.g. IgG4) was also of interest, especially a possible role of GITR which has been previously shown by our group to be a key player mediating the production of IgG4. The possible role of GITR was also analysed in context of the IL-10 signaling pathway because this cytokine is associated with protective immune processes during filariasis. In addition, genetic profiles of three distinct T cell subpopulations (Tregs, $CD4^+$ and $CD8^+$ T cells) of amicrofilaremic and microfilaremic LF infected patients were analysed since these would give a hint which molecules are important in preventing patency and furthermore which molecules could be central targets for future studies with regards to the development of new therapeutic strategies.

2. Patients, Materials and Methods

This section highlights the variety of materials that were used throughout the study, beginning with clarification about how blood samples were collected for each study followed by remarks about the plastic ware and the required antibodies. Afterwards, there is a report of the preparation of different worm extracts, the parasitological examinations of study participants, and the isolation of different cell populations followed by a depiction of the isolation of MF. Furthermore, this sections covers cell culture and immunological assays and molecular biology procedures. The protocols for the use of various equipment, chemicals, reagents, buffers and solutions referred to in this chapter are described in appendices A-D.

2.1 Patients

2.1.1 Onchocerciasis

Blood samples from helminth infected patients and appropriate EN were collected as a part of a collaboration project with partners at the University of Science and Technology, Kumasi (KNUST) Ghana and the Liverpool School of Tropical Medicine. A cohort of 481 individuals was recruited in the Central Region of Ghana (Upper- and Lower Denkyira Districts, Dunkwa on Offin; Amansie Central and Adanse South Districts, Ashanti Region). This area is endemic for onchocerciasis but not for other human filarial infections. Rivers in this areas are breeding sites of the vector black flies *Simulium sanctipauli* that have flight ranges up to 12 km [108]. Individuals eligible for participation were adult men and women aged 18 to 55 years, who were infected with *Onchocerca volvulus.* To inform the target communities, there was first a meeting held with village elders, where the study procedures and rationale were explained. After general consent, the study procedures were explained to the villagers in English by the responsible physician and then again in the local Twi language. Informed consent was obtained from participants and documented by the signatures of two witnesses. A patient questionnaire was completed for each participant and included a patient ID, a village number, age, the time living in the endemic area and history of anti-filarial drug intake during the last two years. Exclusion criteria were absence of onchocercoma, abnormal hepatic and renal enzymes and creatinine, pregnancy, breast-feeding, alcohol or drug abuse. In total, the study included 384 MF^+, 83 MF^- as well as 14 volunteer individuals (EN). The latter subjects were non-infected members of the population.

2.1.2 Lymphatic filariasis

Blood samples from helminth infected patients and appropriate EN were collected as a part of a collaboration project with partners at the University of Science and Technology, Kumasi (KNUST) Ghana and the Liverpool School of Tropical Medicine.

In the first study with LF infected patients, samples were obtained in context of a randomized double-blind placebo-controlled trial. A cohort population of 299 male individuals (18-50 years) from an area in the Western region of Ghana (Ahanta West District), which were infected with *Wuchereria bancrofti,* was investigated. No other filarial species were endemic in this area [78]. Informed consent was obtained as described for the onchocerciasis study participants (see above). Participants were chosen based on the presence of at least one ultrasonographically detectable worm nest. Out of the 299 included patients from the study cohort, 159 individuals were examined in further immunological studies before treatment; these included 92 MF^+ and 67 MF^- individuals and in addition 22 EN. Within the scope of MDA, patients included in this study had had an average of two rounds of anti-filarial therapy (ALB and IVM) with the last intake at least 10 months before blood was taken. Included participants were also screened for other helminth infections via stool and urine analysis. Out of 159 infected individuals 10 (n= 6 MF^+ and n= 4 MF^-) were also positive for other helminth infections (*Ascaris lumricoides* n= 8, *Strongyloides stercoralis* n= 1, *Trichuris trichiura* n= 1). Furthermore, participants were tested for active malaria (Giemsa staining and measurement of body temperature) and subclinical malaria (NADAL Medical test, nal von minden, Moers, Germany). 20 of 181 individuals resulted positive for this subclinical malaria test.

In a second study within a LF endemic area, samples were obtained from a cohort population of 150 individuals (18-60 years) also from the Ahanta West District in Ghana. Fifty of the participants were uninfected individuals who were negative for the CFA test (see section 2.3.1.2) and also for MF (see section 2.3.1.4). The remaining 100 participants were positive in the CFA test, half of them were amicrofilaremic and the other half was patently infected. Exclusion criteria were negative CFA test, abnormal hepatic and renal enzymes and creatinine, pregnancy, breast-feeding, alcohol or drug abuse.

2.1.3 Blood samples

Blood samples used in this study for STAT3 and *in vitro* experiments with MF were collected from healthy European donors and were kindly provided by the Institute for Experimental Haematology and Transfusion Medicine, University Clinic Bonn, Germany. Collection and use of the samples was approved by the University Clinics ethic committee (“Ethikkommission der Medizinischen Fakultät der Rheinischen Friedrich-Wilhelms-Universität Bonn”). PBMCs were separated from heparinized venous blood by gradient centrifugation on Ficoll Plaque (density 1.077; PAA, Pasching, Austria).

2.2 Material

2.2.1 Plastic and glassware

Unless otherwise stated, all plastic and glassware equipment were supplied by one of the following companies: Eppendorf (Hamburg, Germany), Becton Dickinson (Heidelberg, Germany), Nunc (Roskilde, Denmark) or Greiner (Frickenhausen, Germany).

2.2.2 Antibodies and microbeads

Blocking anti-GITR, anti-GITR ligand and their corresponding isotypes controls were obtained from R&D systems (Wiesbaden, Germany). APC-conjugated anti-Foxp3, anti-CD4 FITC, anti-CD8 APC, anti-CD19 PE, anti-CD20 PerCP-Cy5.5, anti-GITR APC and anti-GITR-L APC were from eBioscience (San Diego USA). Anti-CD14 FITC, anti-CD20 PerCP-Cy5.5 and anti-pSTAT3 Alexa Fluor 647 were purchased from BD Biosciences (Heidelberg, Germany); anti-CD25 PE from Miltenyi (Bergisch Gladbach, Germany). Anti-CD3/anti-CD28 T cell expansion beads as well as magnetic cell sorting beads were supplied by Invitrogen (Karlsruhe, Germany). Anti-STAT3 and anti-pSTAT3 were obtained from R&D systems, (Wiesbaden, Germany). Anti-mouse and anti-goat secondary antibodies both coupled to alkaline phosphatase were purchased from DAKO (Hamburg, Germany).

2.2.3 *Onchocerca volvulus* extract

Aqueous soluble *O. volvulus* extract (*O.v*. extract) was prepared from adult worms that were isolated from *O. volvulus* nodules from infected patients. Worms were isolated by collagenase digestion of the nodules and afterwards shock frozen in liquid nitrogen [145]. All steps of the extract preparation were fulfilled on ice and with pre-cooled solutions. Thawed worms were carefully transferred to a Petri dish pre-filled with sterile PBS (PAA, Pasching, Austria). Worms were washed in PBS and then placed inside a glass mortar (VWR, Langenfeld, Germany). Depending on the amount of worms, 3-5 ml of medium (RPMI without supplements) were added and worms were crushed until the solution was homogenous. The extract was then centrifuged for 10 minutes at 300 x g (4°C) in order to remove insoluble material and the resulting supernatant was carefully transferred to a new tube. The protein concentration was determined by Bradford assay (Advanced Protein Assay™, Cytosceleton, Denver, USA) and the extract was stored at -80°C. All procedures were conducted under sterile conditions.

2.2.4 *Brugia malayi* extract

Brugia malayi extract (*B.m.* extract) was kindly provided by John McCall (University of Georgia, Athens, GA) and it was prepared from adult worms of the human filarial parasite *B.*

malayi that were maintained in jirds (*Meriones unguiculatus*). This parasite is closely related to *W. bancrofti*, whose adult worms are generally difficult to obtain since the parasite cannot be maintained in a rodent host and are not easily obtained from man. *B.m.* extract was tested for its endotoxin levels using the kinetic *Limulus amoebocyte* lysate assay (Charles River, Charleston, SC) and level was below 0.16 EU/ml final concentration.

2.2.5 *Litomosoides sigmodontis* extract

For the preparation of aqueous soluble extract of *L. sigmodontis* extract (*L.s*. extract) worms were isolated from the thoracic cavity of infected cotton rats (*Sigmodon hispidus*) and rinsed in sterile PBS before being mechanically minced. Insoluble material was removed by centrifugation for 10 minutes at 300 x g (4°C). Protein concentrations of crude extracts were determined using the Advanced Protein Assay (Cytoskeleton). All procedures were conducted under sterile conditions.

2.3 Methods

2.3.1 Parasitological assessment

2.3.1.1 Examination of onchocercomas

The traditional way to diagnose infection with the parasite *O. volvulus* is palpation of nodules, i.e. capsules of connective tissue in which several parasites aggregate in the skin of infected people [6]. Onchocercomas were found mainly over the hips, over the sacral bone and lower limbs, but also on the thorax and near the knee. All patients included in the onchocerciasis study had at least one palpable nodule.

2.3.1.2 CFA ELISA

All patients included in the LF studies were positive for CFA tested by the TropBio® ELISA (TropBio, Townsville, Australia) according to the manufacturer's protocol. In brief, 100 µl of plasma were added to 300 µl of diluent provided by the company. Samples were boiled for 5 minutes at 100°C and then centrifuged for 15 minutes at 2,000 x g to dissociate antigen/antibody complexes. 50 µl/well of the clear supernatant containing the heat stable antigen were transferred to the pre-coated 96-well plates and incubated together with the appropriate standards for 90 minutes in a humid chamber at room temperature (RT). After three washing steps with the included washing buffer, 50 µl/well of the polyclonal rabbit anti-*Onchocerca* antibody were added and incubated for one hour. Afterwards, plates were washed three times and then incubated for one hour with the diluted anti-rabbit antibody (50 µl/well) conjugated with horseradish peroxidase (HRP). Subsequently, plates were washed

again three times and then 100 µl of substrate (ABTS Chromagen) was added and incubated for one hour. The plates were measured using the SpectraMAX ELISA reader (Molecular devices, Sunyvale, USA with wavelength correction (405 nm and 492 nm).

2.3.1.3 Determination of skin microfilariae

In order to determine the microfilarial load of *O. volvulus* infected individuals, two skin snips from the upper part of each buttock were taken with a corneoscleral (Holth) punch (Koch, Hamburg, Germany), since the worm offspring can be found there. Each skin snip was weighed using an analytical balance (Sartorius electronic balance, Göttingen, Germany) and placed in individual wells of a 96-well microtitre plate and incubated in 100 µl 0.9% NaCl for 6–20 hours at RT. Thereafter, MF were counted at 63-fold magnification using a microscope (Leica Microsystems GmbH, Wetzlar, Germany) [146]. Microfilarial load was calculated per mg of skin.

2.3.1.4 Determination of microfilaremia

Microfilarial burden of *W. bancrofti* infected individuals was determined from venous blood samples taken between 21-23 h since MF show a nocturnal periodicity. Therefore, 1 ml of blood was filtered through a Whatman Nucleopore filter (5 µm pores; Karl Roth, Karlsruhe, Germany) to hold back the worm offspring. Microfilariae were stained using the Giemsa method (Merck KGAA, Darmstadt, Germany) and stained MF on the filters were directly counted using a microscope (Leica Microsystems GmbH, Wetzlar, Germany).

2.3.1.5 Ultrasonography

Additionally to a positive CFA test, all patients in the first study of LF harbored at least one detectable worm nest and were therefore positive for FDS. The number of worm nests was determined by detecting the typical movement pattern of adult worms in the Pulse Wave Doppler mode using a portable ultrasound machine (SONOSITE 180 Plus; Sonosite, Bothell, USA) equipped with a 7.5 MHZ linear transducer. All ultrasound examinations were performed by Dr. med. Sabine Mand.

Furthermore, examinations of lymph dilation in the scrotal area were conducted according to defined parameters. In brief, dilation of lymphatics and lymphatic vessels at the position of the worm nest and the maximum dilation of a lymphatic vessel (without worms) in the supratesticular area were measured in all participants (n=181). This latter parameter was evaluated using a grading system as follows: stage 0, patients without dilation of the scrotal lymphatics; stage 1, patients with minimal dilation up to 0.2 cm; stage 2, patients with mild dilation of 0.21–0.5 cm; stage 3, moderate dilation of 0.51–1 cm; and stage 4, severe dilation

>1 cm [147]. In addition, patients were also screened for the presence of hydrocele according to the staging system described by Mand *et al* [147].

2.3.2 Isolation of PBMCs

Peripheral blood mononuclear cells from heparinized venous blood were isolated using the ficoll based density gradient separation method [148, 149]. The entire procedure was carried out on ice. In brief, blood was diluted 1:2 with PBS (PAA, Pasching, Austria) and then carefully transferred onto a 50 ml falcon tube pre-filled with 15 ml ficoll. The suspension was centrifuged for 20 minutes at 4°C at 800 x g without brake. Thereafter, the white cell layer containing the leucocytes was gently collected with a 5 ml pipette and transferred into a new 50 ml falcon tube. Cell suspensions were filled up with 40 ml complete medium (Appendix C) and washed for 8 minutes at 400 x g and 4°C to remove residual ficoll. The supernatant was discarded and the washing step repeated. Cells were then resuspended in 10 ml cell culture medium (Appendix C). The isolated PBMCs were either immediately used or cryo-preserved (see section 2.3.4).

During field work in Ghana leucosep tubes (Greiner Bio-one, Frickenhausen, Germany) were used to isolate PBMCs. These tubes were already filled with ficoll and contained a porous barrier. 7 ml of patient blood were poured into the leucosep tubes and centrifuged for 20 minutes, 800 x g at 24 °C. Afterwards, plasma samples were removed from the upper phase of the gradient, first stored at -20°C in 1.8 ml cryo tubes (Nunc, Roskilde, Denmark) and then transferred to liquid nitrogen. Plasma samples were used for Ig measurements described in sections 2.3.11 and 2.3.12. The white cell layer was pipetted into a new 15 ml falcon tube and cells were washed twice with PBS. Afterwards, cells were resuspended in 1 ml of cell culture medium and counted.

2.3.3 Cell viability and counting

The number of living cells was determined using the trypan blue (Sigma-Aldrich, Munich, Germany) exclusion method. In short, a small portion of cells was diluted 1:5 or 1:10 with 0.4% trypan blue. Thereafter, 10 µl of the diluted cells were transferred to a cell counting chamber or haemocytometer (LO Laboroptik GmbH, Bad Homburg, Germany). Living cells (non-coloured) were counted and expressed as cell number per ml. Cells were only used if less than 5% of the cells were dead (blue).

2.3.4 Freezing of isolated cells

Cryo-conservation was performed on cell concentration between 5x 10^6 and 1x 10^8 cells per ml. All steps were fulfilled on ice. Freezing medium (Appendix C) was freshly prepared, pre-cooled on ice and added drop-wise to 1 ml of cells. Thereafter, cell suspensions were mixed

and 2 ml of cell suspensions were quickly transferred to cryo tubes and frozen at -80°C for up to one week and then moved to liquid nitrogen.

2.3.5 Thawing of isolated cells

Again all steps were fulfilled on ice. Cryo tubes with frozen cells were taken from the -80°C or the liquid nitrogen and quickly thawed 2-3 minutes between the palms of both hands. Thawed suspensions were pipetted into a new 15 ml falcon tube and then filled up slowly with 10 ml of pre-cooled complete medium under frequent mixing. Cells were centrifuged for 8 minutes at 400 x g (4°C) and then washed again to remove residual freezing medium, which is toxic for the cells. Thereafter, the supernatant was discarded and cells were resuspended in 1 ml of cell culture medium, counted and used for further experiments.

2.3.6 Magnetic cell sorting

2.3.6.1 Isolation of $CD4^+$T cells

$CD4^+$ T cells were isolated using the positive isolation kit from Invitrogen (Darmstadt, Germany) according to the manufacturer's protocol. In brief, 25 µl of Dynabeads were added to 1x 10^7 PBMCs and washed with 1 ml of buffer 1 (1x PBS/0.1% FCS) using the Dynal MPC magnet (Dynal magnetic particle concentrator). Afterwards, cells were resuspended in 1 ml of buffer 1 and co-incubated with prepared beads for 20 minutes at 4°C with gentle tilting and mixing (Dynal Mixer MX1, Invitrogen GmbH, Darmstadt, Germany). Rosetted cells were then washed three times with buffer 1 and resuspended in 100 µl of buffer 2 (complete RPMI/1% FCS). 10 µl of DETACHaBEADS (Invitrogen (Darmstadt, Germany) were added per 1x 10^7 cells; the suspensions were mixed by inversion and incubated for 45 minutes at RT in the mixer MX1. Tubes containing the suspension of the detached beads and the free $CD4^+$ T cells were then decanted on the magnet (two times) and the solutions containing the $CD4^+$ T cells were collected in a new tube, centrifuged, counted and adjusted to the desired concentration. To analyse the purity of the isolated cells, small fractions were stained before and after isolation with FITC-labelled anti-CD4 antibody. Fluorescence was measured using a FACSCanto I flow cytometer (BD, Heidelberg, Germany) and analysis was performed using the FACS Diva software (see section 2.3.7.1). The purity of the isolation was routinely > 97%.

2.3.6.2 Isolation of $CD19^+$ B cells

$CD19^+$ B cells were isolated using the positive isolation kit from Invitrogen (Darmstadt, Germany). Briefly, 25 µl of specific Dynabeads were placed into a 15 ml tube and washed twice with 1 ml of buffer 1 (1x PBS/0.1% FCS) using the Dynal MPC magnet. Thereafter,

beads were resuspended in the same amount of buffer 1 as the initial volume of Dynabeads. Approximately, 1x 10^7 PBMCs were added to $CD19^+$ Dynabeads and incubated for 20 minutes at 4°C under gentle vortexing using the mixer MX1. The rosetted cells were washed three times with buffer 1 and resuspended in 100 µl of buffer 2 (complete RPMI/1% FCS). Then, 10 µl of CD19 DETACHaBEADS (Invitrogen, Darmstadt, Germany) were added and incubated for 45 minutes at RT under gentle rotation in the mixer. The suspensions containing the detached beads detached beads and the free $CD19^+$ cells were then decanted on the magnet (two times) and the solutions containing the $CD19^+$ cells were collected in a new tube. To analyse the purity of the isolated cells, small fractions were stained before and after isolation with PE-labelled anti-CD19 antibody. Fluorescence was measured using a FACSCanto I flow cytometer and analysis was performed using the FACS Diva software (see section 2.3.7.1). Purity of isolated B cells was routinely >97%.

2.3.6.3 Isolation of $CD14^+$ cells

$CD14^+$ monocytes were isolated by using the CD14 positive isolation kit from Miltenyi (CD14 Microbeads, Miltenyi Biotech GmbH, Bergisch Gladbach, Germany) according to the manufacturer's protocol. In brief, 1x 10^7 PBMCs were resuspended in 80 µl of autoMACS running buffer (Miltenyi, Bergisch Gladbach, Germany). Afterwards, 20 µl of CD14 microbeads were added to the cells, mixed and incubated for 15 minutes inside the refrigerator (2-8°C). Cells were washed with 2 ml of running buffer and centrifuged for 10 minutes at 400 x g (4°C). Supernatants were discarded and labelled cells were resuspended in 500 µl of running buffer. MS columns (MS column, Miltenyi Biotech GmbH, Bergisch Gladbach, Germany) were placed in the magnetic field of a suitable MACS separator (Miltenyi Biotech, Bergisch Gladbach, Germany) and prepared by washing them with 500 µl of running buffer. Thereafter, 500 µl of cell suspensions were applied onto the column, flow-through was collected as $CD14^-$ cells. Columns were washed three times with 500 µl running buffer in each washing step. After the last washing step, column was removed from the separator and placed onto a 15 ml falcon tube. Finally, 1 ml of running buffer was pipetted onto the column and labelled cell fractions were flushed out by firmly pushing the plungers into the columns. Collected $CD14^+$ cells were checked for their purity by flow cytometry. Therefore, small fractions were stained before and after isolation with FITC-labelled anti-CD14 antibody. Fluorescence was measured using a FACSCanto I flow cytometer and analysis was performed using the FACS Diva software (see section 2.3.7.1). Purity of isolated $CD14^+$ cells was routinely >95%.

2.3.7 Flow cytometry

2.3.7.1 Surface markers

In order to stain surface markers, up to 1x 10^6 cells per sample were resuspended in 50 µl FACS buffer and blocked with 2 µl normal rat serum (eBioscience, San Diego, USA) for 15 minutes at 4°C. Cells were stained for 30 minutes with the desired antibody at 4°C, followed by two washing steps with 2 ml FACS buffer. Cells were resuspended in 300 µl fixation buffer 1x PBS/4% PFA (Merck KGAA, Darmstadt, Germany). Cells were analysed using the FACSCanto I flow cytometer (BD, Heidelberg, Germany). At least 10,000 events were acquired for each sample. Data were evaluated with the FACSDiva software (BD, Heidelberg, Germany).

2.3.7.2 Intracellular Staining

Intracellular staining of the transcription factor Foxp3 was performed using a Foxp3 kit (eBioscience, San Diego, USA) according to the manufacturer's protocol. To identify Tregs, 1x 10^5 to 1x10^6 cells were first stained with surface markers CD4 and CD25 as described in section 2.3.7.1. Cells were permeabilized for 30 minutes using 1 ml of 1:4 diluted fixation/permeabilization buffer (provided by the supplier). Afterwards, cells were washed twice with 1:10 diluted permeabilization buffer (provided by the supplier), blocked with 2 µl of normal rat serum for 15 minutes in a maximal volume of 100 µl and then stained with 5 µl of anti-Foxp3 antibody for 30 minutes at 4°C. After two additional washing steps, cells were resuspended in approximately 300 µl fixation buffer and acquired with the FACSCanto flow cytometer. Foxp3 expression of T cells was analysed after gating on $CD4^+CD25^{high}$ cells.

Intracellular staining of the signaling protein pSTAT3 was performed using the Phosflow kit (BD, Heidelberg, Germany) according to the manufacturer's protocol. In brief, cells were stained on their surface (CD4 FITC or CD20 PerCP-Cy5.5) and after an incubation period of maximal one hour they were fixed with the equal amount of pre-warmed BD Cytofix Buffer for 10 minutes at 37°C. Cells were then centrifuged for 8 minutes at 400 x g, the supernatant was discarded and the pellet was incubated for 30 minutes with 1 ml of BD Phosflow Perm Buffer, afterwards washed twice and resuspended in BD Pharmingen Stain Buffer. Subsequently cells were stained with 20 µl of anti-pSTAT3 antibody (Alexa Fluor 647) for 30 minutes on ice and finally washed with 1 ml staining buffer and resuspended in FACS buffer.

2.3.7.3 Sorting of lymphocytes

PBMCs from healthy blood donors were thawed and counted as described in sections 2.3.3 and 2.3.5. Cells were stained with either CD20 PerCP-Cy5.5 or CD4 PE and sorted with the FACSDiva cytometer (BD, Heidelberg, Germany). Sorted T and B cells were used for

subsequent analysis of pSTAT3. Furthermore, cryo-conserved cells from LF infected patients (MF^+ and MF^-) as well as cells from endemic controls were thawed and cell surfaces were stained with anti-CD4 FITC, anti-CD25 PE and anti-CD8 APC according to the protocol described in section 2.3.7.1. $CD4^+CD25^+$, $CD4^+CD25^-$ and $CD8^+$ were sorted using the FACS MoFlo cytometer (Beckman Coulter, Miami, USA). Sorted $CD4^+CD25^+$, $CD4^+CD25^-$ and $CD8^+$ cells of each patient were centrifuged and resuspended in 1 ml Qiazol lysis reagent (Qiagen, Hilden, Germany) and subsequently frozen at -80°C to further isolate mRNA.

2.3.8 *In vitro* experiments with microfilariae

2.3.8.1 Isolation of microfilariae

In order to test MF in human *in vitro* assays, the well established animal model of *L. sigmodontis* was used to gain the worm offspring. Peripheral blood from *L. sigmodontis* infected cotton rats (*S. hispidus)* was passed through a saccharose gradient (Sigma-Aldrich, Munich, Germany) to extract MF. In brief, blood was diluted 1:2 with PBS and carefully loaded onto a 15 ml falcon tube pre-filled with 3 ml of 30% and 25% gradients (maximal volume of diluted blood was 5 ml). The prepared suspensions were centrifuged for 30 minutes without brake at RT at 400 x g. After separation, a white layer between the 25% and 30% gradients was aspirated with a sterile 1 ml pipette and transferred into a new 15 ml falcon tube. Isolated MF were washed twice with RPMI (without supplements) for 8 minutes at 400 x g at 4°C. After the second washing step they were resuspended in 1 ml fresh ice-cold RPMI medium without supplements. MF were counted with the counting chamber and immediately frozen.

2.3.8.2 Freezing and thawing of microfilariae

1 ml of pre-cooled freezing medium containing 6% DMSO and 15%FCS was directly added to 1x 10^6 of freshly isolated MF [150-152] and immediately frozen at -80 °C.

Frozen MF were thawed by warming the cryo tubes between the palms of both hands. Thawed MF-freezing suspensions were quickly added to 14 ml of cold RPMI medium without supplements and then centrifuged at 400 x g for 8 minutes at 4°C. The supernatant was discarded, the pellet resuspended in a further 14 ml of cold medium and washed again. After centrifugation the pellet was resuspended in 1 ml RPMI/10% FCS (without antibiotic supplements). Microfilariae were kept 15-30 minutes at 37°C counted afterwards with the Neubauer chamber. Only living (moving) MF were counted and aliquots were only taken if at least 95% of MF were alive.

2.3.9 Cell culture

For *in vitro* cytokine analysis of PBMCs originated from Ghanaian patients and their appropriate control individuals, 2x 10^5 of total PBMCs/well were plated into a 96-well plate (U-shaped, Greiner Bio-One, Frickenhausen, Germany) in triplicate and cells were either left unstimulated or stimulated with the following stimuli: *O. volvulus* extract (*O.v*. extract, 5 µg/ml, kind gift of Dr. Satoguina and Dr. Büttner), *B. malayi* extract (*B.m*. extract, 5 µg/ml), *B. malayi* female extract (*B.m.* female extract, 5 µg/ml, kind gift of Dr. Taylor), anti-CD3/anti-CD28 (10 µg/ml and 2.5 µg/ml), recombinant full-length *Plasmodium falciparum* merozoite surface protein (MSP-1, 0.25 µg/ml, peptide pool, kindly provided by Prof. Hermann Bujard, ZMBH, University Heidelberg, Germany), 50 ng/ml lipopolysaccharide (LPS, *Serratia marescens*, Sigma L6136, Taufkirchen, Germany) and 10 µg/ml purified protein derivative of Mycobacterium (PPD, Statens Serum Institut, Copenhagen, Denmark). Cells were incubated for 72 hours at 37°C and 5% CO_2. Supernatants from triplicates were pooled, frozen for one day in cryo tubes (Nunc, Roskilde, Denmark) at -20°C and afterwards transferred to liquid nitrogen for long time storage. In order to determine the cytokine release of PBMCs stimulated with *L.s.* extract or MF, 2x 10^5 of PBMCs/well from healthy European blood donors were incubated for 24 hours with 50 µg/ml *L.s.* extract or living MF (10,000 MF/well). Afterwards, cells were additionally stimulated for 72 hours with anti-CD3/anti-CD28 (10 µg/ml and 2.5 µg/ml respectively).

2.3.10 Cytokine ELISA

Cultures supernatants from stimulated PBMCs obtained from infected Ghanaian and their appropriate non-infected control individuals were analysed for the production of IL-4, IL-5, IL-6, IL-10, IL-13, IL-17, IFN-γ, TNF and TGF-β using R&D Duo sets (R&D Systems, Wiesbaden-Nordenstadt, Germany) as indicated by the manufacturer. In brief, ELISA plates (Greiner Bio-One, Germany) were coated with 50 µl capture antibody per well overnight. Plates were washed four times with washing buffer (Appendix C) and then blocked for one hour with blocking buffer (Appendix C). The wash step was repeated and subsequently, plates were incubated for two hours with 50 µl/well supernatants and standards. After a further washing step, plates were incubated for two hours with 50 µl/well of detection antibody. The washing step was repeated and plates were afterwards incubated with 50 µl/well Streptavidin-HRP for 20 minutes in the dark. After a final washing step, 50 µl/well substrate solution containing tetramethylbenzidine (TMB) were added to the plates, 30 minutes later the reaction was stopped with 25 µl/well 2N H_2SO_4 (Merck KGAA, Darmstadt, Germany). All steps were fulfilled at RT. Optical density was measured using the SpectraMAX ELISA reader (Molecular devices, Sunyvale, USA with wavelength correction (450 nm and 570 nm). Data were analysed with SOFTmax Pro 3.0 software.

Supernatants from PBMCs of European donors stimulated with *L.s*. extract and MF each in combination with anti-CD3/anti-CD28 were analysed using eBioscience ELISA kits (Ready-SET-Go, eBioscience, San Diego, USA). These ELISAs were basically performed as mentioned above, but blocking was carried out with 1x assay diluted (provided by the manufacturer) and the incubation time with the secondary antibody was one hour instead two. Incubation with avidin-HRP was performed for 30 minutes.

2.3.11 Cytometric Bead Array

Plasma of participants from the LF study were investigated for their amount of total Ig subclasses (total IgG, IgG1, IgG2, IgG3, IgG4 and IgE) using the Cytometric Bead Assay Flex Set (CBA; Becton Dickinson Heidelberg, Germany). In accordance to the manual, plasma were diluted in complete RPMI (IgG total 1:100,000, IgG1 1:100,000, IgG2-4 1:20,000, IgE 1:2,000) and incubated with their appropriate beads (each diluted in the adequate dilution buffer) for one hour at RT. Afterwards, samples were washed with 500 µl washing buffer for 5 minutes at 400 x g and then incubated for two hours in the dark with their appropriate detection antibody (included in the kit). In the last step, samples were washed again, resuspended in 200 µl washing buffer and acquired. Data were analysed using FCAP-Array software and BD FACSArray Bioanalyzer (BD, Heidelberg, Germany).

2.3.12 Antigen-specific Ig ELISA

Individual plasma samples from Ghanaian patients were analysed with regards to their levels of filarial-specific IgE and IgG1-4. In brief, 96-well polysorb plates (Nunc, Roskilde, Denmark) were coated overnight at 4°C with 50 µl/well of 5 µg/ml *B.m.* extract diluted in PBS at pH 9.6. Plates were washed 3 times in washing buffer (Appendix C) and once in PBS. Plates were blocked with 200 µl/well blocking buffer (Appendix C) for one hour at RT. Following an additional washing step, 50 µl/well of diluted plasma was added in triplicate (1:500 for specific IgG1-4 and 1:20 for specific IgE) and incubated overnight at 4°C. After the next washing step, 50 µl/well of the biotinylated secondary antibodies were added for two hours at RT (IgG1-4, Sigma-Aldrich, Germany, IgG1 1: 1,000, IgG2 1:15,000, IgG3 1:4,000, IgG4 1:15,000; IgE Southern Biotech, USA 1:1,000). Following another washing step, 50 µl/well Streptavidin-HRP (Roche Diagnostics, Mannheim, Germany; 1:5,000) were incubated for 45 minutes at RT. After the last wash, 50 µl/well substrate solution containing TMB were added to the wells for 15 minutes and thereafter reaction was stopped with 25 µl/well 2N H_2SO_4 (Merck KGAA, Darmstadt, Germany). Optical density was measured as mentioned before in section 2.3.10. Pooled plasma samples from 10 patients were used for the generation of calibration curves and assigned in arbitrary units (AU) for the specific anti-filarial antibodies.

In plasma samples from healthy European donors filarial IgG1-4 and IgE were not detectable.

2.3.13 Measurement of VEGFs

In order to analyze VEGF-A and VEGF-C, Quantikine Kits from R&D (R&D Systems, Wiesbaden-Nordenstadt, Germany) were used according to the manufacturer's protocol. Briefly, pre-coated plates were incubated for two hours with indicated standards and undiluted plasma of *W. bancrofti* infected patients at RT. After four washing steps, plates were incubated for further two hours with 200 µl conjugate per well. Subsequently, plates were washed again four times and 200 µl of substrate were added. Reactions were stopped with 50 µl stop solution and plates were read using the SpectraMAX ELISA reader (Molecular devices, Sunyvale, USA with wavelength correction (450 nm and 570 nm). Data were analysed with SOFTmax Pro 3.0 software.

2.3.14 Analysis of sVEGFR3

Individual plasma samples of Ghanaian patients were analysed for their levels of soluble VEGF receptor 3 using R&D Duo sets (R&D Systems, Wiesbaden-Nordenstadt, Germany). Procedure was performed as indicated by the manufacturer and described in section 2.3.10. Plasma samples were diluted 1:5 in 1% BSA in PBS.

2.3.15 Intervention/treatment of lymphatic filariasis patients

All *W. bancrofti* patients included in the randomized, double-blind, placebo-controlled trial were treated with one of the following treatment regimens:

Treatment 1: 4 weeks doxycycline 200 mg
Treatment 2: 5 weeks doxycycline 100 mg
Treatment 3: 4 weeks doxycycline 100 mg
Treatment 4: 3 weeks doxycycline 200 mg/rifampicin (10 mg/kg body weight)
Treatment 5: 2 weeks doxycycline 200 mg/rifampicin (10 mg/kg body weight)
Treatment 6: 10 days doxycycline 200 mg/rifampicin (10 mg/kg body weight)
Treatment 7: placebo

All patients received the same amount of capsules per day which were depending on the treatment arm replaced by placebo capsules. 4 months after finishing the treatment, all patients received MDA (IVM/ALB).

2.3.16 Stimulation of cells for Western blot analysis

Indicated numbers of cells were stimulated with recombinant human IL-10 (R&D Systems, Wiesbaden-Nordenstadt, Germany) for one hour at 37°C and 5% CO_2 in a 12-well plate. In

some experiments PBMCs or $CD4^+$ T cells were additionally pre-incubated for 24 hours with anti-GITR (2-20 μg/ml) or anti-GITR-L (15 μg/ml) antibody (R&D Systems, Wiesbaden, Germany) before recombinant IL-10 was added.

2.3.17 Lysis of cells

All steps were fulfilled on ice. After the incubation with the appropriate stimulus, cells were harvested and centrifuged at 400 x g for 8 minutes at 4°C. The supernatant was discarded and the pellet was resuspended in 50 μl RIPA lysis buffer supplemented with phenylmethanesulfonyl fluoride (PMSF), protease inhibitors and sodium orthovanadate (Santa Cruz Biotechnology, Inc., Heidelberg, Germany). Cells were incubated for 30 minutes on ice and passed several times through a 21G needle (Becton Dickinson Heidelberg, Germany). Lysates were then incubated for additional 30 minutes on ice. Afterwards, all samples were centrifuged for 10 minutes at 10,000 x g at 4°C. The supernatant was transferred into new tubes and stored at -20°C until required.

If SDS gel electrophoresis was performed (see following section) equal amounts of cell lysates and 5x loading dye (Appendix C) were mixed and incubated for 5 minutes at 95°C. Finally, suspensions were centrifuged for 10 minutes at 10,000 x g at RT.

2.3.18 Sodium dodecyl sulfate polyacrylamide gel electrophoresis (SDS-PAGE)

SDS-PAGE gel electrophoresis was performed in accordance with Laemmli *et al* [153]. All equipment required for gel electrophoresis was purchased from Bio-Rad (Munich, Germany). Clean glass plates were coupled together with 1.5 mm spacers. A 7% resolving gel solution (Appendix C) was prepared and poured into the apparatus. Whilst the gel was setting, a layer of 10% isopropanol was added. After 20 minutes, isopropanol was discarded and the stacking gel solution (Appendix C) was loaded. Combs of appropriate size and numbers were inserted into the stacking gel layer which was then left to set for 30 minutes. After carefully removing the combs, the gels were assembled into a running tank. Running buffer (Appendix C) was added and the samples and protein markers (MagicMark, Invitrogen, and Darmstadt, Germany) were loaded. The level of the running buffer solution was maintained to ensure good connection between the gels and electrodes. Samples were separated by vertical electrophoresis at 100 V for 15 minutes and then the voltage was increased up to 150 V for approximately 30 minutes.

2.3.19 Western blot

After separating proteins as described above, gels were first soaked in distilled water for 5 minutes. Meanwhile the nitrocellulose membrane (Sigma-Aldrich, Munich, Germany) was saturated for 15 seconds with methanol. Both gel and membrane were soaked twice for 5

minutes in protein transfer buffer (Appendix C). The separated proteins were transferred onto the nitrocellulose paper using the SD semi-dry electrophoretic transfer cell (Bio-Rad, Munich Germany). The membrane, the gel and two blotting papers were stacked and the protein transfer was carried out at 0.8 mA/cm^2 for one hour. The nitrocellulose membranes were afterwards blocked in Roti-Block (Carl Roth, Karlsruhe, Germany) for one hour followed by three washing steps 10 minutes each with the appropriate wash buffer (Appendix C). The membrane was then shrink-wrapped in wrapping film (Staples Advantage, Cologne, Germany) to reduce the amount of used antibody and incubated overnight with the primary antibody (anti-STAT3, anti-pSTAT3 or anti-biotin antibody, all Santa Cruz Biotechnology, Inc., Heidelberg, Germany) on a rocker (Bio-Rad Munich, Germany), each appropriately diluted in 1x Roti-Block. After three 10 minute washes with wash buffer, the membrane was shrink-wrapped again and the appropriate species specific alkaline phosphatase (AP)-labelled secondary antibodies (DAKO, Hamburg, Germany) were added at a dilution of 1:750 and incubated for 90 minutes at RT. After further washings the membranes were placed, in the correct orientation, inside plastic coverings and Immun-Star AP substrate (Bio-Rad, Munich, Germany) reagent was added for two minutes. After different periods of exposure time to Kodak films (Kodak, Stuttgart, Germany), the films were developed manually. In brief, films were soaked for two minutes in developer solution (Kodak, Stuttgart, Germany) followed by a two minutes washing step with water. Thereafter, films were incubated for two minutes with fixer solution and finally washed again with water for two minutes. Films were scanned (Microtek, Willich, Germany) and blots were analysed with the fiji software.

2.3.20 Extraction of RNA

RNA of sorted cells from patients and controls of the LF study was extracted using the miRNeasy Kit from Qiagen (Qiagen, Hilden, Germany) according to the manufacturer's protocol. In brief, samples (each 1 ml) were thawed at RT and 200 µl of chloroform (Sigma-Aldrich GmbH, Munich, Germany) were added. Tubes were shaken for 15 seconds and then placed for further 3 minutes at RT. Thereafter, samples were centrifuged for 15 minutes at 1,000 x g (4°C) and the upper aqueous phase was transferred to a new collection tube. 600 µl of ethanol (Merck KGAA, Darmstadt, Germany) were added to each sample, probes were pipetted into RNeasy Mini columns and centrifuged at 8,000 x g for 30 seconds at RT. 700 µl of RWT buffer were added, samples were centrifuged for 30 seconds at RT at 8,000 x g. Flow through was discarded and the wash steps were repeated with 500 µl of buffer RWT. Then, 500 µl of buffer RPE were pipetted to the columns and samples were centrifuged for two minutes at 8,000 x g at RT. Finally columns were centrifuged at 14,000 x g for 1 minute to get rid of residual fluid. Columns were placed on new labelled tubes and RNA was eluted

with 50 µl of RNase-free water (Qiagen, Hilden, Germany) by centrifugation at 8,000 x g for one minute.

2.3.21 Measurement of RNA concentration

Concentration of RNA was first determined using the NanoDrop1000 (Peqlab, Erlangen, Germany) by measuring 1 µl of extracted RNA and afterwards RNA was re-measured because of low concentration with the more sensitive Agilent RNA 6000 Pico Kit (Agilent Technologies, Waldbronn, Germany). For the latter application, 2 µl of each sample were heat denatured for two minutes at 70°C. In-between the gel matrix was prepared according to the manufacturer's protocol. In brief, 550 µl RNA gel matrix were pipetted into a spin filter and centrifuged at 1,500 x g for 10 minutes at RT. 1 µl of a dye concentrate was transferred to 65 µl of the gel matrix and vortexed for 10 seconds. Thereafter, the gel was centrifuged for 10 minutes at 13,000 x g at RT. 9 µl of the prepared gel-dye mix was loaded onto the chip in the marked position and the chip was primed with the appropriate plunger. In addition, 9 µl of a conditioning solution and two times 9 µl of gel-dye mix were transferred to the marked positions. 5 µl of the Pico marker were pipetted into every well and finally, 1 µl of each sample and 1 µl of the ladder were loaded onto the chip. The chip was vortexed (Agilent Technologies, Waldbronn, Germany) for one minute at 2400 rpm and then measured with the Agilent 2100 bioanalyzer.

2.3.22 RNA amplification

Extracted RNA was further amplified using the TargetAmp 2-Round biotin-aRNA Amplification Kit 3.0 (Epicentre Biotechnologies, Madison, USA) according to the manufacturer's protocol. In brief, 500 pg of poly(A) RNA were first transcribed into first strand cDNA using a T7-oligo(dt) primer. Therefore, 1 µl of the T7-oligo(dt) primer was added to 2 µl of RNA and incubated for 5 minutes at 65°C in a thermocycler. Afterwards, reaction was chilled on ice for one minute and then centrifuged. The master mix for the first strand cDNA synthesis was prepared, which consists of 1.25 µl reverse transcription preMix, 0.25 µl RNase inhibitor, 0.25 µl dithiothreitol (DTT) and 0.25 µl SuperScript III reverse transcriptase (200 U/ml, Invitrogen GmbH, Darmstadt, Germany). 2 µl of this master mix were added to each reaction, gently mixed and incubated for 30 minutes at 50°C in a thermocycler (Biometra GmbH, Göttingen, Germany). Afterwards, the second strand cDNA synthesis was performed by adding 5 µl of ice cold master mix (composed of 4.5 µl TargetAmp DNA polymerase preMix1, 0.5 µl TargetAmp DNA polymerase) to each sample. Reactions were gently mixed and then first incubated for 10 minutes at 65°C in the thermocycler followed by an incubation step at 80°C for 3 minutes. After a short centrifugation step (5,000 x g, 10

seconds), 1 µl of TargetAmp cDNA finishing solution was added to each reaction and incubated for 10 minutes at 37°C followed by an incubation step of 3 minutes at 80 °C (both steps were performed in the thermocycler). Reactions were chilled on ice before starting with the *in vitro* transcription. Therefore, all used components were warmed to RT and then the master mix was prepared (4 µl of TargetAmp T7 transcription buffer 1, 27 µl NTP preMix 1, 4 µl DTT, and 4 µl TargetAmp T7 polymerase). 39 µl of the master mix were added to each sample and incubated for 4 hours at 42°C in the thermocycler. Subsequently, 2 µl of RNase-free DNase I were added to each reaction and incubated for 15 minutes at 37°C followed by the RNA purification step using the RNA Clean & Concentrator™-5 Kit (Zymo Research Cooperation, Irvine, USA) according to the manufacturer's protocol (see section 2.3.23). Afterwards 2 µl of TargetAmp random primers were added to the purified RNA, which was eluted in 8 µl of RNase-free water and incubated for 5 minutes at 65°C in the thermocycler. Samples were chilled on ice for one minute followed by a brief centrifugation (5000 x g, 10 seconds). Meanwhile the master mix for the second round of first strand cDNA synthesis was prepared (1.5 µl TargetAmp reverse transcription preMix, 0.25 µl DTT and 0.25 µl SuperScript II reverse transcriptase). 2 µl of this master mix were added to each sample and after gently mixing, reactions were incubated for 10 minutes at RT followed by an incubation of one hour at 37°C in the thermocycler. 0.5 µl of TargetAmp RNase H were added to each samples and incubated for further 20 minutes at 37°C in the thermocycler followed by an incubation step of 2 minutes at 95°C. Samples were chilled on ice for one minute and then the second round of second-strand cDNA synthesis was performed by adding 1 µl of the TargetAmp T7-oligo(dt) primer 2. Reactions were gently mixed and incubated for 5 minutes at 70°C and then for 10 minutes at 42°C in the thermocycler. Samples were briefly centrifuged and in-between the second-strand cDNA synthesis master mix was prepared (13 µl TargetAmp DNA polymerase PreMix 2, 0.5 µl TargetAmp DNA polymerase 2). 13.5 µl of this master mix were added to each sample, incubated for 10 minutes at 37°C and then for 3 minutes at 80°C in the thermocycler. Samples were briefly centrifuged and the *in vitro* transcription of biotin-aRNA was performed. Therefore, the master mix was prepared (7.5 µl TargetAmp T7 transcription buffer 2, 4.5 µl biotin-UTP, 20 µl NTP PreMix2, 4 µl DTT and 4 µl TargetAmp T7 RNA polymerase) at RT and 40 µl of this master mix were added to each reaction followed by an incubation step of 9 hours at 42°C in the thermocycler. Subsequently, 2 µl of RNase-free DNase I were added to each reaction and the samples were incubated for 15 minutes at 37°C. Afterwards, the biotin-aRNA was purified (see section 2.3.24) and the concentration of biotin-aRNA was determined finally, by measuring the OD with the NanoDrop (see section 2.3.21).

2.3.23 RNA purification I

In order to clean and purify the RNA before performing the second first-strand DNA synthesis, the RNA Clean and Concentrator-5 Kit (Zymo Research Cooperation, Irvine, USA) was used according to the manufacturer' s protocol. In brief, 2 volumes of RNA Binding Buffer were added to each volume of RNA sample. Afterwards, 1 volume ethanol (100%) was added to the mixture from step 1 and mixed well. The mixture from the second step was transferred to the Zymo-Spin IC column in a collection tube and centrifuged at 12,000 x g for 1 minute. Flow-through was discarded and 400 µl of RNA Prep Buffer were added to the column and centrifuged at 12,000 x g for 1 minute. Flow-through was discarded again and 800 µl of RNA wash buffer were added to the column and centrifuged at 12,000 x g for 30 seconds. Flow-through was discarded another time and the wash step repeated with 400 µl RNA wash buffer. The Zymo-Spin IC column was centrifuged in an emptied collection tube at 12,000 x g for 2 minutes and the Zymo-Spin IC column was carefully removed from the collection tube and transferred into an RNase-free tube. Finally, 8 µl (as recommended in the TargetAmp 2-Round biotin-aRNA Amplification Kit) of DNase/RNase-free water were added directly to the column matrix and incubate for one minute at RT. The reaction was centrifuged at 10,000 x g for 30 seconds and the eluted RNA was used for further application.

2.3.24 RNA purification II

In order to purify the biotin-aRNA, the Qiagen RNeasy MiniElute Cleanup kit (Qiagen, Hilden, Germany) was utilized. Therefore, RLT/β-ME solution was prepared by combining 1 ml of RLT buffer with 10 µl of β-mercaptoethanol. 350 µl of this buffer in combination with 38 µl of RNase-free water and 250 µl 100% ethanol were added to each reaction. Samples were applied to the purification kit's spin columns and centrifuged for 15 seconds at 8,000 x g. Flow-through was discarded and 700 µl of RPE solution were applied onto the columns. Centrifugation was repeated for 2 minutes. Flow-through was discarded once more and the spin columns were transferred to a new collection tube and centrifuged at 16,000 x g for one minute. Afterwards the RNA was eluted by applying 20 µl of RNase-free water followed by 2 minutes incubation and centrifugation at 16,000 x g for one minute. The elution step was repeated under the same conditions.

2.3.25 Quality control of amplified cRNA

A polymerase chain reaction (PCR) was performed in order to control the bands of the housekeeping gene β-actin in the amplified RNA. Therfore, 300 ng of cRNA were transcribed with SuperScript III Reverse Transcriptase (200 U/ml, Invitrogen GmbH, Darmstadt, Germany) into cDNA. 300 ng of amplified RNA in a total volume of 11 µl were added to 1 µl

of random decamer primers (50 μM, Ambion, Darmstadt, Germany) and 1 μl of dNTP Mix (10 mM each dATP, dGTP, dCTP, dTTP at neutral pH; Invitrogen GmbH, Darmstadt, Germany). The mixture was incubated for 5 minutes at 65°C following by incubation for one minute on ice. Afterwards, 7 μl of a master mix consisting of 4 μl 5x First-Strand Buffer, 1 μl 0.1 M DTT, 1 μl RNaseOUT recombinant RNase Inhibitor (all Invitrogen GmbH, Darmstadt, Germany) and 1 μl of the SuperScript III RT were added to each sample. The reactions were mixed gently and then incubated for 5 minutes at 25°C. Subsequently, samples were incubated for 45 minutes at 50°C and afterwards for 15 minutes at 70°C in a thermocycler.

The transcribed cDNA was further used in a multiplex PCR in order to amplify two fragments of the β-actin gene, one is localized in the 5' region and one in the 3' region (primer sequence: see Appendix D). Therefore, 12.5 μl of the master mix consisting of 3 μl 10x buffer, 4.5 μl $MgCL_2$ (both Sigma-Aldrich, Munich, Germany), 0.7 μl dNTPs (Invitrogen GmbH, Darmstadt, Germany), 4 μl primer and 0.3 μl Taq polymerase (Sigma-Aldrich, Munich, Germany) for each reaction were added to 17.5 μl of cDNA (2 μl DNA diluted in 15.5 μl RNase-free water). β-actin amplification was performed under the following conditions: initial denaturation at 95°C for 10 minutes, 18 cycles of 95°C for 30 seconds, 58°C for 45 seconds and 72°C for 45 seconds followed by 15 cycles of 95°C for 30 seconds, 40°C for 45 seconds and 72°C for 45 seconds. Subsequently, a final extension of 72°C for 5 minutes was performed. Afterwards, a 1% agarose gel was prepared by dissolving 0.5 g of agarose (Fermentas, St. Leon-Rot, Germany) in 50 ml of tris/borate/EDTA (TBE) buffer (Biomol GmbH, Hamburg, Germany) and 2.5 μl of Redsafe (HISS Diagnostics GmbH, Freiburg, Germany). Afterwards, the solution was heated in a microwave and then poured to an appropriate gel chamber. 10 μl of the PCR product were mixed with 2 μl 6x DNA loading dye (NEW ENGLAND BioLabs, Frankfurt, Germany) and applied into the slots of the gel. The molecular weight was standardized with a DNA molecular weight marker (Quick load 100 bp DNA ladder, NEW ENGLAND BioLabs, Frankfurt, Germany) run on the same gel. Electrophoresis was performed at 150 V for 40 minutes in TBE buffer. Visualization of the two β-actin bands was performed using the BioDocAnalyze digital gel documentation device (Biometra GmbH, Göttingen, Germany). Furthermore the quality of the amplified RNA was monitored with the Agilent RNA 6000 Pico Kit (Agilent Technologies, Waldbronn) as mentioned in section 2.3.21.

2.3.26 Microarray

Microarrays were performed in collaboration with the LIMES institute in Bonn using the Illumina Whole-Genome Gene Expression Direct Hybridization Assay system kit (Direct Hybridization Assay, Illumina Inc., San Diego, USA) according to the manufacturer's protocol. In brief, 750 ng of each sample were prepared for the hybridization by pre-heating

the cRNA for 5 minutes at 65°C, followed by vortexing and pulsed centrifugation step at 250 x g. RNase free water was used to resuspend each sample in a total volume of 5 μl and afterwards 10 μl of the hybridization buffer were added to each sample. The chamber gasket was placed into the hybridization chamber and 200 μl of the humidity control buffer were added into the eight humidifying buffer reservoirs in the hybridization chamber. 15 μl of the DNA sample were pipetted onto the centre of each inlet port and the sample loaded BeadChips were placed into each hybridization chamber which were then put into the Illumina hybridization oven at 58°C for 14-20 hours. BeadChips were washed with diluted E1BC wash buffer inside a beaker. The cover seal from the BeadChip was removed under the buffer and the BeadChip were transferred to a slide rack submerged containing 250 ml wash solution and subsequently placed into the Hybex water bath containing high-temperature wash buffer where they were incubated for 10 minutes. After this incubation time slide racks were transferred to a staining dish containing 250 ml of fresh wash buffer. The staining dish was put on an orbital shaker and shaked at RT for 5 minutes followed by a wash step in 100% ethanol under the same conditions. Furthermore the BeadChips were washed at RT for 2 minutes in fresh wash buffer followed by incubation with 4 ml of block buffer for 10 minutes on a rocker mixer. Finally, BeadChips were washed with distilled water before they were incubated with 2 ml Cy3-Straptavidin (diluted 1:1,000) for 10 minutes on a rocker mixer. Afterwards, BeadChips were washed 5 minutes with wash buffer at room RT and then centrifuged for 4 minutes at 1,400 rpm in order to dry the BeadChips before they were scanned with the HiScan SQ (Illumina Inc., San Diego, USA).

2.3.27 Statistical analysis

Statistics were performed using PRISM 5 programme (GraphPad Software, Inc., La Jolla, USA), SPSS 19 programme (SPSS Schweiz Ag, Zurich, Switzerland) and SAS version 9.2 (SAS Institute Inc. Cary, NC, USA). Statistical significances between different groups were tested with ANOVA and in case of significance followed by t-test in case of Gaussian distribution. If values were non parametric, significance was first analysed with the Kruskal-Wallis followed by the Mann-Whitney test. P values of 0.05 or less were considered significant. Where indicated the Cochran-Armitage test was used to determine a trend. Cytokine and Ig data were assessed using a generalized linear model analysis using age as a covariate where indicated.

Raw data analysis for Illumina BeadChips was conducted using Illumina BeadStudio software version 3.1.3.0. All data analysis was performed using R statistical language and packages from the Bioconductor project and IlliminaGUI as described in Debey-Pascher et al [154].

3. Results

This chapter is divided into four main segments and the first section deals with different findings obtained from immunological aspects of *O. volvulus* infected patients. An immune parameter which is consistently associated with onchocerciasis infections is IL-10, especially with regards to the induction of IgG4. Therefore, the second part describes *in vitro* experiments concerning the signaling pathways of IL-10. Interestingly, the critical source of IL-10 in filariasis is not limited to regulatory cells but also effector T cells produce this immunosuppressive cytokine [155]. To elucidate dominant cytokine and Ig production, immune profiling was also performed in a large cohort of patent and latent LF infected individuals that did not suffer from lymphedema. Within this study cohort, the effect of antibiotic treatment on immune responses was also assessed. Finally, to gain greater insight into the T cell subsets of LF patients gene expression profiles of Tregs, $CD4^+$ and $CD8^+$ T cells were investigated.

3.1 Onchocerciasis

In the present study clinical parameters and immunological profiles were investigated in a cohort of 467 infected individuals and 14 EN from the Central region of Ghana. Participants were part of a clinical study that was conducted in order to improve current drug therapy. Since adult *O. volvulus* filariae form characteristic nodules in the subcutaneous tissue of their hosts [3] patients were recruited to the study if they harbored at least one palpable nodule. To substantiate the field studies, volunteers residing in the same villages (EN) also took part and were free of palpable nodules and skin MF. The focus of the work described here is an analysis of immunological profiles of the individuals before treatment. The analysis of nodules and nodule sites was essential for the study since these two parameters were monitored following treatment to test the efficacy of the applied drugs and moreover, to determine the extent of *Wolbachia* death within surgically removed nodules. These data are not included in this thesis since the studies are still ongoing.

3.1.1 Clinical evaluation of *Onchocerca volvulus* infected patients

Infected individuals of the study cohort were palpated as described in section 2.3.1.1. Thereafter, patients were subdivided into microfilariae positive (MF^+, n=384) and microfilariae negative (MF^-, n=83) individuals according to the presence of MF observed in skin snips as described in section 2.3.1.3. Table 3.1 depicts the characteristics of the study population. Within both infection groups percentages of male and female participants were similar (MF^+: 76.82% males and 23.18% females; MF^-: 71.08% males and 28.92% females). Levels of MF

	MF^+ (n=384)	MF^- (n= 83)	EN (n=14)
age (mean and range)	37.34 (18-55)	39.34 (19-55)	n.d.
number of nodules (mean)	4.07	3.01	0.00
number of sites (mean)	2.35	1.82	0.00
rounds of IVM (mean)	1.17	1.97	n.d.
MF/mg of skin (mean and range)	26.08 (0.06-330.81)	0.00	0.00

Table 3.1. Characteristics of the study population.

differed greatly between patent individuals which is not an unusual phenomenon. It was also determined whether MF influenced any clinical manifestation during infection. Thus, carriers and non-carriers of worm offspring were compared concerning their nodule and site burden, the latter one defined as the position of palpable nodules. Both parameters reflect the amount and tissue distribution of adult worms. The number of sites (figure 3.1A) and the number of palpable nodules (figure 3.1B) were compared in both infected groups. In addition, the rounds of ivermectin treatment were documented and evaluated, since these drugs are given annually as part of the mass drug administration (figure 3.1C). As shown in figure 3.1A patent infected participants harboured significantly more sites in comparison to MF^- infected individuals and in addition the former group also had significantly more nodules (figure 3.1B). Moreover, MF^- individuals were characterized by a significant numerous intake of IVM (figure 3.1C).

3.1.2 MF loads correlate with the number of sites, nodules and rounds of ivermectin

Since there were significant differences between patent and MF^- infected individuals concerning their clinical parameters, we addressed whether the amount of MF correlated with the number of sites, the amount of nodules or the rounds of IVM intake. Indeed, despite low correlation coefficients there were significant positive correlations between MF load and the number of sites (figure 3.2A) and also with the number of nodules (figure 3.2B).

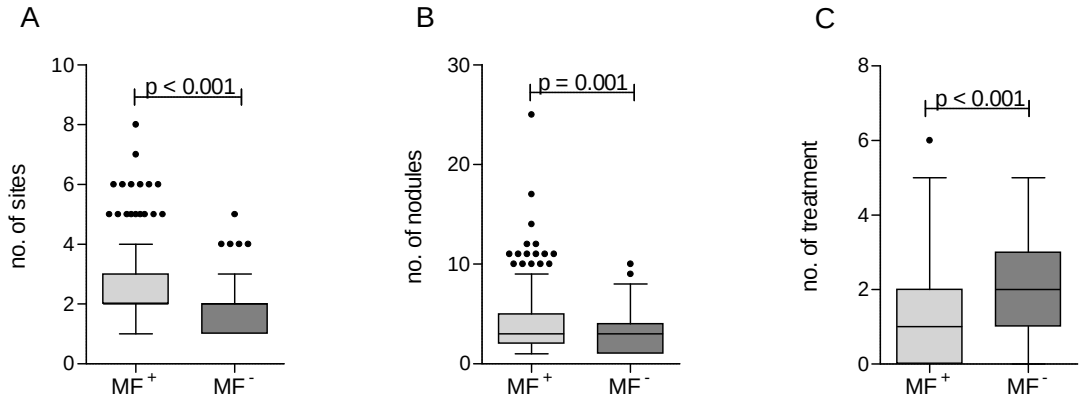

Figure 3.1. MF^+ patients have more worms than MF^- individuals. Infected individuals were examined for (A) the number of sites and (B) the number of nodules by palpation. In addition, participants were also analysed for (C) rounds of IVM intake. Graphs show box whiskers with median, interquartile ranges and outliers. Statistical significances between the indicated groups were obtained after Mann-Whitney tests and significant differences are indicated in the figures.

In contrast, the amount of MF was negatively correlated with the number of previous IVM treatments which is shown in figure 3.2C. If the rounds of IVM intake of all infected patients were correlated with both pathological outcomes, there was only a weak negative correlation between the drug intake and the number of sites (r= -0.096, p= 0.048, data not shown).

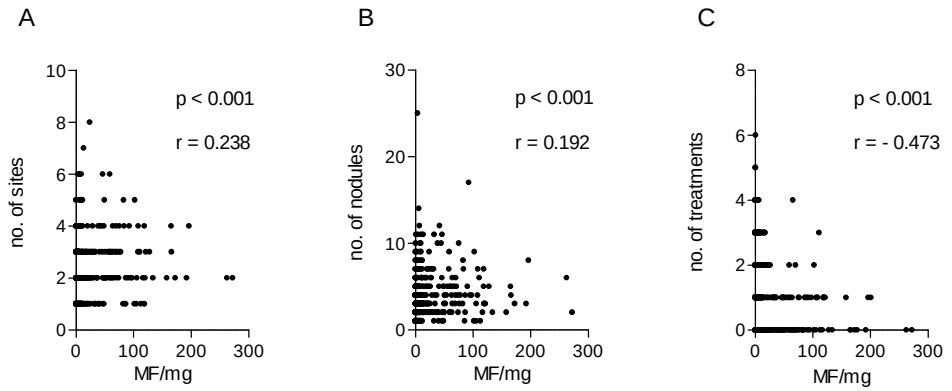

Figure 3.2. Amount of MF correlates with clinical outcome. Microfilarial load was correlated to (A) the number of sites, (B) the number of nodules and (C) the number of IVM treatments. Analysis was performed using the Spearman correlation test. Correlation coefficients r and p values are shown.

3.1.3 Decreased antigen-specific IL-5 secretion in MF^+ patients

Helminth infections and in accordance the presentation of their antigens are associated with inducing Th2 responses which are detected by cytokines like IL-5 and IL-13 [20]. Therefore, PBMCs from MF^+ and MF^- infected individuals and also from EN were monitored for their release of IL-5 (figure 3.3) and IL-13 (figure 3.4) following restimulation with various antigens (*O.v*. extract, anti-CD3/anti-CD28, *B.m*. female extract, MSP-1, LPS and PPD). PBMCs were stimulated with both specific *O.v.* extract and *B.m.* female extract as well in order to see if these different filarial extracts induce similar cytokine profiles because of conserved structures. Numbers in brackets below the graphs indicate how many patients from each group were stimulated with each stimulus. Numbers of patients stimulated with *O.v.* extract are lower than numbers for other applied stimuli since three different batches of *O.v.* extract were used during the study. Therefore, only results for one batch of *O. v.* extract are depicted and correspond to the results obtained when using the batch for the uninfected controls. Infected individuals produced significantly more IL-5 when compared to EN if their PBMCs were stimulated with antigen-specific *O.v.* extract (figure 3.3A), the related *B.m.* female extract (figure 3.3C) and the T-cell stimulus anti-CD3/anti-CD28 (figure 3.3B). In addition, PBMCs from patently infected people secreted significantly less IL-5 than MF^- infected persons after stimulation with either helminth extracts whereas similar levels of IL-5 secretion were obtained after stimulation with anti-CD3/anti-CD28 (figure 3.3B). There were no significant differences between the three groups concerning their IL-5 release after

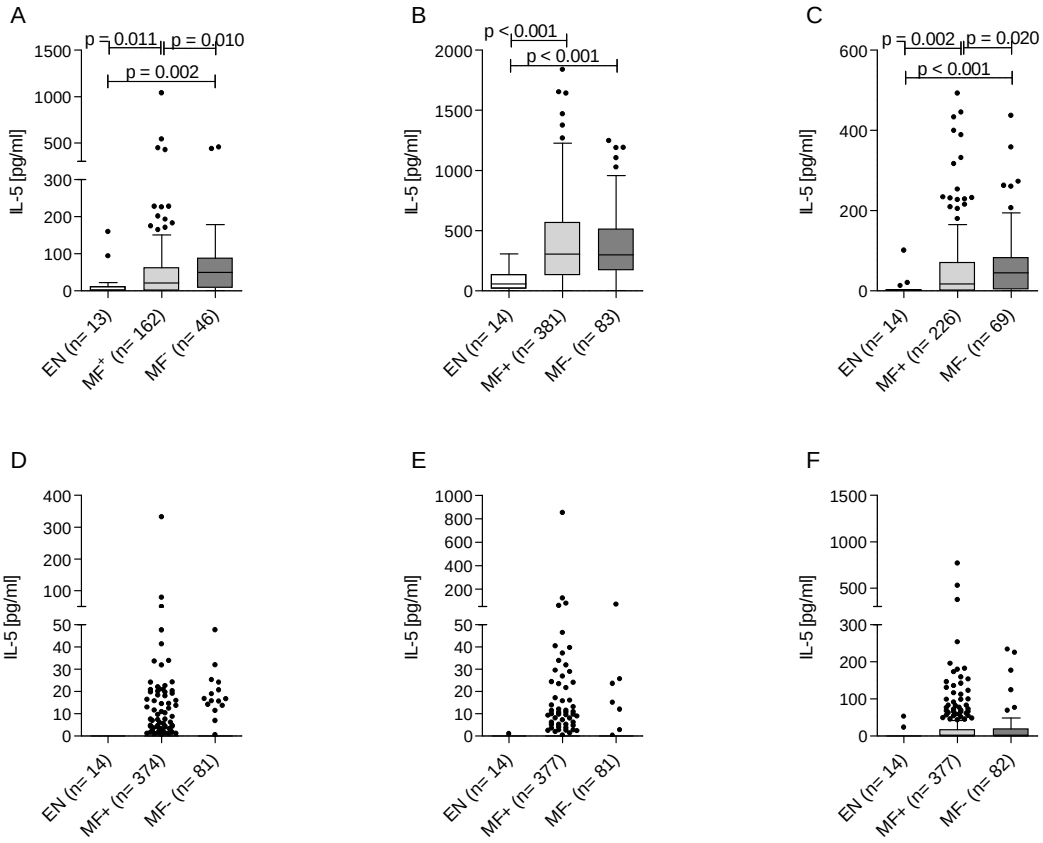

Figure 3.3 Decreased IL-5 productions in patent individuals following filarial-specific stimulation. Isolated PBMCs (2x 10^5/well) from EN or *O.v*. infected MF^+ or MF^- patients were stimulated with either (A) *O.v*. extract (5 μg/ml), (B) anti-CD3/anti-CD28 (10 μg/ml; 2.5 μg/ml), (C) *B.m*. female extract (5 μg/ml), (D) MSP-1 (0.25 μg/ml), (E) LPS (50 ng/ml) or (F) PPD (10 μg/ml) for 72 hours. Thereafter, levels of IL-5 were measured in the culture supernatants via ELISA. Graphs show box whiskers with median, interquartile ranges and outliers after background subtraction. Statistical significances between the indicated groups were obtained after Kruskal-Wallis and Mann-Whitney tests. Numbers in brackets on the x axis legend indicate the amount of stimulated patients within each group.

stimulation with MSP-1 (figure 3.3D), LPS (figure 3.3E) or PPD (figure 3.3F). Percentages of patent and MF^- individuals responding to these stimuli were comparable (MSP-1: 17.9% MF^+ versus 18.5% MF^-; LPS: 14.0% MF^+ versus 8.6% MF^-; PPD: 41.1% MF^+ versus 42.6% MF^-). Figure 3.4 shows the results obtained upon measurement of IL-13. Significant differences were observed following anti-CD3/anti-CD28 stimulation between the infected individuals compared to endemic controls. More precisely, infected individuals produced more IL-13 than the control group but within the infected group there was no significant disparity (figure 3.4B). Additionally, percentages of patients reacting to this stimulation were similar (85.0% MF^+ versus 84.3% MF^-). Antigen-specific stimulation with *O.v.* extract resulted in higher percentages of infected individuals producing IL-13 compared to EN (30.8% EN versus 85.0% MF^+ versus 84.3% MF^-) but there were no significant differences between the worm infected groups. All other applied stimuli did not result in any significant differences in IL-13 secretion and percentages of patients responding to the applied stimuli were also comparable (data not shown).

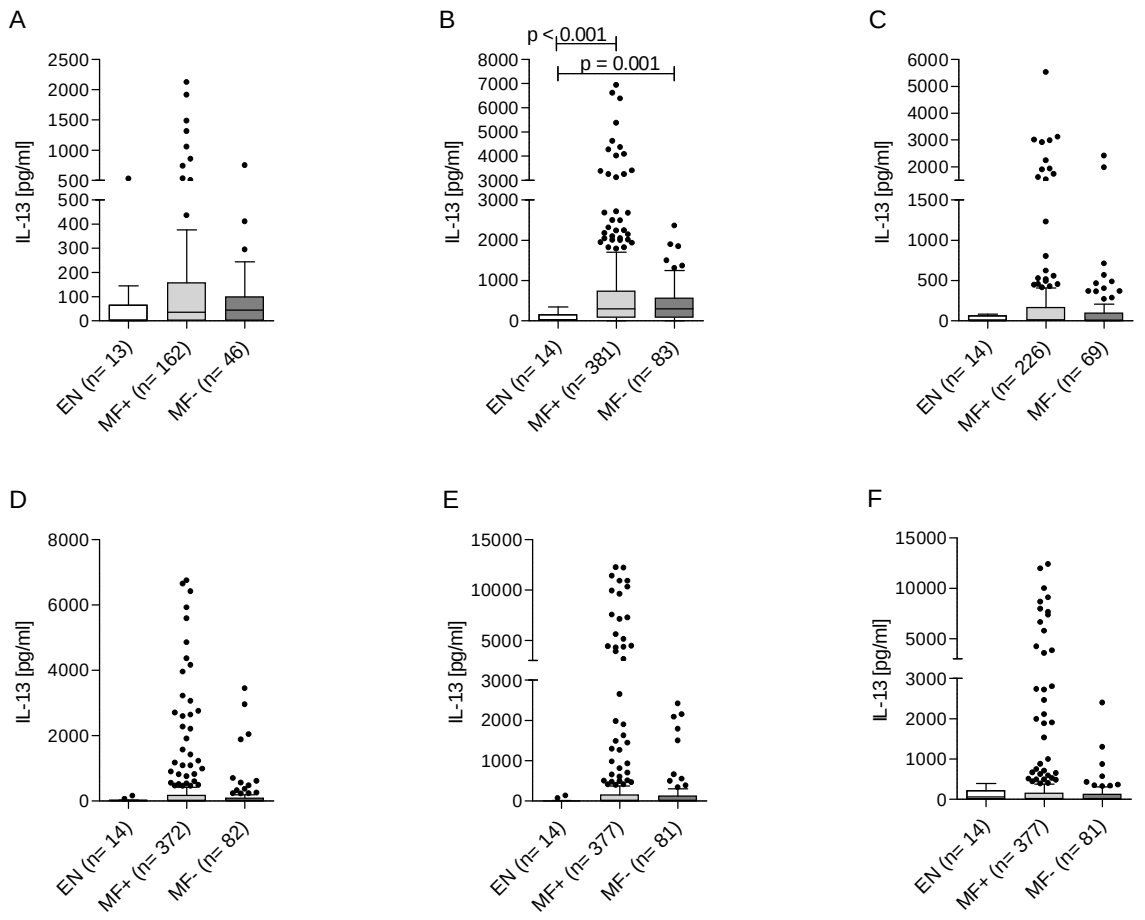

Figure 3.4. Infected individuals secrete higher levels of IL-13. Isolated PBMCs (2x 10^5/well) from EN or *O.v*. infected MF^+ or MF^- patients were stimulated with either (A) *O.v*. extract (5 μg/ml), (B) anti-CD3/anti-CD28 (10 μg/ml; 2.5 μg/ml), (C) *B.m*. female extract (5 μg/ml), (D) MSP-1 (0.25 μg/ml), (E) LPS (50 ng/ml) or (F) PPD (10 μg/ml) for 72 hours. Thereafter, levels of IL-13 were measured in the culture supernatants via ELISA. Graphs show box whiskers with median, interquartile ranges and outliers after background subtraction. Statistical significances between the indicated groups were obtained after Kruskal-Wallis and Mann-Whitney tests. Numbers in brackets on the x axis legend indicate the amount of stimulated patients within each group.

3.1.4 Increased antigen-specific IL-10 production in patent infected individuals

IL-10 is one of the most prominent cytokines in helminthic infections as it is associated with the suppression of pro-inflammatory immune responses and found to be increased in patients with the generalized form of onchocerciasis who do not show any signs of pathology [7]. Thus, stimulated PBMCs from patients within the three different groups were analysed with regards to their levels of secreted IL-10. Their cells were treated as mentioned in section 3.1.3 and IL-10 was measured after 72 hours of cell culture. PBMCs from infected participants secreted significantly more of this immunosuppressive cytokine than uninfected controls upon stimulation with either *O.v.* extract (figure 3.5A) or *B.m.* female extract (figure 3.5C). IL-10 responses following MSP-1 stimulation were also higher in infected populations (figure 3.5D). Furthermore, the MF^+ patients produced significantly more IL-10 after stimulation with *O.v.* extract than MF^- infected patients (figure 3.5A) and also in response to the LPS stimulus (figure 3.5E). Stimulation with anti-CD3/anti-CD28 (figure 3.5B) or PPD (figure 3.5F) did not result in significant differences although there was an observable trend

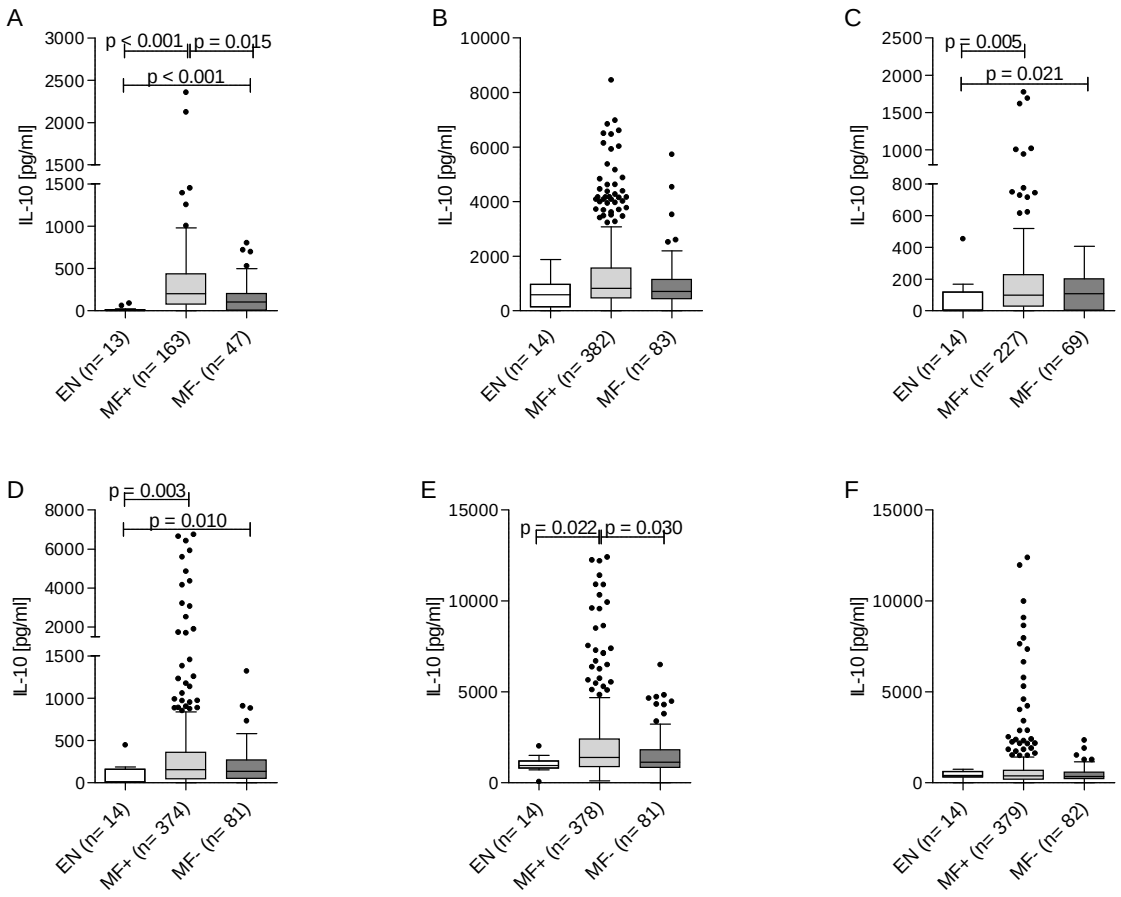

Figure 3.5. MF$^+$ patients produce higher levels of IL-10. Isolated PBMCs (2x 10^5/well) from EN or filarial infected MF$^+$ or MF$^-$ patients were stimulated with either (A) *O.v*. extract (5 μg/ml), (B) anti-CD3/anti-CD28 (10 μg/ml; 2.5 μg/ml), (C) *B.m*. female extract (5 μg/ml), (D) MSP-1 (0.25 μg/ml), (E) LPS (50 ng/ml) or (F) PPD (10 μg/ml) for 72 hours. Thereafter, levels of IL-10 were measured in the culture supernatants via ELISA. Graphs show box whiskers with median, interquartile ranges and outliers after background subtraction. Statistical significances between the indicated groups were obtained after Kruskal-Wallis and Mann-Whitney tests. Numbers in brackets on the x axis legend indicate the amount of stimulated patients within each group.

in terms of higher IL-10 production following anti-CD3/anti-CD28 stimulation in the MF$^+$ group compared to the control group (p= 0.065; figure 3.5B).

3.1.5 Infected individuals show increased IFN-γ secretion to stimulation with MSP-1

As mentioned above, helminthic infections are associated with increased Th2 cytokines which are thought to counterbalance Th1 immune responses that could be detrimental to the host [20]. Moreover, it was shown in LF infections that increased Th1 and Th17 responses are associated with severe pathology (lymphedema) [41]. Therefore, it was analysed if participants of this study produce distinct Th1 and Th17 cytokine responses even though the selected patients did not suffer from severe pathology (like dermatitis or blindness). To address to this question, isolated PBMCs were cultured with the above mentioned panel of stimuli followed by measurement of IFN-γ (figure 3.6) and IL-17 levels (figure 3.7) after three days of incubation. The production of IFN-γ was similar throughout the groups when cells were treated with *O.v.* extract (figure 3.6A), anti-CD3/anti-CD28 (figure 3.6B), *B.m.* female

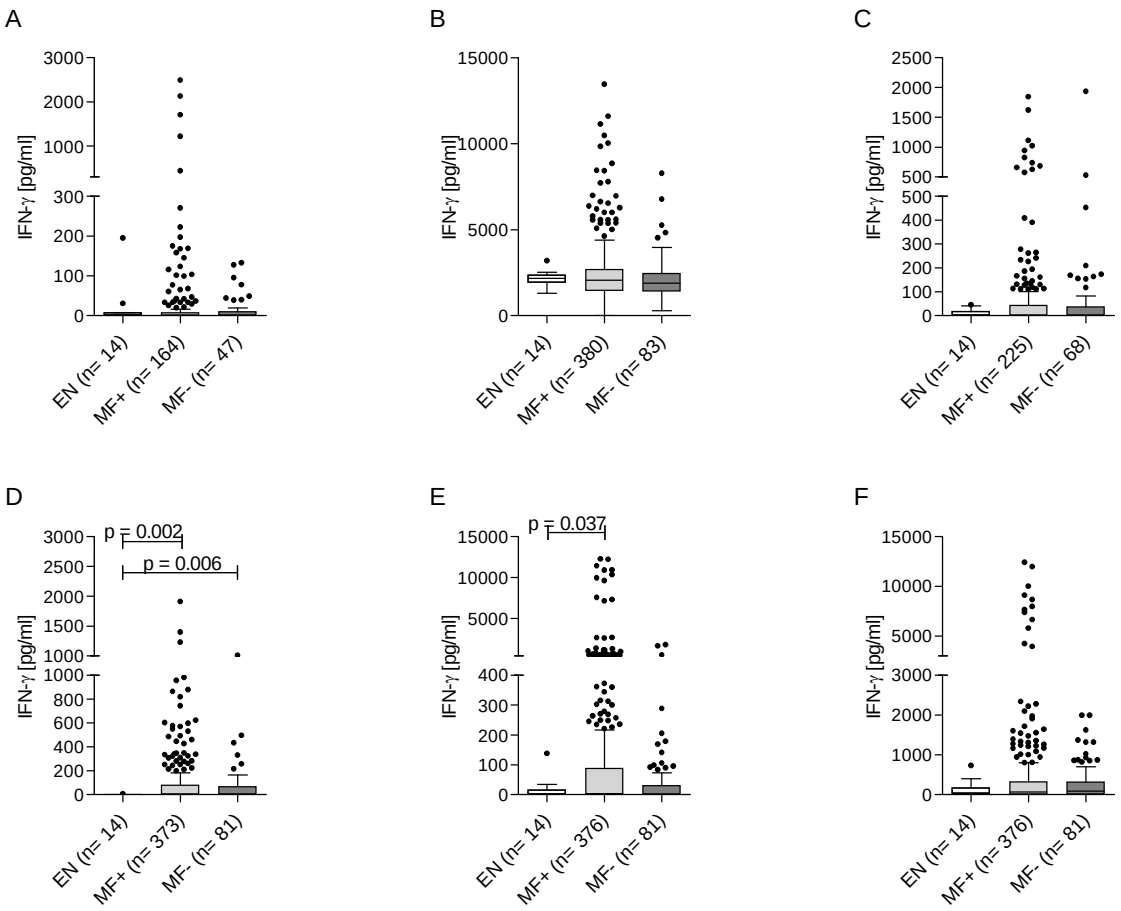

Figure 3.6. Increased IFN-γ production in infected individuals following MSP-1 stimulation. Isolated PBMCs (2x 10^5/well) from EN or filarial infected MF^+ or MF^- patients were stimulated with either (A) *O.v.* extract (5 μg/ml), (B) anti-CD3/anti-CD28 (10 μg/ml; 2.5 μg/ml), (C) *B.m.* female extract (5 μg/ml), (D) MSP-1 (0.25 μg/ml), (E) LPS (50 ng/ml) or (F) PPD (10 μg/ml) for 72 hours. Thereafter, levels of IFN-γ were measured in the culture supernatants via ELISA. Graphs show box whiskers with median, interquartile ranges and outliers after background subtraction. Statistical significances between the indicated groups were obtained after Kruskal-Wallis and Mann-Whitney tests. Numbers in brackets on the x axis legend indicate the amount of stimulated patients within each group.

extract (figure 3.6C) and PPD (figure 3.6F). Both patient groups, however, showed a significantly increased secretion of IFN-γ if their cells were stimulated with MSP-1 (figure 3.6D). In addition, the patent infected group released significantly more IFN-γ than the EN group when LPS was used as stimulus (figure 3.6E). In terms of IL-17 there were no significant differences between the three groups for any of the stimuli (figure 3.7A-F) although a higher percentage of MF^+ individuals responded to the stimulation with MSP-1 (21.4% EN versus 37.1% MF^+ versus 32.9% MF^-) and LPS (14.3% EN versus 26.3% MF^+ versus 19.5% MF^-).

3.1.6 Filarial infected patients display strong pro-inflammatory cytokine profiles upon stimulation

Pro-inflammatory cytokines are described to play a role in the development of pathogenesis in filarial infections and have been shown to be induced by the endosymbiotic bacteria

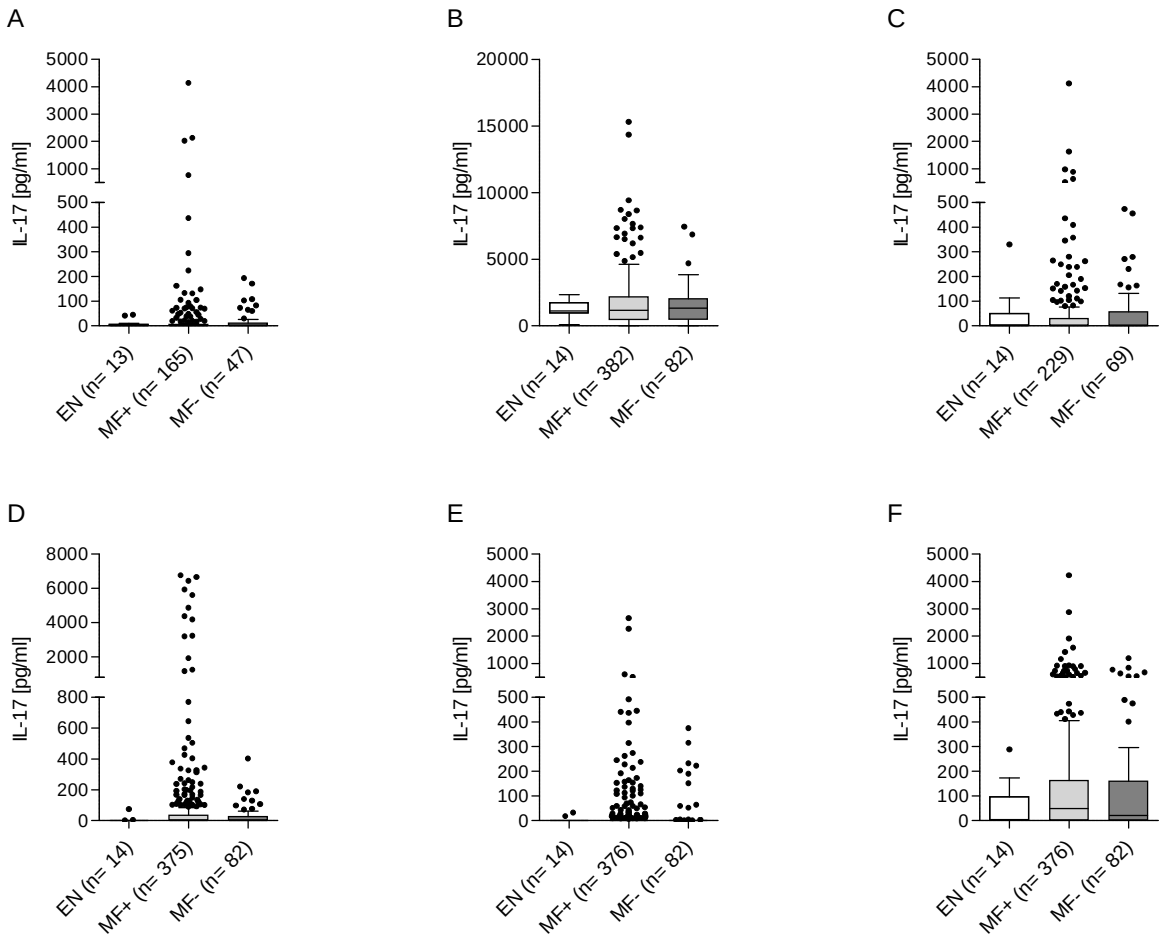

Figure 3.7. Levels of IL-17 secretion are comparable between the analysed groups. Isolated PBMCs (2x 10^5/well) from EN or filarial infected MF^+ or MF^- patients were stimulated with either (A) *O.v.* extract (5 μg/ml), (B) anti-CD3/anti-CD28 (10 μg/ml; 2.5 μg/ml), (C) *B.m*. female extract (5 μg/ml), (D) MSP-1 (0.25 μg/ml), (E) LPS (50 ng/ml) or (F) PPD (10 μg/ml) for 72 hours. Thereafter, levels of IL-17 were measured in the culture supernatants via ELISA. Graphs show box whiskers with median, interquartile ranges and outliers after background subtraction. Statistical significances between the indicated groups were analysed using Kruskal-Wallis and Mann-Whitney tests. Numbers in brackets on the x axis legend indicate the amount of stimulated patients within each group.

Wolbachia [28, 98]. Isolated PBMCs from controls, patent or MF^- infected patients were investigated for their secretion of IL-6 (figure 3.8) or TNF (figure 3.9) in the same manner as described in the previous sections. Incubation of PBMCs from both patient groups with *O.v. extract* resulted in a significant increase of IL-6 and TNF when compared to the response from EN but not in comparison to one another (figure 3.8A and figure 3.9 A). In contrast, treatment with *B.m.* female extract did not lead to any differences between the tested groups with regards to either cytokines (figure 3.8C and figure 3.9C). In the case of stimulation with anti-CD3/anti-CD28 there was also a significant increase in the production of IL-6 in both patient groups compared to the uninfected controls (figure 3.8B) but there were no differences between the infected groups themselves. Regarding TNF release following anti-CD3/anti-CD28 stimulation (figure 3.9B) there were no significant differences at all using the Kruskal-Wallis test. If only TNF production of the control group and the MF^+ group were compared, the latter one showed in the Mann-Whitney test an increased secretion (p= 0.038; figure 3.9B, not depicted in the graph).

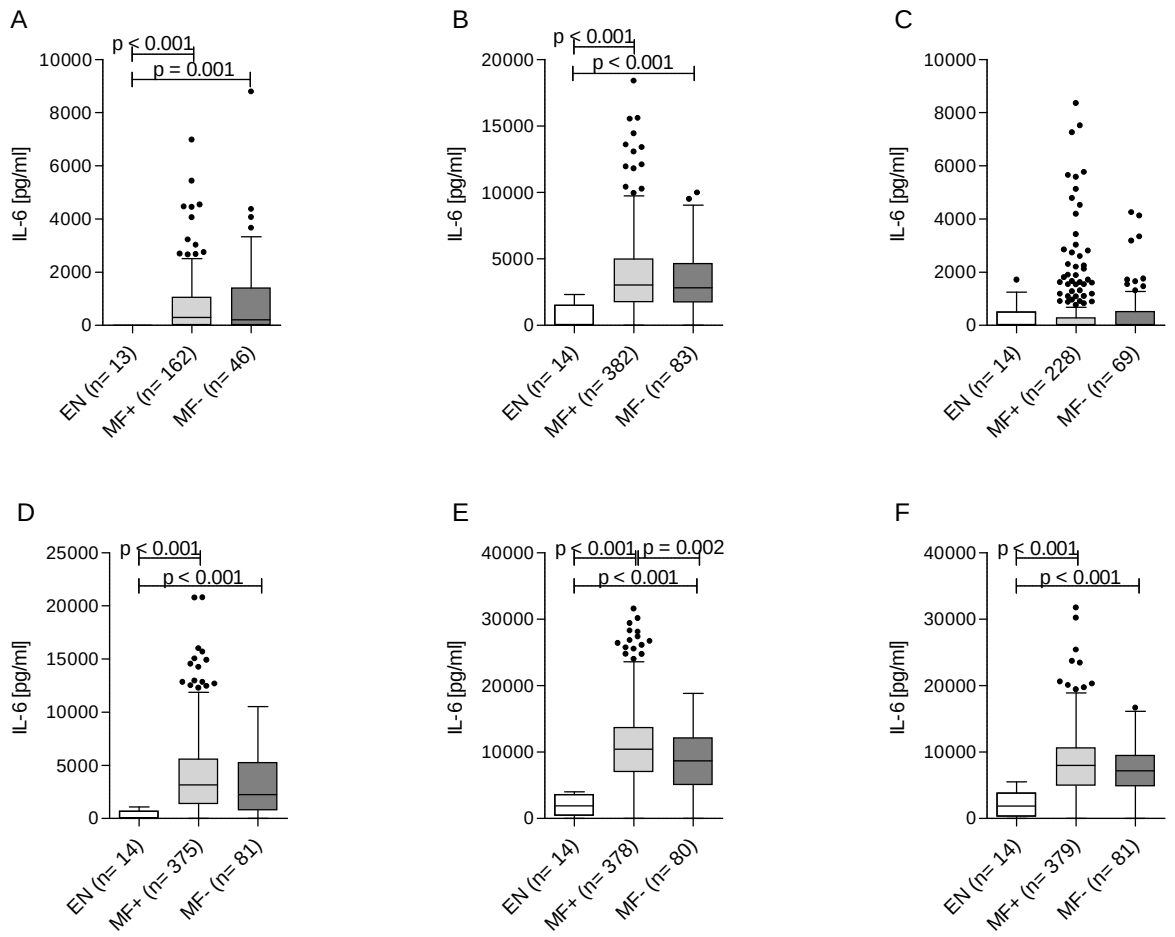

Figure 3.8. Increased IL-6 secretion in helminth infected patients. Isolated PBMCs (2x 10^5/well) from EN or filarial infected MF^+ or MF^- patients were stimulated with either (A) *O.v*. extract (5 μg/ml), (B) anti-CD3/anti-CD28 (10 μg/ml; 2.5 μg/ml), (C) *B.m*. female extract (5 μg/ml), (D) MSP-1 (0.25 μg/ml), (E) LPS (50 ng/ml) or (F) PPD (10 μg/ml) for 72 hours. Thereafter, levels of IL-6 were measured in the culture supernatants via ELISA. Graphs show box whiskers with median, interquartile ranges and outliers after background subtraction. Statistical significances between the indicated groups were obtained after Kruskal-Wallis and Mann-Whitney tests. Numbers in brackets on the x axis legend indicate the amount of stimulated patients within each group.

Stimulation of cells with MSP-1 caused a significant increase in the release of both IL-6 and TNF in the patient groups compared to the uninfected group (figure 3.8D and figure 3.9D). Stimulation with LPS induced the same effects as MSP-1 in terms of a significantly up-regulated secretion in patent and MF^- infected individuals when compared to EN (figure 3.8E and figure 3.9E).

Furthermore, MF^+ patients produced significantly more TNF and IL-6 than the MF^- individuals (figure 3.8E and figure 3.9E). Treatment with PPD induced a significant increase in IL-6 secretion from both patient groups in comparison to controls (figure 3.8F). There was the same outcome for TNF following PPD stimulation albeit not significant (figure 3.9F). In summary, both antigen-specific and bystander stimuli induced secretion of IL-6 and TNF in PBMCs from infected individuals when compared to controls. Interestingly, LPS stimuli elevated the release of both of these innate cytokines in MF^+ patients significantly compared to MF^- individuals.

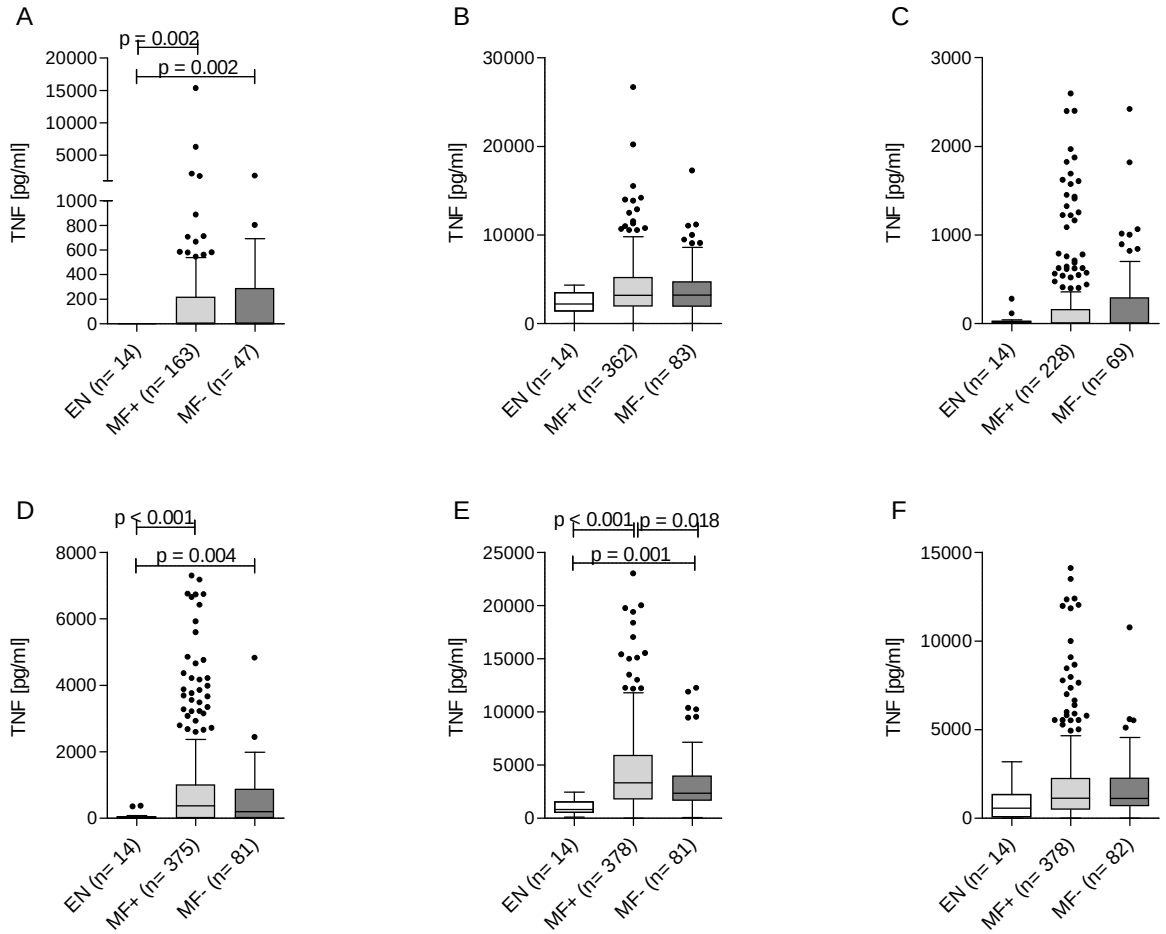

Figure 3.9. Up-regulation of TNF secretion in helminth infected individuals. Isolated PBMCs (2x 10^5/well) from EN or filarial infected MF^+ or MF^- patients were stimulated with either (A) *O.v.* extract (5 μg/ml), (B) anti-CD3/anti-CD28 (10 μg/ml; 2.5 μg/ml), (C) *B.m.* female extract (5 μg/ml), (D) MSP-1 (0.25 μg/ml), (E) LPS (50 ng/ml) or (F) PPD (10 μg/ml) for 72 hours. Thereafter, levels of TNF were measured in the culture supernatants via ELISA. Graphs show box whiskers with median, interquartile ranges and outliers after background subtraction. Statistical significances between the indicated groups were obtained after Kruskal-Wallis and Mann-Whitney tests. Numbers in brackets on the x axis legend indicate the amount of stimulated patients within each group.

3.1.7 Negative correlation of IL-5 with MF burden following filarial stimulation

Previous publications have shown that IL-5 and IL-13 are negatively correlated with the amount of MF if cells were stimulated with the *O.v.* specific extract [29]. In order to confirm these data and to expand analysis also for MF^- individuals, correlation analysis were performed and revealed that indeed the amount of MF was significantly negative correlated to IL-5 secretion after stimulation with *O.v*. extract (figure 3.10A) and furthermore, when cells were stimulated with the related *B.m.* female extract (figure 3.10B). These negative correlations were not found for IL-13 (data not shown). Interestingly, the amount of secreted IL-10 correlated positively with the amount of MF after *O.v*. extract stimulation (figure 3.10C). In addition, levels of secreted cytokines following antigen-specific re-stimulation of all infected patients were also correlated to the rounds of IVM intake and revealed a negative correlation of the latter one with the production of IL-10 (r= -0.177, p= 0.011, data not shown). Since MF^- and patent infected individuals differed significantly with regards to the

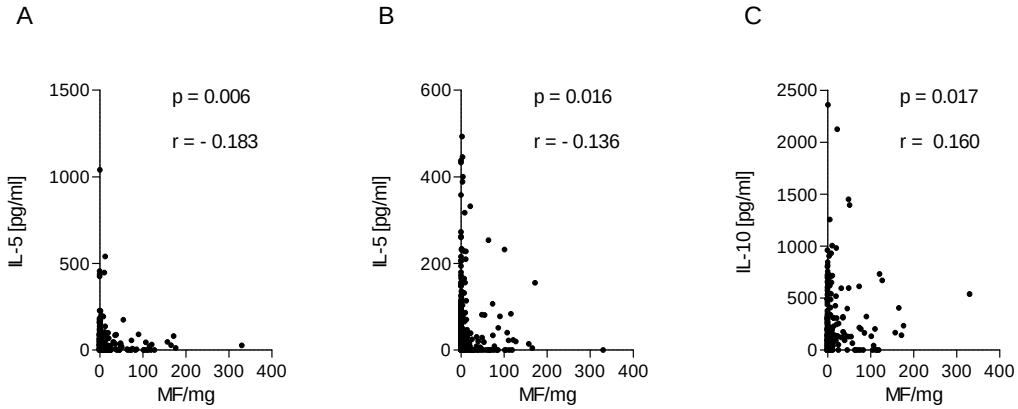

Figure 3.10. MF correlate with cytokine expression. Microfilarial load was correlated to the IL-5 secretion following stimulation with (A) *O.v.* extract (5 μg/ml) and (B) *B.m.* female extract (5 μg/ml). Moreover, MF were correlated to (C) the IL-10 production following *O.v.* extract stimulation. Analysis was performed using Spearman correlation test. Correlation coefficients r and p values are shown.

intake of IVM (see figure 3.1C), correlation analysis was also performed for each subgroup and showed a stronger negative correlation for MF^- infected patients with regards to secretion levels of IL-10 (r= -0.425, p= 0.003, data not shown) whereas there was no such correlation observable for MF^+ patients. There was also no correlation of the amount of nodules or sites with IL-5 or IL-10 following *O.v.* or *B.m.* female extract stimulation.

3.1.8 Specific immunoglobulin profiles in *O. volvulus* infected individuals

The existence of defined immunoglobulin profiles with the asymptomatic filarial infections has been well-established since the early 1980's [51, 102]. More precisely, asymptomatic infected individuals show increased levels of filarial-specific IgG4 in contrast to hyperreactive patients, the latter ones defined by up-regulated levels of IgE, IgG1 and IgG3 [54]. However, the majority of previous studies have focused on the comparison of Ig levels in hyperreactive individuals and patients with GEO form of the disease. Within this work a comparison was performed concerning the immunoglobulin profiles between infected individuals (without severe pathology) versus EN. Moreover, the infected individuals were further subdivided into those presenting MF or not. Levels of filarial-specific Igs from plasma samples were

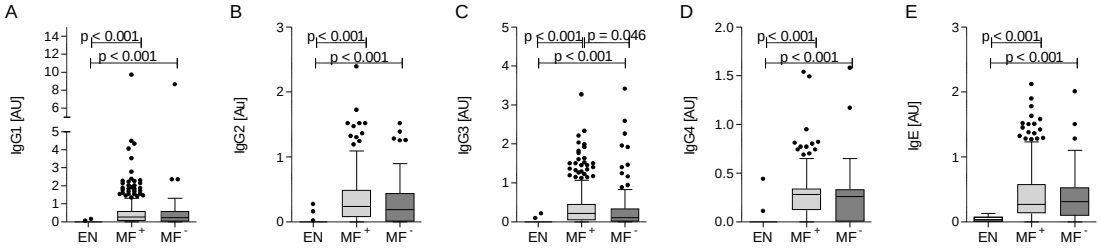

Figure 3.11. Strong production of antigen-specific Igs in helminth infected individuals. Plasma samples from all participants were investigated for the presence of helminth-specific Igs by ELISA. Plates were coated overnight with 5 μg/ml *O.v.* extract in PBS (pH = 9.6), incubated with patient and control plasma overnight and analysed for specific (A-D) IgG1-4 and (E) IgE. Data are depicted as absolute values expressed in arbitrary units [AU]. Graphs show box whiskers with median, interquartile ranges and outliers. Statistical significances between the indicated groups were obtained after Kruskal-Wallis and Mann-Whitney tests.

measured and expressed in arbitrary units (AU). As depicted in figure 3.11A-E all infected individuals had significantly increased levels of specific IgE and IgG subclasses when compared to the control individuals. Upon comparing total levels between the two patient groups, there were only significant differences between specific IgG3 responses, that is, there were higher amounts of circulating IgG3 in patently infected individuals (figure 3.11C).
IgG4 and IgE are often directed at the same antigenic epitope and deciphering the ratio between these two isotypes provides insightful information when determining whether the antigen triggers an IgE-mediated hypersensitivity response or whether IgG4 can act as a blocking antibody [69]. Therefore, the ratios of IgG4 to IgE and to other IgG subclasses were compared for the infected individuals (figure 3.12). Analysing the ratio of IgG4 to the other Ig subclasses revealed no significant differences at all between patent and MF^- individuals (figure 3.12A-C). The ratio of IgG4/IgE was increased in MF^+ patients compared to MF^- individuals albeit not significantly (p= 0.085) as demonstrated in figure 3.12D. This was also reflected by the percentages of patients giving a signal for IgG4 in the specific ELISA, thus 85.90% of MF^+ gave a positive signal compared to only 74.07% of MF^- individuals (for IgE: MF^+: 92.81 and MF^- 92.59) indicating that MF^+ individuals are more "protected" from developing inflammation. Correlating IL-10 and IgG4 did not reveal any significant result (data not shown).

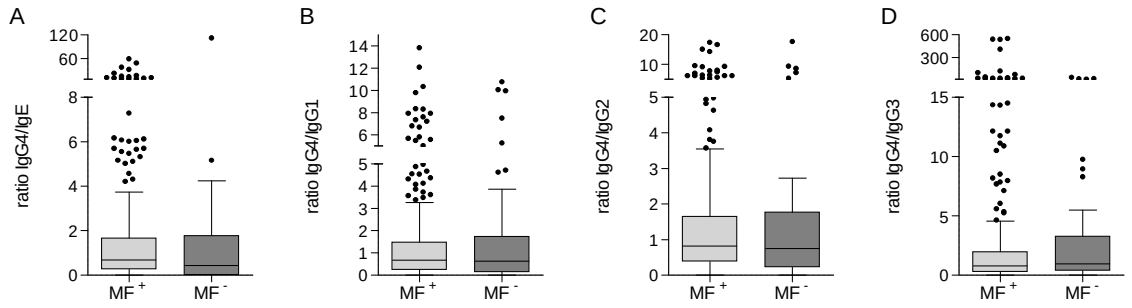

Figure 3.12. Determination of IgG4 ratios. Plasma samples from all participants were investigated for the presence of helminth-specific Igs by ELISA. Plates were coated overnight with 5 μg/ml *O.v.* extract in PBS (pH = 9.6), incubated with patient and control plasma overnight and analysed for specific IgG1-4 and IgE. A-D show the ratio of the antigen-specific antibodies IgG4/IgE (A), IgG4/IgG1 (B), IgG4/IgG2 (C) and IgG4/IgG3 (D). Graphs show box whiskers with median, interquartile ranges and outliers. Statistical significances were analysed using Kruskal-Wallis and Mann-Whitney tests.

3.2 Analysis of pSTAT3 expression

Previous studies from our department have revealed an important role of IL-10 during filarial infections since this immunoregulatory cytokine is involved in the induction of immunosuppression in hyporesponsive patients [18]. In the results mentioned above, it was demonstrated that *O. volvulus* infected patients produce significantly more IL-10 than the control individuals. Additionally, it was also shown in previous experiments that regulatory T cell clones from hyporeactive patients are characterized by high expression of IL-10 which in turn facilitates their ability to induce IgG4 from B cells [18, 49]. Besides cell-cell contact this

Treg:B cell interaction is dependent on GITR and its ligand and also on the interaction of TGF-β with its receptor. In brief, *in vitro* experiments using cell clones of human IL-10-producing Tregs, in co-culture with autologous B cells, demonstrated that blocking GITR or GITR-L selectively prevented IgG4 production [50]. The same outcome was found after adding anti-IL-10 and anti-TGF-β antibodies to the Treg:B cell co-cultures. In order to investigate more in-depth the mechanisms of IL-10 in inducing IgG4 production, the signaling pathway of IL-10 was analysed with regards to pSTAT3 since its phosphorylation reflects activation of the IL-10 pathway [21]. The long term aim was to determine in co-culture assays of B cells and Tregs which cell population is activated via the IL-10 pathway. Furthermore, the influence of GITR and its ligand should be investigated.

3.2.1 Dose-dependent induction of pSTAT3 by IL-10 in PBMCs

First of all a system was established to induce the phosphorylation of STAT3. Therefore, PBMCs of healthy blood donors were isolated as mentioned in section 2.3.2. In brief, 2x 10^6 cells per well were stimulated for one hour with IL-10 (concentrations ranged from 3 ng/ml to 100 ng/ml). Thereafter, cells were harvested, lysed and loaded onto SDS gels before further analysis by Western blot as described in section 2.3.19. Data in figure 3.13 show cells unstimulated and stimulated with different concentrations of recombinant IL-10. There was a

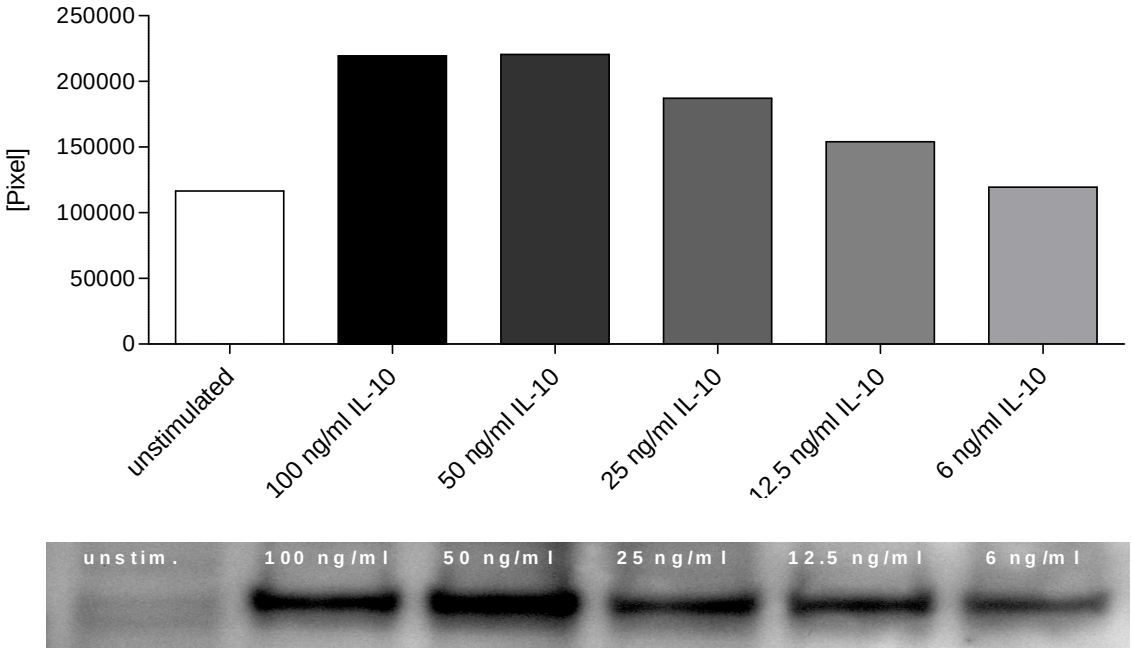

Figure 3.13. Dose dependent phosphorylation of STAT3 by IL-10 in PBMCs. 2x 10^6 PBMCs were either left unstimulated or stimulated for one hour in the presence of increasing doses of recombinant IL-10 followed by SDS gel electrophoresis and Western blotting. Depicted are results from one representative of two independent donors. Bars in the upper part show pixel intensity, whereas the lower part shows Western blot bands. Analysis of blot bands was performed using fiji software.

clear dose-dependent induction of pSTAT3 in PBMCs upon activation with recombinant IL-10 peaking at a dose of 50 ng/ml. However, even 6 ng/ml of IL-10 induced the phosphorylation of STAT3. Stimulation with 3 ng/ml of IL-10 did not result in a clear band on the Western blot (data not shown). In conclusion, stimulation of PBMCs for one hour with at least 6 ng/ml of recombinant IL-10 was sufficient to induce phosphorylation of STAT3.

3.2.2 Phosphorylation of STAT3 in T and B cells

The results mentioned above showed phosphorylation of STAT3 following stimulation with 100 ng/ml IL-10. Thus, the same experiment was performed with $CD4^+$ T and $CD19^+$ B cells instead of PBMCs because the long-term aim was the setup of a co-culture system of T and B cells. Cells were isolated as described in section 2.3.6.1 and 2.3.6.2. Purity of enriched cells was routinely >95%. 1x 10^6 cells per well were stimulated for one hour with 100 ng/ml IL-10 and afterwards harvested, lysed and loaded onto SDS gels before analysed by Western blot. Data in figure 3.14 depict pSTAT3 expression in unstimulated and stimulated cells of both subpopulations, each graph consisting of data from three donors. Following IL-10 stimulation STAT3 was phosphorylated in $CD4^+$ T cells (figure 3.14A) and also in $CD19^+$ B cells (figure 3.14B) albeit to a much lesser extent than in PBMCs.

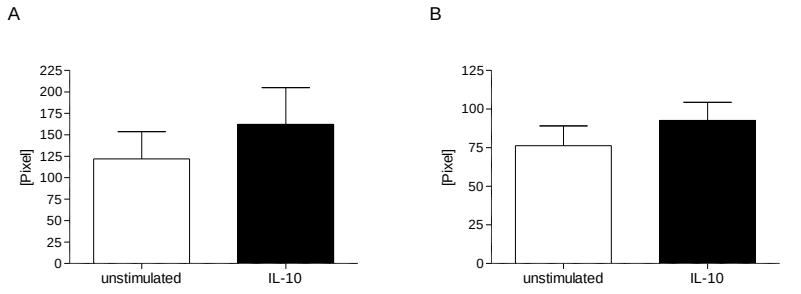

Figure 3.14. Phosphorylation of STAT3 in T and B cells. 1x 10^6 enriched (A) $CD4^+$ T (n=3) or (B) $CD19^+$ B cells (n=3) were either left unstimulated or stimulated for one hour with 100 ng/ml recombinant IL-10 followed by SDS gel electrophoresis and Western blot analysis.

3.2.3 No significant alteration of pSTAT3 following blockade of GITR or GITR-L

In order to determine the effect of anti-GITR (figure 3.15A) or anti-GITR-L (figure 3.15B) antibodies during the signaling process of IL-10, PBMCs from healthy donors were incubated in presence of these blocking antibodies. 2x 10^6 cells per well of six donors were either left untreated or treated for 24 hours with 1 μg/ml of anti-GITR antibody or 15 ng/ml anti-GITR-L antibody. The concentrations of the antibodies were chosen on their ability to block activity of IgG4 production in the co-culture assays mentioned above [50]. Afterwards, cells were left unstimulated or stimulated for one hour with 50 ng/ml recombinant IL-10, then lysed and used for subsequent Western blot analysis. Normalization was performed by calculating the ratio of pixel intensity of stimulated cells compared to the intensity of unstimulated cells with the fiji software. The same experimental setup was performed with isolated $CD4^+$ T cells.

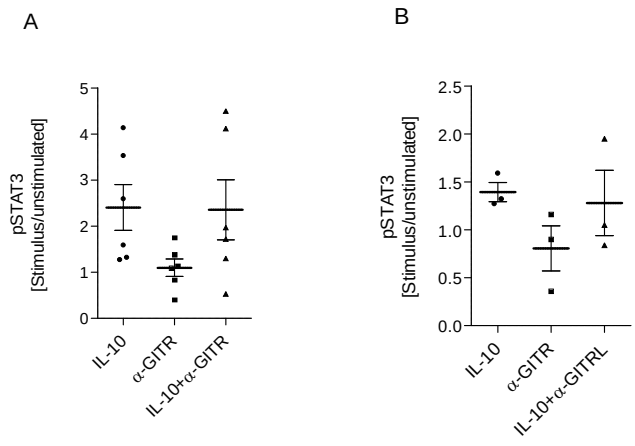

Figure 3.15. No significant effect of α–GITR or α–GITR-L on phosphorylation status of STAT3. 2x 10^6 PBMCs were incubated for 24 hours in presence of (A) 2 μg/ml αGITR (n=6) or (B) 15 μg/ml αGITR-L (n=3) followed by stimulation with 100 ng/ml IL-10 for one hour. SDS gel electrophoresis and Western blot analysis were conducted. Normalization was performed by calculating the ratio of pixel intensity of stimulated cells compared to the intensity of unstimulated cells using fiji software.

As shown in figure 3.15A and B, there was an induction of pSTAT3 when cells were stimulated with IL-10 alone. As expected, treatment with anti-GITR (figure 3.15A) or anti-GITR-L antibody alone (figure 3.15B) did not trigger the phosphorylation of STAT3. The results obtained with prior blocking of the cells with anti-GITR or anti-GITR-L before stimulation with IL-10 proved difficult to interpret since the phosphorylation status was only partially reduced (figure 3.15A and B). In addition, blocking of GITR did not modulate the phosphorylation of STAT3 in isolated $CD4^+$ T cells significantly (data not shown).

3.2.4 No effect of anti-GITR with decreasing doses of IL-10

As can be seen from figure 3.15, distribution of pSTAT3 expression was heterogeneous in anti-GITR/IL-10 stimulated cells of different blood donors. As mentioned above, levels of pSTAT3 expression were compared on the individual donor level and the obtained results were contradictory regarding the effect of anti-GITR. More precisely, although some donors showed a down-regulation of pSTAT3 signal following GITR blockage others did not. Therefore, increasing concentrations of anti-GITR antibody were applied and concentrations

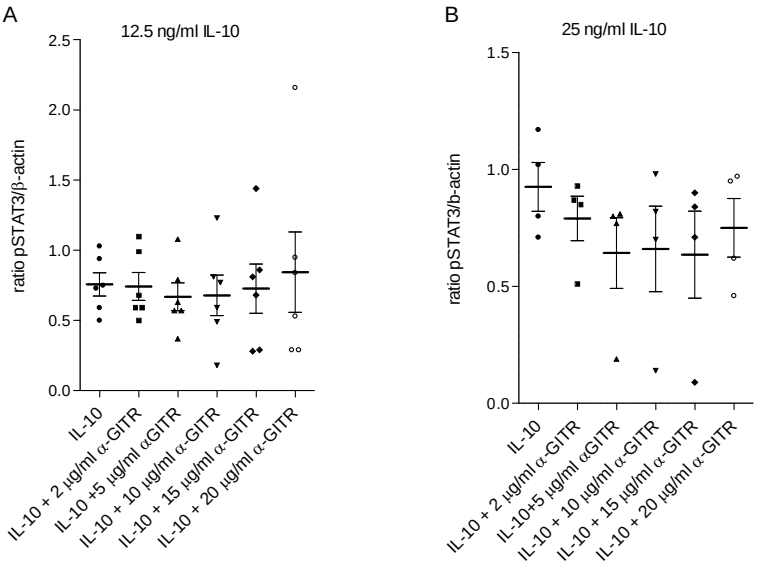

Figure 3.16. Increasing doses of α–GITR do not alter phosphorylation status of STAT3. 2x 10^6 PBMCs were incubated for 24 hours with 2-20 μg/ml α–GITR followed by stimulation with (A) 12.5 ng/ml (n=6) or (B) 25 ng/ml IL-10 (n=3) for one hour. Then, SDS gel electrophoresis and Western blot analysis were conducted. Normalization was performed by calculating the ratio of pixel intensity of bands of pSTAT3 against those of β-actin using fiji software.

of recombinant IL-10 were decreased to 12.5 ng/ml (figure 3.16A) and 25 ng/ml (figure 3.16B). The described titration assay at the beginning of this section showed clear bands of pSTAT3 following stimulation with these lower doses of recombinant IL-10. PBMCs from healthy donors were isolated and 2x 10^6 cells were stimulated with either 12.5 or 25 ng/ml IL-10 in the absence or presence of increasing concentrations of anti-GITR antibody (2-20 ng/ml) as shown in figure 3.16A and B respectively. Bands of stimulated cells were normalized against bands of β-actin. As can be seen in figure 3.16 there were no significant reductions of pSTAT3 in the presence of increasing doses of blocking anti-GITR antibody independent of the IL-10 concentration. Again, analysis of individual donors revealed different results, thus in some individuals blocking GITR might play a role regarding the phosphorylation of STAT3 whereas in other donors the signaling pathway is not directly influenced by GITR.

3.2.5 Recombinant GITR does not alter phosphorylation of STAT3

In a further Western blot experiment concerning the possible effect of GITR on the IL-10 signaling pathway, recombinant GITR was added to PBMCs of healthy donors in order to see if this application would increase the phosphorylation of STAT3. PBMCs were pre-incubated for 24 hours with increasing doses of recombinant human GITR (5-100 ng/ml) and afterwards stimulated with IL-10 (12.5 ng/ml) for one hour. Bands of stimulated cells were normalized against the bands of β-actin. As depicted in figure 3.17, there were no significant alterations in the expression of pSTAT3 in the presence of recombinant GITR, independent of the applied concentrations. In conclusion, there appears to be no direct influence of recombinant GITR on the expression of pSTAT3.

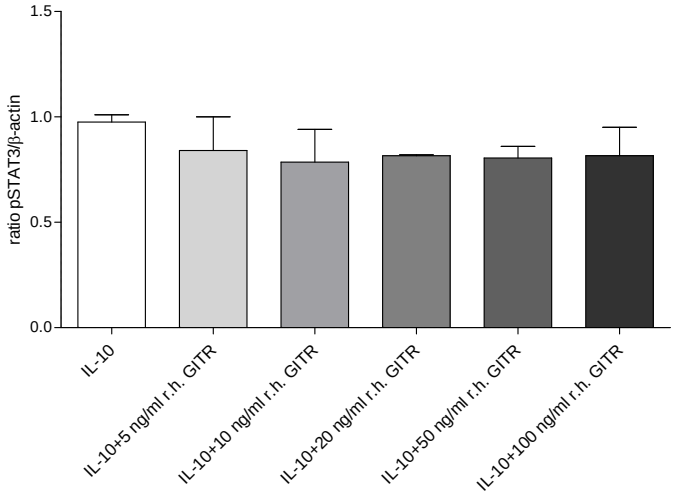

Figure 3.17. Increasing doses of recombinant GITR do not alter the phosphorylation status of STAT3. 2x 10^6 PBMCs were incubated for 24 hours with increasing concentrations of recombinant human (r.h.) GITR (5-100 ng/ml) followed by stimulation with 12.5 ng/ml IL-10 (n=2) for one hour. Subsequently SDS gel electrophoresis and Western blot analysis were performed. Normalization was done by calculating the ratio of pixel intensity of bands of pSTAT3 against those of β-actin using fiji software.

3.2.6 Cell surface expression of GITR and GITR-L

In order to see if PBMCs of individual donors express GITR and GITR-L in comparable amounts, cell surface expression of these markers was determined. Hence, isolated PBMCs from 16 blood donors were stained for their GITR and GITR-L cell surface expression as described in section 2.3.7.1 and results are depicted in figure 3.18. Measurement of GITR and GITR-L revealed different percentages in individual PBMCs ranging from less than 30 and up to 67% for GITR and between 42 and 77% for GITR-L respectively. These data highlight that different background expression patterns might be a possible explanation for the inconclusive results obtained from the blocking experiments with anti-GITR. Further analysis on B and T cells should be performed.

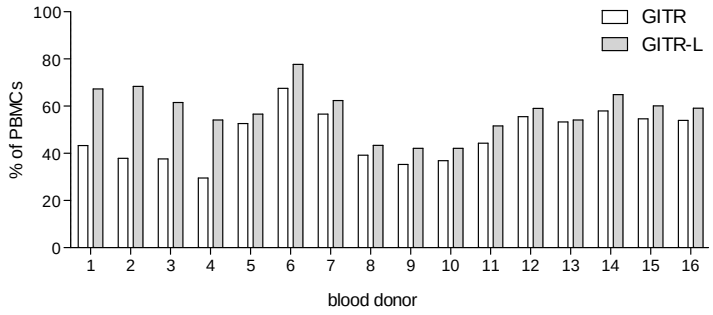

Figure 3.18. Cell surface expression of GITR and GITR-L in PBMCs. 2x 10^5 PBMCs of healthy blood donors were analysed by FACS for their expression of GITR or GITR-L. Bars represent percentages of GITR or GITR-L for each individual blood donor (n=16) after gating on lymphocyte gate. Data were analysed with FACS Diva software.

3.2.7 Phosflow experiments

As mentioned above, previous studies have shown that co-cultivation of B cells and IL-10-producing Tregs induce the secretion of IgG4 in a cell-contact-dependent-manner [49, 50]. Blocking antibodies against IL-10 or TGF-β decreased the production of IgG4. In parallel to the Western blot studies described above, an attempt to elucidate which of these two cell populations is activated via IL-10 was conducted using intracellular FACS staining to determine phosphorylation status of STAT3. PBMCs of healthy individuals were isolated and B cell and T cell fractions were sorted after staining with their appropriate surface markers (CD20 and CD4 respectively) as described in section 2.3.7.3. 1x 10^6 lymphocytes per well were incubated for one hour in the presence or absence of 100 ng/ml IL-10. Cells were subsequently stained for pSTAT3 as described in section 2.3.7.2. In contrast to the results from Western blot assays (figure 3.13) stimulation of sorted cells with IL-10 did not result in any increase of pSTAT3 signal. Figure 3.19 shows a representative flow cytometry analysis of pSTAT3 staining in PBMCs, isolated $CD4^+$ T cells and isolated $CD20^+$ B cells. There was only a weak signal for pSTAT3 but even with increasing doses of IL-10 or elongated incubation times the fluorescence could not be significantly intensified (data not shown) indicating that cells were not optimally treated to receive an increased signal for pSTAT3. Therefore, no conclusions could be drawn from these experiments.

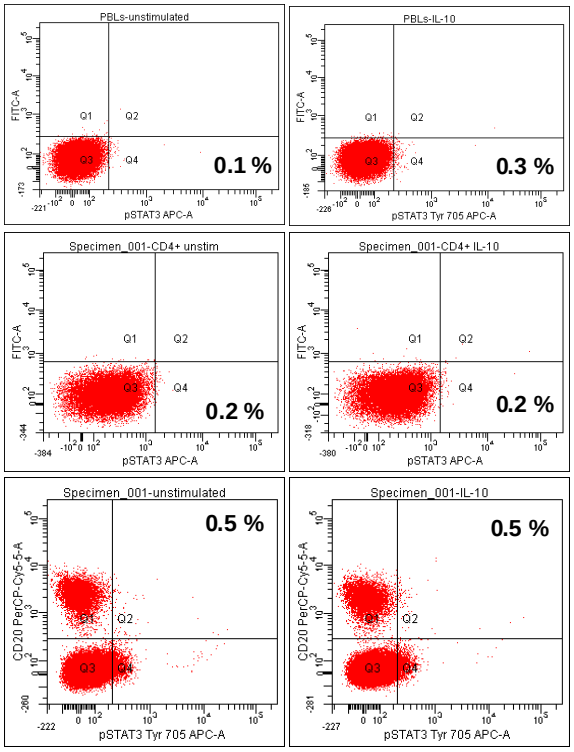

Figure 3.19. No increase of pSTAT3 signals following IL-10 stimulation. 1x 10^6 cells were either left unstimulated (left panel) or stimulated for one hour with 100 ng/ml recombinant IL-10 (right panel) and analysed for the presence of pSTAT3. Phosphorylated STAT3 expression of PBMCs (upper row), sorted $CD4^+$ T (middle row) or sorted $CD20^+$ B cells (lower row) was determined. Data were analysed using FACS Diva software. In case of the $CD4^+$ T cells (middle row), only pre-gated $CD4^+$ T cells are depicted.

3.3 Lymphatic filariasis

Within this section, aspects of the immunological status of a cohort of *W. bancrofti* infected patients are highlighted pre- and post-treatment. In this study, male individuals from the Western region of Ghana were investigated for the presence of CFA and for the presence of detectable worm nests in the scrotal area. All included participants did not suffer from lymphedema determined according to Debrah *et al* [78]. The study cohort consisted of 181 individuals that were subdivided into 92 microfilaremic and 67 amicrofilaremic patients and 22 endemic individuals. Before included individuals were treated with different treatment regiments, cytokine secretion levels were assessed upon antigen-specific or bystander stimulation. In addition, unspecific and antigen-specific Ig levels of included individuals were determined using plasma samples. Moreover, 12 months post-treatment, alterations in Ig profiles or cytokine levels following antigen-specific and bystander stimulations were also assessed in the differently treated groups. This parameter was also analysed 24 months after treatment.

3.3.1 Clinical evaluation of *Wuchereria bancrofti* infected patients

Infection with *W. bancrofti* leads to dilation of lymphatic vessels since adult worms residue inside the vascular system [140]. In order to investigate the level of dilation of lymph vessels and the actual number of worm nests within the scrotal region ultrasonography was performed (see section 2.3.1.5) on the above mentioned cohort. The number of worm nests was determined by detecting the movement of adult worms, termed filarial dance sign. Dilation of lymphatics and lymphatic vessels at the position of the worm nest and the

	MF$^+$ (n=92)	MF$^-$ (n= 67)	EN (n=22)
age (mean and range)	34.68 (18-50)	34.61 (19-55)	32.50 (19-45)
FDS	positive	positive	negative
CFA	positive	positive	negative
rounds of IVM/ALB (mean)	2.17	2.09	n.d.
number of scrotal worm nests (mean)	1.80	1.28	0.00
m-mode average (cm, mean)	0.41	0.36	0.00
MF/ml (mean and range)	971.16 (1-7,590)	0.00	0.00

Table 3.2. Characteristics of the study population.

maximum dilation of a lymphatic vessel (without worms) in the supratesticular area were evaluated using a grading system from stage 0 to stage 4 according to Debrah *et al* [78] as described in section 2.3.1.5. Determination of hydroceles was also performed and revealed 12 patients with clinical hydrocele (MF$^+$ n= 7 and MF$^-$ n=5) according to Mand *et al* [147] but all patients were negative for lymphedema. Table 3.2 depicts the characteristics of the study population which includes the degree of clinical manifestations within each group and the rounds of MDA for the CFA positive groups that was determined using the CFA test. In contrast to the onchocerciasis study, only males were included since the presence of at least one scrotal worm nest was an inclusion criterion. With regards to CFA, we found a positive correlation (r= 0.68, p<0.001, data not shown) between the concentration of CFA and MF. No significant differences could be observed in the extent of dilation of lymphatic vessels at worm nest locations between the MF$^+$ and MF$^-$ groups (figure 3.20A). However, the microfilaremic patients showed a significant increase in the number of scrotal worm nests in comparison to MF$^-$ patients (figure 3.20B), which was confirmed by the Cochran-Armitage trend test (p<0.001). Whereas figure 3.20A illustrates the local dilation of lymphatic vessels around the detected worm nests, figure 3.20C depicts the maximal detectable lymph dilation within the whole scrotal tissue, including the area of the spermatic cord which is not necessarily co-localized with the position of the worm nest. No significant differences between the two *W. bancrofti* infected groups could be detected (MF$^+$ versus MF$^-$ p= 0.180,

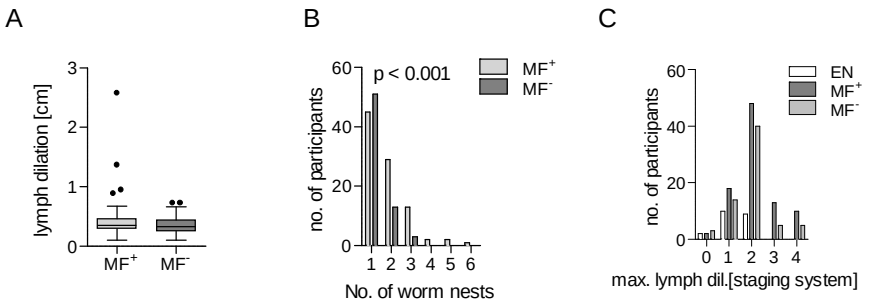

Figure 3.20. Active circulation of MF is associated with the number of worm nests. Using ultrasound, participants were examined for dilation of lymphatic vessels around the worm nests (A) and for the amount of worm nests (B). They were also examined for the maximum degree of dilation of supratesticular lymph vessels (C), presented as a staging system. Box whisker plots in A show median, interquartile ranges and outliers of individually tested patients. Bars in B and C show the number of patients and their correlating amount of worm nests or lymph dilation. Data in B were tested for significance with the Cochran-Armitage trend test (p< 0.001).

figure 3.20C). In EN individuals, which were CFA, MF and FDS negative, the maximal dilation of scrotal lymphatic vessels was also assessed and they displayed dilation of lymphatic vessels between grades 0 and 2, but these individuals had significantly less dilation of lymphatic vessels than either the patent or the latent group (MF^+ versus EN: p= 0.001, MF^- versus EN: p= 0.006; figure 3.20C). The number of detectable worm nests however, was positively correlated with the amount of circulating MF (r = 0.356, p<0.001, figure 3.21B) whereas there was no such correlation with any of the dilation parameters, neither at the worm nests nor at the maximal detectable dilation of lymphatic vessels (figure 3.21A and C). Moreover, there were no correlations found between the rounds of drug intake and any of the clinical parameters (data not shown).

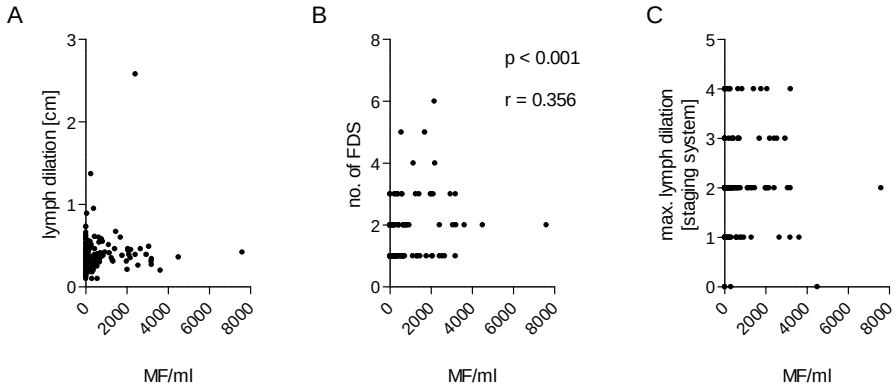

Figure 3.21. The amount of MF correlates with the number of worm nests. Microfilarial load was correlated to the dilation of lymphatic vessels (A), the number of worm nests (B) and the maximal dilation of lymphatic vessels (C). Analysis was performed using Spearman correlation test. Correlation coefficients r are only shown if p values were <0.05.

3.3.2 Similar numbers of PBMCs in infected and uninfected individuals

PBMCs of *W. bancrofti* infected patients were isolated as described in section 2.3.2 and subsequently incubated with various stimuli for three days in order to investigate their cytokine profiles. The amount of isolated cells from each individual from all three groups was compared and is depicted in figure 3.22. There were no significant differences in terms of higher or lower cell concentrations.

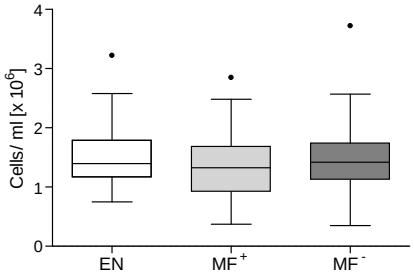

Figure 3.22. Similar amounts of PBMCs in infected and uninfected individuals. PBMCs of EN, MF^+ and MF^- individuals were isolated using ficoll gradients. The amount of viable cells was determined using the trypan blue exclusion method. Graphs show box whiskers with median, interquartile ranges and outliers. Statistical significances between the indicated groups were tested using Kruskal-Wallis and Mann-Whitney tests.

3.3.3 Filarial-specific IL-5 responses are elevated in latently infected individuals

Although much is known about the immunological differences between patients presenting low and severe pathology, little is known about the differences in antigen-specific responses of MF^+ and MF^- groups. To address the immunological profile of MF^+ and MF^- patients, PBMCs were stimulated with anti-CD3/anti-CD28, *B.m.* extract, MSP-1 and LPS. As mentioned in section 2.2.5, *B.m.* extract was used instead of *W. bancrofti* extract because the latter parasite cannot be maintained in a rodent host in contrast to the closely related *B. malayi*. Since Th2 cytokines are typical hallmarks of helminth infections, levels of IL-5 (figure 3.23A-D) and IL-13 (figure 3.23E-H) were determined. Levels of IL-4 were also measured but the obtained results were all under the ELISA detection limit (data not shown). Figure 3.23A and E show that upon T cell activation, all groups produced IL-5 and IL-13 and there were no differences between the infected groups or to EN. With regards to filarial-specific responses, MF^- patients made significantly more IL-5 than MF^+ individuals (figure 3.23B), whereas EN hardly responded to this antigen at all. IL-13 was also strongly produced by all infected individuals in response to the filarial extract but no significant differences between the MF^+ and MF^- groups could be determined. Both groups, however, secreted significantly higher levels of IL-13 when compared to EN (figure 3.23F). In response to MSP-1 and LPS, there were no significant alterations between the two infection groups (figure 3.23C, D, G and H). However, in contrast to IL-5 there was secretion of IL-13 upon stimulation with MSP-1 and

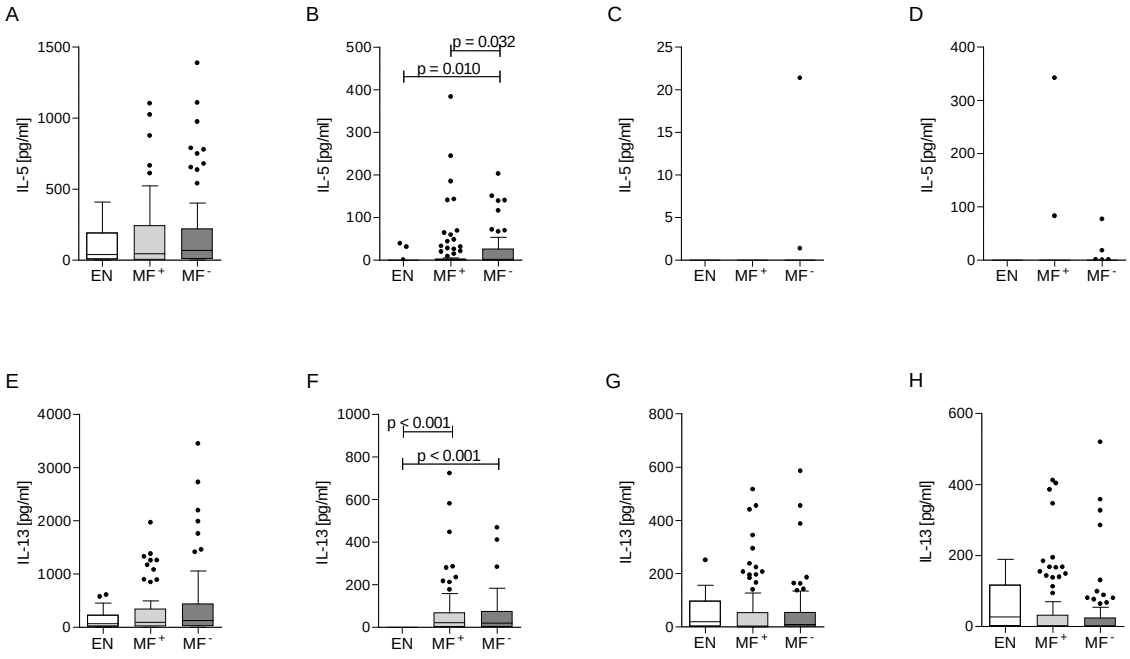

Figure 3.23. Patent infection alters filarial-specific Th2 responses. Isolated PBMCs (2x 10^5/well) from EN or *W. bancrofti* infected MF^+ or MF^- patients were stimulated with either anti-CD3/anti-CD28 (10 µg/ml; 2.5 µg/ml; A and E), *B.m.* extract (5 µg/ml; B and F), MSP-1 (0.25 µg/ml; C and G) or LPS (50 ng/ml; D and H) for 72 hours. Thereafter, levels of IL-5 (A-D) or IL-13 (E-H) were measured in the culture supernatants via ELISA. Graphs show box whiskers with median, interquartile ranges and outliers after background subtraction. Statistical significances between the indicated groups were obtained after Kruskal-Wallis and Mann-Whitney tests.

LPS. In conclusion, these data show that there is a distinct filaria-specific expression of the key cytokine IL-5 between amicrofilaremic and patent individuals.

3.3.4 Amicrofilaremic patients present elevated Th-17 responses

To observe whether there were any alterations in the Th1 and Th17 profiles of microfilaremic and amicrofilaremic patients the secreted levels of IFN-γ (figure 3.24A-D) and IL-17 (figure 3.24E-H) were also measured. Only a limited number of patients presented cytokine responses upon re-stimulation with *B.m.* extract (figure 3.24B and F). Similarly few responders were observed upon stimulation with MSP-1 (figure 3.24C and G) or LPS (figure 3.24D and H). Indeed, only MF^- patients responded to MSP-1 in terms of IL-17 production. These responders did not correlate with those patients that had a subclinical plasmodial infection. Albeit only a small portion of the study cohort (20/181), further statistical analysis revealed that these subclinical malaria patients did not differ in any of their responses when compared to the malaria negative patients. Interestingly, when compared to patently infected patients and EN, the MF^- group also showed significantly elevated IL-17 responses upon anti-CD3/anti-CD28 stimulation (figure 3.24E). Although non-significant, after stimulation with anti-CD3/anti-CD28 the IFN-γ response of MF^+ patients was lower than either of the other two groups (figure 3.24A). This result emphasizes again that upon MF production host adaptive responses are dampened.

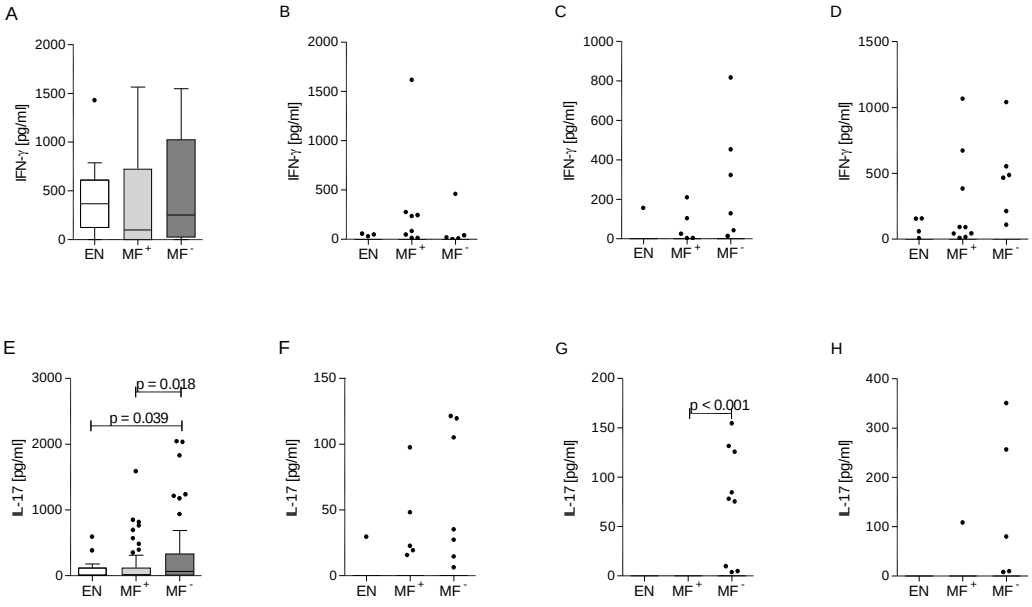

Figure 3.24. Latent infected patients show elevated Th17 but not Th1 responses. Isolated PBMCs (2x 10^5/well) from EN) or MF^+ or MF^- patients suffering from LF were stimulated with either anti-CD3/anti-CD28 (10 µg/ml; 2.5µg/ml; A and E), *B.m.* extract (5 µg/ml; B and F), MSP-1 (0.25 µg/ml; C and G) or LPS (50 ng/ml; D and H) for 72 hours. Thereafter, levels of IFN-γ (A-D) or IL-17 (E-H) were measured in the culture supernatants via ELISA. Graphs show box whiskers with median, interquartile ranges and outliers after background subtraction. Statistical significances between the indicated groups were obtained after Kruskal-Wallis and Mann-Whitney tests.

3.3.5 Filarial-specific IL-10 is enhanced in latently infected individuals

Next, the IL-10 and TGF-β production from stimulated PBMCs of infected patients were analysed since increased levels of TGF-β and IL-10 have been associated with the asymptomatic form of LF [41, 156]. In the patient cohort, IL-10 responses from MF^+ patients were lower than those from MF^- patients irrespective of the applied stimulus. Interestingly, there was a significantly up-regulated IL-10 response in the latent group following antigen-specific stimulation compared to the MF^+ individuals. Moreover, in response to malaria peptides (figure 3.25C) and LPS (figure 3.25D) MF^+ patients produced significantly lower amounts of IL-10 when compared to responses from EN and MF^- patients. These data indicate that MF are able to immunomodulate responses upon filarial-specific stimulation, upon TLR triggering and in response to other parasitic antigens such as those derived from malaria species. Due to high background production of TGF-β, no differences could be determined within the different groups, irrespective of antigen stimulus (data not shown). With regards to IL-6, there was a general down-regulation in the microfilaremic patients when compared to uninfected individuals independent of the applied stimulus (figure 3.25E-H). In the case of T cell activation with anti-CD3/anti-CD28 there was also a significant difference between the two infection groups concerning the release of IL-6 (figure 3.25E).

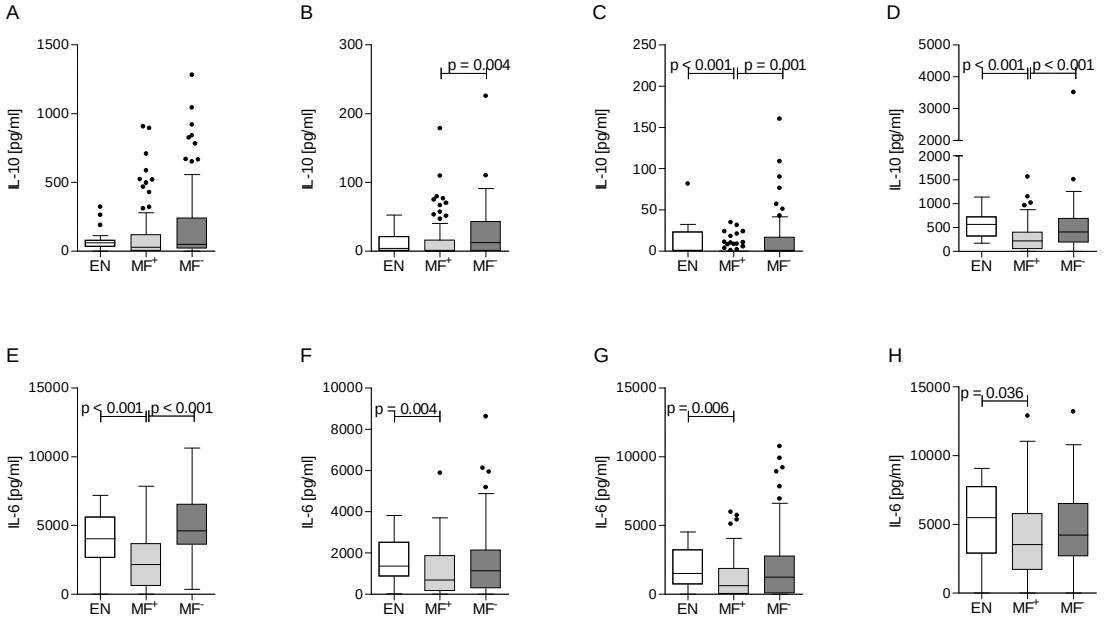

Figure 3.25. Regulatory responses are enhanced in latently-infected individuals. Isolated PBMCs (2x 10^5/well) from EN or patients infected with *W. bancrofti* were stimulated with anti-CD3/anti-CD28 (10 µg/ml; 2.5 µg/ml; A), *B.m.* extract (5 µg/ml, B), MSP-1 (0.25 µg/ml; C) or LPS (50 ng/ml, D) for 72 hours. Thereafter, culture supernatant was tested via ELISA for cytokine release of IL-10 and IL-6. Graphs show box whiskers with median, interquartile ranges and outliers after background subtraction. Statistical significances between the indicated groups were obtained after Kruskal-Wallis and Mann-Whitney tests.

3.3.6 Circulating MF dampen TNF responses

The TNF production has been shown to be a feature of acute infection during human bancroftian filariasis [98] but intriguingly *in vitro* studies have implicated that the elicited TNF stems from the endosymbiotic bacteria and not the worm [157]. Therefore, stimulated PBMCs were investigated for the production of this cytokine. Strikingly, after stimulation with anti-CD3/anti-CD28, MSP-1 or LPS there was a significant suppression of TNF release from cells of MF^+ patients when compared to EN or the latent infected group (figure 3.26A, C and D). Upon stimulation with *B.m*. extract, significant differences could be detected between the two infected groups (figure 3.26B). These data highlight, that by dampening TNF responses, whether adaptive or innate, there is a potential benefit for the helminth since reduced responses to MF, either directly or indirectly, would enhance the chances for its survival and in essence completion of the life-cycle.

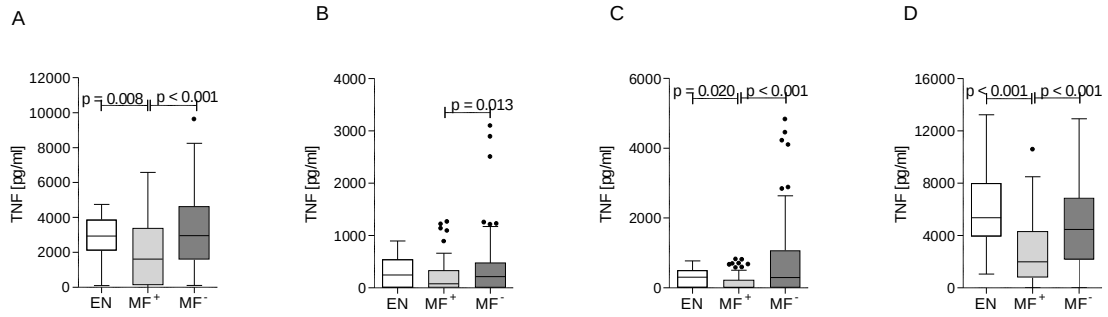

Figure 3.26. Circulating MF dampen release of TNF. Isolated PBMCs (2x 10^5/well) from EN or patients suffering from LF were stimulated with (A) anti-CD3/anti-CD28 (10 µg/ml; 2.5 µg/ml), (B), *B.m.* extract (5 µg/ml), (C) LPS (50 ng/ml) or with (D) MSP-1 (0.25 µg/m) for 72 hours. Thereafter, culture supernatant was tested via ELISA for cytokine release of TNF. Graphs show box whiskers with median, interquartile ranges and outliers after background subtraction. Statistical significances between the indicated groups were obtained after Kruskal-Wallis and Mann-Whitney tests.

3.3.7 Microfilariae stimulate IL-1β and IL-17 release from PBMCs of healthy donors

Since the results obtained above indicated that circulating MF are able to suppress cytokine responses, additional experiments with PBMCs from European blood donors were performed in order to investigate if the worm's offspring is competent in immunomodulating T cell dependent responses. Microfilariae from infected cotton rats were freshly isolated using a saccharose gradient as described in section 2.3.8.1. Furthermore, an antigen extract from adult *L. sigmodontis* worms was used in the same setup of experiments which was prepared as described in section 2.2.6. Cells from 13 different blood donors were incubated for 24 hours in the presence or absence of live MF (5,000/well) or *L.s.* extract (50 µg/ml) in order to mimic the situation of a patent or latent infection. Afterwards, cells were stimulated with anti-CD3/anti-CD28 (10 and 2.5 µg/ml respectively) for additional 72 hours.

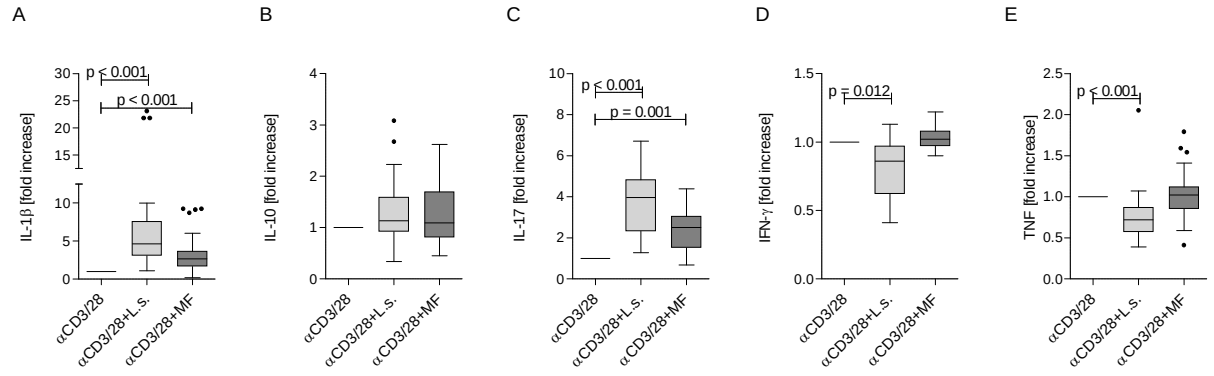

Figure 3.27. MF increase IL-1β and IL-17 secretion in PBMCs from healthy individuals. 2x 10^5 isolated PBMCs from healthy blood donors (n=13) were either left unstimulated or incubated with *L.s*. extract (50 μg/ml) or MF (5,000/well) for 24 hours followed by stimulated with anti-CD3/anti-CD28 (10 μg/ml; 2.5 μg/ml) for further 72 hours. Thereafter, culture supernatant was tested via ELISA for cytokine release of (A) IL-1β, (B) IL-10, (C) IL-17, (D) IFN-γ or (E) TNF. Cytokine data are depicted as fold increase over anti-CD3/anti-CD28 stimulation. Graphs show box whiskers with median, interquartile ranges and outliers. Statistical significances between the indicated groups were obtained after Kruskal-Wallis and Mann-Whitney tests.

Cytokine data are shown as fold increase over basal anti-CD3/anti-CD28 stimulation levels. As depicted in figure 3.27 the presence of MF was not sufficient to suppress anti-CD3/anti-CD28 induced cytokine responses. However, there was a significant up-regulation of IL-1β (figure 3.27A) and IL-17 (figure 3.27C) secretion when MF were used in combination with anti-CD3/anti-CD28. Interestingly, incubation with *L.s*. extract resulted in the same outcome concerning the production of IL-1β (figure 3.27A) and IL-17 (figure 3.27C) but in contrast reduced the levels of TNF significantly (figure 3.27E). Secreted levels of IL-10 were not significantly altered by MF or the *L.s.* extract (figure 3.27B) but the IFN-γ response was significantly decreased in presence of *L.s*. extract (figure 3.27 D). In summary, the initial presence of MF is not sufficient enough to induce strong immunosuppression in healthy donors.

3.3.8 Quantitative assessment of IgG and IgE levels

Alongside IL-5, elevated levels of IgE are a hallmark of helminth infection but as mentioned above most LF studies have focused on the comparison between patients with severe pathology and microfilaremic individuals. Since the cytokine levels of infected patients differed between the amicrofilaremic and microfilaremic individuals, concentrations of total IgG and total IgE were investigated to determine whether the presence of MF also modulates the humoral immune responses. Thus, levels of unspecific IgE and IgG subclasses from all study participants and from the uninfected volunteers were measured and compared (figure 3.28). Microfilaremic patients had significantly more IgE when compared to EN (figure 3.28A). In addition, these levels were also more pronounced when compared to the latent infected group (figure 3.28A). With regards to the IgG subclasses, no differences in levels of total IgG1 and IgG3 could be observed between individuals of any of the study groups (figure

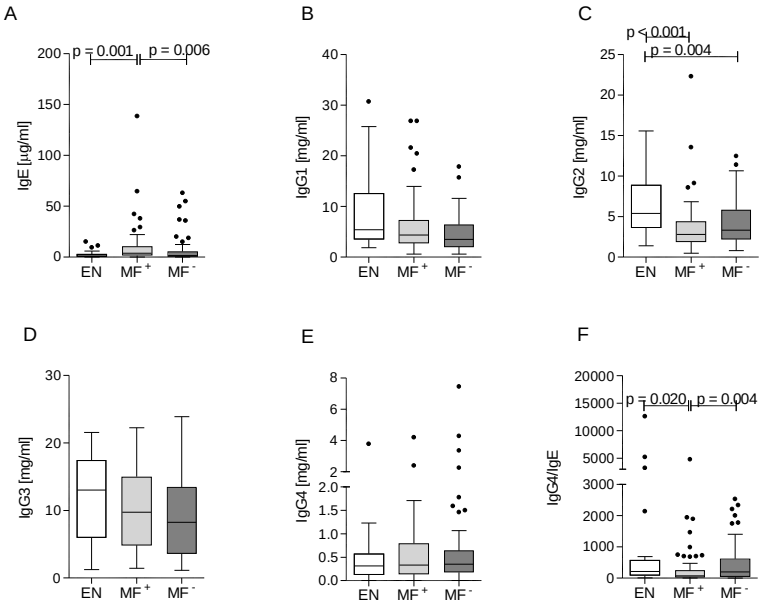

Figure 3.28. Patently infected individuals present elevated levels of total IgE. Plasma samples from all three groups were analysed for the production of total IgG1 (A), IgG2 (B), IgG3 (C), IgG4 (D) and IgE (E) with the Cytometric Bead Array. Figure 6G shows the ratio of IgG4 and IgE. Graphs show box whiskers with median, interquartile ranges and outliers. Statistical significances between the indicated groups were obtained after Kruskal-Wallis and Mann-Whitney tests.

3.28B and D). However, both patient groups showed a significant reduction of IgG2 when compared to EN (figure 3.28C). In addition, in comparison to amicrofilaremic individuals there was a decrease in IgG2 levels in the MF^+ patients albeit non significant (p = 0.058).No differences could be observed in the concentration of IgG4 (figure 3.28E) but the ratio of IgG4 and IgE was significantly reduced in the microfilaremic group when compared to MF^- and EN individuals (figure 3.28F).

3.3.9 MF^+ patients display a predominant antigen-specific IgG4 phenotype

Finally, individual patients were analysed for their helminth-specific IgG and IgE levels (figure 3.29). Determination of the absolute values of antigen-specific IgE and IgG subclasses revealed no significant differences between the patent and latent infected individuals (figure

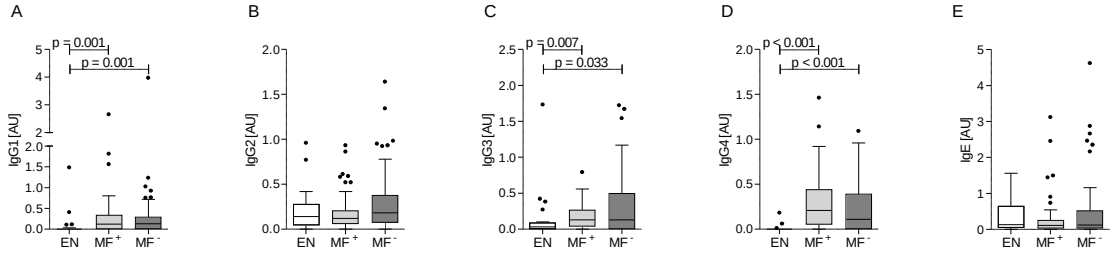

Figure 3.29. Infected individuals have higher levels of specific IgG1, IgG3 and IgG4 than EN. Plasma samples from all participants were investigated for the presence of helminth-specific immunoglobulins by ELISA. Plates were coated overnight with 5 µg/ml *B.m.* extract in PBS (pH = 9.6), incubated with patient and control plasma overnight and analysed for specific IgG1-4 and IgE. Data are depicted as absolute values expressed in arbitrary units [AU]. Graphs show box whiskers with median, interquartile ranges and outliers. Statistical significances between the indicated groups were obtained after Kruskal-Wallis and Mann-Whitney tests.

3.29A-E) but both patient groups were characterized by increased levels of IgG1 (figure 3.29A), IgG3 (figure 3.29C) and IgG4 (figure 3.29D) when compared to EN. Since IgG4 and IgE compete for the same binding sites, determining the ratio provides an indication about the pathophysiological conditions, that is, whether the antigen triggers an IgE mediated hypersensitivity response, or whether this response can be blocked by IgG4 [59]. Patients within the control group were characterized by having only background levels of specific helminth antibodies. In contrast to the data generated on the presence of total IgE and IgG4 (figure 3.28), MF^+ patients showed a dominant expression of helminth-specific IgG4 rather than IgE (figure 3.30D and E). In fact, ratios of antigen-specific IgG4/IgE, IgG4/IgG1, IgG4/IgG2 and IgG4/IgG3 (figure 3.30A-D) in the microfilaremic group were all significantly higher compared to the EN group. Significant differences between MF^+ and MF^- groups were found in the ratios of IgG4/IgE (figure 3.30A), IgG4/IgG2 (figure 3.30C) and IgG4/IgG3 (figure 3.30D). In summary, patently infected individuals display a strong expression of filarial-specific IgG4 indicating that circulating MF also influence B cell responses.

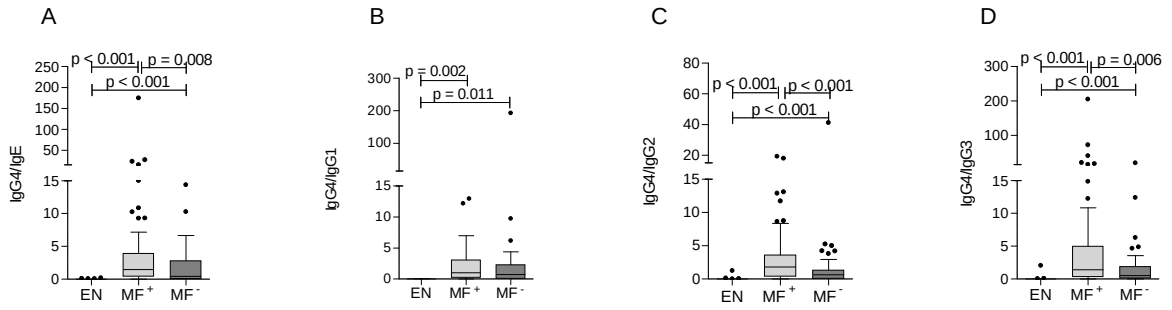

Figure 3.30. Patent infected patients produce more filarial-specific IgG4. Plasma samples from all participants were investigated for the presence of helminth-specific immunoglobulins by ELISA. Plates were coated overnight with 5 μg/ml *B.m.* extract in PBS (pH = 9.6), incubated with patient and control plasma overnight and analysed for specific IgG1-4 and IgE. A-D show the ratio of the antigen-specific antibodies IgG4/IgE (A), IgG4/IgG1 (B), IgG4/IgG2 (C) and IgG4/IgG3 (D). Graphs show box whiskers with median, interquartile ranges and outliers. Statistical significances between the indicated groups were obtained after Kruskal-Wallis and Mann-Whitney tests.

3.3.10 Elevated immune responses of MF^- patients are independent of age

Age has been shown to play a role with regards to cytokine production during filariasis [158] which was also seen within our LF study group, more precisely, an increase in age correlated with increased immune responses. Of note, age distribution was equal between the infected groups (figure 3.31). Therefore, a regression analysis was performed using age as a covariate and all data were log transformed [log (concentration+0.5)] to correct for skewness [159, 160]. Statistically correction for age did not change the overall results, that is, PBMCs from latently infected individuals had elevated levels of cytokines upon re-stimulation with various stimuli and also the results for the immunoglobulin responses stayed the same. An additional significant differences did become apparent in the scenario of IL-10 production following anti-CD3/anti-CD28 stimulation since MF^+ patients produced significantly less IL-10 when compared to MF^- individuals (p=0.005) which was in line with the statistical responses

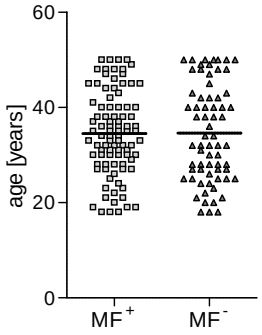

Figure 3.31. Equal age distribution amongst filarial-infected individuals. Age distribution amongst infected males was assessed. No significant differences could be observed. Symbols represent individuals within each group MF^+ (n=92) and MF^- (n=67).

observed with the other stimuli (figure 3.25B-D). The only variable for which we found an interaction between age and MF status was total IgG3 secretion: here increases in age correlated with elevated IgG3 in MF^- but less IgG3 in MF^+ patients still the latter group had more IgG3. All statistical outcomes remained the same if the 12 clinical hydrocele patients were removed from the analysis as with the exception of TNF secretion upon *B.m*. specific re-stimulation. Here however, the trend remained (data not shown).

3.3.11 Analysis of lymphangiogenesis factors

Previous studies have revealed that patients suffering from severe pathology have increased levels of vascular angiogenesis factors in their plasma and depletion of the endosymbiotic *Wolbachia* with doxycycline leads to a decrease of these factors [78, 79, 161] arguing for an association between the endosymbiont and these factors. Therefore, a comparative analysis of microfilaremic and amicrofilaremic individuals was performed in order to gain information about the status of VEGFs in these asymptomatic individuals. Plasma samples of both patient groups were investigated concerning their levels of VEGF-A, VEGF-C and soluble VEGF-R3 as described in sections 2.3.13 and 2.3.14. Figure 3.32 A-C demonstrates that there were no significant differences at all with regards to the levels of VEGF-A, VEGF-C and the soluble receptor VEGF-R3 indicating that these factors are not influenced by the presence of circulating MF. If these lymphangiogenesis factors were correlated with one

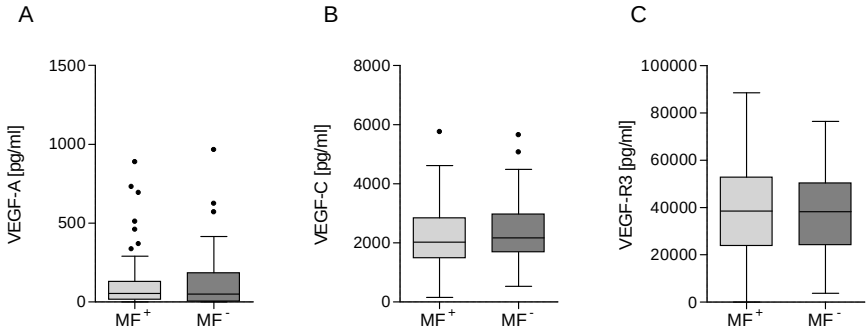

Figure 3.32. Lymphangiogenesis factors of infected individuals. Plasma samples from all participants were investigated for the presence of (A) VEGF-A, (B) VEGF-C and (C) VEGF-R3. Graphs show box whiskers with median, interquartile ranges and outliers. Statistical significances between both groups were tested with Mann-Whitney tests.

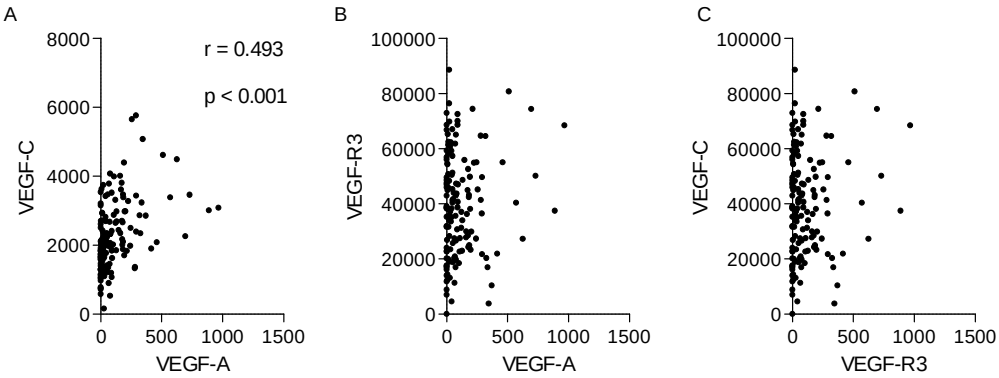

Figure 3.33. VEGF-A and VEGF-C correlate with each other. Lymphangiogenesis factors measured from plasma samples were correlated to one other. Analysis was performed using Spearman correlation test. Correlation coefficients r are only shown if p values were <0.05.

other (figure 3.33), there was only a significant positive correlation between VEGF-A and VEGF-C (figure 3.33A). Moreover, there were no correlations of any of these factors with the number of circulating MF and the number of worm nests (data not shown). However, VEGF-A correlated negatively with the maximal lymph dilation (figure 3.34A) in contrast to VEGF-R3 which correlated positively with this clinical parameter (figure 3.34C) if all infected individuals were analysed. If infected individuals were further subdivided into MF^+ and MF^-, there was a positive correlation between VEGF-R3 and the maximal dilation of lymphatic vessels and also with the dilation of lymph vessels at worm nests location (r= 0.215, p= 0.048; data not shown). Correlations between the levels of angiogenesis factors and rounds of IVM/ALB intake were only seen for MF^- with regards to VEGF-R3 (r= 0.317, p= 0.012, data not shown).

3.4 Lymphatic filariasis – post-treatment

The mutualistic association between *Wolbachia* and their filarial hosts has provided an alternative approach for novel chemotherapeutic strategies in filariasis. It has been shown in

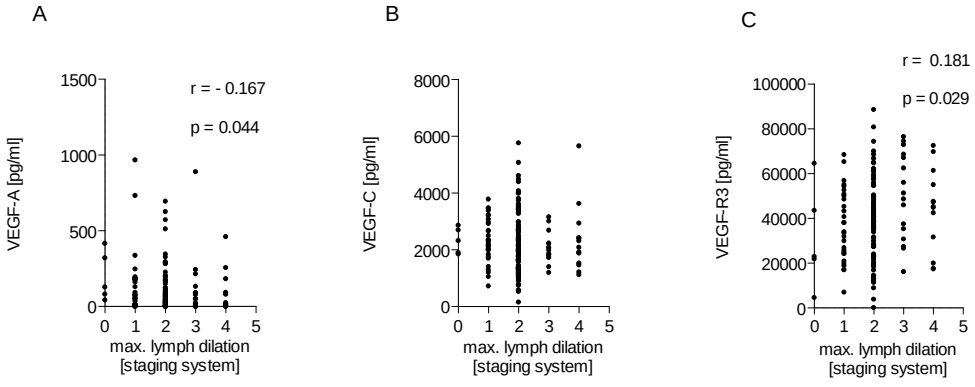

Figure 3.34. Correlation of lymphangiogenesis factors with clinical parameters. Lymphangiogenesis factors were correlated to the maximal dilation of lymphatic vessels. Analysis was performed using Spearman correlation test. Correlation coefficients r are only shown if p values were <0.05.

several field studies that treatment regimes of 3-8 weeks with doxycycline lead to elimination of MF, female filariae sterility (due to interruption of embryogenesis), inhibition of larval development and adult worm death indicating macrofilaricidal effects as well [137-139]. However, improvement to the therapy is still required in order to shorten the time span of treatment which would consequentially increase compliance. For example, experimental trials with the already registered antibiotic rifampicin have also shown good activity against *Wolbachia* in mice [143]. In addition, a preliminary study in humans revealed that treatment of onchocerciasis with rifampicin causes a significant reduction of *Wolbachia* [144] and furthermore a pilot study showed that the combination of doxycycline with rifampicin is effective in patients infected with *W. bancrofti* [129]. As a follow up to the study described in section 3.3, *W. bancrofti* infected patients were analysed 12 and 24 months post-treatment with regards to changes in their immunological profile. All patients were part of a registered clinical study and herewith treated with one of the seven mentioned treatment arms as described in section 2.3.15.

3.4.1 Reduction of microfilarial load 12 months post-treatment

All participants of the study received doxycycline, doxycycline in combination with rifampicin or placebo followed by a single dose of IVM/ALB four months later. Figure 3.35 shows a schematic overview of study participants that finished their treatment and those that were included in the cytokine analysis 12 months post-treatment. Treatment regimes were 200 mg doxycycline for 4 weeks (treatment 1), 100 mg for 5 weeks (treatment 2), 100 mg for 4 weeks (treatment 3) or a combination of doxycycline (200 mg) and rifampicin (10 mg per kg body

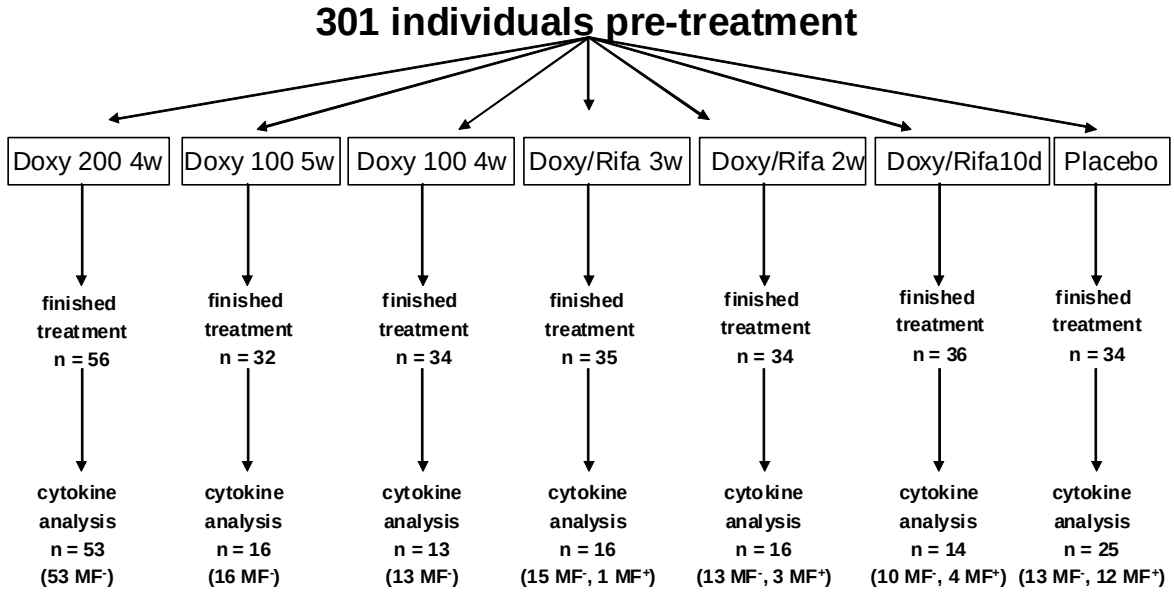

Figure 3.35. Schematic overview of patients included in cytokine analysis 12 months post-treatment. Scheme shows amount of participants that finished treatment and was included in cytokine analysis 12 months after treatment. Within each group the amount of MF^+ and MF^- individuals was further determined.

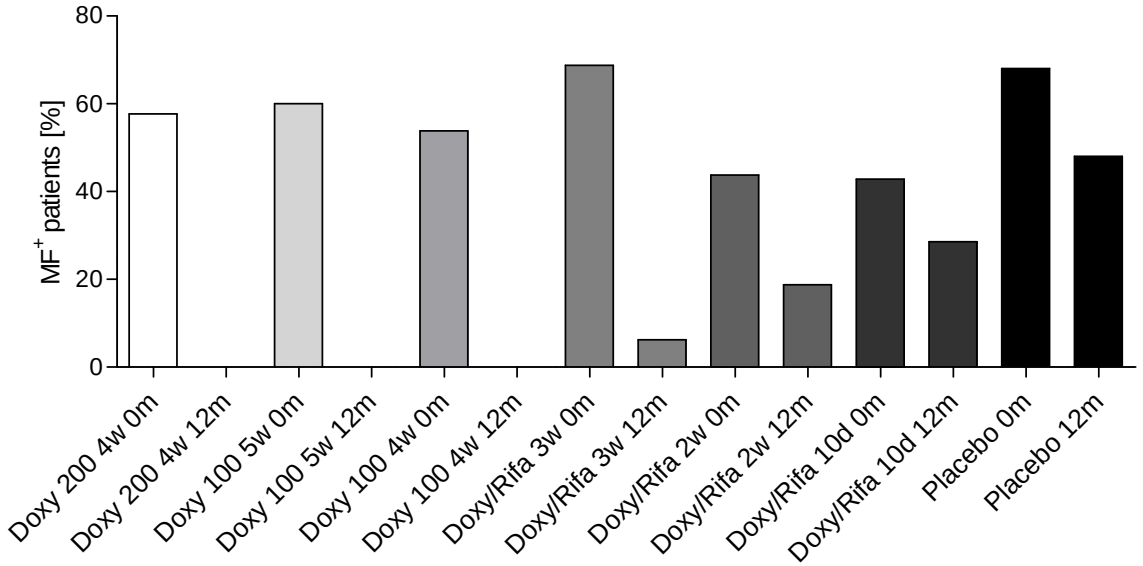

Figure 3.36. Microfilaremia 12 months after treatment of LF infected patients. Percentages of MF^+ *W. bancrofti* infected individuals were determined pre- (0 months) and post-treatment (12 months) and are depicted as bar graphs for each treatment arm and placebo for both time points.

weight) for either 3 weeks, 2 weeks or 10 days (treatment arms 4-6 respectively). Moreover, 34 patients were randomly allocated into the placebo group. 12 months post-treatment, blood was taken from each individual and analysed for microfilarial load as described in section 2.3.1.4. In addition, changes in cytokine profiles were assessed in culture supernatant obtained from PBMCs that were re-stimulated with filarial specific antigens, anti-CD3/anti-CD28, MSP-1 and LPS. These data are described in the following section.

With regards to MF load, treatment with doxycycline alone, regardless of duration or dose resulted in a complete loss of MF. In contrast, in treatment group of combined antibiotic therapy several patients were MF positive. Previous studies have documented that following IVM/ALB therapy MF reappear in 77% of infected patients after 12 months [162]. In order to demonstrate the efficacy of individual treatments, microfilaremia was calculated as percentages pre- and post-treatment as depicted in figure 3.36. Within the placebo group 12 out of 25 patients were found to be MF^+ reflecting 48.0% compared to 68.0% MF^+ individuals pre-treatment. However, comparing amounts of MF pre- and post-treatment those in 2009

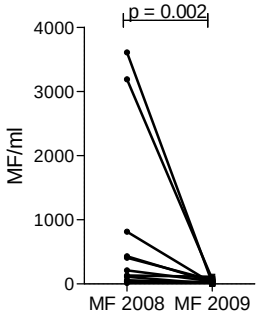

Figure 3.37. Reduction of microfilaremia. The amount of microfilaremia was compared within the MF^+ placebo group (n=12) 0 and 12 months post-treatment. Statistical significance between the indicated groups was obtained after Wilcoxon matched-pairs signed rank test.

were significantly reduced compared to levels before treatment as illustrated in figure 3.37. These data indicate that the treatment arms with doxycycline alone followed by a single dose of IVM/ALB were 100% microfilaricidal for a long time period. This was in contrast to the placebo treated group where MF reappeared within one year although all individuals took IVM/ALB four months after placebo intake.

3.4.2 Analysis of Th2 responses following doxycycline treatment

In order to discover the putative effects of the applied pharmaceuticals on the immunological profile, cell culture assays were performed as mentioned in section 2.3.9 with the same setup of stimuli. Results from the pre-treatment study demonstrated that cytokine profiles of patent and latent infected patients differed. More precisely, there was a general down-regulation of the immune responses in MF^+ patients. Thus, individuals of the placebo group were split according to their microfilarial status in 2009 (reflecting the time point 12 months post-treatment) at the time blood was taken and their responses were then compared to the differently treated participants. Following this analysis strategy, measurement of IL-5 and

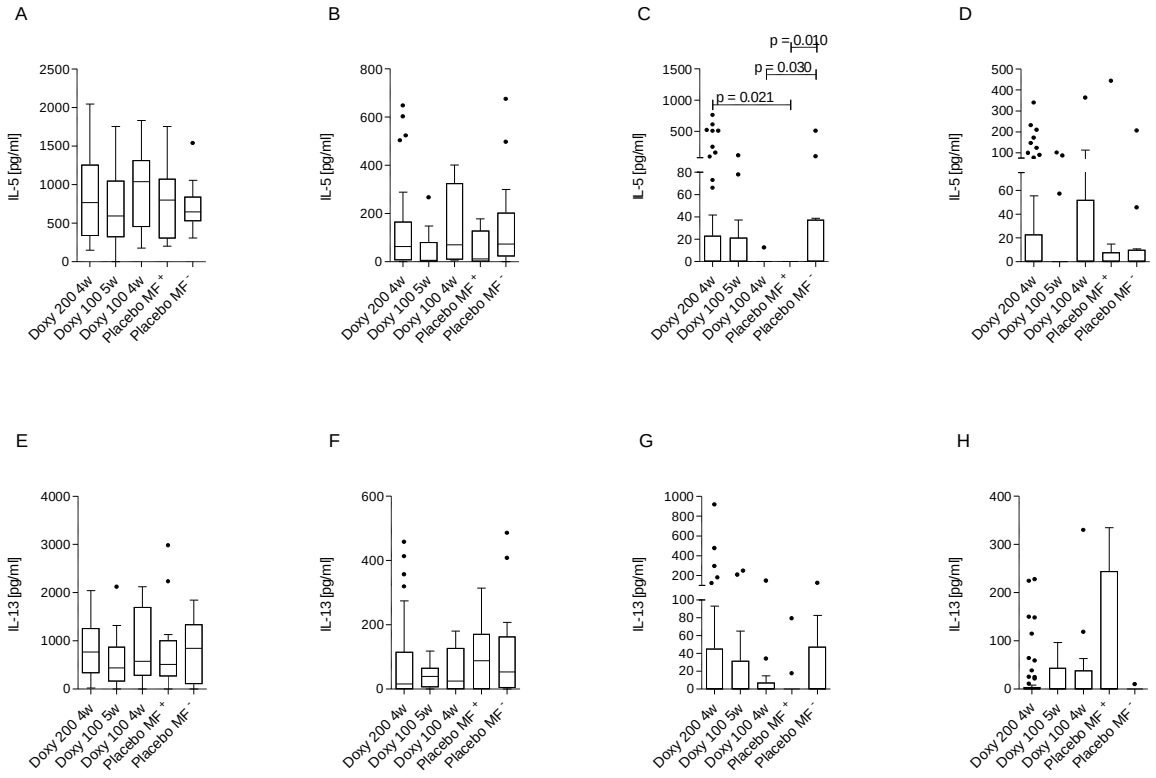

Figure 3.38. Influence of treatment on Th2 responses. Isolated PBMCs (2x 10^5/well) of doxycycline or placebo treated individuals were stimulated with either anti-CD3/anti-CD28 (10 µg/ml; 2.5 µg/ml; A and E), *B.m.* extract (5 µg/ml; B and F), MSP-1 (0.25 µg/ml; C and G) or LPS (50 ng/ml; D and H) for 72 hours. Thereafter, levels of IL-5 (A-D) or IL-13 (E-H) were measured in the culture supernatants via ELISA. Individuals of the placebo group were split according to their MF status at the time blood was taken. Different durations and concentrations of doxycycline intake are indicated in each graph. Graphs show box whiskers with median, interquartile ranges and outliers after background subtraction. Statistical significances between the indicated groups were obtained after Kruskal-Wallis and Mann-Whitney tests.

IL-13 (figure 3.38) did not reveal any significant differences between the different groups after stimulation with the T cell stimulus (figure 3.38A and E), the filarial-specific antigen (figure 3.38B and F) or LPS (figure 3.38D and H). Nevertheless, IL-5 secretion of PBMCs from individuals of the placebo group was decreased in MF^+ patients following stimulation with *B.m.* extract when compared to MF^- individuals (figure 3.38B), albeit not significant. These data confirmed the results from the pre-treatment study concerning IL-5 release (figure 3.23). Interestingly, IL-5 production was significantly increased in the first treatment group compared to the placebo MF^+ individuals (figure 3.38C) following MSP-1 stimulation and also MF^+ placebo treated individuals produced less IL-5 compared to amicrofilaremic placebo group (figure 3.38C).

3.4.3 Alteration of IFN-γ production following treatment

In addition to the Th2 immune responses described above, IFN-γ and IL-17 were also measured from the same cell culture supernatants (figure 3.39). Regarding the production of IL-17, there were no significant differences between the groups and this was independent of the applied stimulus (figure 3.39E-H).

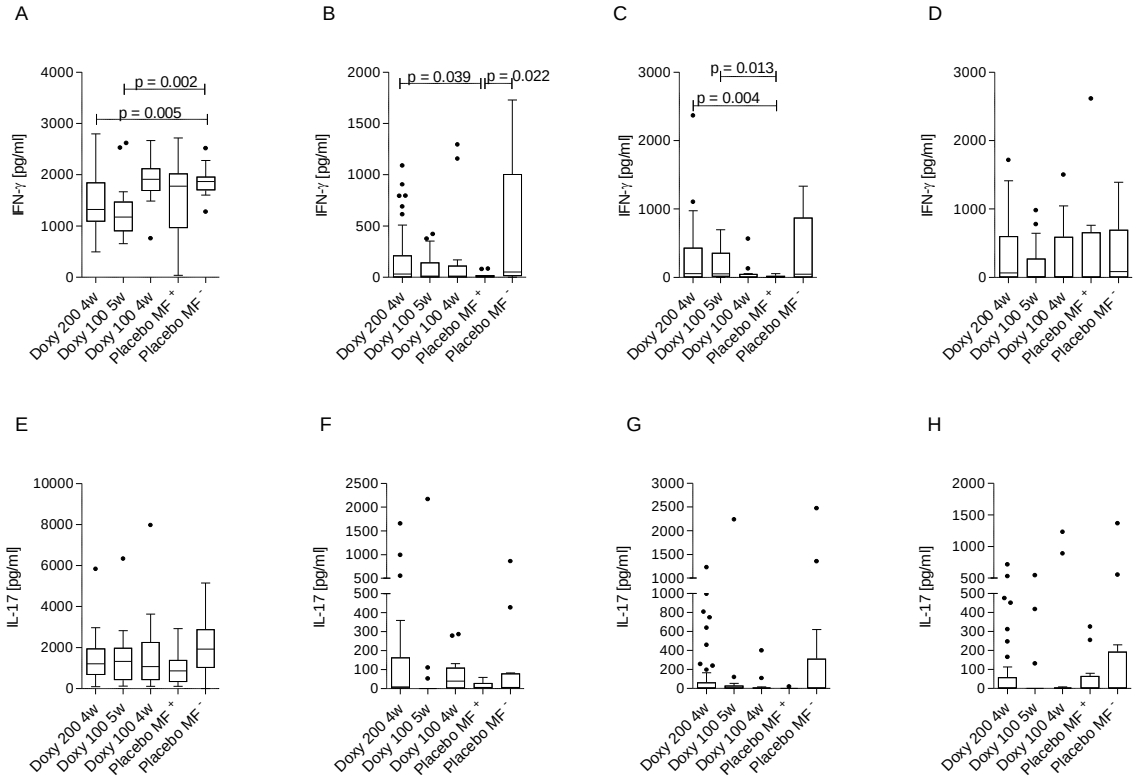

Figure 3.39. Doxycycline reduces T cell induced IFN-γ production. Isolated PBMCs (2x 10^5/well) of doxycycline or placebo treated individuals were stimulated with either anti-CD3/anti-CD28 (10 µg/ml; 2.5 µg/ml; A and E), *B.m.* extract (5 µg/ml; B and F), MSP-1 (0.25 µg/ml; C and G) or LPS (50 ng/ml; D and H) for 72 hours. Thereafter, levels of IFN-γ (A-D) or IL-17 (E-H) were measured in the culture supernatants via ELISA. Individuals of the placebo group were split according to their MF status at the time blood was taken. Different durations and concentrations of doxycycline intake are indicated in each graph. Graphs show box whiskers with median, interquartile ranges and outliers after background subtraction. Statistical significances between the indicated groups were obtained after Kruskal-Wallis and Mann-Whitney tests.

Secretion of IFN-γ was significantly reduced in the first and second treatment groups when compared to PBMCs from MF^- individuals in the placebo group. After stimulation with *B.m.* extract there was a significant increase of the IFN-γ production in the case of the first treatment group compared to the MF^+ placebo group and these patients also secrete less IFN-γ when compared to the MF^- patients (figure 3.39B). Furthermore, individuals of the first and second treatment group produced significantly more IFN-γ following MSP-1 stimulation compared to the MF^+ placebo group (figure 3.39C).

3.4.4 Doxycycline modulates T cell-specific IL-10 and IL-6 secretion

Supernatants from PBMC cultures of different treated individuals were investigated for the release of IL-10 and IL-6 (figure 3.40). Stimulation of PBMCs with anti-CD3/anti-CD28 resulted in significantly reduced levels of IL-10 in the second treatment group compared to the MF^- placebo treated individuals (figure 3.40A) whereas the production of IL-6 was increased compared to the microfilaremic placebo treated patients (figure 3.40E). Interestingly, MF^+ individuals produced less IL-6 and significantly less IL-10 than MF^- patients within the placebo group following T cell specific stimulation (figure 3.40A and E) which was

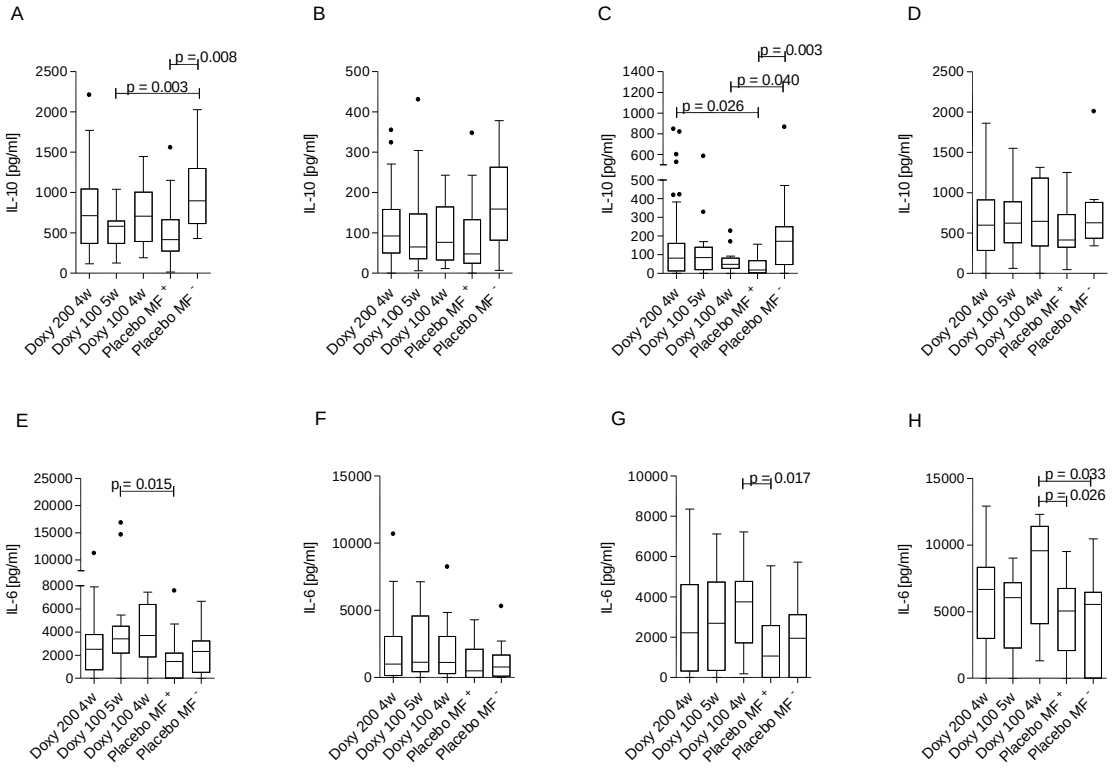

Figure 3.40. Doxycycline alters T cell induced IL-10 and IL-6 secretion. Isolated PBMCs (2x 10^5/well) of doxycycline or placebo treated individuals were stimulated with either anti-CD3/anti-CD28 (10 µg/ml; 2.5 µg/ml; A and E), *B.m.* extract (5 µg/ml; B and F), MSP-1 (0.25 µg/ml; C and G) or LPS (50 ng/ml; D and H) for 72 hours. Thereafter, levels of IL-10 (A-D) or IL-6 (E-H) were measured in the culture supernatants via ELISA. Individuals of the placebo group were split according to their MF status at the time blood was taken. Different durations and concentrations of doxycycline intake are indicated in each graph. Graphs show box whiskers with median, interquartile ranges and outliers after background subtraction. Statistical significances between the indicated groups were obtained after Kruskal-Wallis and Mann-Whitney tests.

in line with results from the pre-treatment study. Stimulation with *B.m*. extract and LPS did not induce significant differences between any of the indicated groups (figure 3.40B, D, F and H). With regards to stimulation with MSP-1 there was a significant down-regulation of IL-6 in the MF^+ patients when compared to the third treatment group and this stimulus did induce also a significantly higher IL-10 release in the MF^- placebo patients when compared to MF^+ individuals and the patients from the first and third treatment group (figure 3.40C).

3.4.5 Determination of TNF response following treatment

Finally, TNF was measured from the above mentioned supernatants (figure 3.41). In the pre-treatment study, TNF release from re-stimulated PBMCs of MF^+ individuals was strongly suppressed and this was independent of the stimuli (figure 3.26). Interestingly, when comparing responses of PBMCs isolated from MF^- and MF^+ individuals post IVM/ALB treatment, these suppressed responses were seen following treatment with all stimuli (figure 3.41 A-D), albeit only significantly for MSP-1 (figure 3.41C). With regards to the doxycycline groups, treatment 3 induced higher levels of TNF following stimulation with anti-CD3/anti-CD28 and LPS when compared to MF^+ individuals (figure 3.41A and D). Relating to MSP-1 stimulation, cells from the first treatment group showed also significantly higher levels of TNF when compared patent infected patients from the placebo group (figure 3.41C).

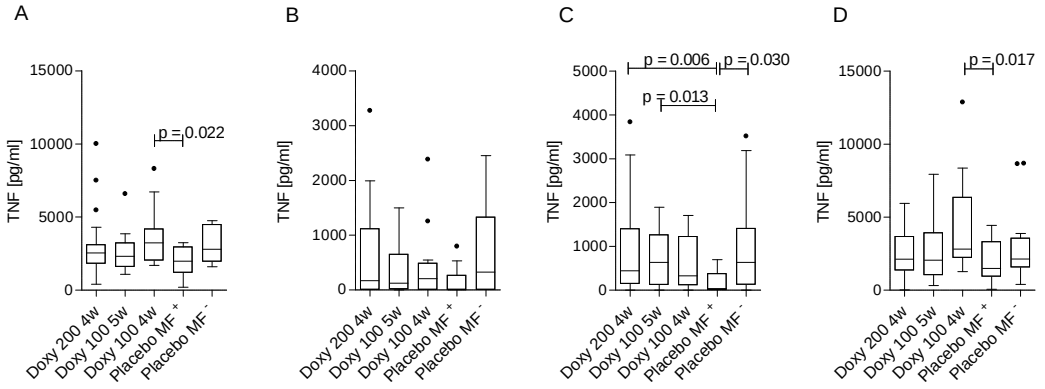

Figure 3.41. TNF production following doxycycline treatment. Isolated PBMCs (2x 10^5/well) of doxycycline or placebo treated individuals were stimulated with either (A) anti-CD3/anti-CD28 (10 µg/ml; 2.5 µg/ml), (B) *B.m.* extract (5 µg/ml), (C) MSP-1 (0.25 µg/ml) or (D) LPS (50 ng/ml) for 72 hours. Thereafter, levels of TNF were measured in the culture supernatants via ELISA. Individuals of the placebo group were split according to their MF status at the time blood was taken. Different durations and concentrations of doxycycline intake are indicated in each graph. Graphs show box whiskers with median, interquartile ranges and outliers after background subtraction. Statistical significances between the indicated groups were obtained after Kruskal-Wallis and Mann-Whitney tests.

3.4.6 Analysis of antigen-specific immunoglobulins 12 months post-treatment

One year after treatment plasma samples of included participants were analysed for antigen-specific Igs as described in section 2.3.12. As can be seen from the absolute values in figure 3.42 there were no significant differences between the indicated groups. In addition, even the ratios of IgG4 to IgE (figure 3.43A) and to the other Ig subclasses (figure 3.43B-D) did not

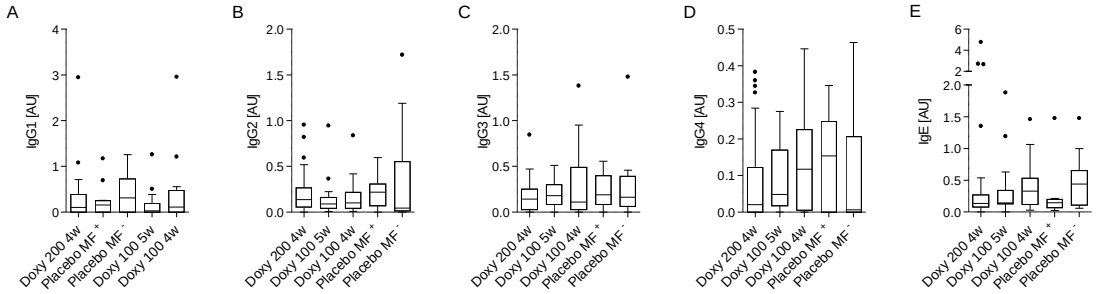

Figure 3.42. Specific Ig levels following doxycycline treatment. Plasma samples of doxycycline or placebo treated individuals were investigated for the presence of filarial-specific Igs by ELISA 12 months after treatment. Plates were coated overnight with 5 μg/ml *B.m.* extract in PBS (pH = 9.6), incubated with patient and control plasma overnight and analysed for specific IgG1-4 and IgE. Data are depicted as absolute values expressed in arbitrary units [AU]. Individuals of the placebo group were split according to their MF status at the time blood was taken. Graphs show box whiskers with median, interquartile range and outliers. Statistical significances between the indicated groups were analysed using Kruskal-Wallis and Mann-Whitney tests.

show any significant differences. However, levels of IgE were lower in MF^+ compared to MF^- placebo treated individuals (figure 3.42E) which was further reflected in a higher ratio of IgG4 to IgE (figure 3.43A), albeit not significantly. These data were again in line with results from the pre-treatment study concerning MF^+ and MF^- patients but indicate also that treatment had no significant influence on Ig levels 12 months post-treatment.

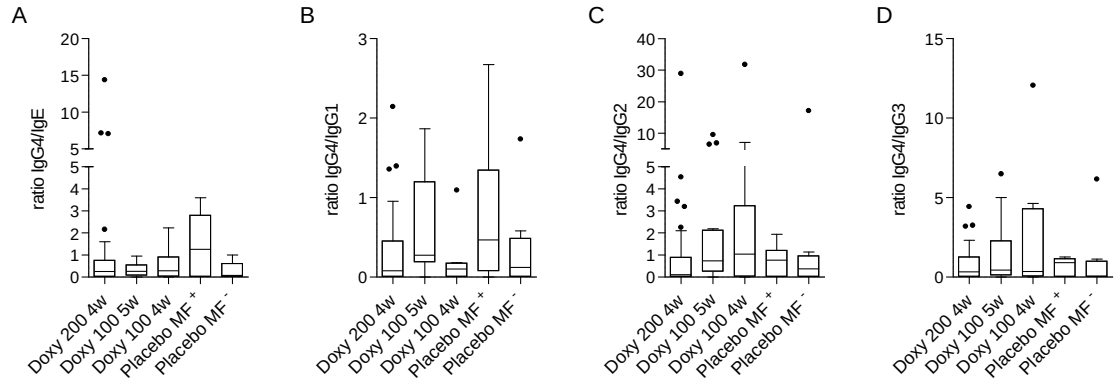

Figure 3.43. Ratios of filarial-specific Igs are not significantly altered 12 months after treatment. Plasma samples of doxycycline or placebo treated individuals were investigated for the presence of filarial-specific Igs by ELISA 12 months after treatment. Plates were coated overnight with 5 μg/ml *B.m.* extract in PBS (pH = 9.6), incubated with patient and control plasma overnight and analysed for specific IgG1-4 and IgE. Figures A-D show the ratio of the antigen-specific antibodies IgG4/IgE (A), IgG4/IgG1 (B), IgG4/IgG2 (C) and IgG4/IgG3 (D). Individuals of the placebo group were split according to their MF status at the time blood was taken. Graphs show box whiskers with median, interquartile ranges and outliers. Statistical significances between the indicated groups were analysed using Kruskal-Wallis and Mann-Whitney tests.

3.4.7 Microfilaremia 24 months post-treatment

In order to determine long-term effects of the different applied treatment arms, participants were analysed 24 months after treatment with regards to their antigen-specific Ig levels as described in section 2.3.12. Figure 3.44 shows a schematic overview of those patients that completed treatment and were included in Ig analysis two years later.

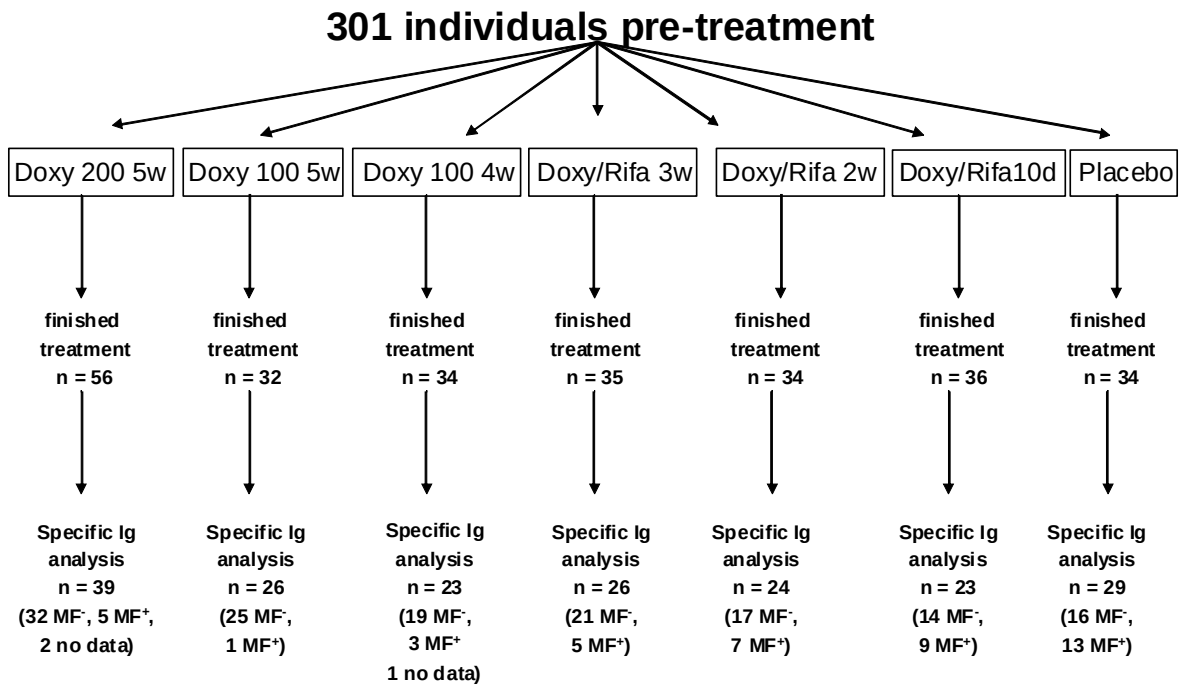

Figure 3.44. Schematic overview of patients included in immunoglobulin analysis 24 months post-treatment. Scheme shows amount of participants that finished treatment and was included in Ig analysis 24 months after treatment. Within each group the numbers of MF^+ and MF^- individuals were further determined.

Furthermore, microfilaremia was again evaluated and calculated as percentages for each individual treatment arm. As can be seen in figure 3.45 treatment group 2 had the longest microfilaricidal effect, whereas in all other treatment arms more MF were detected indicating that a longer treatment is required to achieve long term effects concerning the depletion of circulating MF and that a lower dose of 100 mg is also efficient.

Analysis of the absolute values of Igs revealed that patients treated with 100 mg doxycycline for 5 weeks had significantly lower levels of specific IgG1 compared to both placebo groups

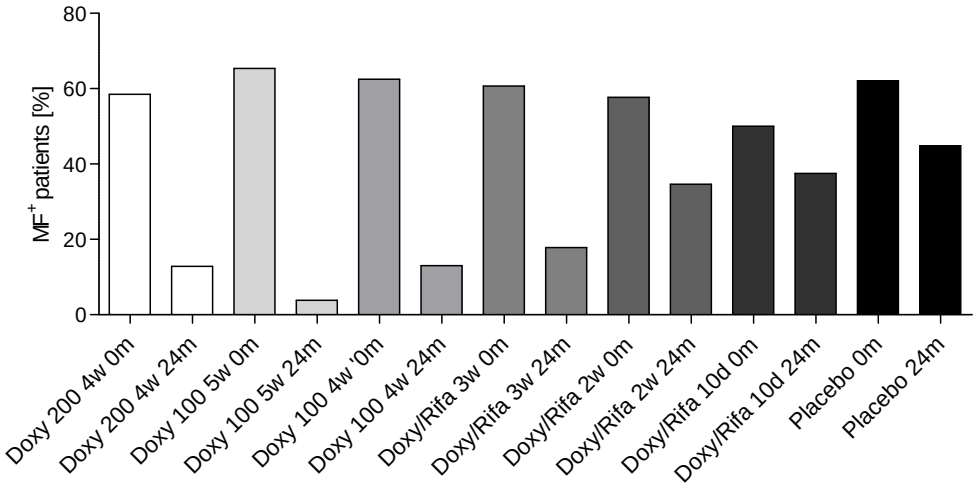

Figure 3.45. Microfilaremia 24 months after treatment of LF infected patients. Percentages of MF^+ *W. bancrofti* infected individuals were determined pre- (0 months) and post-treatment (24 months) and are depicted as bar graphs for each treatment arm and placebo for both time points.

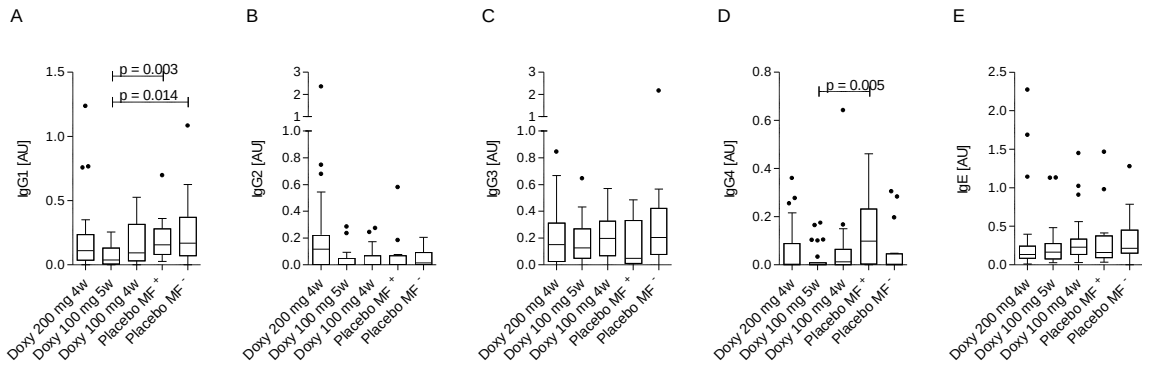

Figure 3.46. Reduction of antigen-specific IgG1 levels 24 months after treatment. Plasma samples of doxycycline or placebo treated individuals were investigated for the presence of helminth-specific Igs by ELISA 24 months after treatment. Plates were coated overnight with 5 μg/ml *B.m.* extract in PBS (pH = 9.6), incubated with patient and control plasma overnight and analysed for specific IgG1-4 and IgE. Data are depicted as absolute values expressed in arbitrary units [AU]. Individuals of the placebo group were split according to their MF status at the time blood was taken. Graphs show box whiskers with median, interquartile ranges and outliers. Statistical significances between the indicated groups were obtained after Kruskal-Wallis and Mann-Whitney tests.

(figure 3.46A) and decreased amounts of specific IgG4 compared to the MF^+ placebo treated individuals (figure 3.46D). With regards to the ratios of IgG4 to the other subclasses, there were significant lower ratios of IgG4/IgE (figure 3.47A), IgG4/IgG1 (figure 3.47B) and IgG4/IgG3 (figure 3.47D) in the second treatment group when compared to the MF^+ placebo patients. Interestingly, the difference in the IgG4/IgE ratio between MF^+ and MF^- was seen in the pre-treatment study and also 12 months later whereas the significant up-regulated IgG4/IgG1 ratio between both placebo groups observed here was not seen in the pre-treatment data.

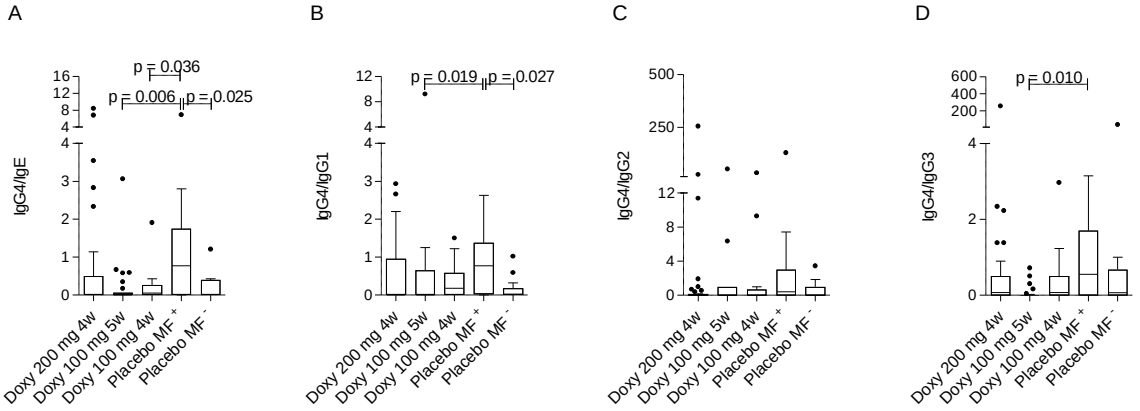

Figure 3.47. Ratios of IgG4/IgE and IgG4/IgG3 are modulated by doxycycline treatment. Plasma samples of doxycycline or placebo treated individuals were investigated for the presence of helminth-specific Igs by ELISA 24 months after treatment. Plates were coated overnight with 5 μg/ml *B.m.* extract in PBS (pH = 9.6), incubated with patient and control plasma overnight and analysed for specific IgG1-4 and IgE. A-D show the ratio of the antigen-specific antibodies IgG4/IgE (A), IgG4/IgG1 (B), IgG4/IgG2 (C) and IgG4/IgG3 (D). Graphs show box whiskers with median, interquartile ranges and outliers. Statistical significances between the indicated groups were analysed using Kruskal-Wallis and Mann-Whitney tests.

3.5 Gene expression in T cells of *W. bancrofti* patients and endemic individuals

In order to obtain more in-depth information about differentially expressed genes in *W. bancrofti* infected individuals, distinct T cell subpopulations from EN, patent or latent infected individuals were sorted and analysed with a microarray. The FACS sorting was performed with the MoFlo cell sorter in the core facility at the Technical University in Munich. Cells were stained with anti-CD4, anti-CD25 and anti-CD8 as described in section 2.3.7.1.

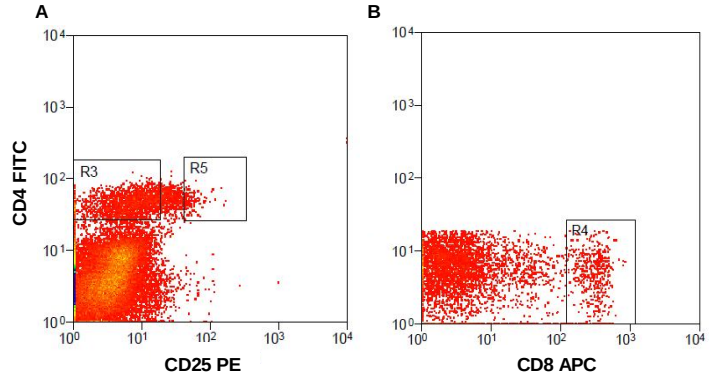

Figure 3.48. Gating strategy of sorted $CD4^+CD25^{high}$, $CD4^+CD25^-$ and $CD8^+$ T cells. Cells of EN, MF^+ or MF^- individuals were stained with αCD4 FITC, αCD25 PE and αCD8 APC antibodies and sorted using the MoFlo sorter. Graphs show representative gating strategy for each subpopulation: R3 depicts $CD4^+CD25^-$ T effector cells, R5 $CD4^+CD25^+$ Tregs and R4 $CD8^+$ T cells.

Figure 3.48 depicts the gating strategy for each subpopulation of T cells and is representative of one participant. PBMC samples contained a maximum of 5x 10^6 cells and sorted cell populations ranged between 5x 10^3 and 5x 10^4 for Treg populations, 3x 10^3 and 4x 10^5 for $CD4^+CD25^-$ populations and 4x 10^3 to 5x 10^5 for $CD8^+$ T cells. Afterwards, sorted cells were resuspended in 1 ml Trizol and frozen at -80°C.

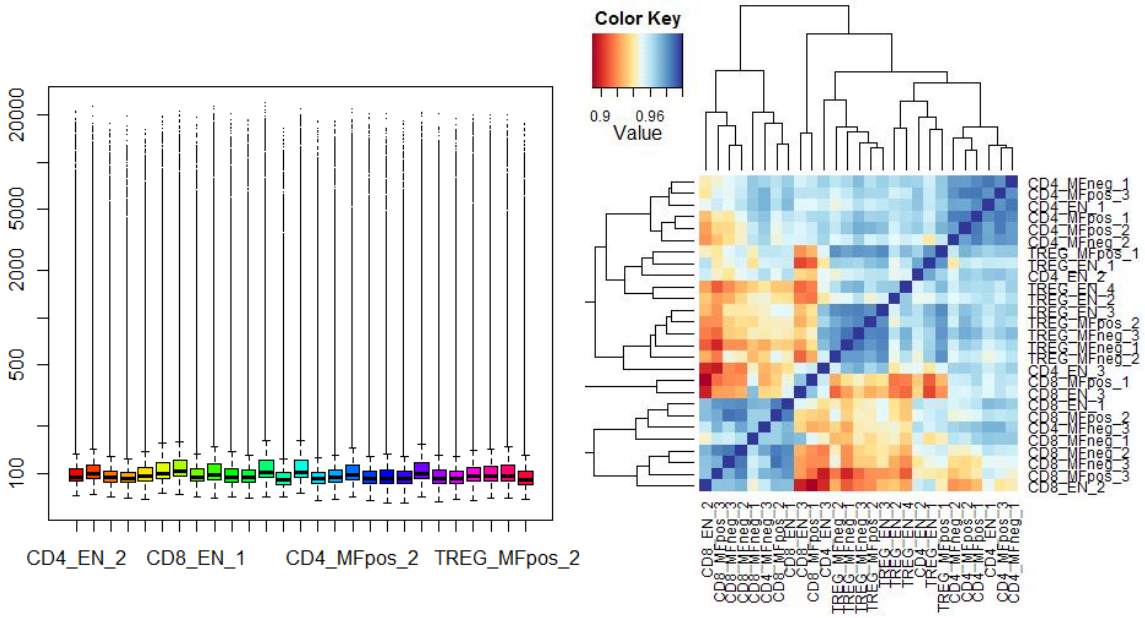

Figure 3.49. Quality control box plots and quality correlations (quantile data) of sorted T cell subpopulations. Box plots on the left side show the fluorescence intensity of each sample before quantile normalization was performed (depicted is the median, 25 and 75% percentile). The heat map on the right side depicts correlations (Pearson) of all used samples after performing quantile normalization. Courtesy of Dr. Svenja Debey-Pascher.

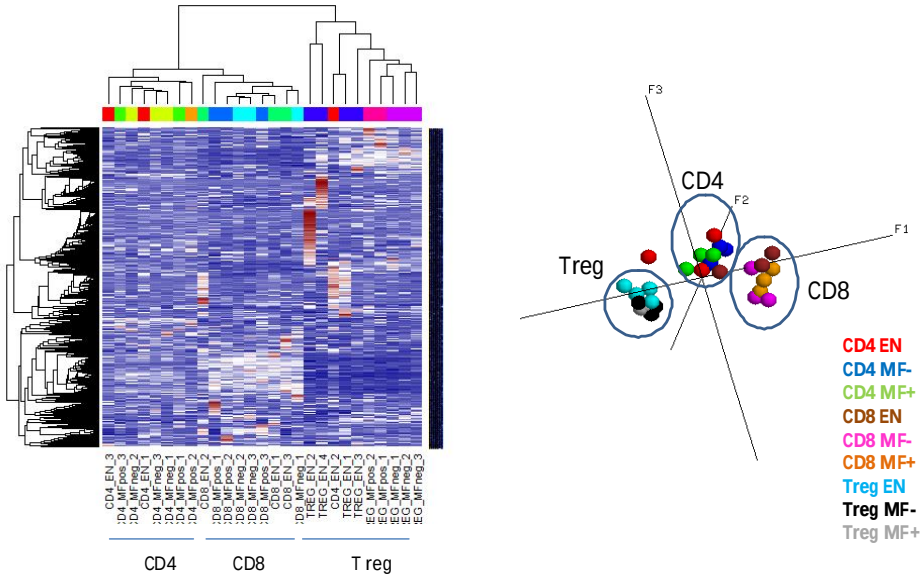

Figure 3.50. Cluster and PCA variable genes (n = 820). Hierarchical clustering (left side) and principal component analysis (right sides) were performed on quantile normalized data using the most variable genes in the dataset. Courtesy of Dr. Svenja Debey-Pascher.

RNA extraction was performed in the LIMES institute in Bonn as mentioned in section 2.3.20. Due to the small cell number extracted RNA amounts were to low for microarray analysis and were therefore amplified with an amplification kit as described in section 2.3.22. Determination of differentially expressed genes was performed using an Illumina microarray (HT12V4 Array, containing 47.231 probes) and analysis was conducted by Dr. Debey-Pascher, Genomics and immunoregulation, LIMES Institute Universität Bonn (working group Prof. Joachim Schultze; see figures 3.49 and 3.50).

$CD4^+$ T effector cells ($CD4^+CD25^-$) of 3 individuals per group (EN, patent and latent infected individuals) were analysed with the Illumina microarray as described in section 2.3.26. The same amount of samples was determined with regards to $CD8^+$ T cells. For Tregs ($CD4^+CD25^{high}$) 5 samples of infected individuals (2 MF^+ and 3 MF^-) and 4 probes from EN were determined. Signal intensities of all tested samples were within the normal range arguing for a sufficient control of the probes (figure 3.49 and 3.50). To identify differentially regulated genes within the three cell populations, a combination of filtering for absolute (max-min 100) and relative (max/min 1.5) changes in average expression signals across all conditions, and statistical testing (t-test) was applied. The amounts of differentially expressed genes within each cell population are depicted in table 3.3. Concerning the expression profiles in Tregs when comparing all infected patients versus EN, there were actually only 68 genes that were differentially expressed. Within this list of 68 genes, 13 were down- and 55 were up-regulated in the infected group (e.g. the STAT1 gene). Upon closer inspection 191 genes were differentially expressed between MF^+ and EN (57 down- and 134 up-regulated). These included genes such as C-C chemokine receptor type 3 (CCR3), CD84, and STAT1. Similar amount of genes (194) were differentially regulated when comparing amicrofilaremic

and microfilaremic patients (86 down- and 108 up-regulated). Here, major histocompatibility complex, class II, DQ beta 1 (HLA-DQR) and nucleotide-binding oligomerization domain containing 1 (Nod1) were up-regulated genes whilst CD83 was one of the most strong down-regulated genes. When comparing MF^- and EN, there was almost a 50% reduction in the number of regulated genes (106), of which 29 were down- and 77 up-regulated. With regards to the effector $CD4^+$ T cells, comparison of the EN and the infected groups revealed 100 differentially expressed genes (34 down- and 66 up-regulated, e.g. lymphocyte transmembrane adaptor 1 (LAX1), VEGF-B, caspase 3) whereas patent infected individuals had 184 genes that were differentially regulated compared to EN (64 down- and 120 up-regulated). Amicrofilaremic patients had 99 genes that were distinct from EN (40 down- and 59 up-regulated) and the two infected groups were diverse in reference to 90 genes (40 were down-regulated in MF^- individuals and 50 up-regulated, e.g. IL-15). Finally, with regards to the $CD8^+$ T cell populations, all three groups had differences in their gene expression. Disparity involved only 41 genes between the infected and the EN individuals (17 down- and 24 up-regulated) and here superoxide dismutase 2 (SOD2), serum/glucocorticoid regulated kinase (SGK) and Krueppel-like factor 4 (KLF4) were the most prominently down-regulated genes in the former group. Amongst the groups, 69 genes were regulated between MF^+ and EN (37 down- and 32 up-regulated), 78 genes between MF^- and EN (42 down- and 36 up-regulated) and finally also 78 genes between the latent and patent infected patients (31 down- and 47 up-regulated). These data reveal that not only immunological profiles but also gene expression levels are altered depending on the infectious state of the patient. With regards to $CD8^+$ T cells, apoptosis-associated genes like B-cell lymphoma 6 protein (Bcl-6), inhibitor of growth 2 (ING2) and SUMO1/sentrin specific peptidase 5 (SENP5) are interesting candidates for further research since apoptosis was already linked to filariasis beforehand. From these up- and downregulated genes we have begun to cheery pick the most relevant and interesting genes for further investigation. These genes cover the field of cytokines (e.g. IL-10 receptor β, TGF-β receptor, IL-15), apoptosis (e.g. BCL-6, SGK), tumor necrosis factor (ligand) superfamily member 10 (TRAIL)), immune regulation (e.g. CD83), effector function (e.g. CXCR4) and cell signaling (e.g. STAT1). The functional relevance of these genes with regards to filarial infection is discussed in more detail in the following section.

	$CD4^+CD25^+$	**$CD4^+CD25^-$**	**$CD8^+$**
Infected versus EN	68	100	41
MF^+ versus EN	191	184	69
MF^- versus EN	106	99	78
MF^+ versus MF^-	194	90	78

Table 3.3. Overview of regulated genes within all T cell subpopulations.

4. Discussion

Onchocerciasis and LF are neglected diseases in tropical regions and affect more than 150 million people. Moreover, 1.3 billion people are estimated to be at risk of infection [3, 131]. These impressive numbers highlight the impact of both diseases and why they are considered major health problems with socioeconomic consequences. Although filarial infections are well established as tropical helminth diseases there are still many unresolved questions about the immunological processes that drive pathology. Both filarial species are renowned for their ability to immunomodulate the host's immune system to ensure reproduction and long-term survival which accounts for the asymptomatic form of infection. Nevertheless, severe pathology can occur in the form of visual impairment, blindness, acute and chronic skin disease in onchocerciasis [5] and as hydrocele, lymphedema or elephantiasis and others in LF [74]. Since the two major poles of infections are reflected by asymptomatic infections and severe pathology, most previous studies focused on the comparison of hyperreactive and asymptomatic individuals or sometimes on the assessment of immunological responses in patent infected patients versus EN. However, an in-depth analysis on the possible differences between MF^+ and MF^- infected patients in both infections has never been performed and was therefore a primary objective of this thesis. Data obtained over the last few years have revealed that MF^+ and MF^- LF and onchocerciasis patients can be identified by distinct immunological profiles with regards to cytokine release and Ig levels. Moreover, in the case of LF infection further characterisation was obtained on a genetic level. In general, these results showed that the degree of immunomodulation was differently regulated between both filarial diseases.

4.1 Interplay between MF status and pathology

As mentioned above, an in-depth analysis of immune responses in MF^- individuals has not been previously addressed. Actually MF^- *O. volvulus* infected individuals have been a neglected cohort because of the difficulties to identify these patients due to the lack of an available antigen test and determination of nodules by palpation requires experienced medical training. In contrast, a conclusive determination of the infection status in LF can be achieved through the rapid card test [115, 116]. Nevertheless, up to the studies performed in this thesis this latent LF patient group was also neglected. These MF^- patients are of considerable interest because they represent a dead end in parasite transmission and preventing the completion of the lifecycle is one of the main goals of programmes like the APOC and GPELF.

Analyzing the pathological aspects in both diseases revealed that asymptomatic MF^+ patients had higher parasite burden since the presented either increased amounts of nodules

and nodule sites or a higher number of scrotal worm nests. In contrast, in LF lymph dilation at either the worm nest location or maximal lymph dilation according to the staging system employed did not reveal any significant differences between latent and patent infected individuals. Interestingly, EN also possessed a certain degree of lymph dilation. Since there remains no available data for the spread of lymph dilation in non-endemic normals or healthy Europeans, it is difficult to conclude if these EN have already enlarged lymph vessels or if this represents the normal physiological situation.

In line with this aspect was the observation that a certain percentage of individuals in the LF study possessed hydroceles which was also determined via ultrasonography. Hydroceles are a common manifestation in man with bancroftian filariasis infection and can be graded according to their developmental stage and size. In contrast to scrotal palpation, ultrasonography allows the detection of both subclinical (stage 1-2) and clinical (stage 3-4) manifestations [163]. Ultrasound studies have shown that many males in endemic areas with normal clinical examinations have subclinical hydroceles that can be asymptomatic [164-166]. Patients with severe pathology are usually characterized by the absence of adult worms, but patients within this study all possessed adult filariae. Interestingly, our results showed that the presence of hydrocele did not influence the outcome of dampened responses in the patently LF infected group, indicating that these two separate pathological outcomes can influence the immune responses in a different manner. Therefore, we conclude that the presence of MF is more important to influence the immunological profile than the hydrocele status which is line with previous publications [167].

Nevertheless, further associations between the presence of MF and pathology were reflected by the positive correlation of MF load and the number of sites and nodules in *O. volvulus* infected persons and between MF and the amount of worm nests in LF patients. The application of ultrasonography has already shown a positive association of FDS with the amount of circulating MF in *W. bancrofti* infected individuals from Brazil [168]. However, no data have been accumulated regarding this aspect in endemic areas of Africa. In general, these findings indicate that although patently infected individuals have obviously more worms that are competing for the same ecological niches, there is still efficient down-modulation of the immune system since they did not suffer from severe pathology like lymphedema or symptomatic hydrocele. This is in accordance with previous findings describing that immunosuppression rises with parasite burden [25]. Interestingly, there was a negative correlation between the amount of MDA intake and the amount of MF in *O. volvulus* infected patients but this was not observed in LF infected individuals. This negative correlation in onchocerciasis patients indicates that MF^- infected individuals were not “latently” infected as seen in LF but that MF levels had not recovered from previous IVM treatments and this was already described in earlier studies [16]. However, this scenario could be ruled out for

individuals of the LF study since patients were only included if they had not received MDA during the least 10 months and previous studies described that following such therapy MF reappear after 12 months in 77% of *W. bancrofti* infected patients [162].

4.2 Are cytokine profiles of onchocerciasis and lymphatic filariasis infected individuals really comparable?

Although both *O. volvulus* and *W. bancrofti* belong to filariae and share some general features, results described within this thesis show that there are major differences between both diseases with regards to the immunological profiles of MF^+ and MF^- individuals. Clearance of helminth infections is mediated by Th2 cells and includes cytokines like IL-3, IL-4, IL-5, IL-9, IL-10, IL-13, the presence of IgG1, IgG4 and IgE, and expanded cell populations such as eosinophils, basophils and mast cells [20]. IL-5 is considered to be a hallmark of helminth infections [169] and moreover, IL-5 induces eosinophils and also IgE [170]. Therefore, it was interesting to compare the level of IL-5 in both infection scenarios and between patent and MF^- infected individuals. Interleukin-5 was significantly down-regulated following filarial-specific stimulation of cells from patent infected individuals when compared to the MF^- group in both diseases (see table 4.1). This was in contrast to a previous publication of Dimock *et al* [105] but in line with *in vivo* studies using the murine model of filariasis which showed that infected IL-5 deficient mice possessed higher levels of MF [171, 172]. Moreover, a human study revealed that IL-5 was negatively correlated with the amount of MF in *O. volvulus* infected individuals [29]. Interestingly, *O. volvulus* infected patent patients also produced significantly less IL-5 in response to an extract from *B.m*. females which could possibly be explained through cross-reactivity due to the close ancestral relationship between both filarial species. If levels of MF in *O. volvulus* infected individuals were correlated to IL-5 secretion following stimulation with *O.v*. extract or *B.m*. female extract, there was a significant negative correlation for both stimulation scenarios. This indicates that rising levels of MF induce down-regulation of IL-5 which can be detrimental to the parasite but also to the host itself due to the induction of eosinophils and also IgE which are both associated with pathology [170]. Although such negative correlation could not be confirmed between the amount of MF and secreted levels of IL-5 in LF, it could be shown that microfilaremic individuals produced less IL-5. However, reduced levels of the Th2 cytokine IL-5 in patently infected patients was not reflected in IL-13 secretion since there were no significant differences between both infected groups with regards to both diseases. Reports have described that PI individuals in *O. volvulus* endemic areas have a strong Th1/Th2 mixed response. For example, when compared with those from GEO patients, both IFN-γ and IL-5 production in response to filarial-specific stimulation are readily detected and such profiles are thought to prevent establishment of active infection [13, 24, 57].

	W. bancrofti	*O. volvulus*
IL-5	↓	↓
IL-13	-	-
IL-10	↓	↑
IL-17	-	-
IL-6	(↓)	-
TNF	↓	-
IFN-γ	-	-

Table 4.1. Cytokine secretion from PBMCs of MF^+ infected individuals following stimulation of filarial specific antigen in comparison to MF^- individuals.

However, the results described here do not confirm these data since Th1 responses (assessed through IFN-γ production) by PBMCs were similar for all three groups following antigen-specific stimulation. Stimulation with anti-CD3/anti-CD28 or PPD did also not result in any significant differences between the compared groups in the onchocerciasis cohort and this is in line with previous results [23]. Nonetheless, when compared to EN, IFN-γ secretion was significantly increased in both *O. volvulus* infected groups following MSP-1 stimulation and also in response to LPS in the case of MF^+ individuals. In general, PBMCs from EN of the onchocerciasis study were characterized by lower cytokine secretion with regards to Th1 and Th2 independent of the applied stimulus. Differences in results compared to those presented in previous publications could be explained by the use of varying experimental setups including different batches of antigen in varying concentrations, analysis of individuals from different genetic backgrounds or belonging to different endemic areas [15, 56, 57, 173, 174]. Secretion of IFN-γ from LF infected patients was not detectable for any of the tested stimuli except direct T cell activation, which showed that microfilaremic patients produced less IFN-γ than latent infected individuals, albeit insignificantly.

4.3 MF presence alters IgG4 and IL-10 levels

Beside cytokines, Igs are also valuable tools in deciphering immunological processes since antibodies play an important role in the progress of parasite infections. In general, depending on the Ig subtype they can promote different functional mechanisms like opsonisation, neutralization of toxins, complement activation and antibody dependent cell-mediated cytotoxicity. In helminth infections and allergy, high levels of IgG4 are associated with moderate symptoms whereas high levels of IgE are common in patients with severe pathology [13, 67, 169]. IgG4 is a non-complement fixating Ig that can bind weakly to effector cell Fc receptors and then compete with IgE for antigen-binding sites.

	W. bancrofti	*O. volvulus*
IgG4/IgG1	-	-
IgG4/IgG2	↑	-
IgG4/IgG3	↑	-
IgG4/IgGE	↑	(↑)

Table 4.2. Ratio of filarial-specific IgG4 to other Ig subclasses of MF^+ in comparison to MF^- individuals.

Therefore, the relationship of the two Igs is of special interest during filariasis infections since their presence usually reflects the pathophysiological situation of the host [53, 175]. The quantities of specific IgG4 produced in LF patients can be remarkably high. In patients presenting elephantiasis, IgG4 levels are similar to those found in EN (57% and 55% of filarial-specific IgG respectively) whereas in MF^+ carriers the amount is significantly higher (88%) [101]. Immunohistological stainings of nodules from hyperreactive or asymptomatic onchocerciasis patients have shown that IgG4 expression of the former is down-regulated supporting it's important role in immunomodulation [9]. Upon analyzing filarial-specific Ig levels in the onchocerciasis study, both infected groups revealed significant differences in all Igs when compared to EN but not with each other. Significant differences between patent and MF^- individuals were only found with regards to IgG3, which was increased in MF^+ patients. Levels of IgG4 were slightly increased in MF^+ patients when compared to MF^- individuals, albeit not significant. Due to the competition between IgG4 and IgE for the same binding sites, determining the ratio provides essential insight about the pathophysiological conditions, that is, whether the antigen triggers an IgE mediated hypersensitivity response, or whether this response can be blocked by IgG4 [69]. In general, the prevalence of IgG4 dominated filarial-specific Ig secretion was much more obvious in MF^+ LF infected patients since the ratios of IgG4 to IgE, to IgG2 and to IgG3 were all significantly increased when compared to amicrofilaremic patients. MF^+ onchocerciasis individuals showed only a trend concerning the IgG4/IgE ratio ($p = 0.085$) although MF^+ and MF^- patients produced significantly more antigen-specific Igs compared to the EN which is in line with previous reports [52, 176]. This increased ratio of IgG4 to IgE confirms studies performed by Jaoko *et al* in East Africa with *W. bancrofti* infected individuals and interestingly, this group found that specific antibodies levels reflect infection status rather than lymphatic disease [167]. Moreover, in the study performed here, patent LF infected individuals also had elevated polyclonal IgE levels when compared to latent individuals. Such high levels of IgE may facilitate the persistence of infection through the production of irrelevant (not parasite Ag-specific) Igs, that saturate high affinity IgE receptors expressed on mast cells which renders them unable to be specifically cross-linked by parasite antigen [94].

Besides IgG4, IL-10 is also known to be a key player during filarial infections [74] and its presence is clearly connected with a protective immunological scenario in onchocerciasis: high IgG4, IL-10 and Tregs are associated with low pathology whereas high levels of IgE, IL-4 and eosinophilia are common in patients with severe pathology [9, 13, 67, 169]. However, the source of IL-10 remains inconclusive since studies have depicted that $CD4^+$ (and not $CD25^+$) T cells are the predominant IL-10 producing cells in the circulation of filaria infected patients [155, 156] whereas other studies have shown that IL-10 production is mediated by Tregs [18, 24]. Interestingly, there was an up-regulation of antigen-specific

induced IL-10 secretion in patent *O. volvulus* infected individuals which was further emphasized by a positive correlation between IL-10 levels and the amount of MF but there was no direct correlation between IL-10 and IgG4. In contrast, MF^+ LF patients had significantly lower levels of IL-10 than amicrofilaremic individuals although the former ones were also characterized by elevated levels of antigen-specific IgG4. Therefore, one could conclude that in LF the observed immunoregulation is less dependent on IL-10 or there are some redundant mechanisms blocking inflammation and inducing IgG4. Interestingly, gene expression profiles of Tregs of MF^- LF patients demonstrated a significant up-regulation of the IL-10 receptor β compared to MF^+. This was in line with data obtained from the re-stimulation assays although we used whole PBMCs in these assays and not isolated fractions of T cells. In contrast, MF^+ patients had higher levels of this receptor in their effector T cells compared to EN.

As mentioned above, patent *O. volvulus* infected patients had significantly up-regulated IL-10 levels compared to MF^- individuals but the differences concerning the anti-inflammatory IgG4 were not as clear as in LF. Since the MF in *O. volvulus* infected individuals are found in the skin and not in the blood, one might speculate that the analysis of skin samples may reveal a difference with regards to antigen-specific Igs between MF^- and patent patients and thus reflecting the results found in LF MF^+ and MF^- individuals. A previous study of Korten *et al* has already shown reduced levels of TGF-β in the skin of hyperreactive patients in contrast to GEO individuals [9]. Therefore, it would be of special interest to analyze skin samples of MF^+ and MF^- patients concerning their expression of immunomodulatory factors and also of Igs.

4.4 Role of IL-10

As mentioned above, the regulatory cytokine IL-10 is quite dominant in certain subsets of filarial infected patients. Previous studies from our group have also demonstrated the necessity of this cytokine in inducing the secretion of IgG4 by B cells in a co-culture assay [50]. In this model, Tregs were shown to induce IgG4 production by B cells and this process was dependent of IL-10, TGF-β and GITR/GITR-L [50]. Thus, the signaling pathway of IL-10 was investigated through the phosphorylation of the transcription factor STAT3 since its activation reflects IL-10 production. A future aspect of the studies performed here would be the identification of the cellular source of IL-10.

Experiments using Western blot analysis could demonstrate that phosphorylation of STAT3 could only be induced by stimulation of PBMCs with recombinant IL-10 whereas the unphosphorylated form of STAT3 was constitutively expressed (data not shown). The induction of STAT3 phosphorylation could also be observed in isolated $CD4^+$ and $CD19^+$ B cells. However, these results could not be reproduced if flow cytometry was applied because

in this experimental setup IL-10 did not induce the phosphorylation of STAT3 compared to unstimulated cells. It has to be considered that the applied experimental setup consists of several isolation steps which could also influence intracellular signaling. With the Western blot setup, further experiments that pre-blocked GITR or GITR-L did not show any significant alterations with regards to STAT3 phosphorylation although an association of IL-10, GITR and IgG4 has been demonstrated in the aforementioned previous experiments [50]. Increasing doses of anti-GITR and parallel decreasing doses of recombinant IL-10 did also not significantly modify the phosphorylation status of STAT3. If analysis was performed on individual donor level the results were contradictory since some individuals revealed an influence on pSTAT3 expression when GITR was blocked whereas some did not. Therefore, basal levels of GITR and GITR-L expression on the cell surface were determined. Indeed, the levels of these molecules varied quite broadly between individuals and this could account for the different results observed via Western blots. The previous results that demonstrated an association between IL-10, GITR and IgG4 have used homogeneous cell populations (clones), therefore no conclusions can be drawn from these experiments and the ones performed within this study. In addition, since IL-10 does not only activate STAT3 but also STAT1 and, in certain cell types STAT5 [21] these transcriptions factors should be also analysed in future studies in order to rule out that blocking GITR does not interfere with the IL-10 pathway.

Interestingly, analysis of differentially regulated genes in isolated Tregs of EN and infected individuals revealed that the transcription factor STAT1 was significantly up-regulated in infected individuals. STAT1 is an essential effector of IFNs since binding of IFN-γ or IFN-α to their appropriate receptors induces the final the phosphorylation of STAT1 which is then translocated to the nucleus where it acts as a transcription factor of several genes. Due to the association between IFN-γ and STAT1 one would have perhaps expected a decrease of this gene in the infected group but this was not the case. As mentioned above, IL-10 can also act via STAT1 [177, 178], therefore a hypothetical explanation could be that $CD25^+$ T cells from infected individuals produce more IL-10 in an autocrine manner or react to IL-10 production (for example secreted by AAMs) which leads to the subsequent up-regulation of STAT1. If analysis of this gene expression was further divided into the groups of MF^+ and MF^- patients there was an up-regulation of STAT1 in both infected groups compared to EN but the fold change was higher in latently infected individuals which is in line with the up-regulated secretion of IL-10 in MF^- patients following antigenic stimulation when compared to patent infected individuals. The next step would be an analysis on protein level and furthermore, using our *in vitro* cell stimulation analysis, a proof of principle experiment to demonstrate that IL-10 induces alterations in STAT1 signaling. Analysis of regulated genes also revealed that STAT1 was up-regulated in effector T cells from infected individuals. Again

one can argue here that STAT1 is an essential transcription factor of IL-10-mediated responses.

4.5 Novel aspects for future filarial-specific T cell research

Several reports have deciphered the immunological status of MF^+ LF infected patients and compared it to those presenting severe pathology. These studies have implied that the balance between Th1/Th2, Treg and the Ig milieu, alongside genetic factors of both the parasite and host, may define whether the infected individual is asymptomatic or develops pathology [92]. However, as mentioned above, little has been reported about the strength and character of immune responses elicited in asymptomatic amicrofilaremic individuals, a cohort of patients which are epidemiologically interesting since as mentioned beforehand they represent a dead end for the parasite's transmission.

Analysis of the gene expression profiles of T cell populations from LF infected MF^+ and MF^- individuals demonstrated that novel chemokine and cytokine related genes were found to be differentially regulated. When comparing the gene expression of Tregs from MF^+ LF infected individuals and EN, most of the regulated genes were part of translation processes but some were involved in protein binding and phosphatase activity. Interestingly, CD84 was significantly up-regulated in MF^+ individuals when compared to MF^- patients and EN. CD84 is a self-binding receptor from the CD150 (or signaling lymphocyte activation molecule (SLAM) family and it is broadly expressed on hematopoietic cells including NK, NK T cells, B cells, T cells, monocytes, platelets, DC, eosinophils and neutrophils. Ligation of CD84 is associated with the enhanced induction of IFN-γ in activated T cells [179-181]. Moreover, previous experiments have revealed that CD84 contributes to T:B cell-mediated adhesion and also participates in stable T:B cell interactions *in vitro*. Interestingly, recently published results have demonstrated that CD84 is associated with a negative regulation of IgE high-affinity receptor signaling in human mast cells. In addition it was shown that CD84 deficient mice have defects in the formation of germinal centers [182] and all of these studies strengthen the arguments for the relevance of CD84 as a player in adaptive immunity and humoral responses. As mentioned beforehand helminthic parasites can trigger highly polarized immune responses which are typically characterized by increased numbers of Th2 cells, eosinophils, mast cells and IgE [37, 183]. It was also shown that CD84 can self-interact at a very high affinity in a "head to head" interaction, suggesting that CD84 could cooperate with another CD84 molecule on another cell rather than on the same cell [179, 184]. Since studies have also demonstrated that Tregs may interact with mast cells [185] a hypothetical scenario begins to emerge: CD84 on Tregs could serve as an inhibitory signal with regards to the up-regulation of IgE receptors on mast cells in order to prevent IgE binding and thus the induction of histamines.

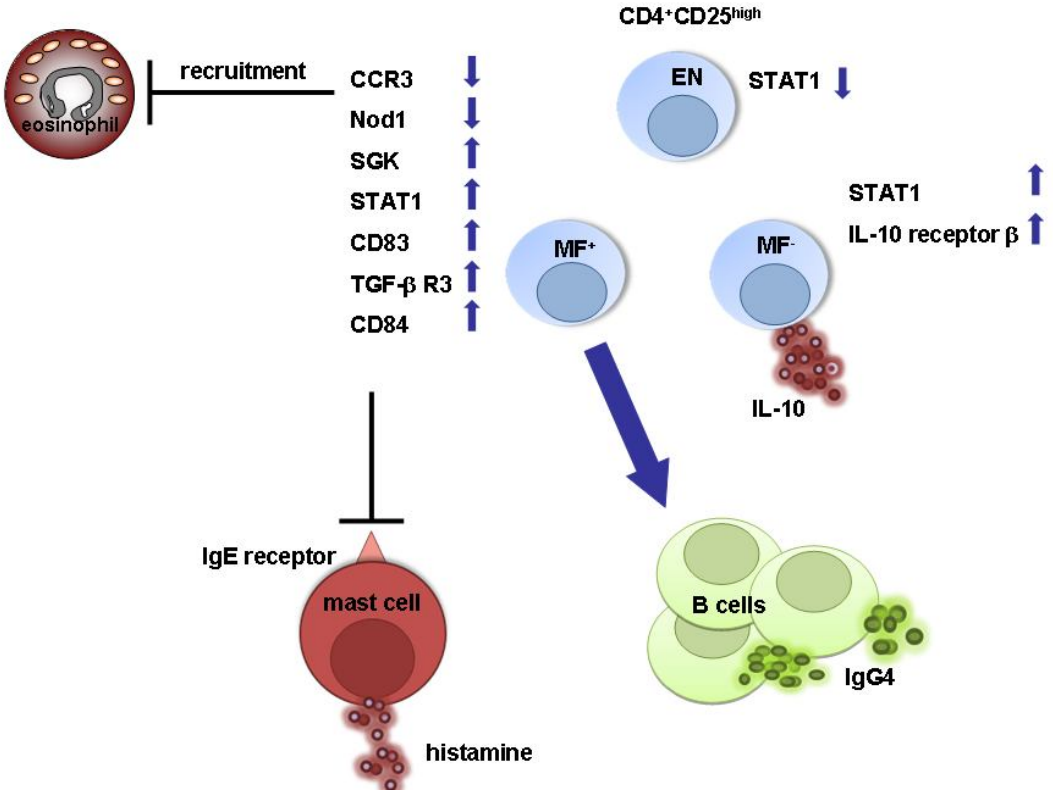

Figure 4.1. Hypothetical cooperation of Tregs in the context of LF infection according to their gene expression profiles.

Given that LF infected MF^+ patients were shown to have increased IgG4:IgE ratios, these mechanisms would be a further possibility to avert unwarranted IgE responses. In addition, CCR3 was down-regulated in the Treg population of MF^+ patients when compared to EN and this receptor is associated with the enhanced recruitment of eosinophils by chemotaxis [186]. As mentioned before, eosinophils are involved in tissue damage during filarial infection [170] and prevention of their activation would be another possibility to prevent damaging immune responses. If Tregs of MF^+ and MF^- patients were further compared there were some more differences with regards to the immunological marker CD83: Tregs from MF^+ individuals were characterized by a significantly up-regulated expression of this marker. This molecule belongs to the Ig superfamily and is associated with the maturation of dendritic cells. Besides its role during DC maturation, it was also shown that the soluble form of CD83 has inhibitory functions in terms of cell activation mediated by DCs resulting in decreased proliferation of T cells [187, 188]. Further studies have demonstrated that CD83 can also be found on T and B cells [187, 189]. Moreover, murine studies have demonstrated that naturally occurring Tregs are characterized by an increased expression of CD83 mRNA and overexpression of CD83 confers suppressive capacity to naïve cells *in vitro* [190]. Together these studies indicate that CD83 represents a mechanism to control immune responses. This is in line with results mentioned before with regards to asymptomatic MF^+ patients since these individuals were characterized by suppressed immune responses in terms of cytokine and Ig production.

Interestingly, the significant differences concerning CD83 were only detected within the infected group and not in comparison to EN. Given that previous results have shown that soluble CD83 molecules can be found in sera of healthy individuals [191] this offers a possibility to analyze the differences observed on the gene level with activities found on protein levels although murine studies have already shown that increased mRNA levels of CD83 in Tregs were not associated with increased protein expression [190]. In line with the pronounced immune regulation of MF^+ patients was the finding that these individuals were characterized by increased levels of TGF-β receptor and also by increased levels of the SGK mRNA when compared to latently infected individuals, the latter one is known to play a role in the prevention of apoptosis [192].

An additional interesting finding was the fact that Tregs from MF^+ individuals had a significantly down-regulated expression of the intracellular receptor Nod1 when compared to MF^- patients. This receptor belongs to a specialized group of intracellular proteins that play a critical role in the regulation of the host's innate immune response [193]. It is widely expressed in many cell types and organs and detects fragments of bacterial peptidoglycans found in Gram-negative bacteria and some Gram-positive bacterial species [194]. Activation of Nod1 results mainly in the activation of nuclear factor (NF)-κB or mitogen-activated protein kinases (MAPKs) which drive the transcription of numerous genes involved in both innate and adaptive immune responses [193]. Interestingly, it was already shown that LF infected patients suffering from severe pathology show increased mRNA levels of Nod1 and Nod2 in contrast to asymptomatic individuals following re-stimulation with the specific filarial antigen [41]. In our study, differences in Nod1 gene expression were only found between MF^+ and MF^- patients and not in comparison to EN thus highlighting again that immune suppression is increased in MF^+ patients.

Comparing the gene expression profiles of $CD4^+$ T effector cells revealed that most of the differences between infected and EN were found with regards to protein binding. One interesting candidate was the lymphocyte transmembrane adaptor 1 (LAX1) which was significantly up-regulated in $CD4^+$ T cells of infected compared to uninfected individuals. This protein belongs to the transmembrane adapter protein (TRAPs) family and is able to exert both positive and negative effects on the complex signaling pathways that regulate immune responses in a variety of hematopoietic cells. LAX is expressed in B and T cells as well as NK cells and monocytes [195]. Interestingly, it was shown in murine studies that LAX1 is negatively associated with lymphocyte activation since T and B cells of mice deficient for LAX1 were hyperresponsive to stimulation via T cell or B cell receptor (TCR, BCR respectively). Moreover, it was shown that LAX1 blocks some signaling pathways although the mechanisms by which LAX1 negatively functions in TCR-mediated signaling are unclear [196]. Lack of T cell proliferation is a hallmark of asymptomatic filariasis infections [74]. Thus,

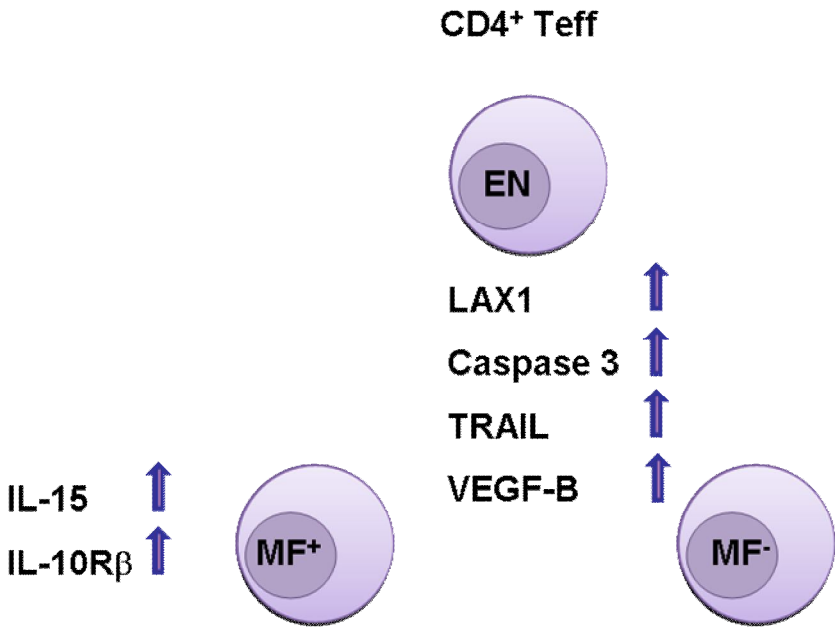

Figure 4.2. Overview of regulated genes within the CD4$^+$ effector T cell subpopulation.

up-regulation of LAX1 and subsequent block of proliferation could be one mechanism induced by the parasite in order to suppress unwarranted immune reactions mediated by effector T cells. In line with this, levels of caspase 3 and TNF ligand superfamily member 10 (also known as TRAIL) were also both significantly up-regulated in infected individuals compared to EN. Caspases are highly conserved through evolution and they play an important role during programmed cell death (apoptosis) [197]. Along with other members of the TNF family of cytokines, TRAIL transduces apoptotic signals through direct protein–protein interactions [198] and as mentioned above apoptosis has been linked with various parasitic infections. For example, Babu *et al* have shown that NK cells from healthy donor samples became apoptotic following stimulation with live L3 in a caspase-dependent process [199]. Also, a TRAIL-dependent apoptosis was seen in monocyte derived DCs from healthy donors if they were incubated with live MF [200]. In addition, it was shown in a different helminth infection model that *Schistosoma mansoni* induced apoptosis in murine T cells [201]. All these studies indicate that parasites are able to modulate the immune system of their hosts via induction of apoptosis in order to evade immune responses which may be detrimental for the parasite and the host as well.

In addition in the microarray analysis, IL-15 was found to be exclusively up-regulated in the T effector cell population of MF$^+$ individuals. This pleiotropic cytokine has a broad range of biological functions in many diverse cell types and the effects of IL-15 expressing CD4$^+$ T lymphocyte subsets differs according to their developmental and activation stage [202]. Although some reports have described that under normal conditions the homeostatic proliferation of CD4$^+$ lymphocytes requires IL-15 [203], the general nature of IL-15 activity is critically dependent on the activation status of the T cells. For example, in the absence of a

TCR signal IL-15 induces a quiescent phenotype but during TCR engagement, T cells are resistant against TCR-induced cell death and can strongly proliferate [204]. *In vitro*, it was further shown that memory B cells develop into IgG secreting plasma cells in the presence of IL-15 [205] and a recent publication showed that IL-15 is important for the development of IgG-antibody secreting cells (ASC) and moreover, decreases the number of IgE-ASCs [206]. Since the LF infected MF^+ patients were characterized by decreased total IgG4/IgE ratios, it would be of interest to determine whether levels of secreted IL-15 differed upon helminth-specific stimulation.

4.6 $CD8^+$ T cells: a neglected player during helminth infection?

In general, $CD8^+$ T cells play a central role during adaptive immune responses since they are important for the recognition and clearance of cells infected by intracellular pathogens and moreover they are key players in anti-tumor immune response [207]. Surprisingly, there are only very few publications concerning their involvement during filarial infections. It was shown however, that in comparison to asymptomatic MF^+ individuals isolated PBMC fraction from elephantiasis patients contained higher proportions of $CD8^+$ T cells [208]. These T cells were also found to be increased in limb biopsies of patients suffering from lymphedema and elephantiasis in comparison to asymptomatic individuals [209]. Both studies indicate that $CD8^+$ T cells are involved in severe pathology. On the other hand, it was demonstrated that $CD8^+$ T cells of filarial infected persons are able to produce IL-10 [155] and they are the main producers of IL-5 in CFA^- patients with chronic disease in contrast to MF^+ patients [210]. Moreover, $CD8^+$ T cells of MF^+ patients were also characterized by increased levels of CTLA-4 compared to latent infected individuals [211]. Since CTLA-4 is a potent inhibitor of T cells and is involved in mediating T cell anergy and tolerance [212] these observations indicate that $CD8^+$ T cells play also a protective role during filarial infections. Along these lines, it was shown in *B. pahangi* infected rats that $CD8^+$ T cells were able to induce a non-specific immune suppression [213].

Gene expression analysis performed in this study revealed that between infected and EN individuals only 41 genes were differentially regulated. One such gene was KLF4 which increased in $CD8^+$ T cells from EN and this factor has been associated with the induction of cell cycle arrest of naïve $CD8^+$ T cells in mice [214]. In contrast, SOD2 was the most strongly down-regulated gene in infected individuals when compared to EN. These SODs are a family of metalloenzymes involved in intracellular and extracellular antioxidant defense which they achieve through catalyzing the dismutation of superoxide radicals into hydrogen peroxide and oxygen in order to avoid toxicity mediated by these reactive oxygen species [215]. Thereby, SODs have been shown to be important factors in ameliorating and coping with injury from oxidative damage and they can help maintain redox homeostasis [216]. They are

also considered to play a prominent role in protection against many apoptotic stimuli [217] an aspect already heavily described during filariasis infections [86, 200]. In line with this assumption was the finding that SGK was also down-regulated in $CD8^+$ T cells of infected patients because as mentioned before SGK is associated with protection from apoptosis [192] indicating that T cells from filarial infected patients are more susceptible to apoptosis. This was further highlighted by increased expression levels of transcription factor Dp-1 (TFDP1) in MF^+ patients compared to latent infected individuals since up-regulation of TFDP1 has been also associated with the induction of apoptosis [218]. Interestingly, MF^- patients had higher levels of SENP5 compared to patently infected individuals. Since SENP5 is required for cell division [219] one could speculate that $CD8^+$ T cells from MF^+ patients are more tightly regulated or suppressed than those from MF^- patients. Along these lines, we observed a down-regulation of the BCL-6 which was decreased in infected patients when compared to EN. In fact, BCL-6 is important for the generation and maintenance of memory $CD8^+$ T cells [220] indicating that filarial infection can modulate activity of $CD8^+$ T cells. Another apoptosis associated gene is ING2 [221] and this was up-regulated in cells from MF^+ patients when compared to MF^- individuals. In addition, $CD8^+$ T cells from EN also expressed more ING2 than T cells from MF^- patients. Moreover, the F-box protein 11 (FBXO11) was also found to be up-regulated in $CD8^+$ T cells from MF^+ patients when compared to EN and this protein is connected to TGF-β signaling pathways in mice [222]. Recently, ING2 was also associated with the mediation of TGF-β-dependent responses [223]. These two genes could confirm previous findings which have demonstrated that TGF-β is associated with the asymptomatic form of filarial infections [9, 32].

Up-regulation of the prostaglandin D2 (PTGD) receptor (PTGDR) was observed in $CD8^+$ T cells from all infected individuals, especially those that were MF^+, when compared to EN. Interestingly, PTGDRs are linked with the inhibition of effector cell function in lymphocytes since binding of prostaglandin 2 increases intracellular cyclic adenosine monophosphate (cAMP) concentrations. In T cells and other inflammatory cells, the accumulation of cAMP is generally associated with the inhibition of effector cell functions [224] and cAMP represents a key regulator of human Treg function [225]. These receptors are broadly expressed and it was shown that stimulation with their ligands decreased levels of secreted IL-2 and IFN-γ in human $CD8^+$ T cells [226]. Inhibition of IFN-γ and IL-2 production may skew the immune system towards a more Th2-like response which is a hallmark of filarial infection. Interestingly, it was shown that certain pathogens synthesize PTGD which in turn may subvert the host‘s immune functions. For example, the production of PTGD2 by the skin-penetrating life-stage of *S. mansoni* inhibits the migration of epidermal Langerhans cells and the subsequent accumulation of DCs in the draining lymph nodes during murine schistosomiasis [227]. These effects were mediated by the PTGDR [228] since the secreted

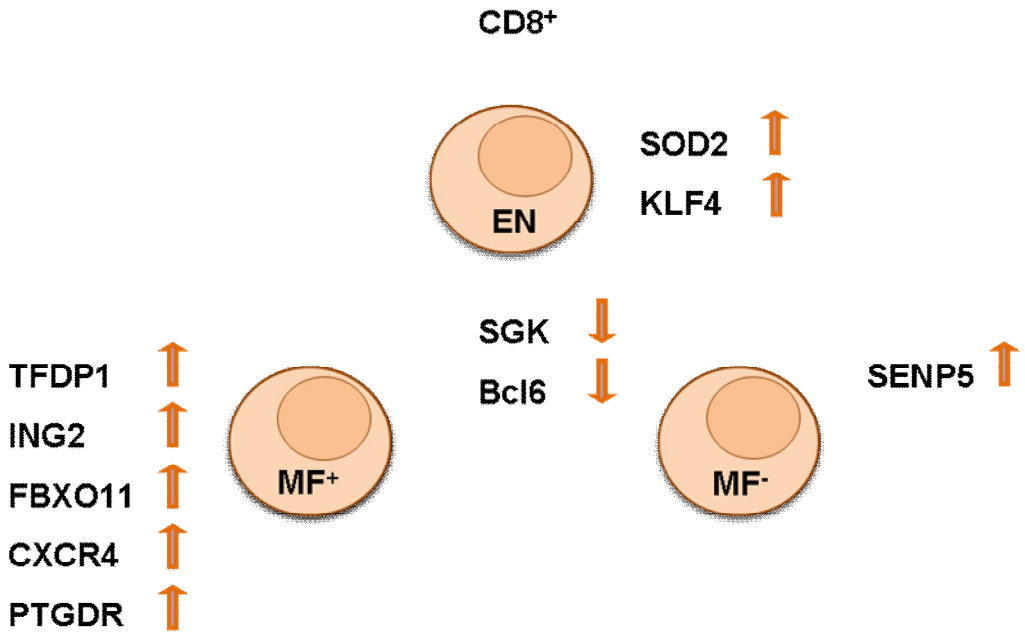

Figure 4.3. Overview of regulated genes within the CD8$^+$ T cell subpopulation.

PTGD2 homologue from *Schistosoma* binds to this receptor. This mechanism may be used by the parasite in order to evade the host's immune system. No doubt there are still numerous mechanisms and immunomodulatory pathways that we are still unaware of. Another gene that warrants future investigations is CXCR4 which was up-regulated in MF$^+$ patients when compared to latently infected individuals. This gene is actually associated with angiogenesis [229] and moreover, CXCR4 was previously shown to be present in nodules from *O. volvulus* infected patients [230]. Previous publications revealed that CXCR4 is highly expressed on naive subsets of human CD8$^+$ T cells and that its surface expression is down-regulated during differentiation from memory to effector subsets. Moreover, the expression of CXCR4 is negatively correlated with that of perforin [231] the latter one is part of the cytotoxic cell granule secretory pathway which is essential for host defense [232].

4.7 Helminth modulation of innate cells

Previous publications have already depicted the importance of innate immune responses during filarial diseases. For example, there have been various reports describing the involvement of TNF during LF [68, 89, 98]. However, the majority of these studies have investigated differences between infected and EN, between infected and CP patients or between MF$^+$ patients and those with episodes of acute filariasis (adenolymphangitis). In studies with acute filariasis individuals had elevated levels of TNF in their sera when compared to MF$^+$ patients [233]. In another study that compared EN with MF$^+$ patients, TNF responses from PBMCs of microfilaremic patients were again dampened if their cells were stimulated with either live L3, live MF and also following stimulation with the filarial antigen

[68]. Reduced levels of TNF were also observed in asymptomatic patients (microfilaremia not determined) when compared to those with severe pathology [41]. Results obtained within this study showed that cells from patent LF infected individuals secreted less TNF and this was independent of the applied stimulus. Naturally, the dampening of not only antigen-specific responses but those to bystander antigens would greatly enhance the parasites chance of survival. Thus, in accordance with the findings of this study the presence of circulating MF in LF infected patients dampens TNF responses regardless of whether these are antigen-specific, bystander or innate. Intriguingly, *in vitro* studies have implicated that *Wolbachia* endobacteria, but not the worm itself, elicit TNF secretion from innate host cells in a TLR-dependent manner [28, 110] and that persistent exposure to *Wolbachia*, but not bacteria-free nematode extracts, drives homologous and heterologous tolerance of macrophages to TLR and CD40 ligands and protection from endotoxin shock *in vivo* [157]. Other studies have also linked TNF with promoting the production of VEGFs such as VEGF-C and VEGF-A [99, 234] which reportedly contribute to the development of lymphodema and hydrocele [78, 79]. Indeed, during LF levels of VEGFs are elevated in the plasma of CP patients and depletion of *Wolbachia* by doxycycline results in decreased levels of VEGF-A and VEGF-C [78, 79]. In addition to the decreased secretion of TNF from PBMCs of patently infected individuals there were also suppressed IL-17 responses. Interestingly, *in vitro* rIL-17 can drive TNF production in macrophages [235] and a combination of rIL-17 and rTNF was shown to increase the production of angiogenic factors like VEGF from fibroblasts [100]. Since there were also differences in IL-6 production between MF^+ and amicrofilaremic LF infected individuals and it is well known that human IL-17 is induced by IL-6 in combination with TGF-β [236] a hypothetical scenario began to emerge: worm death could promote the release of *Wolbachia* and in turn elicit TNF production by triggering TLR [237]. Thus, enhanced TNF, and possibly IL-6, coupled to stronger IL-17 responses could instigate the production of VEGF and deviate the onset of pathology. In association, studies revolving around the immune responses of severe pathology patients observed elevated levels of IL-17 and TNF [41]. The presence of this cytokine combination in our latent LF individuals may reflect a higher susceptibility to pathology especially since a cross-sectional study has indicated that the onset of severe pathology is linked to the amicrofilaremic status [238]. Theoretically, the normal release of MF could counterbalance this immunological milieu circumventing unwarranted responses. However, in this study levels of VEGFs were not significantly different between latent and patent infected individuals, although one has to consider that included patients did not suffer from severe pathology like lymphedema. Moreover, the majority of them were not even aware that they were infected. The similar levels of VEGFs detected between both groups are also in line with the levels of lymph dilation which were also comparable between both groups. Again, the only way to determine if the aforementioned factors are prerequisites for

the induction of pathology would be long term surveillance of infected individuals but this would require no intake of MDA which is not feasible due to ethical reasons.

In contrast to the results obtained within the LF study, the onchocerciasis study presented here demonstrated that secretion of IL-6 was significantly increased in PBMCs from infected individuals when compared to EN following all stimulation scenarios except *B.m*. extract. In addition, IL-6 release was higher in MF^+ compared to MF^- patients after stimulation with LPS in onchocerciasis. The same outcome could be observed for another pro-inflammatory cytokine, namely TNF. These increased levels could possibly be the result of the higher concentrations of endosymbiotic *Wolbachia* within MF^+ patients, since the latter ones are found in all developmental stages of *O. volvulus* including MF. Nevertheless, patent individuals have also shown higher levels of immunosuppressive IL-10 which could counterbalance the effects induced by pro-inflammatory cytokines. Also, in contrast to *W. bancrofti* infected individuals, IL-17 production was not altered between all three groups with regards to all used stimuli within the onchocerciasis cohort. Until now, the role of IL-17 during onchocerciasis infection has not been intensively analysed. However, since it is already described that IL-17 plays a role during pathogenesis in LF [41] and in addition, the presence of angiogenic and lymphangiogenic factors needed for vessel formation was already identified in onchocercomas, it would be interesting to determine if patients suffering of dermatitis or visual impairment have altered IL-17 levels in comparison to asymptomatic individuals.

Interestingly, on the gene level, VEGF-B expression was higher in $CD4^+$ T cells from LF infected patients when compared to EN. In fact, VEGF-B is an angiogenic factor but its actual role remains controversial. This factor is able to directly stimulate endothelial-cell growth and migration but some studies have revealed that it can indirectly stimulate angiogenesis by recruiting pro-angiogenic cells. In addition, under most conditions, VEGF-B has been shown to be dispensable for blood vessel growth but is critically required for blood vessel survival [239]. Additionally, some authors have claimed that VEGF-B is more an anti-apoptotic rather than a lymphangiogenesis marker [240]. A recent study further indicated that VEGF-B is involved in the regulation of energy metabolism by regulating fatty acid uptake since VEGF-B was co-expressed with mitochondrial protein genes. Mice deficient for VEGF-B showed less uptake of fatty acids but increased amounts of body fat and body weight [241, 242] highlighting the indispensable role of VEGF-B in metabolism. Another murine study revealed that in type-1 diabetes mRNA levels of VEGF-B were decreased [243]. Interestingly, it was already shown that mice infected with filariae are protected from developing type-1 diabetes [244] and human studies also demonstrated an inverse relationship between the prevalence of LF and diabetes [245, 246]. In conclusion, it is tempting to speculate that VEGF-B may be

an important factor induced during filarial infections and may be a factor in preventing the onset of diabetes.

4.8 Influence of MF on PBMCs of healthy donors

Since results from the LF study demonstrated an important role of MF with regards to immunosuppression, it was investigated if this influence of worm offspring was strong enough to induce the same effects in PBMCs from healthy individuals, e.g. blood donors that have never had contact with these parasites. Determination of cytokine levels of PBMCs cultivated in the presence of isolated MF and T cell specific stimulus anti-CD3/anti-CD28 revealed no differences concerning IL-10 and IFN-γ release. Also, TNF was not affected, although data from LF infected patients have showed a clear decrease in the release of this cytokine in presence of MF and these results were independent of the applied stimulus. However, production of the pro-inflammatory cytokines IL-1β and IL-17 were significantly increased if MF or worm extract were added. In accordance with this result previous studies have shown that live *B. malayi* MF induced pro-inflammatory cytokine production (IL-1β, IL-8, TNF) by monocyte derived DCs of healthy donors and additionally the up-regulation of apoptotic markers [86]. Interestingly, stimulation with *L.s*. extract resulted in a diminished TNF secretion and decreased IFN-γ response which seems to be in contrast to the results obtained for IL-1β and IL-17. Given that MF were isolated from infected cotton rats one could speculate that the immunomodulatory effects seen using human cells are species-specific or more precisely, suppression of pro-inflammatory cytokines requires either a well-adapted parasite-host interaction or an established infection. Therefore, it would be interesting to use MF from human *W. bancrofti* infections in order to see if they are able to alter the immune system of a “naïve” host but since huge numbers of MF are necessary for such assays this is not feasible. In principle, only MF from *B. malayi* infected jirds can be taken for these types of assays since the *Brugia* cycle can be maintained in an animal model in contrast to *W. bancrofti* whose adult worms are not generally obtainable because of the difficulty of maintaining this parasite outside the human host [103].

4.9 Analysis of immunological profiles following treatment

Control of human LF infections currently depends on chemotherapeutic strategies given as MDA annually or biannually [5, 62]. Since these drugs are mainly microfilaricidal, mass treatment has to continue at least as long as adult worms survive in humans. In an attempt to shorten such long-term treatments, doxycycline is used since it is efficient in inducing worm sterility and worm death rendering patients amicrofilaremic and thereby breaking transmission [2]. Utility of this drug for routine field use remains an issue of concern because doxycycline has to be given in extended daily dose regimen which involves huge logistical

challenges. Furthermore doxycycline is not suitable for children below 9 years, pregnant or breastfeeding women. Since pilot studies with the combination of doxycycline and rifampicin have shown promising results with regards to *Wolbachia* depletion [129] a large-scale study was conducted in order to confirm these results and moreover to test different periods of drug intake as well as different combinations. As part of this study, immunological profiles of participants were also analysed. Cytokine to specific and bystander antigens were analysed 12 months post-treatment and filarial-specific Ig levels 12 and 24 months post-treatment. Of note, all participants received a 4 month post-treatment single dose of IVM/ALB including the placebo treated patients.

Interestingly, in contrast to the combination regimens of doxycycline and rifampicin, treatment with doxycycline alone resulted in a complete loss of circulating MF 12 months post-treatment independent of the concentration or duration of doxycycline intake. This picture was even more obvious 24 months post-treatment since a higher percentage of individuals became microfilaremic after intake of the combination of both drugs in comparison to patients treated only with doxycycline. Decrease of MF burden in the placebo treated group was a result of IVM/ALB intake 4 months post-treatment but MF recovered after 12 months within this group and even more after 24 months although to a lesser extent than before. However, treatment for 5 weeks with 100 mg doxycycline showed the best results with regards to MF depletion indicating that the period of drug intake is also an important factor. Moreover, reduction of drug dosages is always preferable in terms of compliance. Since results from the pre-treatment study have shown that patent and latent patients behave differentially with regards to their cytokine and antigen-specific Ig production, analysis of immunological profiles post-treatment was also performed as comparison of doxycycline or rifampicin treated individuals to the placebo group, the latter one divided into MF^+ and MF^- patients. In addition, within the drug treated participants, only those were included that obtained doxycycline as drug regimen since only these patients were characterized by a long-term reduction of MF. Although treatment with doxycycline in any of the applied regimens did not result in significant differences with regards to the production of the key cytokine IL-5, following *B.m*. extract stimulation, treatment with 100 mg doxycycline for 5 weeks seems to decrease the amount of IL-5 to a comparable level as seen by cells from patients in the placebo MF^+ group, albeit not significantly. Interestingly, IL-5 levels were decreased in MF^+ patients of the placebo group in comparison to MF^- individuals which reflects data from the pre-treatment study. The same picture was seen with regards to IL-10 following anti-CD3/anti-CD28 stimulation and treatment regimen 2 significantly decreased the amount of IL-10 released from PBMCs of MF^+ patients when compared to amicrofilaremic placebo treated individuals. Furthermore, MF^+ produced less TNF than MF^- patients as was seen in the pre-treatment study. In summary, analysis of cytokines 12 months after treatment

did not reveal any clear picture with regards to different treatment arms since there was no stringent up- or down-regulation of the measured cytokines. One has to consider again that all included participants received additionally IVM/ALB which could also influence immune responses. Earlier publications have shown that PBMCs of *O. volvulus* patients produce more IL-2 and IFN-γ but less IL-4 following treatment with IVM [247] and also monocytes of *W. bancrofti* infected individuals start to produce higher levels of IL-1α, IL-8 and IL-10 [248]. Therefore, in order to evaluate possible effects of different regimens of doxycycline on the immunological profile of infected individuals one has to perform this type of studies without any application of IVM/ALB but this would not be in accordance with any ethical rules since individuals have to be given the best available treatment. Alternatively, analysis could be performed in the interval between antibiotic treatment and IVM/ALB administration to observe immediate alterations in the patients. In addition, it would be interesting to carry out longitudinal studies, thus measure cytokines profiles after two or more years of treatment in order to analyse the long-lasting effects of the used drugs.

Regarding levels of antigen-specific Igs there were no significant alterations 12 months post-treatment independent of the applied treatment although levels of IgE were reduced in MF^+ patients of the placebo group compared to MF^- which confirms previous findings. This was further reflected in the ratios of IgG4 to IgE and IgG1 but here again treatment could not show any significant differences. Interestingly, data from the 24 month post-treatment study showed a significant decrease with regards to IgG1 following treatment regimen 2 in comparison to both placebo treated groups and also reduced levels of IgG4 after treatment with regimen 2 when compared to MF^+ individuals. In addition, the ratio of IgG4 to IgE was decreased in this group and also following treatment 3 when compared to MF^+ patients. The ratios of IgG4/IgG1 and IgG4/IgG3 were decreased in treatment group 2 in comparison to the patent placebo treated patients. Moreover, within the placebo treated group there were significant differences with regards to the IgG4/IgE and IgG4/IgG1 ratio which highlights again the stronger immunosuppression of MF^+ patients when compared to latent infected individuals. In summary, treatment with 100 mg doxycycline for 5 weeks had the strongest effect on the production of filarial-specific immunoglobulins.

4.10 Conclusion

Results from this study highlight immunological disparity between patent and MF^- infected individuals. With regards to infection with *O. volvulus* it was shown that patently infected patients were characterized by lower levels of IL-5 when compared to MF^- individuals upon filarial-specific stimulation whereas the opposite was found for filarial-induced IL-10 secretion and antigen-specific IgG4/IgE ratios. The picture of immunoregulation in patently infected patients was more obvious in LF infected indiviudals. In summary, upon comparison with MF^+

individuals, amicrofilaremic LF patients display an increased immune profile of TNF, Th17, IL-10, IL-6 and filarial specific Th2 responses. This elevated cytokine milieu, both filarial-specific and bystander induced, may contribute to the induction of other immunological pathways such as VEGF which in turn promotes overt pathology. In contrast, the immunosuppressive pattern in LF MF^+ patients is complemented by the high ratio of specific IgG4/IgE. In general the prevalence of IgG4 provides protection to both host and parasite since it presents a mechanism in order to counter-regulate high IgE and thus avoid excessive immunopathology. Interestingly, the described differences between the two infected groups, which did not suffer from severe pathology, indicate again that the presence of MF seems to be relevant to induce immunosuppression in an established infection. Such tempered immune responses would provide an environment that benefits the transmission phase of the parasite. The findings herein provide novel insight into the immunology of asymptomatic MF^- individuals, a previously neglected cohort of patients. Their elevated immune responses may provide the key into elucidating alternative therapeutic treatments which would essentially block transmission and consequently eliminate the infection. In addition, since infected MF^- individuals were characterized by higher levels of antigen-specific IL-5, that is associated with induction of pathology, one might speculate that these patients are more prone to develop severe pathology which is further reflected by their decreased ratios of IgG4/IgE. In principle, only long term studies could demystify the questions regarding the development of severe pathology but this would not be in accordance with ethical clearance and moreover with MDA programmes which aim to break transmission and to eliminate the infection. However, in the small *in vitro* study with non-endemic normals we observed an alteration of IL-1β and IL-17 secretion upon stimulation with MF whereas, unexpectedly, IL-10 was not affected, although this cytokine is strongly associated with filariasis. Nevertheless, IL-1β and IL-17 are interesting candidates for prospective in-depths experiments in the context of filarial infections and the same appears for molecules like CD84 or cytokines like IL-15 that were found to be differentially regulated between the compared groups.

5. References

1. Taylor, M.J., A. Hoerauf, and M. Bockarie, *Lymphatic filariasis and onchocerciasis.* Lancet, 2010. **376**: p. 1175-85.
2. Hoerauf, A., et al., *Filariasis in Africa-treatment challenges and prospects.* Clin Microbiol Infect, 2011. **17**(7): p. 977-85.
3. Hoerauf, A.M., *Onchocerciasis*, in *Tropical Infectious Diseases: Principles, Pathogens and Practice*. 2010, R. L. Guerrant, D. H. Walker, Peter F. Weller,.
4. WHO-APOC. *Onchocerciasis – the disease and its impact*. 2011; Available from: http://www.who.int/apoc/onchocerciasis/disease/en/index.html.
5. Tamarozzi, F., et al., *Onchocerciasis: the role of wolbachia bacterial endosymbionts in parasite biology, disease pathogenesis, and treatment.* Clin Microbiol Rev, 2011. **24**(3): p. 459-68.
6. Duerr, H.P., G. Raddatz, and M. Eichner, *Diagnostic value of nodule palpation in onchocerciasis.* Trans R Soc Trop Med Hyg, 2008. **102**(2): p. 148-54.
7. Brattig, N.W., *Pathogenesis and host responses in human onchocerciasis: impact of Onchocerca filariae and Wolbachia endobacteria.* Microbes Infect, 2004. **6**(1): p. 113-28.
8. Hoerauf, A., et al., *Efficacy of 5-week doxycycline treatment on adult Onchocerca volvulus.* Parasitol Res, 2009. **104**(2): p. 437-47.
9. Korten, S., et al., *Low levels of transforming growth factor-beta (TGF-beta) and reduced suppression of Th2-mediated inflammation in hyperreactive human onchocerciasis.* Parasitology, 2010. **138**(1): p. 35-45.
10. Ottesen, E.A., *Immune responsiveness and the pathogenesis of human onchocerciasis.* J Infect Dis, 1995. **171**(3): p. 659-71.
11. King, C.L. and T.B. Nutman, *Regulation of the immune response in lymphatic filariasis and onchocerciasis.* Immunol Today, 1991. **12**(3): p. A54-8.
12. Hise, A.G., et al., *Innate immune responses to endosymbiotic Wolbachia bacteria in Brugia malayi and Onchocerca volvulus are dependent on TLR2, TLR6, MyD88, and Mal, but not TLR4, TRIF, or TRAM.* J Immunol, 2007. **178**(2): p. 1068-76.
13. Hoerauf, A. and N. Brattig, *Resistance and susceptibility in human onchocerciasis--beyond Th1 vs. Th2.* Trends Parasitol, 2002. **18**(1): p. 25-31.
14. Hoerauf, A., et al., *Onchocerciasis.* BMJ, 2003. **326**(7382): p. 207-10.
15. Soboslay, P.T., et al., *The diverse expression of immunity in humans at distinct states of Onchocerca volvulus infection.* Immunology, 1997. **90**(4): p. 592-9.
16. Lechner, C.J., et al., *Chemokines and cytokines in patients with an occult Onchocerca volvulus infection.* Microbes Infect, 2011.
17. Hoerauf, A., et al., *The variant Arg110Gln of human IL-13 is associated with an immunologically hyper-reactive form of onchocerciasis (sowda).* Microbes Infect, 2002. **4**(1): p. 37-42.
18. Satoguina, J., et al., *Antigen-specific T regulatory-1 cells are associated with immunosuppression in a chronic helminth infection (onchocerciasis).* Microbes Infect, 2002. **4**(13): p. 1291-300.
19. Maizels, R.M., et al., *Regulation of pathogenesis and immunity in helminth infections.* J Exp Med, 2009. **206**(10): p. 2059-66.
20. Allen, J.E. and R.M. Maizels, *Diversity and dialogue in immunity to helminths.* Nat Rev Immunol, 2011. **11**(6): p. 375-88.
21. Sabat, R., et al., *Biology of interleukin-10.* Cytokine Growth Factor Rev, 2010. **21**(5): p. 331-44.
22. Goswami, R. and M.H. Kaplan, *A brief history of IL-9.* J Immunol, 2011. **186**(6): p. 3283-8.

23. Steel, C. and T.B. Nutman, *Regulation of IL-5 in onchocerciasis. A critical role for IL-2.* J Immunol, 1993. **150**(12): p. 5511-8.
24. Doetze, A., et al., *Antigen-specific cellular hyporesponsiveness in a chronic human helminth infection is mediated by T(h)3/T(r)1-type cytokines IL-10 and transforming growth factor-beta but not by a T(h)1 to T(h)2 shift.* Int Immunol, 2000. **12**(5): p. 623-30.
25. Maizels, R.M. and M. Yazdanbakhsh, *Immune regulation by helminth parasites: cellular and molecular mechanisms.* Nat Rev Immunol, 2003. **3**(9): p. 733-44.
26. Smits, H.H., et al., *Chronic helminth infections protect against allergic diseases by active regulatory processes.* Curr Allergy Asthma Rep, 2010. **10**(1): p. 3-12.
27. Mahanty, S., et al., *Stage-specific induction of cytokines regulates the immune response in lymphatic filariasis.* Exp Parasitol, 1996. **84**(2): p. 282-90.
28. Brattig, N.W., et al., *The major surface protein of Wolbachia endosymbionts in filarial nematodes elicits immune responses through TLR2 and TLR4.* J Immunol, 2004. **173**(1): p. 437-45.
29. Brattig, N.W., et al., *Onchocerca volvulus-exposed persons fail to produce interferon-gamma in response to O. volvulus antigen but mount proliferative responses with interleukin-5 and IL-13 production that decrease with increasing microfilarial density.* J Infect Dis, 2002. **185**(8): p. 1148-54.
30. Schnoeller, C., et al., *A helminth immunomodulator reduces allergic and inflammatory responses by induction of IL-10-producing macrophages.* J Immunol, 2008. **180**(6): p. 4265-72.
31. Babu, S., V. Kumaraswami, and T.B. Nutman, *Alternatively activated and immunoregulatory monocytes in human filarial infections.* J Infect Dis, 2009. **199**(12): p. 1827-37.
32. Korten, S., et al., *Transforming growth factor-beta expression by host cells is elicited locally by the filarial nematode Onchocerca volvulus in hyporeactive patients independently from Wolbachia.* Microbes Infect, 2010. **12**(7): p. 555-64.
33. Babu, S., et al., *Cutting edge: diminished T cell TLR expression and function modulates the immune response in human filarial infection.* J Immunol, 2006. **176**(7): p. 3885-9.
34. Sakaguchi, S., et al., *Regulatory T cells and immune tolerance.* Cell, 2008. **133**(5): p. 775-87.
35. Sasisekhar, B., et al., *Diminished monocyte function in microfilaremic patients with lymphatic filariasis and its relationship to altered lymphoproliferative responses.* Infect Immun, 2005. **73**(6): p. 3385-93.
36. Babu, S., et al., *Diminished expression and function of TLR in lymphatic filariasis: a novel mechanism of immune dysregulation.* J Immunol, 2005. **175**(2): p. 1170-6.
37. Kreider, T., et al., *Alternatively activated macrophages in helminth infections.* Curr Opin Immunol, 2007. **19**(4): p. 448-53.
38. Gordon, S. and F.O. Martinez, *Alternative activation of macrophages: mechanism and functions.* Immunity, 2010. **32**(5): p. 593-604.
39. Saint Andre, A., et al., *The role of endosymbiotic Wolbachia bacteria in the pathogenesis of river blindness.* Science, 2002. **295**(5561): p. 1892-5.
40. Daehnel, K., et al., *Filaria/Wolbachia activation of dendritic cells and development of Th1-associated responses is dependent on Toll-like receptor 2 in a mouse model of ocular onchocerciasis (river blindness).* Parasite Immunol, 2007. **29**(9): p. 455-65.
41. Babu, S., et al., *Filarial lymphedema is characterized by antigen-specific Th1 and th17 proinflammatory responses and a lack of regulatory T cells.* PLoS Negl Trop Dis, 2009. **3**(4): p. 1-9.
42. Babu, S., et al., *Filarial Lymphatic Pathology Reflects Augmented TLR-mediated, MAPK-mediated Pro-inflammatory Cytokine Production.* Infect Immun, 2011: p. 4600–4608.
43. Li, M.O., et al., *Transforming growth factor-beta regulation of immune responses.* Annu Rev Immunol, 2006. **24**: p. 99-146.

44. Debrah, A.Y., et al., *Transforming growth factor-beta1 variant Leu10Pro is associated with both lack of microfilariae and differential microfilarial loads in the blood of persons infected with lymphatic filariasis.* Hum Immunol, 2011: p. 1143-1148.
45. Korten, S., et al., *The nematode parasite Onchocerca volvulus generates the transforming growth factor-beta (TGF-beta).* Parasitol Res, 2009. **105**(3): p. 731-41.
46. Ouyang, W., et al., *Regulation and functions of the IL-10 family of cytokines in inflammation and disease.* Annu Rev Immunol, 2011. **29**: p. 71-109.
47. Pestka, S., et al., *Interleukin-10 and related cytokines and receptors.* Annu Rev Immunol, 2004. **22**: p. 929-79.
48. Cooper, P.J., et al., *Early human infection with Onchocerca volvulus is associated with an enhanced parasite-specific cellular immune response.* J Infect Dis, 2001. **183**(11): p. 1662-8.
49. Satoguina, J.S., et al., *T regulatory-1 cells induce IgG4 production by B cells: role of IL-10.* J Immunol, 2005. **174**(8): p. 4718-26.
50. Satoguina, J.S., et al., *Tr1 and naturally occurring regulatory T cells induce IgG4 in B cells through GITR/GITR-L interaction, IL-10 and TGF-beta.* Eur J Immunol, 2008. **38**(11): p. 3101-13.
51. Ottesen, E.A., et al., *Prominence of IgG4 in the IgG antibody response to human filariasis.* J Immunol, 1985. **134**(4): p. 2707-12.
52. Dafa'alla, T.H., et al., *The profile of IgG and IgG subclasses of onchocerciasis patients.* Clin Exp Immunol, 1992. **88**(2): p. 258-63.
53. Hussain, R. and E.A. Ottesen, *IgE responses in human filariasis. IV. Parallel antigen recognition by IgE and IgG4 subclass antibodies.* J Immunol, 1986. **136**(5): p. 1859-63.
54. Adjobimey, T. and A. Hoerauf, *Induction of immunoglobulin G4 in human filariasis: an indicator of immunoregulation.* Ann Trop Med Parasitol, 2010. **104**(6): p. 455-64.
55. Korten, S., et al., *Mast cells in onchocercomas from patients with hyperreactive onchocerciasis (sowda).* Acta Trop, 1998. **70**(2): p. 217-31.
56. Elson, L.H., et al., *Immunity to onchocerciasis: putative immune persons produce a Th1-like response to Onchocerca volvulus.* J Infect Dis, 1995. **171**(3): p. 652-8.
57. Turaga, P.S., et al., *Immunity to onchocerciasis: cells from putatively immune individuals produce enhanced levels of interleukin-5, gamma interferon, and granulocyte-macrophage colony-stimulating factor in response to Onchocerca volvulus larval and male worm antigens.* Infect Immun, 2000. **68**(4): p. 1905-11.
58. Doetze, A., et al., *Production of both IFN-gamma and IL-5 by Onchocerca volvulus S1 antigen-specific CD4+ T cells from putatively immune individuals.* Int Immunol, 1997. **9**(5): p. 721-9.
59. Hussain, R., R.W. Poindexter, and E.A. Ottesen, *Control of allergic reactivity in human filariasis. Predominant localization of blocking antibody to the IgG4 subclass.* J Immunol, 1992. **148**(9): p. 2731-7.
60. WHO, *Weekly epidemiological record - African Programme for Onchocerciasis Control – report of the sixth meeting of national task forces, October 2009*. 2010. p. 21-28.
61. WHO, *Global programme to eliminate lymphatic filariasis (GPELF). Progress report 2000-2009 and strategic plan 2010-2020.* 2010: p. 1-79.
62. Bockarie, M.J. and R.M. Deb, *Elimination of lymphatic filariasis: do we have the drugs to complete the job?* Curr Opin Infect Dis, 2010. **23**(6): p. 617-20.
63. Ramaiah, K.D., et al., *The economic burden of lymphatic filariasis in India.* Parasitol Today, 2000. **16**(6): p. 251-3.
64. Ramaiah, K.D., et al., *Functional impairment caused by lymphatic filariasis in rural areas of south India.* Trop Med Int Health, 1997. **2**(9): p. 832-8.

65. Ottesen, E.A., *Lymphatic filariasis: Treatment, control and elimination.* Adv Parasitol, 2006. **61**: p. 395-441.
66. Manguin, S., et al., *Review on global co-transmission of human Plasmodium species and Wuchereria bancrofti by Anopheles mosquitoes.* Infect Genet Evol, 2010. **10**(2): p. 159-77.
67. Hoerauf, A., et al., *Immunomodulation by filarial nematodes.* Parasite Immunol, 2005. **27**(10-11): p. 417-29.
68. Babu, S., et al., *Regulatory networks induced by live parasites impair both Th1 and Th2 pathways in patent lymphatic filariasis: implications for parasite persistence.* J Immunol, 2006. **176**(5): p. 3248-56.
69. Maizels, R.M., et al., *T-cell activation and the balance of antibody isotypes in human lymphatic filariasis.* Parasitol Today, 1995. **11**(2): p. 50-6.
70. Nutman, T.B. and V. Kumaraswami, *Regulation of the immune response in lymphatic filariasis: perspectives on acute and chronic infection with Wuchereria bancrofti in South India.* Parasite Immunol, 2001. **23**(7): p. 389-99.
71. Addiss, D.G. and M.A. Brady, *Morbidity management in the Global Programme to Eliminate Lymphatic Filariasis: a review of the scientific literature.* Filaria J, 2007. **6**: p. 1-19.
72. Dreyer, G., et al., *Acute attacks in the extremities of persons living in an area endemic for bancroftian filariasis: differentiation of two syndromes.* Trans R Soc Trop Med Hyg, 1999. **93**(4): p. 413-7.
73. Simonsen, P.E., *Filariases*, in *Manson's tropical diseases*. 2009. p. 1477-1513.
74. Pfarr, K.M., et al., *Filariasis and lymphoedema.* Parasite Immunol, 2009. **31**(11): p. 664-72.
75. Jungmann, P., J. Figueredo-Silva, and G. Dreyer, *Bancroftian lymphadenopathy: a histopathologic study of fifty-eight cases from northeastern Brazil.* Am J Trop Med Hyg, 1991. **45**(3): p. 325-31.
76. Ottesen, E.A., *Immunopathology of Lymphatic Filariasis in Man.* Springer Semininars Immunopathology, 1980. **2**: p. 373-385.
77. Shenoy, R.K., *Clinical and pathological aspects of filarial lymphedema and its management.* Korean J Parasitol, 2008. **46**(3): p. 119-25.
78. Debrah, A.Y., et al., *Doxycycline reduces plasma VEGF-C/sVEGFR-3 and improves pathology in lymphatic filariasis.* PLoS Pathog, 2006. **2**(9): p. 0829-43.
79. Debrah, A.Y., et al., *Plasma vascular endothelial growth Factor-A (VEGF-A) and VEGF-A gene polymorphism are associated with hydrocele development in lymphatic filariasis.* Am J Trop Med Hyg, 2007. **77**(4): p. 601-8.
80. Ong, R.K. and R.L. Doyle, *Tropical pulmonary eosinophilia.* Chest, 1998. **113**(6): p. 1673-9.
81. Solanki, A. and J. Ahluwalia, *Asymptomatic filariasis.* Blood, 2011. **117**(14): p. 3707.
82. Lobos, E., et al., *A major allergen of lymphatic filarial nematodes is a parasite homolog of the gamma-glutamyl transpeptidase.* Mol Med, 1996. **2**(6): p. 712-24.
83. Dreyer, G., et al., *Pathogenesis of lymphatic disease in bancroftian filariasis: a clinical perspective.* Parasitol Today, 2000. **16**(12): p. 544-8.
84. Steel, C., et al., *Long-term effect of prenatal exposure to maternal microfilaraemia on immune responsiveness to filarial parasite antigens.* Lancet, 1994. **343**(8902): p. 890-3.
85. Semnani, R.T., et al., *Filarial antigens impair the function of human dendritic cells during differentiation.* Infect Immun, 2001. **69**(9): p. 5813-22.
86. Semnani, R.T., et al., *Brugia malayi microfilariae induce cell death in human dendritic cells, inhibit their ability to make IL-12 and IL-10, and reduce their capacity to activate CD4+ T cells.* J Immunol, 2003. **171**(4): p. 1950-60.
87. Semnani, R.T., et al., *Filaria-induced immune evasion: suppression by the infective stage of Brugia malayi at the earliest host-parasite interface.* J Immunol, 2004. **172**(10): p. 6229-38.

88. Babu, S. and T.B. Nutman, *Proinflammatory cytokines dominate the early immune response to filarial parasites.* J Immunol, 2003. **171**(12): p. 6723-32.
89. Das, B.K., P.K. Sahoo, and B. Ravindran, *A role for tumour necrosis factor-alpha in acute lymphatic filariasis.* Parasite Immunol, 1996. **18**(8): p. 421-4.
90. Mahanty, S. and T.B. Nutman, *Immunoregulation in human lymphatic filariasis: the role of interleukin 10.* Parasite Immunol, 1995. **17**(8): p. 385-92.
91. Semnani, R.T. and T.B. Nutman, *Toward an understanding of the interaction between filarial parasites and host antigen-presenting cells.* Immunol Rev, 2004. **201**: p. 127-38.
92. King, C.L., et al., *Immunologic tolerance in lymphatic filariasis. Diminished parasite-specific T and B lymphocyte precursor frequency in the microfilaremic state.* J Clin Invest, 1992. **89**(5): p. 1403-10.
93. Mahanty, S., et al., *High levels of spontaneous and parasite antigen-driven interleukin-10 production are associated with antigen-specific hyporesponsiveness in human lymphatic filariasis.* J Infect Dis, 1996. **173**(3): p. 769-73.
94. King, C.L., et al., *Cytokine control of parasite-specific anergy in human lymphatic filariasis. Preferential induction of a regulatory T helper type 2 lymphocyte subset.* J Clin Invest, 1993. **92**(4): p. 1667-73.
95. Nutman, T.B., V. Kumaraswami, and E.A. Ottesen, *Parasite-specific anergy in human filariasis. Insights after analysis of parasite antigen-driven lymphokine production.* J Clin Invest, 1987. **79**(5): p. 1516-23.
96. Maizels, R.M., et al., *Vaccination against helminth parasites--the ultimate challenge for vaccinologists?* Immunol Rev, 1999. **171**: p. 125-47.
97. Ottesen, E.A., P.F. Weller, and L. Heck, *Specific cellular immune unresponsiveness in human filariasis.* Immunology, 1977. **33**(3): p. 413-21.
98. Satapathy, A.K., et al., *Human bancroftian filariasis: immunological markers of morbidity and infection.* Microbes Infect, 2006. **8**(9-10): p. 2414-23.
99. Ristimaki, A., et al., *Proinflammatory cytokines regulate expression of the lymphatic endothelial mitogen vascular endothelial growth factor-C.* J Biol Chem, 1998. **273**(14): p. 8413-8.
100. Numasaki, M., M.T. Lotze, and H. Sasaki, *Interleukin-17 augments tumor necrosis factor-alpha-induced elaboration of proangiogenic factors from fibroblasts.* Immunol Lett, 2004. **93**(1): p. 39-43.
101. Kurniawan, A., et al., *Differential expression of IgE and IgG4 specific antibody responses in asymptomatic and chronic human filariasis.* J Immunol, 1993. **150**(9): p. 3941-50.
102. Hussain, R., et al., *IgE responses in human filariasis. I. Quantitation of filaria-specific IgE.* J Immunol, 1981. **127**(4): p. 1623-9.
103. Hussain, R., M. Grogl, and E.A. Ottesen, *IgG antibody subclasses in human filariasis. Differential subclass recognition of parasite antigens correlates with different clinical manifestations of infection.* J Immunol, 1987. **139**(8): p. 2794-8.
104. Ravindran, B., et al., *Protective immunity in human lymphatic filariasis: problems and prospects.* Med Microbiol Immunol, 2003. **192**(1): p. 41-6.
105. Dimock, K.A., M.L. Eberhard, and P.J. Lammie, *Th1-like antifilarial immune responses predominate in antigen-negative persons.* Infect Immun, 1996. **64**(8): p. 2962-7.
106. Steel, C., A. Guinea, and E.A. Ottesen, *Evidence for protective immunity to bancroftian filariasis in the Cook Islands.* J Infect Dis, 1996. **174**(3): p. 598-605.
107. Hoerauf, A., et al., *Doxycycline in the treatment of human onchocerciasis: Kinetics of Wolbachia endobacteria reduction and of inhibition of embryogenesis in female Onchocerca worms.* Microbes Infect, 2003. **5**(4): p. 261-73.
108. Hoerauf, A., et al., *Wolbachia endobacteria depletion by doxycycline as antifilarial therapy has macrofilaricidal activity in onchocerciasis: a randomized placebo-controlled study.* Med Microbiol Immunol, 2008. **197**(3): p. 295-311.

109. Taylor, M.J. and A. Hoerauf, *Wolbachia bacteria of filarial nematodes.* Parasitol Today, 1999. **15**(11): p. 437-42.
110. Turner, J.D., et al., *Wolbachia lipoprotein stimulates innate and adaptive immunity through Toll-like receptors 2 and 6 to induce disease manifestations of filariasis.* J Biol Chem, 2009. **284**(33): p. 22364-78.
111. Brattig, N.W., et al., *Lipopolysaccharide-like molecules derived from Wolbachia endobacteria of the filaria Onchocerca volvulus are candidate mediators in the sequence of inflammatory and antiinflammatory responses of human monocytes.* Microbes Infect, 2000. **2**(10): p. 1147-57.
112. Pfarr, K.M., K. Fischer, and A. Hoerauf, *Involvement of Toll-like receptor 4 in the embryogenesis of the rodent filaria Litomosoides sigmodontis.* Med Microbiol Immunol, 2003. **192**(1): p. 53-6.
113. Osei-Atweneboana, M.Y., et al., *Prevalence and intensity of Onchocerca volvulus infection and efficacy of ivermectin in endemic communities in Ghana: a two-phase epidemiological study.* Lancet, 2007. **369**(9578): p. 2021-9.
114. Palumbo, E., *Filariasis: diagnosis, treatment and prevention.* Acta Biomed, 2008. **79**(2): p. 106-9.
115. Weil, G.J., P.J. Lammie, and N. Weiss, *The ICT Filariasis Test: A rapid-format antigen test for diagnosis of bancroftian filariasis.* Parasitol Today, 1997. **13**(10): p. 401-4.
116. Simonsen, P.E. and S.K. Dunyo, *Comparative evaluation of three new tools for diagnosis of bancroftian filariasis based on detection of specific circulating antigens.* Trans R Soc Trop Med Hyg, 1999. **93**(3): p. 278-82.
117. Turner, P., et al., *A comparison of the Og4C3 antigen capture ELISA, the Knott test, an IgG4 assay and clinical signs, in the diagnosis of Bancroftian filariasis.* Trop Med Parasitol, 1993. **44**(1): p. 45-8.
118. Dreyer, G., et al., *Ultrasonographic evidence for stability of adult worm location in bancroftian filariasis.* Trans R Soc Trop Med Hyg, 1994. **88**(5): p. 558.
119. Mand, S., et al., *Animated documentation of the filaria dance sign (FDS) in bancroftian filariasis.* Filaria J, 2003. **2**(1): p. 1-11.
120. Shenoy, R.K., et al., *Apparent failure of ultrasonography to detect adult worms of Brugia malayi.* Ann Trop Med Parasitol, 2000. **94**(1): p. 77-82.
121. Mand, S., et al., *Detection of adult Brugia malayi filariae by ultrasonography in humans in India and Indonesia.* Trop Med Int Health, 2006. **11**(9): p. 1375-81.
122. Haarbrink, M., et al., *Anti-filarial IgG4 in men and women living in Brugia malayi-endemic areas.* Trop Med Int Health, 1999. **4**(2): p. 93-7.
123. Moreno, Y., et al., *Ivermectin disrupts the function of the excretory-secretory apparatus in microfilariae of Brugia malayi.* Proc Natl Acad Sci U S A, 2010. **107**(46): p. 20120-5.
124. Fernando, S.D., C. Rodrigo, and S. Rajapakse, *Current evidence on the use of antifilarial agents in the management of bancroftian filariasis.* J Trop Med, 2011. **2011**: p. 1-12.
125. Omura, S. and A. Crump, *The life and times of ivermectin - a success story.* Nat Rev Microbiol, 2004. **2**(12): p. 984-9.
126. Ottesen, E.A. and W.C. Campbell, *Ivermectin in human medicine.* J Antimicrob Chemother, 1994. **34**(2): p. 195-203.
127. Horton, J., *Albendazole: a broad spectrum anthelminthic for treatment of individuals and populations.* Curr Opin Infect Dis, 2002. **15**(6): p. 599-608.
128. Dadzie, K.Y., et al., *Ocular findings in a double-blind study of ivermectin versus diethylcarbamazine versus placebo in the treatment of onchocerciasis.* Br J Ophthalmol, 1987. **71**(2): p. 78-85.
129. Debrah, A.Y., et al., *Macrofilaricidal Activity in Wuchereria bancrofti after 2 Weeks Treatment with a Combination of Rifampicin plus Doxycycline.* J Parasitol Res, 2011. **2011**: p. 1-9.

130. WHO, *weekly epidemiological record: InterAmerican Conference on Onchocerciasis, 2010: progress towards eliminating river blindness in the WHO Region of the Americas.* 2011. **86**(38): p. 417-424.
131. WHO, *Global Programme to Eliminate Lymphatic Filariasis: progress report on mass drug administration, 2010.* 2011. **86**: p. 377–388.
132. Hoerauf, A., *Filariasis: new drugs and new opportunities for lymphatic filariasis and onchocerciasis.* Curr Opin Infect Dis, 2008. **21**(6): p. 673-81.
133. Osei-Atweneboana, M.Y., et al., *Phenotypic evidence of emerging ivermectin resistance in Onchocerca volvulus.* PLoS Negl Trop Dis, 2011. **5**(3): p. e998.
134. Cross, H.F., et al., *Severe reactions to filarial chemotherapy and release of Wolbachia endosymbionts into blood.* Lancet, 2001. **358**(9296): p. 1873-5.
135. Hoerauf, A., et al., *Endosymbiotic bacteria in worms as targets for a novel chemotherapy in filariasis.* Lancet, 2000. **355**(9211): p. 1242-3.
136. Hoerauf, A., et al., *Tetracycline therapy targets intracellular bacteria in the filarial nematode Litomosoides sigmodontis and results in filarial infertility.* J Clin Invest, 1999. **103**(1): p. 11-8.
137. Hoerauf, A., et al., *Doxycycline as a novel strategy against bancroftian filariasis-depletion of Wolbachia endosymbionts from Wuchereria bancrofti and stop of microfilaria production.* Med Microbiol Immunol, 2003. **192**(4): p. 211-6.
138. Taylor, M.J., et al., *Macrofilaricidal activity after doxycycline treatment of Wuchereria bancrofti: a double-blind, randomised placebo-controlled trial.* Lancet, 2005. **365**(9477): p. 2116-21.
139. Mand, S., D.W. Buttner, and A. Hoerauf, *Bancroftian filariasis--absence of Wolbachia after doxycycline treatment.* Am J Trop Med Hyg, 2008. **78**(6): p. 854-5.
140. Mand, S., et al., *Macrofilaricidal activity and amelioration of lymphatic pathology in bancroftian filariasis after 3 weeks of doxycycline followed by single-dose diethylcarbamazine.* Am J Trop Med Hyg, 2009. **81**(4): p. 702-11.
141. Coulibaly, Y.I., et al., *A randomized trial of doxycycline for Mansonella perstans infection.* N Engl J Med, 2009. **361**(15): p. 1448-58.
142. Hoerauf, A., et al., *Depletion of wolbachia endobacteria in Onchocerca volvulus by doxycycline and microfilaridermia after ivermectin treatment.* Lancet, 2001. **357**(9266): p. 1415-6.
143. Volkmann, L., et al., *Antibiotic therapy in murine filariasis (Litomosoides sigmodontis): comparative effects of doxycycline and rifampicin on Wolbachia and filarial viability.* Trop Med Int Health, 2003. **8**(5): p. 392-401.
144. Specht, S., et al., *Efficacy of 2- and 4-week rifampicin treatment on the Wolbachia of Onchocerca volvulus.* Parasitol Res, 2008. **103**(6): p. 1303-9.
145. Schulz-Key, H., E.J. Albiez, and D.W. Buttner, *Isolation of living adult Onchocerca volvulus from nodules.* Tropenmed Parasitol, 1977. **28**(4): p. 428-30.
146. Mand, S., et al., *Frequent detection of worm movements in onchocercal nodules by ultrasonography.* Filaria J, 2005. **4**(1): p. 1-11.
147. Mand, S., et al., *The role of ultrasonography in the differentiation of the various types of filaricele due to bancroftian filariasis.* Acta Trop, 2010. **120 S**: p. S23-32.
148. Ayad, S.R., M. Fox, and D. Winstanley, *The use of ficoll gradient centrifugation to produce synchronous mouse lymphoma cells.* Biochem Biophys Res Commun, 1969. **37**(4): p. 551-8.
149. Arakaki, D.T. and R.S. Sparkes, *Microtechnique for Culturing Leukocytes from Whole Blood.* Cytogenetics, 1963. **85**: p. 57-60.
150. Lowrie, R.C., Jr., *Cryopreservation of the microfilariae of Brugia malayi, Dirofilaria corynodes, and Wuchereria bancrofti.* Am J Trop Med Hyg, 1983. **32**(1): p. 138-45.

151. Klonisch, T., et al., *The sheaths of Brugia microfilariae: isolation and composition.* Parasitol Res, 1991. **77**(5): p. 448-51.
152. Al-Qaoud, K.M., et al., *Infection of BALB/c mice with the filarial nematode Litomosoides sigmodontis: role of CD4+ T cells in controlling larval development.* Infect Immun, 1997. **65**(6): p. 2457-61.
153. Laemmli, U.K., *Cleavage of structural proteins during the assembly of the head of bacteriophage T4.* Nature, 1970. **227**(5259): p. 680-5.
154. Debey-Pascher, S., et al., *RNA-stabilized whole blood samples but not peripheral blood mononuclear cells can be stored for prolonged time periods prior to transcriptome analysis.* J Mol Diagn, 2011. **13**(4): p. 452-60.
155. Mitre, E., D. Chien, and T.B. Nutman, *CD4(+) (and not CD25+) T cells are the predominant interleukin-10-producing cells in the circulation of filaria-infected patients.* J Infect Dis, 2008. **197**(1): p. 94-101.
156. Metenou, S., et al., *At Homeostasis Filarial Infections Have Expanded Adaptive T Regulatory but Not Classical Th2 Cells.* J Immunol, 2010. **184**(9): p. 5375-82.
157. Turner, J.D., et al., *Wolbachia endosymbiotic bacteria of Brugia malayi mediate macrophage tolerance to TLR- and CD40-specific stimuli in a MyD88/TLR2-dependent manner.* J Immunol, 2006. **177**(2): p. 1240-9.
158. Sartono, E., et al., *Depression of antigen-specific interleukin-5 and interferon-gamma responses in human lymphatic filariasis as a function of clinical status and age.* J Infect Dis, 1997. **175**(5): p. 1276-80.
159. Sweiss, N.J., et al., *Linkage of type I interferon activity and TNF-alpha levels in serum with sarcoidosis manifestations and ancestry.* PLoS One, 2011. **6**(12): p. e29126.
160. Hubner, M.P., et al., *Echinococcus multilocularis metacestodes modulate cellular cytokine and chemokine release by peripheral blood mononuclear cells in alveolar echinococcosis patients.* Clin Exp Immunol, 2006. **145**(2): p. 243-51.
161. Bennuru, S., et al., *Elevated levels of plasma angiogenic factors are associated with human lymphatic filarial infections.* Am J Trop Med Hyg, 2010. **83**(4): p. 884-90.
162. Dunyo, S.K., F.K. Nkrumah, and P.E. Simonsen, *Single-dose treatment of Wuchereria bancrofti infections with ivermectin and albendazole alone or in combination: evaluation of the potential for control at 12 months after treatment.* Trans R Soc Trop Med Hyg, 2000. **94**(4): p. 437-43.
163. Hussein, O., et al., *Duplex Doppler sonographic assessment of the effects of diethylcarbamazine and albendazole therapy on adult filarial worms and adjacent host tissues in Bancroftian filariasis.* Am J Trop Med Hyg, 2004. **71**(4): p. 471-7.
164. Senbagavalli, P., et al., *Heightened measures of immune complex and complement function and immune complex-mediated granulocyte activation in human lymphatic filariasis.* Am J Trop Med Hyg, 2011. **85**(1): p. 89-96.
165. Tobian, A.A., et al., *Sensitivity and specificity of ultrasound detection and risk factors for filarial-associated hydroceles.* Am J Trop Med Hyg, 2003. **68**(6): p. 638-42.
166. Faris, R., et al., *Bancroftian filariasis in Egypt: visualization of adult worms and subclinical lymphatic pathology by scrotal ultrasound.* Am J Trop Med Hyg, 1998. **59**(6): p. 864-7.
167. Jaoko, W.G., et al., *Filarial-specific antibody response in East African bancroftian filariasis: effects of host infection, clinical disease, and filarial endemicity.* Am J Trop Med Hyg, 2006. **75**(1): p. 97-107.
168. Noroes, J., et al., *Occurrence of living adult Wuchereria bancrofti in the scrotal area of men with microfilaraemia.* Trans R Soc Trop Med Hyg, 1996. **90**(1): p. 55-6.
169. Yazdanbakhsh, M., A. van den Biggelaar, and R.M. Maizels, *Th2 responses without atopy: immunoregulation in chronic helminth infections and reduced allergic disease.* Trends Immunol, 2001. **22**(7): p. 372-7.

170. Chitkara, R.K. and G. Krishna, *Parasitic pulmonary eosinophilia.* Semin Respir Crit Care Med, 2006. **27**(2): p. 171-84.
171. Volkmann, L., et al., *Murine filariasis: interleukin 4 and interleukin 5 lead to containment of different worm developmental stages.* Med Microbiol Immunol, 2003. **192**(1): p. 23-31.
172. Saeftel, M., et al., *Synergism of gamma interferon and interleukin-5 in the control of murine filariasis.* Infect Immun, 2003. **71**(12): p. 6978-85.
173. Brattig, N., et al., *Differences in cytokine responses to Onchocerca volvulus extract and recombinant Ov33 and OvL3-1 proteins in exposed subjects with various parasitologic and clinical states.* J Infect Dis, 1997. **176**(3): p. 838-42.
174. Soboslay, P.T., et al., *Regulatory effects of Th1-type (IFN-gamma, IL-12) and Th2-type cytokines (IL-10, IL-13) on parasite-specific cellular responsiveness in Onchocerca volvulus-infected humans and exposed endemic controls.* Immunology, 1999. **97**(2): p. 219-25.
175. Aalberse, R.C., et al., *Immunoglobulin G4: an odd antibody.* Clin Exp Allergy, 2009. **39**(4): p. 469-77.
176. Brattig, N.W., et al., *Strong IgG isotypic antibody response in sowdah type onchocerciasis.* J Infect Dis, 1994. **170**(4): p. 955-61.
177. Finbloom, D.S. and K.D. Winestock, *IL-10 induces the tyrosine phosphorylation of tyk2 and Jak1 and the differential assembly of STAT1 alpha and STAT3 complexes in human T cells and monocytes.* J Immunol, 1995. **155**(3): p. 1079-90.
178. Wehinger, J., et al., *IL-10 induces DNA binding activity of three STAT proteins (Stat1, Stat3, and Stat5) and their distinct combinatorial assembly in the promoters of selected genes.* FEBS Lett, 1996. **394**(3): p. 365-70.
179. Martin, M., et al., *CD84 functions as a homophilic adhesion molecule and enhances IFN-gamma secretion: adhesion is mediated by Ig-like domain 1.* J Immunol, 2001. **167**(7): p. 3668-76.
180. Tangye, S.G., et al., *Functional requirements for interactions between CD84 and Src homology 2 domain-containing proteins and their contribution to human T cell activation.* J Immunol, 2003. **171**(5): p. 2485-95.
181. Alvarez-Errico, D., et al., *CD84 Negatively Regulates IgE High-Affinity Receptor Signaling in Human Mast Cells.* J Immunol, 2011: p. 5577-86.
182. Cannons, J.L., et al., *Optimal germinal center responses require a multistage T cell:B cell adhesion process involving integrins, SLAM-associated protein, and CD84.* Immunity, 2010. **32**(2): p. 253-65.
183. Maizels, R.M., et al., *Helminth parasites--masters of regulation.* Immunol Rev, 2004. **201**: p. 89-116.
184. Yan, Q., et al., *Structure of CD84 provides insight into SLAM family function.* Proc Natl Acad Sci U S A, 2007. **104**(25): p. 10583-8.
185. Gri, G., et al., *CD4+CD25+ regulatory T cells suppress mast cell degranulation and allergic responses through OX40-OX40L interaction.* Immunity, 2008. **29**(5): p. 771-81.
186. Shakoory, B., et al., *The role of human mast cell-derived cytokines in eosinophil biology.* J Interferon Cytokine Res, 2004. **24**(5): p. 271-81.
187. Lechmann, M., et al., *The extracellular domain of CD83 inhibits dendritic cell-mediated T cell stimulation and binds to a ligand on dendritic cells.* J Exp Med, 2001. **194**(12): p. 1813-21.
188. Lechmann, M., et al., *CD83 on dendritic cells: more than just a marker for maturation.* Trends Immunol, 2002. **23**(6): p. 273-5.
189. Breloer, M. and B. Fleischer, *CD83 regulates lymphocyte maturation, activation and homeostasis.* Trends Immunol, 2008. **29**(4): p. 186-94.
190. Reinwald, S., et al., *CD83 expression in CD4+ T cells modulates inflammation and autoimmunity.* J Immunol, 2008. **180**(9): p. 5890-7.

191. Hock, B.D., et al., *A soluble form of CD83 is released from activated dendritic cells and B lymphocytes, and is detectable in normal human sera.* Int Immunol, 2001. **13**(7): p. 959-67.
192. Mikosz, C.A., et al., *Glucocorticoid receptor-mediated protection from apoptosis is associated with induction of the serine/threonine survival kinase gene, sgk-1.* J Biol Chem, 2001. **276**(20): p. 16649-54.
193. Franchi, L., et al., *Function of Nod-like receptors in microbial recognition and host defense.* Immunol Rev, 2009. **227**(1): p. 106-28.
194. Magalhaes, J.G., et al., *What is new with Nods?* Curr Opin Immunol, 2011. **23**(1): p. 29-34.
195. Fuller, D.M. and W. Zhang, *Regulation of lymphocyte development and activation by the LAT family of adapter proteins.* Immunol Rev, 2009. **232**(1): p. 72-83.
196. Zhu, M., et al., *Negative regulation of lymphocyte activation by the adaptor protein LAX.* J Immunol, 2005. **174**(9): p. 5612-9.
197. Hengartner, M.O., *The biochemistry of apoptosis.* Nature, 2000. **407**(6805): p. 770-6.
198. Choi, E.H., et al., *Genetic polymorphisms in molecules of innate immunity and susceptibility to infection with Wuchereria bancrofti in South India.* Genes Immun, 2001. **2**(5): p. 248-53.
199. Babu, S., C.P. Blauvelt, and T.B. Nutman, *Filarial parasites induce NK cell activation, type 1 and type 2 cytokine secretion, and subsequent apoptotic cell death.* J Immunol, 2007. **179**(4): p. 2445-56.
200. Semnani, R.T., et al., *Induction of TRAIL- and TNF-alpha-dependent apoptosis in human monocyte-derived dendritic cells by microfilariae of Brugia malayi.* J Immunol, 2008. **181**(10): p. 7081-9.
201. Chen, L., et al., *Skin-stage schistosomula of Schistosoma mansoni produce an apoptosis-inducing factor that can cause apoptosis of T cells.* J Biol Chem, 2002. **277**(37): p. 34329-35.
202. Perera, P.Y., J.H. Lichy, and L.P. Perera, *The role of interleukin-15 in inflammation and immune responses to infection: Implications for its therapeutic use.* Microbes Infect, 2011.
203. van Leeuwen, E.M., J. Sprent, and C.D. Surh, *Generation and maintenance of memory CD4(+) T Cells.* Curr Opin Immunol, 2009. **21**(2): p. 167-72.
204. Dooms, H., et al., *Quiescence-inducing and antiapoptotic activities of IL-15 enhance secondary CD4+ T cell responsiveness to antigen.* J Immunol, 1998. **161**(5): p. 2141-50.
205. Bernasconi, N.L., E. Traggiai, and A. Lanzavecchia, *Maintenance of serological memory by polyclonal activation of human memory B cells.* Science, 2002. **298**(5601): p. 2199-202.
206. Esen, M., et al., *Effect of IL-15 on IgG versus IgE antibody-secreting cells in vitro.* J Immunol Methods, 2011: p. 7-13
207. Strioga, M., V. Pasukoniene, and D. Characiejus, *CD8+ CD28- and CD8+ CD57+ T cells and their role in health and disease.* Immunology, 2011. **134**(1): p. 17-32.
208. Lal, R.B., et al., *Lymphocyte subpopulations in Bancroftian filariasis: activated (DR+) CD8+ T cells in patients with chronic lymphatic obstruction.* Clin Exp Immunol, 1989. **77**(1): p. 77-82.
209. Freedman, D.O., et al., *Predominant CD8+ infiltrate in limb biopsies of individuals with filarial lymphedema and elephantiasis.* Am J Trop Med Hyg, 1995. **53**(6): p. 633-8.
210. de Almeida, A.B., et al., *The presence or absence of active infection, not clinical status, is most closely associated with cytokine responses in lymphatic filariasis.* J Infect Dis, 1996. **173**(6): p. 1453-9.
211. Steel, C. and T.B. Nutman, *CTLA-4 in filarial infections: implications for a role in diminished T cell reactivity.* J Immunol, 2003. **170**(4): p. 1930-8.
212. Taylor, M.D., et al., *CTLA-4 and CD4+ CD25+ regulatory T cells inhibit protective immunity to filarial parasites in vivo.* J Immunol, 2007. **179**(7): p. 4626-34.
213. Owhashi, M., et al., *Non-specific immune suppression by CD8+ T cells in Brugia pahangi-infected rats.* Int J Parasitol, 1990. **20**(7): p. 951-6.
214. Yamada, T., et al., *Transcription factor ELF4 controls the proliferation and homing of CD8+ T cells via the Kruppel-like factors KLF4 and KLF2.* Nat Immunol, 2009. **10**(6): p. 618-26.

215. Henkle-Duhrsen, K., et al., *Localization and functional analysis of the cytosolic and extracellular CuZn superoxide dismutases in the human parasitic nematode Onchocerca volvulus.* Mol Biochem Parasitol, 1997. **88**(1-2): p. 187-202.
216. Miao, L. and D.K. St Clair, *Regulation of superoxide dismutase genes: implications in disease.* Free Radic Biol Med, 2009. **47**(4): p. 344-56.
217. Pardo, M., J.A. Melendez, and O. Tirosh, *Manganese superoxide dismutase inactivation during Fas (CD95)-mediated apoptosis in Jurkat T cells.* Free Radic Biol Med, 2006. **41**(12): p. 1795-806.
218. Hitchens, M.R. and P.D. Robbins, *The role of the transcription factor DP in apoptosis.* Apoptosis, 2003. **8**(5): p. 461-8.
219. Di Bacco, A., et al., *The SUMO-specific protease SENP5 is required for cell division.* Mol Cell Biol, 2006. **26**(12): p. 4489-98.
220. Ichii, H., et al., *Role for Bcl-6 in the generation and maintenance of memory CD8+ T cells.* Nat Immunol, 2002. **3**(6): p. 558-63.
221. Ythier, D., et al., *Sumoylation of ING2 regulates the transcription mediated by Sin3A.* Oncogene, 2010. **29**(44): p. 5946-56.
222. Rye, M.S., et al., *FBXO11, a regulator of the TGFbeta pathway, is associated with severe otitis media in Western Australian children.* Genes Immun, 2011. **12**(5): p. 352-9.
223. Sarker, K.P., et al., *ING2 as a novel mediator of transforming growth factor-beta-dependent responses in epithelial cells.* J Biol Chem, 2008. **283**(19): p. 13269-79.
224. Tilley, S.L., T.M. Coffman, and B.H. Koller, *Mixed messages: modulation of inflammation and immune responses by prostaglandins and thromboxanes.* J Clin Invest, 2001. **108**(1): p. 15-23.
225. Klein, M., et al., *Repression of Cyclic Adenosine Monophosphate Upregulation Disarms and Expands Human Regulatory T Cells.* J Immunol, 2011.
226. Tanaka, K., et al., *Effects of prostaglandin D2 on helper T cell functions.* Biochem Biophys Res Commun, 2004. **316**(4): p. 1009-14.
227. Angeli, V., et al., *Role of the parasite-derived prostaglandin D2 in the inhibition of epidermal Langerhans cell migration during schistosomiasis infection.* J Exp Med, 2001. **193**(10): p. 1135-47.
228. Herve, M., et al., *Pivotal roles of the parasite PGD2 synthase and of the host D prostanoid receptor 1 in schistosome immune evasion.* Eur J Immunol, 2003. **33**(10): p. 2764-72.
229. Petit, I., D. Jin, and S. Rafii, *The SDF-1-CXCR4 signaling pathway: a molecular hub modulating neo-angiogenesis.* Trends Immunol, 2007. **28**(7): p. 299-307.
230. Attout, T., et al., *Lymphatic vascularisation and involvement of Lyve-1+ macrophages in the human onchocerca nodule.* PLoS One, 2009. **4**(12): p. e8234.
231. Kobayashi, N., et al., *Down-regulation of CXCR4 expression on human CD8+ T cells during peripheral differentiation.* Eur J Immunol, 2004. **34**(12): p. 3370-8.
232. Metkar, S.S., et al., *Perforin rapidly induces plasma membrane phospholipid flip-flop.* PLoS One, 2011. **6**(9): p. e24286.
233. Metenou, S., et al., *Filarial Infection Suppresses Malaria-Specific Multifunctional Th1 and Th17 Responses in Malaria and Filarial Coinfections.* J Immunol, 2011. **186**(8): p. 4725-33.
234. Asano-Kato, N., et al., *TGF-beta1, IL-1beta, and Th2 cytokines stimulate vascular endothelial growth factor production from conjunctival fibroblasts.* Exp Eye Res, 2005. **80**(4): p. 555-60.
235. Jovanovic, D.V., et al., *IL-17 stimulates the production and expression of proinflammatory cytokines, IL-beta and TNF-alpha, by human macrophages.* J Immunol, 1998. **160**(7): p. 3513-21.
236. Kimura, A. and T. Kishimoto, *IL-6: regulator of Treg/Th17 balance.* Eur J Immunol, 2010. **40**(7): p. 1830-5.

237. Keiser, P.B., et al., *Bacterial endosymbionts of Onchocerca volvulus in the pathogenesis of posttreatment reactions.* J Infect Dis, 2002. **185**(6): p. 805-11.
238. Dissanayake, S., *In Wuchereria bancrofti filariasis, asymptomatic microfilaraemia does not progress to amicrofilaraemic lymphatic disease.* Int J Epidemiol, 2001. **30**(2): p. 394-9.
239. Zhang, F., et al., *VEGF-B is dispensable for blood vessel growth but critical for their survival, and VEGF-B targeting inhibits pathological angiogenesis.* Proc Natl Acad Sci U S A, 2009. **106**(15): p. 6152-7.
240. Li, X., et al., *VEGF-B: a survival, or an angiogenic factor?* Cell Adh Migr, 2009. **3**(4): p. 322-7.
241. Hagberg, C.E., et al., *Vascular endothelial growth factor B controls endothelial fatty acid uptake.* Nature, 2010. **464**(7290): p. 917-21.
242. Li, X., *VEGF-B: a thing of beauty.* Cell Res, 2010. **20**(7): p. 741-4.
243. Kivela, R., et al., *Exercise-induced expression of angiogenic growth factors in skeletal muscle and in capillaries of healthy and diabetic mice.* Cardiovasc Diabetol, 2008. **7**: p. 13.
244. Hubner, M.P., J.T. Stocker, and E. Mitre, *Inhibition of type 1 diabetes in filaria-infected non-obese diabetic mice is associated with a T helper type 2 shift and induction of FoxP3+ regulatory T cells.* Immunology, 2009. **127**(4): p. 512-22.
245. Aravindhan, V., et al., *Decreased prevalence of lymphatic filariasis among diabetic subjects associated with a diminished pro-inflammatory cytokine response (CURES 83).* PLoS Negl Trop Dis, 2010. **4**(6): p. e707.
246. Aravindhan, V., et al., *Decreased prevalence of lymphatic filariasis among subjects with type-1 diabetes.* Am J Trop Med Hyg, 2010. **83**(6): p. 1336-9.
247. Soboslay, P.T., et al., *Ivermectin-facilitated immunity in onchocerciasis; activation of parasite-specific Th1-type responses with subclinical Onchocerca volvulus infection.* Clin Exp Immunol, 1994. **96**(2): p. 238-44.
248. Semnani, R.T., et al., *Filaria-induced monocyte dysfunction and its reversal following treatment.* Infect Immun, 2006. **74**(8): p. 4409-17.

Appendix A: Equipment

Automatic pipettes (10-1000µl)	Eppendorf AG, Hamburg, Germany
Automatic pipettes (10-1000µl)	Biohit, Rosbach v. d. Höhe, Germany
BD FACSCanto™ I flow cytometer	BD™ Biosciences, Heidelberg, Germany
BD FACS Diva flow cytometer	BD™ Biosciences, Heidelberg, Germany
Bioanalyzer Agilent 2100	Agilent Technologies, Waldbronn, Germany
Centrifuge (Eppendorf 5415 R)	Eppendorf AG, Hamburg, Germany
Centrifuge (Multifuge 4KR)	Heraeus Holding GmbH, Hanau, Germany
Combs (1.5 mm)	Bio-Rad, Munich, Germany
ELISA Plate reader (Spectra Max 340pc384)	Molecular Devices, Sunnyvale, USA
Films	Kodak, Stuttgart, Germany
Filter (Whatman Nucleopore, 5 µm)	Carl Roth, Karlsruhe, Germany
Freezer (-20°C)	Bosch GmbH, Stuttgart, Germany
Freezer (-80°C)	Heraeus Holding GmbH, Hanau, Germany
Fridge	Bosch GmbH, Stuttgart, Germany
Gel tray	Bio-Rad, Munich, Germany
Gel documentation (BioDocAnalyze digital)	Biometra GmbH, Göttingen, Germany
Glass pipettes (1-20 ml)	Brand GmbH & Co KG, Wertheim, Germany
Glass mortar	VWR, Langenfeld, Germany
Glass plates (1.5 mm)	Bio-Rad, Munich, Germany
Glassware	Schott AG, Mainz, Germany
Heating Block	Eppendorf AG, Hamburg, Germany
Ice machine (Scotsman AF 80)	Gastro Handel GmbH, Wien, Austria
Incubator	Binder GmbH, Tuttlingen, Germany
MACS® columns (MS)	Miltenyi Biotech GmbH, Bergisch Gladbach Germany
MACS® separator	Miltenyi Biotech GmbH, Bergisch Gladbach, Germany
Magnet (Dynal MPC®)	Invitrogen GmbH, Darmstadt, Germany
Microscope (Leica DM IL)	Leica Microsystems GmbH, Wetzlar, Germany
Microarray Scanning(Illumina HiScan SQ)	Illumina Inc., San Diego, USA
Mixer (Dynal MX1)	Invitrogen GmbH, Darmstadt, Germany
MoFlo	Beckman Coulter, Miami, USA
Nanodrop	Peqlab, Erlangen, Germany
Needles (BD Microlance™, 21G)	BD™ Biosciences, Heidelberg, Germany
Neubauer counting chamber	LO Laboroptik GmbH, Bad Homburg, Germany
PH meter	Mettler Toledo GmbH, Giessen, Germany
Pipetboy (pipetus®-akku)	Hirschmann Laborgeräte, Eberstadt, Germany
Power supply	Bio-Rad, Munich, Germany
Punch (Holth corneoscleral punch 2mm)	Koch, Hamburg, Germany
PVDF membrane (0.45 µm)	Sigma-Aldrich GmbH, Munich, Germany
Reflotron® Plus	Roche Diagnostics, Mannheim, Germany

Rocker	Bio-Rad, Munich, Germany
Scanner ScanMaker i900	Microtek, Willich, Germany
Sedgewick rafter chamber	VWR, Langenfeld, Germany
Spacer (1.5 mm)	Bio-Rad, Munich, Germany
Syringes (5 ml, 10 ml)	BD™ Biosciences, Heidelberg, Germany
Thermocycler	Biometra GmbH, Göttingen, Germany
Thermo magnetic stirrer	IKA® GmbH & Co.KG, Staufen, Germany
Trans-blot semi dry transfer cell	Bio-Rad, Munich, Germany
Ultrasound machine (Sonosite 180 Plus)	Sonosite, Bothell, USA
Vortex mixer (Minishaker)	IKA® GmbH & Co.KG, Staufen, Germany
Water bath	VWR, Langenfeld, Germany
Water purifier Milli-Q plus	Millipore, Schwalbach, Germany
Weighing machine	Sartorius AG, Göttingen, Germany
Western blotting filter paper	Bio-Rad, Munich, Germany
Wrapping film	Staples Advantage, Cologne, Germany

Appendix B: Chemicals and Reagents

Advanced Protein Assay™	Cytoskeleton, Inc., Denver, USA
Agarose	Fermentas. St. Leon-Rot, Germany
Agilent RNA 6000 Pico Kit	Agilent Technologies, Waldbronn, Germany
Ammoniumpersulfate (10%)	Sigma-Aldrich GmbH, Munich, Germany
autoMACS running buffer	Miltenyi Biotech GmbH, Bergisch Gladbach, Germany
B cell isolation kit	Invitrogen GmbH, Darmstadt, Germany
BD Phosflow starter kit	BD™ Biosciences, Heidelberg, Germany
β-Mercaptoethanol	Sigma-Aldrich GmbH, Munich, Germany
Bromophenol blue	Sigma-Aldrich GmbH, Munich, Germany
BSA	PAA Laboratories GmbH, Pasching, Austria
CD14 Microbeads	Miltenyi Biotech GmbH, Bergisch Gladbach, Germany
$CD4^+$ T cell isolation kit	Invitrogen GmbH, Darmstadt, Germany
Chloroform	Sigma-Aldrich GmbH, Munich, Germany
Cytometric bead assay (IgG1, IgG2, IgG3, IgG4, IgE)	BD™ Biosciences, Heidelberg, Germany
DMSO	Sigma-Aldrich GmbH, Munich, Germany
DNA Loading dye (6x)	Fermentas. St. Leon-Rot, Germany
dNTP Mix (10 mM each)	Invitrogen GmbH, Darmstadt, Germany
ELISA kits Ready-SET-Go (IL-6, IL-10, IFN-γ, TNF)	eBiosciences, Inc., San Diego, USA
ELISA kits (IL-5, IL-6, IL-10, IL-13, IL-17, IFN-γ, TNF)	R&D, Wiesbaden-Nordenstadt, Germany
Ethanol	Merck KGAA, Darmstadt, Germany

FCS	PAA Laboratories GmbH, Pasching, Austria
Gel Loading Dye, Blue (6X)	NEW ENGLAND BioLabs, Frankfurt, Gemany
Gentamycin	PAA Laboratories GmbH, Pasching, Austria
Giemsa's azur eosin methylene blue solution	Merck KGAA, Darmstadt, Germany
Hydrogen peroxide (H_2O_2)	Sigma-Aldrich GmbH, Munich, Germany
Illumina® Whole-Genome Gene Expression Direct Hybridization Assay system	Illumina Inc., San Diego, USA
Immun-Star™ AP substrate	Bio-Rad, Munich, Germany
Isopropanol	Merck KGAA, Darmstadt, Germany
Leucosep tubes	Greiner Bio-one, Frickenhausen, Germany
L-glutamine	PAA Laboratories GmbH, Pasching, Austria
Limulus amoebocyte lysate assay	Charles River, Wilmington, USA
Liquid nitrogen	Linde, Düsseldorf, Germany
LPS	Sigma-Aldrich GmbH, Munich, Germany
LSM 1077	PAA Laboratories GmbH, Pasching, Austria
Malaria test (Nadal® Malaria test 4species)	Nal von Minden, Moers, Germany
miRNeasy Kit	Qiagen, Hilden, Germany
Monosodium phosphate	Merck KGAA, Darmstadt, Germany
Normal Rat serum	eBiosciences, Inc., San Diego, USA
Paraformaldehyde	Merck KGAA, Darmstadt, Germany
PBS (endotoxin free)	PAA Laboratories GmbH, Pasching, Austria
Penicillin/Streptomycin	PAA Laboratories GmbH, Pasching, Austria
Potassium chloride (KCl)	Merck KGAA, Darmstadt, Germany
Potassium dihydrogen phosphate	Merck KGAA, Darmstadt, Germany
Protein Standard (MagicMark™)	Invitrogen GmbH, Darmstadt, Germany
PPD	Statens Serum Institut, Copenhagen, Denmark
Random decamer primers	Ambion, Darmstadt, Germany
Recombinant human IL-10	R&D, Wiesbaden-Nordenstadt, Germany
RedSafe™ Nucleic Acid Staining Solution	HISS Diagnostics GmbH, Freiburg, Germany
RIPA lysis buffer	Santa Cruz Biotechnology Inc., Heidelberg, Germany
RNA Clean & Concentrator™- 5	Zymo Research Cooperation, Irvine, USA
RNase-free water	Qiagen, Hilden, Germany
RNaseOUT™ Recombinant Ribonuclease Inhibitor	Invitrogen GmbH, Darmstadt, Germany
RNeasy MiniElute Cleanup Kit	Qiagen, Hilden, Germany
RNA ladder	Invitrogen GmbH, Darmstadt, Germany
Roti®-block	Carl Roth, Karlsruhe, Germany
RPMI-1640	PAA Laboratories GmbH, Pasching, Austria
Saccharose	Sigma-Aldrich GmbH, Munich, Germany
Sodium chloride (NaCl)	Merck KGAA, Darmstadt, Germany

Stop solution 2N H_2SO_4	Merck KGAA, Darmstadt, Germany
Streptavidin-Peroxidase	Roche Diagnostics, Mannheim, Germany
SuperScript III Reverse Transcriptase	Invitrogen GmbH, Darmstadt, Germany
SuperScript II Reverse Transcriptase	Invitrogen GmbH, Darmstadt, Germany
TargetAmp™ 2-Round Biotin aRNA Amplification Kit 3.0	Epicentre Biotechnologies, Madison, USA
TBE buffer 10x	Biomol GmbH, Hamburg, Germany
TEMED	Bio-Rad, Munich, Germany
TMB	Sigma-Aldrich GmbH, Munich, Germany
TropBio® ELISA	TropBio, Townsville, Australia
Tris	Merck KGAA, Darmstadt, Germany
Trizol (Qiazol lysis reagent)	Qiagen, Hilden, Germany
Trypan Blue	Sigma-Aldrich GmbH, Munich, Germany
Tween 20	Sigma-Aldrich GmbH, Munich, Germany

Appendic C: Buffers, Media and Solutions

20x phosphate buffer saline (PBS):

360 g NaCl

8.0 g KCl

46.4 g Na_2HPO_4

8.0 g KH_2PO_4

Volume was then adjusted to 1 liter of distilled water.

For 1x phosphate buffer saline (PBS): 50 ml of 20x PBS solution was diluted in 900 ml distilled water. The pH was adjusted to 7.3 and the solution was topped up to 1 liter and autoclaved.

Fetal calf serum

FCS used for medium supplementations was heated for 30 minutes at 56°C to inactivate the complement factors. Aliquots were then stored at -20°C until required.

Cells culture reagents

Complete medium

RPMI 1640

2 mM L-glutamine

50 μg/ml penicillin/streptomycin

50 μg/ml gentamicin

Cell culture medium

RPMI 1640

2 mM L-glutamine

50 μg/ml penicillin/streptomycin

50 μg/ml gentamicin

10% FCS

Freezing medium

80% FCS

20% Dimethylsulfoxid (DMSO)

ELISA:

Coating solution

0.1 M $NaHCO_3$, pH 9.6

Washing buffer

1x PBS

0.05% Tween 20

Blocking solution

1x PBS

1% BSA

Substrate buffer

0.1 M $NaH_2PO_4.2H_2O$, pH 5.5

Substrate

3,3', 5,5' Tetramethylbenzidine, dissolved to a concentration of 6 mg/ml in DMSO.

Substrate solution

12 ml substrate buffer

200 µl substrate

1.2 µl 30% H_2O_2

Stop solution

2N H_2SO_4

SDS-Page and Western blot

7% separation gel (total volume 15 ml)

7.75 ml H_20

3.5 ml Acrylamide (30%)

3.75 ml 4x Lower Tris TEMED

30 µl APS (10%)

5% stacking gel (total volume 10 ml)

6.5 ml H_20

1.3 ml Acrylamide (30%)

2.5 ml 4x Upper Tris

30 µl TEMED

30 µl APS (10%)

Laemmli buffer (pH 6.8)

4% SDS

0.5% bromophenol blue

1% β-mercaptoethanol

0.5% glycerol

0.5 M Tris-HCl

Electrophoresis running buffer (pH 8.3)

192 mM glycine

25 mM Tris,

0.1% SDS

Transfer buffer (pH 8.53)

10 mM Tris

100 mM glycine

20% methanol

Western blot wash buffer

1x PBS

0.15% Tween 20

Flow cytometry

FACS buffer

1x PBS

1% FCS

Fixation buffer

1x PBS

4% Paraformaldehyde

Appendix D: Primer sequences

5´ß-Aktin Fragment: 269 bp

fw primer 5`end:	TGGTGGGCATGGGTCAGA
rv primer 5`end:	GTACATGGCTGGGGTGTTGA

3´ß-Aktin Fragment: 456 bp

fw primer 3`end:	AACAAGATGAGATTGGCA
rv primer 3`end:	GACCAAAAGCCTTCATACAT

Appendix E: Software

BD FACSDiva software 3.0

Flow cytometry software obtained from BD™ Biosciences, Heidelberg, Germany.

Fiji software

Fiji is an open source imaging software.

GraphPad Prism 5

Analyze, Graph and Organize Software obtained from GraphPad Software, Inc., La Jolla, USA.

SoftMax Pro

Microplate Data Acquisition and Analysis Software obtained from Molecular Devices, Sunnyvale, USA.

Appendix F: Microarray data

Comparison $CD4^{+}CD25^{hihg}$ T cells of infected individuals versus EN

Symbol	Definition	mean_Treg_inf	mean_Treg_healthy	FC	pvalue	diff
C14orf80	Homo sapiens chromosome 14 open reading frame 80 (C14orf80), mRNA.	130.96	343.55	-2.62	0.017	212.59
EMILIN2	Homo sapiens elastin microfibril interfacer 2 (EMILIN2), mRNA.	261.48	495.64	-1.90	0.019	234.16
WDR36	Homo sapiens WD repeat domain 36 (WDR36), mRNA.	163.35	298.22	-1.83	0.001	134.87
EIF4A1	Homo sapiens eukaryotic translation initiation factor 4A, isoform 1 (EIF4A1), mRNA.	310.14	560.08	-1.81	0.012	249.94
RARS	Homo sapiens arginyl-tRNA synthetase (RARS), mRNA.	657.38	1121.84	-1.71	0.020	464.47
C6orf125	Homo sapiens chromosome 6 open reading frame 125 (C6orf125), mRNA.	182.46	309.35	-1.70	6.00E-04	126.89
PGM1	Homo sapiens phosphoglucomutase 1 (PGM1), mRNA.	596.24	1003.63	-1.68	0.004	407.39
C7orf26	Homo sapiens chromosome 7 open reading frame 26 (C7orf26), mRNA.	263.03	436.54	-1.66	5.00E-04	173.51
CHKB	Homo sapiens choline kinase beta (CHKB), transcript variant 1, mRNA.	569.14	936.93	-1.65	0.009	367.79
ZFYVE20	Homo sapiens zinc finger, FYVE domain containing 20 (ZFYVE20), mRNA.	170.40	274.60	-1.61	0.000	104.19
DGUOK	Homo sapiens deoxyguanosine kinase (DGUOK), nuclear gene encoding mitochondrial protein, transcript variant 1, mRNA.	551.51	857.06	-1.55	0.040	305.55
TDRD1	Homo sapiens tudor domain containing 1 (TDRD1), mRNA.	216.45	333.79	-1.54	0.020	117.35
C15orf17	Homo sapiens chromosome 15 open reading frame 17 (C15orf17), mRNA.	219.38	335.64	-1.53	0.000	116.26
DENR	Homo sapiens density-regulated protein (DENR), mRNA.	852.71	566.85	1.50	0.029	285.86
LOC728855	Homo sapiens hypothetical LOC728855 (LOC728855), non-coding RNA.	1308.39	860.91	1.52	0.012	447.47
CCDC115	Homo sapiens coiled-coil domain containing 115 (CCDC115), mRNA.	509.65	325.20	1.57	0.025	184.46
ST6GAL1	Homo sapiens ST6 beta-galactosamide alpha-2,6-sialyltranferase 1 (ST6GAL1), transcript variant 2, mRNA.	923.78	588.98	1.57	0.040	334.8
CAPRIN2	Homo sapiens caprin family member 2 (CAPRIN2), transcript variant 1, mRNA.	311.54	197.38	1.58	0.015	114.15
SETD3	Homo sapiens SET domain containing 3 (SETD3), transcript variant 1, mRNA.	2673.25	1691.14	1.58	0.000	982.11
C18orf25	Homo sapiens chromosome 18 open reading frame 25 (C18orf25), transcript variant 2, mRNA.	477.45	296.84	1.61	0.012	180.61
PRKAB2	Homo sapiens protein kinase, AMP-activated, beta 2 non-catalytic subunit (PRKAB2), mRNA.	303.61	183.34	1.66	0.007	120.27
SRP54	Homo sapiens signal recognition particle 54kDa (SRP54), mRNA.	980.97	589.69	1.66	0.043	391.28
COPS5	Homo sapiens COP9 constitutive photomorphogenic homolog subunit 5 (Arabidopsis) (COPS5), mRNA.	1241.43	743.49	1.67	0.047	497.94
COPS3	Homo sapiens COP9 constitutive photomorphogenic homolog subunit 3 (Arabidopsis) (COPS3), mRNA.	715.53	424.61	1.69	0.006	290.92
STAT1	Homo sapiens signal transducer and activator of transcription 1, 91kDa (STAT1), transcript variant alpha, mRNA.	2180.10	1290.43	1.69	0.002	889.67
EIF2B1	Homo sapiens eukaryotic translation initiation factor 2B, subunit 1 alpha, 26kDa (EIF2B1), mRNA.	647.37	381.63	1.70	0.013	265.75
GMFB	Homo sapiens glia maturation factor, beta (GMFB), mRNA.	659.24	381.72	1.73	0.012	277.52
ADCY7	Homo sapiens adenylate cyclase 7 (ADCY7), mRNA.	504.66	289.77	1.74	0.032	214.89
PNKP	Homo sapiens polynucleotide kinase 3'-phosphatase (PNKP), mRNA.	358.86	206.21	1.74	0.027	152.65
ATP6V1D	Homo sapiens ATPase, H+ transporting, lysosomal 34kDa, V1 subunit D (ATP6V1D), mRNA.	889.84	508.36	1.75	0.003	381.48
CPNE3	Homo sapiens copine III (CPNE3), mRNA.	487.84	277.73	1.76	0.038	210.11
SRP54	PREDICTED: Homo sapiens signal recognition particle 54kDa (SRP54), mRNA.	925.94	527.47	1.76	0.034	398.47
ACLY	Homo sapiens ATP citrate lyase (ACLY), transcript variant 2, mRNA.	874.16	487.06	1.79	0.002	387.1
COPB2	Homo sapiens coatomer protein complex, subunit beta 2 (beta prime) (COPB2), mRNA.	354.97	197.46	1.80	0.024	157.51
SEC11C	Homo sapiens SEC11 homolog C (S. cerevisiae) (SEC11C), mRNA.	1063.33	589.43	1.80	0.025	473.9
TBK1	Homo sapiens TANK-binding kinase 1 (TBK1), mRNA.	781.06	433.53	1.80	0.002	347.53
PIAS4	Homo sapiens protein inhibitor of activated STAT, 4 (PIAS4), mRNA.	226.26	125.07	1.81	0.048	101.2
LOC651894	PREDICTED: Homo sapiens similar to ribosomal protein S12 (LOC651894), mRNA.	852.84	468.03	1.82	0.003	384.82
WDR19	Homo sapiens WD repeat domain 19 (WDR19), mRNA.	232.33	126.52	1.84	0.000	105.81
SEC23IP	Homo sapiens SEC23 interacting protein (SEC23IP), mRNA.	226.32	122.39	1.85	0.006	103.93
ZNF845	Homo sapiens zinc finger protein 845 (ZNF845), mRNA. XM_039908	238.56	128.06	1.86	0.000	110.5

ST3GAL5	Homo sapiens ST3 beta-galactoside alpha-2,3-sialyltransferase 5 (ST3GAL5), transcript variant 2, mRNA.	367.35	196.8	1.87	0.000	170.55
ZNF721	Homo sapiens zinc finger protein 721 (ZNF721), mRNA.	345.94	185.12	1.87	0.024	160.83
AKR1A1	Homo sapiens aldo-keto reductase family 1, member A1 (aldehyde reductase) (AKR1A1), transcript variant 1, mRNA.	822.73	431.33	1.91	0.005	391.4
GSPT2	Homo sapiens G1 to S phase transition 2 (GSPT2), mRNA.	261.17	136.22	1.92	0.003	124.95
ATAD1	Homo sapiens ATPase family, AAA domain containing 1 (ATAD1), mRNA.	243.02	124.18	1.96	5.00E-04	118.84
ITGB1	Homo sapiens integrin, beta 1 (fibronectin receptor, beta polypeptide, antigen CD29 includes MDF2, MSK12) (ITGB1), transcript variant 1D, mRNA.	353.74	179.21	1.97	0.033	174.52
ZHX2	Homo sapiens zinc fingers and homeoboxes 2 (ZHX2), mRNA.	359.92	182.89	1.97	0.046	177.04
LACTB	Homo sapiens lactamase, beta (LACTB), nuclear gene encoding mitochondrial protein, transcript variant 1, mRNA.	715.05	360.78	1.98	0.043	354.27
HDDC3	Homo sapiens HD domain containing 3 (HDDC3), mRNA.	324.36	163.04	1.99	0.001	161.32
SNX5	Homo sapiens sorting nexin 5 (SNX5), transcript variant 2, mRNA.	235.08	116.14	2.02	0.014	118.94
TOR1AIP1	Homo sapiens torsin A interacting protein 1 (TOR1AIP1), mRNA.	331.58	162.42	2.04	0.000	169.16
CDK7	Homo sapiens cyclin-dependent kinase 7 (MO15 homolog, Xenopus laevis, cdk-activating kinase) (CDK7), mRNA.	602.30	294.32	2.05	0.011	307.98
C13orf23	Homo sapiens chromosome 13 open reading frame 23 (C13orf23), transcript variant 1, mRNA.	272.86	131.32	2.08	0.004	141.54
C13orf23	Homo sapiens chromosome 13 open reading frame 23 (C13orf23), transcript variant 1, mRNA.	280.37	132.94	2.11	0.001	147.44
PRKAR1A	Homo sapiens protein kinase, cAMP-dependent, regulatory, type I, alpha (tissue specific extinguisher 1) (PRKAR1A), transcript variant 3, mRNA.	727.01	345.24	2.11	0.035	381.77
SDAD1	Homo sapiens SDA1 domain containing 1 (SDAD1), mRNA.	714.28	331.02	2.16	0.003	383.26
FBXO28	Homo sapiens F-box protein 28 (FBXO28), mRNA.	227.92	104.97	2.17	0.041	122.95
ZNHIT6	Homo sapiens zinc finger, HIT type 6 (ZNHIT6), mRNA.	262.49	120.79	2.17	0.007	141.7
C8orf76	Homo sapiens chromosome 8 open reading frame 76 (C8orf76), mRNA.	412.7	179.1	2.30	0.040	233.6
C17orf97	Homo sapiens chromosome 17 open reading frame 97 (C17orf97), mRNA.	221.92	93.73	2.37	0.012	128.19
DHX29	Homo sapiens DEAH (Asp-Glu-Ala-His) box polypeptide 29 (DHX29), mRNA.	269.91	113.53	2.38	0.003	156.37
PSMB5	Homo sapiens proteasome (prosome, macropain) subunit, beta type, 5 (PSMB5), mRNA.	447.32	187.96	2.38	0.013	259.36
HAVCR2	Homo sapiens hepatitis A virus cellular receptor 2 (HAVCR2), mRNA.	290.16	121.52	2.39	0.004	168.64
RSBN1	Homo sapiens round spermatid basic protein 1 (RSBN1), mRNA.	304.85	125.89	2.42	0.003	178.96
TOR1AIP1	Homo sapiens torsin A interacting protein 1 (TOR1AIP1), mRNA.	646.24	267.27	2.42	0.013	378.97
DHX29	Homo sapiens DEAH (Asp-Glu-Ala-His) box polypeptide 29 (DHX29), mRNA.	424.44	161.47	2.63	0.000	262.96
FAM69A	Homo sapiens family with sequence similarity 69, member A (FAM69A), mRNA.	335.09	105.31	3.18	0.004	229.78

Comparison $CD4^{+}CD25^{high}$ T cells of MF^{-} versus MF^{+} individuals

Symbol	Definition	mean_Treg_MFneg	mean_Treg_MFpos	FC	pvalue	diff
MYOM2	Homo sapiens myomesin (M-protein) 2, 165kDa (MYOM2), mRNA.	170.21	1021.80	-6.00	0.000	851.59
CD83	Homo sapiens CD83 molecule (CD83), transcript variant 2, mRNA.	187.41	567.67	-3.03	0.000	380.26
MYNN	Homo sapiens myoneurin (MYNN), mRNA.	122.18	340.64	-2.79	0.000	218.46
NBPF20	Homo sapiens neuroblastoma breakpoint family, member 20 (NBPF20), mRNA.	161.62	421.89	-2.61	0.000	260.27
RCBTB2	Homo sapiens regulator of chromosome condensation (RCC1) and BTB (POZ) domain containing protein 2 (RCBTB2), mRNA.	151.19	393.09	-2.60	0.000	241.90
VCAN	Homo sapiens versican (VCAN), mRNA.	151.84	392.22	-2.58	0.000	240.38
CD83	Homo sapiens CD83 molecule (CD83), transcript variant 1, mRNA.	113.99	282.12	-2.47	0.000	168.13
SNORD3A	Homo sapiens small nucleolar RNA, C/D box 3A (SNORD3A), small nucleolar RNA.	519.25	1213.06	-2.34	0.000	693.82
SGK	Homo sapiens serum/glucocorticoid regulated kinase (SGK), mRNA.	129.41	296.34	-2.29	0.001	166.92
GART	Homo sapiens phosphoribosylglycinamide formyltransferase, phosphoribosylglycinamide synthetase, phosphoribosylaminoimidazole synthetase (GART), transcript variant 1, mRNA.	390.16	873.82		0.031	483.66
FLJ38717	Homo sapiens FLJ38717 protein (FLJ38717), mRNA.	167.65	368.09	-2.20	1.00E-04	200.44
TNFRSF19	Homo sapiens tumor necrosis factor receptor superfamily, member 19 (TNFRSF19), transcript variant 2, mRNA.	151.24	328.88	-2.17	0.000	177.64
COBLL1	Homo sapiens COBL-like 1 (COBLL1), mRNA.	123.80	267.01	-2.16	4.00E-04	143.22
ZNF529	Homo sapiens zinc finger protein 529 (ZNF529), mRNA.	117.02	246.89	-2.11	0.000	129.87

PPARBP	Homo sapiens PPAR binding protein (PPARBP), mRNA.	127.65	268.68	-2.10	0.011	141.03
TGFBR3	Homo sapiens transforming growth factor, beta receptor III (TGFBR3), mRNA.	179.21	369.13	-2.06	0.015	189.92
ZYG11B	Homo sapiens zyg-11 homolog B (C. elegans) (ZYG11B), mRNA.	337.69	692.25	-2.05	0.000	354.56
KLF11	PREDICTED: Homo sapiens Kruppel-like factor 11 (KLF11), mRNA.	337.11	687.70	-2.04	0.003	350.59
PHC3	Homo sapiens polyhomeotic homolog 3 (Drosophila) (PHC3), mRNA.	134.84	275.28	-2.04	0.012	140.45
OXR1	Homo sapiens oxidation resistance 1 (OXR1), mRNA.	123.74	249.60	-2.02	0.000	125.86
RAB12	Homo sapiens RAB12, member RAS oncogene family (RAB12), mRNA.	106.62	212.86	2.00	0.004	106.24
C14orf131	Homo sapiens chromosome 14 open reading frame 131 (C14orf131), mRNA.	378.02	747.81	-1.98	0.300	369.80
TAGAP	Homo sapiens T-cell activation RhoGTPase activating protein (TAGAP), transcript variant 3, mRNA.	115.15	226.91	-1.97	0.010	111.76
FBXO11	Homo sapiens F-box protein 11 (FBXO11), transcript variant 1, mRNA.	425.99	831.65	-1.95	0.000	405.66
NDFIP1	Homo sapiens Nedd4 family interacting protein 1 (NDFIP1), mRNA.	124.99	242.02	-1.94	1.00E-04	117.04
C7orf54	Homo sapiens chromosome 7 open reading frame 54 (C7orf54), mRNA.	173.22	333.43	-1.92	8.00E-04	160.21
CD84	Homo sapiens CD84 molecule (CD84), mRNA.	138.65	261.99	-1.89	0.000	123.35
SMAD5	Homo sapiens SMAD family member 5 (SMAD5), transcript variant 1, mRNA.	162.96	303.99	-1.87	0.000	141.02
STAMBP	Homo sapiens STAM binding protein (STAMBP), transcript variant 1, mRNA.	354.05	662.07	-1.87	0.015	308.02
LOC727762	PREDICTED: Homo sapiens similar to NADH dehydrogenase (ubiquinone) 1 beta subcomplex, 4, 15kDa, transcript variant 1 (LOC727762), mRNA.	196.75	365.27	-1.86	0.002	168.53
SNRNP200	Homo sapiens small nuclear ribonucleoprotein 200kDa (U5) (SNRNP200), mRNA.	258.14	478.61	-1.85	0.000	220.47
RNF38	Homo sapiens ring finger protein 38 (RNF38), transcript variant 1, mRNA.	581.75	1064.1	-1.83	0.029	482.35
STAMBPL1	Homo sapiens STAM binding protein-like 1 (STAMBPL1), mRNA.	419.75	766.15	-1.83	0.041	346.39
CEP350	Homo sapiens centrosomal protein 350kDa (CEP350), mRNA.	140.95	254.90	-1.81	0.000	113.96
ERP27	Homo sapiens endoplasmic reticulum protein 27 kDa (ERP27), mRNA.	185.14	334.80	-1.81	0.008	149.65
EEF1G	Homo sapiens eukaryotic translation elongation factor 1 gamma (EEF1G), mRNA. XM_935976 XM_935977 XM_935978 XM_935979	937.36	1686.19	-1.80	0.008	748.83
MTX3	Homo sapiens metaxin 3 (MTX3), mRNA.	224.07	401.29	-1.79	0.013	177.21
TAGAP	Homo sapiens T-cell activation RhoGTPase activating protein (TAGAP), transcript variant 2, mRNA.	151.71	270.95	-1.79	0.000	119.24
PLEKHA1	Homo sapiens pleckstrin homology domain containing, family A (phosphoinositide binding specific) member 1 (PLEKHA1), transcript variant 2, mRNA.	184.52	327.88	-1.78	0.000	143.36
SMG1	Homo sapiens PI-3-kinase-related kinase SMG-1 (SMG1), mRNA.	292.75	516.87	-1.77	0.019	224.12
LOC644033	PREDICTED: Homo sapiens similar to similar to RPL23AP7 protein (LOC644033), mRNA.	348.13	613.32	-1.76	0.000	265.19
CHRAC1	Homo sapiens chromatin accessibility complex 1 (CHRAC1), mRNA.	241.90	421.73	-1.74	0.017	179.82
A2LD1	Homo sapiens AIG2-like domain 1 (A2LD1), mRNA.	168.01	288.9	-1.72	0.000	120.89
CMAS	Homo sapiens cytidine monophosphate N-acetylneuraminic acid synthetase (CMAS), mRNA.	240.33	413.22	-1.72	1.00E-04	172.89
GAB2	Homo sapiens GRB2-associated binding protein 2 (GAB2), transcript variant 1, mRNA.	141.78	241.98	-1.71	0.003	100.20
NKTR	Homo sapiens natural killer-tumor recognition sequence (NKTR), mRNA.	1069.57	1825.25	-1.71	0.019	755.68
SH3BGRL	Homo sapiens SH3 domain binding glutamic acid-rich protein like (SH3BGRL), mRNA.	474.03	810.42	-1.71	0.000	336.38
C14orf138	Homo sapiens chromosome 14 open reading frame 138 (C14orf138), transcript variant 1, mRNA.	153.93	261.76	-1.70	0.004	107.83
S100A8	Homo sapiens S100 calcium binding protein A8 (S100A8), mRNA.	205.20	348.86	-1.70	0.000	143.66
VAMP4	Homo sapiens vesicle-associated membrane protein 4 (VAMP4), transcript variant 1, mRNA.	186.81	317.31	-1.70	0.000	130.50
AGTPBP1	Homo sapiens ATP/GTP binding protein 1 (AGTPBP1), mRNA.	367.79	623.15	-1.69	0.000	255.36
MAP3K7	Homo sapiens mitogen-activated protein kinase kinase kinase 7 (MAP3K7), transcript variant B, mRNA.	604.31	1023.03	-1.69	6.00E-04	418.71
TMED2	Homo sapiens transmembrane emp24 domain trafficking protein 2 (TMED2), mRNA.	595.09	1008.2	-1.69	0.000	413.11
JMJD1C	Homo sapiens jumonji domain containing 1C (JMJD1C), transcript variant 1, mRNA.	264.42	441.62	-1.67	1.00E-04	177.2
ZNF211	Homo sapiens zinc finger protein 211 (ZNF211), transcript variant 1, mRNA.	201.07	335.95	-1.67	6.00E-04	134.87
CBLL1	Homo sapiens Cas-Br-M (murine) ecotropic retroviral transforming sequence-like 1 (CBLL1), mRNA.	350.97	584.23	-1.66	0.000	233.26
YOD1	Homo sapiens YOD1 OTU deubiquinating enzyme 1 homolog (S. cerevisiae) (YOD1), mRNA.	154.36	256.00	-1.66	0.009	101.64
DOCK11	Homo sapiens dedicator of cytokinesis 11 (DOCK11), mRNA.	1020.09	1681.86	-1.65	0.000	661.77
UFSP2	Homo sapiens UFM1-specific peptidase 2 (UFSP2), mRNA.	222.47	368.01	-1.65	0.000	145.55
BCLAF1	Homo sapiens BCL2-associated transcription factor 1 (BCLAF1), transcript variant 2, mRNA.	510.77	837.68	-1.64	0.023	326.91
DOCK10	Homo sapiens dedicator of cytokinesis 10 (DOCK10), mRNA.	672.35	1098.04	-1.63	0.000	425.69
GNPDA1	Homo sapiens glucosamine-6-phosphate deaminase 1 (GNPDA1), mRNA.	535.09	872.63	-1.63	0.004	337.54

NGDN	Homo sapiens neuroguidin, EIF4E binding protein (NGDN), transcript variant 1, mRNA.	229.23	374.18	-1.63	9.00E-04	144.95
SNORD3C	Homo sapiens small nucleolar RNA, C/D box 3C (SNORD3C), small nucleolar RNA.	363.57	588.02	-1.62	0.000	224.45
AMY2A	Homo sapiens amylase, alpha 2A (pancreatic) (AMY2A), mRNA.	265.38	427.12	-1.61	8.00E-04	161.74
ZNF786	Homo sapiens zinc finger protein 786 (ZNF786), mRNA.	385.91	620.53	-1.61	0.000	234.62
DTWD2	Homo sapiens DTW domain containing 2 (DTWD2), mRNA.	529.28	845.09	-1.60	0.000	315.82
RNF130	Homo sapiens ring finger protein 130 (RNF130), mRNA.	280.52	444.43	-1.58	0.000	163.91
FBXO34	Homo sapiens F-box protein 34 (FBXO34), mRNA.	254.13	398.71	-1.57	8.00E-04	144.58
SRGN	Homo sapiens serglycin (SRGN), mRNA.	314.56	493.47	-1.57	1.00E-04	178.9
COQ5	Homo sapiens coenzyme Q5 homolog, methyltransferase (S. cerevisiae) (COQ5), mRNA.	317.64	494.53	-1.56	0.015	176.89
LOC401397	PREDICTED: Homo sapiens hypothetical LOC401397 (LOC401397), mRNA.	218.92	341.58	-1.56	0.034	122.66
TMEM126B	Homo sapiens transmembrane protein 126B (TMEM126B), mRNA.	303.41	473.28	-1.56	0.000	169.87
C8orf45	Homo sapiens chromosome 8 open reading frame 45 (C8orf45), mRNA.	1343.16	2083.5	-1.55	0.031	740.34
C21orf24	Homo sapiens chromosome 21 open reading frame 24 (C21orf24), mRNA.	1136.36	1735.72	-1.53	0.043	599.36
CBX6	Homo sapiens chromobox homolog 6 (CBX6), mRNA.	199.65	306.03	-1.53	1.00E-04	106.38
PAG1	Homo sapiens phosphoprotein associated with glycosphingolipid microdomains 1 (PAG1), mRNA.	700.59	1074.96	-1.53	0.002	374.38
PRKAR1A	Homo sapiens protein kinase, cAMP-dependent, regulatory, type I, alpha (tissue specific extinguisher 1) (PRKAR1A), transcript variant 3, mRNA.	599.31	918.57	-1.53	0.045	319.26
CMPK1	Homo sapiens cytidine monophosphate (UMP-CMP) kinase 1, cytosolic (CMPK1), mRNA.	224.74	342.10	-1.52	0.026	117.37
CYP20A1	Homo sapiens cytochrome P450, family 20, subfamily A, polypeptide 1 (CYP20A1), mRNA.	200.36	304.64	-1.52	0.000	104.28
DYRK1A	Homo sapiens dual-specificity tyrosine-(Y)-phosphorylation regulated kinase 1A (DYRK1A), transcript variant 4, mRNA.	301.70	459.56	-1.52	0.017	157.87
FAM73A	Homo sapiens family with sequence similarity 73, member A (FAM73A), mRNA.	380.31	576.57	-1.52	0.000	196.26
KCTD5	Homo sapiens potassium channel tetramerisation domain containing 5 (KCTD5), mRNA.	260.91	397.48	-1.52	0.003	136.56
SNRK	Homo sapiens SNF related kinase (SNRK), mRNA.	825.21	1257.22	-1.52	0.042	432.01
PAXIP1	Homo sapiens PAX interacting (with transcription-activation domain) protein 1 (PAXIP1), mRNA.	250.21	378.33	-1.51	0.000	128.12
SLC11A2	Homo sapiens solute carrier family 11 (proton-coupled divalent metal ion transporters), member 2 (SLC11A2), mRNA.	325.37	488.83	-1.50	0.021	163.46
EFTUD1	Homo sapiens elongation factor Tu GTP binding domain containing 1 (EFTUD1), transcript variant 1, mRNA.	479.11	319.05	1.50	0.028	160.05
ECHDC2	Homo sapiens enoyl Coenzyme A hydratase domain containing 2 (ECHDC2), mRNA.	1747.48	1156.02	1.51	0.000	591.46
GNAI2	Homo sapiens guanine nucleotide binding protein (G protein), alpha inhibiting activity polypeptide 2 (GNAI2), transcript variant 1, mRNA.	826.69	541.38	1.53	0.009	285.31
HNRNPAB	Homo sapiens heterogeneous nuclear ribonucleoprotein A/B (HNRNPAB), transcript variant 2, mRNA.	879.72	573.68	1.53	0.002	306.04
LOC100129681	PREDICTED: Homo sapiens similar to NPC-A-7 (LOC100129681), mRNA.	959.20	625.10	1.53	0.023	334.10
SAPS3	Homo sapiens SAPS domain family, member 3 (SAPS3), mRNA.	498.23	326.39	1.53	0.000	171.84
STK40	Homo sapiens serine/threonine kinase 40 (STK40), mRNA.	508.60	332.58	1.53	0.000	176.02
EGLN2	Homo sapiens egl nine homolog 2 (C. elegans) (EGLN2), transcript variant 3, mRNA.	1273.21	828.64	1.54	0.017	444.57
LOC641768	PREDICTED: Homo sapiens similar to ribosomal protein S26, transcript variant 2 (LOC641768), mRNA.	1642.73	1061.34	1.55	0.041	581.38
MVP	Homo sapiens major vault protein (MVP), transcript variant 2, mRNA.	1117.34	720.61	1.55	0.008	396.73
SAMM50	Homo sapiens sorting and assembly machinery component 50 homolog (S. cerevisiae) (SAMM50), mRNA.	1698.49	1092.58	1.55	0.000	605.92
TMEM63A	Homo sapiens transmembrane protein 63A (TMEM63A), mRNA.	650.13	419.42	1.55	0.003	230.71
TPP1	Homo sapiens tripeptidyl peptidase I (TPP1), mRNA.	889.66	575.17	1.55	0.009	314.49
TRADD	Homo sapiens TNFRSF1A-associated via death domain (TRADD), transcript variant 1, mRNA.	843.72	545.55	1.55	0.000	298.18
RAB37	Homo sapiens RAB37, member RAS oncogene family (RAB37), transcript variant 3, mRNA.	1303.31	834.26	1.56	0.020	469.05
MRPL18	Homo sapiens mitochondrial ribosomal protein L18 (MRPL18), nuclear gene encoding mitochondrial protein, mRNA.	591.86	377.79	1.57	2.00E-04	214.07
BLOC1S1	Homo sapiens biogenesis of lysosome-related organelles complex-1, subunit 1 (BLOC1S1), mRNA.	303.72	191.69	1.58	0.002	112.03
SHISA5	Homo sapiens shisa homolog 5 (Xenopus laevis) (SHISA5), mRNA.	1783.58	1128.14	1.58	0.000	655.44
VPS28	Homo sapiens vacuolar protein sorting 28 homolog (S. cerevisiae) (VPS28), transcript variant 1, mRNA.	415.45	262.99	1.58	2.00E-04	152.46
ARL6IP4	Homo sapiens ADP-ribosylation-like factor 6 interacting protein 4 (ARL6IP4), transcript variant 1, mRNA.	430.51	270.01	1.59	2.00E-04	160.50
ZNF277	Homo sapiens zinc finger protein 277 (ZNF277), mRNA.	379.85	238.36	1.59	0.036	141.49
PEBP1	Homo sapiens phosphatidylethanolamine binding protein 1 (PEBP1), mRNA.	571.59	356.94	1.60	0.000	214.65
SMCR7L	Homo sapiens Smith-Magenis syndrome chromosome region, candidate 7-like (SMCR7L), mRNA.	609.14	381.57	1.60	0.000	227.57
DEDD2	Homo sapiens death effector domain containing 2 (DEDD2), mRNA.	929.83	578.22	1.61	1.00E-04	351.61
FRYL	Homo sapiens FRY-like (FRYL), mRNA.	1042.33	649.17	1.61	0.024	393.16

GZMK	Homo sapiens granzyme K (granzyme 3; tryptase II) (GZMK), mRNA.	307.37	190.50	1.61	0.003	116.87
MYO1G	Homo sapiens myosin IG (MYO1G), mRNA.	925.41	576.45	1.61	0.000	348.96
RASAL3	Homo sapiens RAS protein activator like 3 (RASAL3), mRNA.	472.20	291.32	1.62	1.00E-04	180.88
SAMD9	Homo sapiens sterile alpha motif domain containing 9 (SAMD9), mRNA.	634.27	391.36	1.62	0.019	242.91
C20orf100	Homo sapiens chromosome 20 open reading frame 100 (C20orf100), mRNA.	329.44	201.95	1.63	0.017	127.48
TRIM21	Homo sapiens tripartite motif-containing 21 (TRIM21), mRNA.	278.21	170.94	1.63	0.050	107.26
IL10RB	Homo sapiens interleukin 10 receptor, beta (IL10RB), mRNA.	1123.71	685.83	1.64	0.013	437.87
MSRB2	Homo sapiens methionine sulfoxide reductase B2 (MSRB2), mRNA.	366.04	223.77	1.64	0.045	142.27
SEC22B	Homo sapiens SEC22 vesicle trafficking protein homolog B (S. cerevisiae) (SEC22B), mRNA.	355.74	216.87	1.64	0.000	138.88
JMJD6	Homo sapiens jumonji domain containing 6 (JMJD6), transcript variant 2, mRNA.	273.77	166.14	1.65	0.011	107.63
NDUFA6	Homo sapiens NADH dehydrogenase (ubiquinone) 1 alpha subcomplex, 6, 14kDa (NDUFA6), nuclear gene encoding mitochondrial protein, mRNA.	495.87	300.79	1.65	2.00E-04	195.07
PDCL3	Homo sapiens phosducin-like 3 (PDCL3), mRNA.	306.94	186.47	1.65	0.014	120.48
FAM53C	Homo sapiens family with sequence similarity 53, member C (FAM53C), mRNA.	534.85	322.13	1.66	0.005	212.71
LIME1	Homo sapiens Lck interacting transmembrane adaptor 1 (LIME1), mRNA.	1091.52	658.49	1.66	0.002	433.03
NUP133	Homo sapiens nucleoporin 133kDa (NUP133), mRNA.	363.05	219.07	1.66	0.000	143.98
DHPS	Homo sapiens deoxyhypusine synthase (DHPS), transcript variant 2, mRNA.	412.48	246.29	1.67	0.000	166.19
GGA3	Homo sapiens golgi associated, gamma adaptin ear containing, ARF binding protein 3 (GGA3), transcript variant long, mRNA.	451.54	270.32	1.67	0.000	181.22
LDLRAP1	Homo sapiens low density lipoprotein receptor adaptor protein 1 (LDLRAP1), mRNA.	263.00	157.86	1.67	0.034	105.14
KLHDC3	Homo sapiens kelch domain containing 3 (KLHDC3), mRNA.	559.83	332.27	1.68	0.003	227.56
RIPK3	Homo sapiens receptor-interacting serine-threonine kinase 3 (RIPK3), mRNA.	280.32	166.48	1.68	0.041	113.84
NOL11	Homo sapiens nucleolar protein 11 (NOL11), mRNA.	740.98	437.53	1.69	0.000	303.46
C5orf51	Homo sapiens chromosome 5 open reading frame 51 (C5orf51), mRNA.	276.35	162.89	1.70	0.002	113.46
CIAO1	Homo sapiens cytosolic iron-sulfur protein assembly 1 homolog (S. cerevisiae) (CIAO1), mRNA.	898.86	528.02	1.70	0.022	370.83
MRPS15	Homo sapiens mitochondrial ribosomal protein S15 (MRPS15), nuclear gene encoding mitochondrial protein, mRNA.	582.83	342.20	1.70	0.012	240.63
PIK3CD	Homo sapiens phosphoinositide-3-kinase, catalytic, delta polypeptide (PIK3CD), mRNA.	646.39	379.88	1.70	0.035	266.50
LOC88523	Homo sapiens CG016 (LOC88523), mRNA.	641.30	375.85	1.71	0.039	265.45
URM1	Homo sapiens ubiquitin related modifier 1 homolog (S. cerevisiae) (URM1), mRNA.	827.47	482.73	1.71	0.043	344.75
B9D2	Homo sapiens B9 protein domain 2 (B9D2), mRNA.	304.10	176.79	1.72	0.000	127.31
ECHS1	Homo sapiens enoyl Coenzyme A hydratase, short chain, 1, mitochondrial (ECHS1), nuclear gene encoding mitochondrial protein, mRNA.	569.00	330.88	1.72	0.006	238.13
GRAP	Homo sapiens GRB2-related adaptor protein (GRAP), mRNA.	925.18	538.24	1.72	0.002	386.94
SCYL1	Homo sapiens SCY1-like 1 (S. cerevisiae) (SCYL1), transcript variant A, mRNA.	970.52	564.64	1.72	0.006	405.88
ATG16L1	Homo sapiens ATG16 autophagy related 16-like 1 (S. cerevisiae) (ATG16L1), transcript variant 1, mRNA.	1611.24	933.75	1.73	0.000	677.48
NUCB2	Homo sapiens nucleobindin 2 (NUCB2), mRNA.	421.54	243.80	1.73	1.00E-04	177.74
SUMF2	Homo sapiens sulfatase modifying factor 2 (SUMF2), transcript variant 4, mRNA.	1141.24	650.91	1.75	0.000	490.33
DHPS	Homo sapiens deoxyhypusine synthase (DHPS), transcript variant 2, mRNA.	342.87	194.38	1.76	0.000	148.49
RALGDS	Homo sapiens ral guanine nucleotide dissociation stimulator (RALGDS), transcript variant 1, mRNA.	613.44	348.98	1.76	0.000	264.46
TYSND1	Homo sapiens trypsin domain containing 1 (TYSND1), transcript variant 2, mRNA.	363.75	206.31	1.76	0.000	157.44
APPL2	Homo sapiens adaptor protein, phosphotyrosine interaction, PH domain and leucine zipper containing 2 (APPL2), mRNA.	361.89	204.40	1.77	0.001	157.50
GBA	Homo sapiens glucosidase, beta; acid (includes glucosylceramidase) (GBA), transcript variant 3, mRNA.	347.99	195.50	1.78	0.023	152.49
MRPL23	Homo sapiens mitochondrial ribosomal protein L23 (MRPL23), nuclear gene encoding mitochondrial protein, mRNA.	449.72	252.15	1.78	0.000	197.57
EGLN2	Homo sapiens egl nine homolog 2 (C. elegans) (EGLN2), transcript variant 1, mRNA.	473.73	264.25	1.79	0.007	209.47
PPP4C	Homo sapiens protein phosphatase 4 (formerly X), catalytic subunit (PPP4C), mRNA.	597.57	332.64	1.80	0.000	264.94
PRPF8	Homo sapiens PRP8 pre-mRNA processing factor 8 homolog (S. cerevisiae) (PRPF8), mRNA.	1361.06	756.23	1.80	0.000	604.84
ZBTB33	Homo sapiens zinc finger and BTB domain containing 33 (ZBTB33), mRNA.	704.50	389.31	1.81	0.034	315.20
ATG16L1	Homo sapiens ATG16 autophagy related 16-like 1 (S. cerevisiae) (ATG16L1), transcript variant 2, mRNA.	841.75	462.89	1.82	0.000	378.86
ERCC3	Homo sapiens excision repair cross-complementing rodent repair deficiency, complementation group 3 (xeroderma pigmentosum group B complementing) (ERCC3), mRNA.	465.83	256.63	1.82	8.00E-04	209.20
MRPL27	Homo sapiens mitochondrial ribosomal protein L27 (MRPL27), nuclear gene encoding mitochondrial protein, transcript variant 2, mRNA.	310.38	170.10	1.82	0.015	140.28
DNTTIP1	Homo sapiens deoxynucleotidyltransferase, terminal, interacting protein 1 (DNTTIP1), mRNA.	242.40	130.77	1.85	1.00E-04	111.64

TCP1	Homo sapiens t-complex 1 (TCP1), transcript variant 1, mRNA.	219.72	117.51	1.87	6.00E-04	102.21
IDH3G	Homo sapiens isocitrate dehydrogenase 3 (NAD+) gamma (IDH3G), nuclear gene encoding mitochondrial protein, transcript variant 2, mRNA.	467.25	248.57	1.88	7.00E-04	218.67
TMEM101	Homo sapiens transmembrane protein 101 (TMEM101), mRNA.	291.48	155.27	1.88	0.009	136.21
FAM160A2	Homo sapiens family with sequence similarity 160, member A2 (FAM160A2), transcript variant 2, mRNA.	287.42	152.37	1.89	7.00E-04	135.05
HAX1	Homo sapiens HCLS1 associated protein X-1 (HAX1), transcript variant 1, mRNA.	968.01	512.48	1.89	0.000	455.53
RP9	Homo sapiens retinitis pigmentosa 9 (autosomal dominant) (RP9), mRNA.	547.28	289.12	1.89	0.000	258.16
PGLS	Homo sapiens 6-phosphogluconolactonase (PGLS), mRNA.	476.49	249.59	1.91	0.000	226.89
ATP6V0E2	Homo sapiens ATPase, H+ transporting V0 subunit e2 (ATP6V0E2), transcript variant 1, mRNA.	985.70	513.44	1.92	0.002	472.26
TULP4	Homo sapiens tubby like protein 4 (TULP4), transcript variant 2, mRNA.	269.50	140.40	1.92	0.000	129.10
SCYL1	Homo sapiens SCY1-like 1 (S. cerevisiae) (SCYL1), mRNA.	465.74	241.81	1.93	0.000	223.93
P4HTM	Homo sapiens prolyl 4-hydroxylase, transmembrane (endoplasmic reticulum) (P4HTM), transcript variant 3, mRNA.	316.89	163.24	1.94	0.001	153.65
PRKAG1	Homo sapiens protein kinase, AMP-activated, gamma 1 non-catalytic subunit (PRKAG1), transcript variant 1, mRNA.	271.27	139.80	1.94	0.033	131.48
DYRK4	Homo sapiens dual-specificity tyrosine-(Y)-phosphorylation regulated kinase 4 (DYRK4), mRNA.	274.69	140.59	1.95	0.000	134.10
CBY1	Homo sapiens chibby homolog 1 (Drosophila) (CBY1), transcript variant 1, mRNA.	232.57	118.06	1.97	0.000	114.50
SELS	Homo sapiens selenoprotein S (SELS), transcript variant 2, mRNA.	391.24	197.35	1.98	0.000	193.89
WDR51A	Homo sapiens WD repeat domain 51A (WDR51A), mRNA.	207.80	104.13	2.00	1.00E-04	103.67
SLC5A6	Homo sapiens solute carrier family 5 (sodium-dependent vitamin transporter), member 6 (SLC5A6), mRNA.	389.67	192.21	2.03	0.000	197.46
TMEM115	Homo sapiens transmembrane protein 115 (TMEM115), mRNA.	315.32	155.13	2.03	0.017	160.19
CEP55	Homo sapiens centrosomal protein 55kDa (CEP55), mRNA.	198.52	97.15	2.04	0.024	101.38
SLC24A6	Homo sapiens solute carrier family 24 (sodium/potassium/calcium exchanger), member 6 (SLC24A6), mRNA.	306.31	149.95	2.04	0.000	156.37
DSCR3	Homo sapiens Down syndrome critical region gene 3 (DSCR3), mRNA.	518.76	253.28	2.05	0.000	265.48
WDR23	Homo sapiens WD repeat domain 23 (WDR23), transcript variant 1, mRNA.	866.31	416.77	2.08	0.000	449.54
NOD1	Homo sapiens nucleotide-binding oligomerization domain containing 1 (NOD1), mRNA.	325.70	156.03	2.09	0.000	169.68
PKP4	Homo sapiens plakophilin 4 (PKP4), transcript variant 1, mRNA.	519.08	243.16	2.13	0.007	275.92
ABCB6	Homo sapiens ATP-binding cassette, sub-family B (MDR/TAP), member 6 (ABCB6), nuclear gene encoding mitochondrial protein, mRNA.	234.42	107.92	2.17	0.042	126.50
PLIN2	Homo sapiens perilipin 2 (PLIN2), mRNA.	737.37	331.91	2.22	0.005	405.46
PTPN4	Homo sapiens protein tyrosine phosphatase, non-receptor type 4 (megakaryocyte) (PTPN4), mRNA.	675.95	303.08	2.23	0.032	372.87
ZBTB42	Homo sapiens zinc finger and BTB domain containing 42 (ZBTB42), mRNA.	254.34	109.84	2.32	0.000	144.50
CISH	Homo sapiens cytokine inducible SH2-containing protein (CISH), mRNA.	355.92	152.46	2.33	0.010	203.46
C1orf50	Homo sapiens chromosome 1 open reading frame 50 (C1orf50), mRNA.	349.97	134.85	2.60	0.022	215.13
PRPF4	Homo sapiens PRP4 pre-mRNA processing factor 4 homolog (yeast) (PRPF4), mRNA.	453.50	170.42	2.66	0.019	283.08
ZBP1	Homo sapiens Z-DNA binding protein 1 (ZBP1), mRNA.	432.80	160.00	2.71	0.000	272.80
HLA-DQB1	Homo sapiens major histocompatibility complex, class II, DQ beta 1 (HLA-DQB1), mRNA.	405.82	148.33	2.74	1.00E-04	257.49
NUSAP1	Homo sapiens nucleolar and spindle associated protein 1 (NUSAP1), transcript variant 2, mRNA.	437.93	151.71	2.89	0.030	286.22
C19orf12	Homo sapiens chromosome 19 open reading frame 12 (C19orf12), transcript variant 1, mRNA.	744.45	196.04	3.80	0.000	548.41

Comparison $CD4^{+}CD25^{high}$ T cells of MF^{-} individuals versus EN

Symbol	Definition	mean_Treg_MFneg	mean_Treg_EN	FC	pvalue	diff
ZNF25	Homo sapiens zinc finger protein 25 (ZNF25), mRNA.	167.95	414.44	-2.47	0.005	246.49
C14orf80	Homo sapiens chromosome 14 open reading frame 80 (C14orf80), mRNA.	139.80	343.55	-2.46	0.016	203.76
C5orf28	Homo sapiens chromosome 5 open reading frame 28 (C5orf28), mRNA.	461.16	962.96	-2.09	0.003	501.80
KLF11	PREDICTED: Homo sapiens Kruppel-like factor 11 (KLF11), mRNA.	337.11	673.06	-2.00	0.050	335.94
EMILIN2	Homo sapiens elastin microfibril interfacer 2 (EMILIN2), mRNA.	256.94	495.64	-1.93	0.033	238.70
NUFIP2	Homo sapiens nuclear fragile X mental retardation protein interacting protein 2 (NUFIP2), mRNA.	463.78	885.99	-1.91	0.005	422.21
LOC100128098	PREDICTED: Homo sapiens hypothetical protein LOC100128098 (LOC100128098), mRNA.	350.72	660.87	-1.88	0.039	310.15
WDR36	Homo sapiens WD repeat domain 36 (WDR36), mRNA.	161.41	298.22	-1.85	0.010	136.8

CTBS	Homo sapiens chitobiase, di-N-acetyl- (CTBS), mRNA.	138.56	248.84	-1.80	0.000	110.28
EIF4A1	Homo sapiens eukaryotic translation initiation factor 4A, isoform 1 (EIF4A1), mRNA.	316.44	560.08	-1.77	0.011	243.63
TNFSF15	Homo sapiens tumor necrosis factor (ligand) superfamily, member 15 (TNFSF15), mRNA.	144.89	254.41	-1.76	0.012	109.52
NDUFS3	Homo sapiens NADH dehydrogenase (ubiquinone) Fe-S protein 3, 30kDa (NADH-coenzyme Q reductase) (NDUFS3), mRNA.	736.94	1286.87	-1.75		549.92
TGFBR3	Homo sapiens transforming growth factor, beta receptor III (TGFBR3), mRNA.	179.21	310.57	-1.73	0.002	131.35
GSTTP2	Homo sapiens glutathione S-transferase theta pseudogene 2 (GSTTP2), non-coding RNA. XM_941198 XM_945014 XM_945016	159.46	270.16	-1.69	0.038	110.69
C7orf26	Homo sapiens chromosome 7 open reading frame 26 (C7orf26), mRNA.	262.59	436.54	-1.66	0.000	173.94
CDCA4	Homo sapiens cell division cycle associated 4 (CDCA4), transcript variant 14, mRNA.	253.65	418.88	-1.65		165.23
DUSP19	Homo sapiens dual specificity phosphatase 19 (DUSP19), mRNA.	1280.88	2112.64	-1.65	0.039	831.75
HCG2P7	Homo sapiens HLA complex group 2 pseudogene 7 (HCG2P7), non-coding RNA.	1651.11	2713.9	-1.64	0.033	1062.8
RARS	Homo sapiens arginyl-tRNA synthetase (RARS), mRNA.	685.23	1121.84	-1.64	0.050	436.62
TDRD1	Homo sapiens tudor domain containing 1 (TDRD1), mRNA.	206.62	333.79	-1.62	0.004	127.17
CREB1	Homo sapiens cAMP responsive element binding protein 1 (CREB1), transcript variant A, mRNA.	907.14	1458.17	-1.61	0.015	551.03
FCAR	Homo sapiens Fc fragment of IgA, receptor for (FCAR), transcript variant 9, mRNA.	175.43	280.67	-1.60	0.039	105.24
FAM63A	Homo sapiens family with sequence similarity 63, member A (FAM63A), transcript variant 1, mRNA.	292.52	463.15	-1.58	0.014	170.63
SNAPC1	Homo sapiens small nuclear RNA activating complex, polypeptide 1, 43kDa (SNAPC1), mRNA.	176.48	279.15	-1.58	0.026	102.67
C15orf17	Homo sapiens chromosome 15 open reading frame 17 (C15orf17), mRNA.	213.69	335.64	-1.57	0.006	121.95
C6orf125	Homo sapiens chromosome 6 open reading frame 125 (C6orf125), mRNA.	198.26	309.35	-1.56	0.003	111.09
DGUOK	Homo sapiens deoxyguanosine kinase (DGUOK), nuclear gene encoding mitochondrial protein, transcript variant 1, mRNA.	548.61	857.06	-1.56	0.025	308.45
C9orf80	Homo sapiens chromosome 9 open reading frame 80 (C9orf80), mRNA.	1759.62	2725.44	-1.55	0.024	965.82
ZNF577	Homo sapiens zinc finger protein 577 (ZNF577), mRNA.	289.07	445.30	-1.54	0.016	156.23
HDGF	Homo sapiens hepatoma-derived growth factor (high-mobility group protein 1-like) (HDGF), mRNA.	403.88	268.45	1.50	0.000	135.43
POLR3GL	Homo sapiens polymerase (RNA) III (DNA directed) polypeptide G (32kD)-like (POLR3GL), mRNA.	1282.69	854.63	1.50	0.042	428.06
SASH3	Homo sapiens SAM and SH3 domain containing 3 (SASH3), mRNA.	509.26	336.81	1.51	0.004	172.46
LOC728855	Homo sapiens hypothetical LOC728855 (LOC728855), non-coding RNA.	1310.43	860.91	1.52	0.036	449.52
MTDH	Homo sapiens metadherin (MTDH), mRNA.	486.72	319.40	1.52	0.034	167.32
ACTB	Homo sapiens actin, beta (ACTB), mRNA.	7970.05	5201.06	1.53	0.024	2768.98
COPZ1	Homo sapiens coatomer protein complex, subunit zeta 1 (COPZ1), mRNA.	521.25	339.61	1.53	0.000	181.64
HLA-H	Homo sapiens major histocompatibility complex, class I, H (pseudogene) (HLA-H), non-coding RNA.	2708.25	1771.84	1.53	0.043	936.41
LRP10	Homo sapiens low density lipoprotein receptor-related protein 10 (LRP10), mRNA.	1079.75	705.31	1.53	0.024	374.44
ACTB	Homo sapiens actin, beta (ACTB), mRNA.	6116.64	3933.68	1.55	0.016	2182.96
AP1G2	Homo sapiens adaptor-related protein complex 1, gamma 2 subunit (AP1G2), mRNA.	403.43	260.67	1.55	0.040	142.76
ACTL6A	Homo sapiens actin-like 6A (ACTL6A), transcript variant 1, mRNA.	300.87	192.68	1.56	0.036	108.19
	full-length cDNA clone CS0DI056YK21 of Placenta Cot 25-normalized of Homo sapiens (human)	4649.60	2989.98	1.56	0.047	1659.63
CMTM6	Homo sapiens CKLF-like MARVEL transmembrane domain containing 6 (CMTM6), mRNA.	491.17	312.14	1.57	0.027	179.04
TMED9	Homo sapiens transmembrane emp24 protein transport domain containing 9 (TMED9), mRNA.	759.35	484.26	1.57	0.024	275.09
UGP2	Homo sapiens UDP-glucose pyrophosphorylase 2 (UGP2), transcript variant 1, mRNA.	767.97	489.61	1.57	0.034	278.36
ZFP106	Homo sapiens zinc finger protein 106 homolog (mouse) (ZFP106), mRNA.	374.39	238.15	1.57	0.030	136.24
NUCB2	Homo sapiens nucleobindin 2 (NUCB2), mRNA.	421.54	266.81	1.58	0.022	154.73
C2orf28	Homo sapiens chromosome 2 open reading frame 28 (C2orf28), transcript variant 2, mRNA.	1143.09	717.91	1.59	0.001	425.18
C5orf51	Homo sapiens chromosome 5 open reading frame 51 (C5orf51), mRNA.	276.35	171.79	1.61	9.00E-04	104.56
SETD3	Homo sapiens SET domain containing 3 (SETD3), transcript variant 1, mRNA.	2732.58	1691.14	1.62	1.00E-04	1041.44
PTPRCAP	Homo sapiens protein tyrosine phosphatase, receptor type, C-associated protein (PTPRCAP), mRNA.	1199.45	725.18	1.65	0.007	474.27
ZHX2	Homo sapiens zinc fingers and homeoboxes 2 (ZHX2), mRNA.	302.63	182.89	1.65	0.004	119.74
LOC647000	PREDICTED: Homo sapiens similar to tubulin, beta 5 (LOC647000), mRNA.	574.26	345.86	1.66	0.026	228.40
TRAPPC6A	Homo sapiens trafficking protein particle complex 6A (TRAPPC6A), mRNA.	1005.63	599.62	1.68	0.030	406.01
EFTUD1	Homo sapiens elongation factor Tu GTP binding domain containing 1 (EFTUD1), transcript variant 1, mRNA.	479.11	284.22	1.69	0.006	194.89
GBP1	Homo sapiens guanylate binding protein 1, interferon-inducible, 67kDa (GBP1), mRNA.	576.91	341.13	1.69	0.025	235.79
GGA3	Homo sapiens golgi associated, gamma adaptin ear containing, ARF binding protein 3 (GGA3), transcript variant long, mRNA.	451.54	265.21	1.70	0.042	186.33
HAX1	Homo sapiens HCLS1 associated protein X-1 (HAX1), transcript variant 1, mRNA.	968.01	569.18	1.70	4.00E-04	398.83

CCDC115	Homo sapiens coiled-coil domain containing 115 (CCDC115), mRNA.	555.72	325.20	1.71	0.005	230.52
LOC651894	PREDICTED: Homo sapiens similar to ribosomal protein S12 (LOC651894), mRNA.	799.74	468.03	1.71	0.048	331.71
STRADB	Homo sapiens STE20-related kinase adaptor beta (STRADB), mRNA.	369.55	216.63	1.71	0.005	152.93
PRKAB2	Homo sapiens protein kinase, AMP-activated, beta 2 non-catalytic subunit (PRKAB2), mRNA.	317.91	183.34	1.73	4.00E-04	134.58
PAPSS1	Homo sapiens 3'-phosphoadenosine 5'-phosphosulfate synthase 1 (PAPSS1), mRNA.	258.25	148.80	1.74	0.026	109.45
ACLY	Homo sapiens ATP citrate lyase (ACLY), transcript variant 2, mRNA.	852.70	487.06	1.75	0.014	365.64
KATNA1	Homo sapiens katanin p60 (ATPase-containing) subunit A 1 (KATNA1), mRNA.	394.41	225.13	1.75	0.031	169.29
EFTUD1	Homo sapiens elongation factor Tu GTP binding domain containing 1 (EFTUD1), transcript variant 1, mRNA.	470.30	267.29	1.76	3.00E-04	203.00
SEC11C	Homo sapiens SEC11 homolog C (S. cerevisiae) (SEC11C), mRNA.	1051.34	589.43	1.78	0.011	461.91
STAT1	Homo sapiens signal transducer and activator of transcription 1, 91kDa (STAT1), transcript variant alpha, mRNA.	2334.42	1290.43	1.81	1.00E-04	1043.99
ATAD1	Homo sapiens ATPase family, AAA domain containing 1 (ATAD1), mRNA.	226.36	124.18	1.82	6.00E-04	102.18
MTMR10	Homo sapiens myotubularin related protein 10 (MTMR10), mRNA.	249.05	135.66	1.84	0.013	113.39
UNG	Homo sapiens uracil-DNA glycosylase (UNG), nuclear gene encoding mitochondrial protein, transcript variant 1, mRNA.	801.35	435.34	1.84	0.031	366.01
KIAA1712	Homo sapiens KIAA1712 (KIAA1712), mRNA.	240.55	130.18	1.85	0.007	110.38
TYW1	Homo sapiens tRNA-yW synthesizing protein 1 homolog (S. cerevisiae) (TYW1), mRNA.	269.78	145.52	1.85	0.021	124.26
GBP1	Homo sapiens guanylate binding protein 1, interferon-inducible, 67kDa (GBP1), mRNA.	798.38	425.20	1.88	0.001	373.18
ST3GAL5	Homo sapiens ST3 beta-galactoside alpha-2,3-sialyltransferase 5 (ST3GAL5), transcript variant 2, mRNA.	370.70	196.80	1.88	0.000	173.90
NMRAL1	Homo sapiens NmrA-like family domain containing 1 (NMRAL1), mRNA.	404.64	214.63	1.89	0.040	190.01
CDK7	Homo sapiens cyclin-dependent kinase 7 (MO15 homolog, Xenopus laevis, cdk-activating kinase) (CDK7), mRNA.	567.30	294.32	1.93	0.047	272.98
ATP6V1D	Homo sapiens ATPase, H+ transporting, lysosomal 34kDa, V1 subunit D (ATP6V1D), mRNA.	986.61	508.36	1.94	4.00E-04	478.25
CCT4	Homo sapiens chaperonin containing TCP1, subunit 4 (delta) (CCT4), mRNA.	211.97	108.48	1.95	0.005	103.48
ZNF721	Homo sapiens zinc finger protein 721 (ZNF721), mRNA.	364.58	185.12	1.97	0.015	179.46
ZC3HC1	Homo sapiens zinc finger, C3HC-type containing 1 (ZC3HC1), mRNA.	595.91	297.95	2.00	0.045	297.96
ZNF845	Homo sapiens zinc finger protein 845 (ZNF845), mRNA. XM_039908	255.64	128.06	2.00	1.00E-04	127.57
TOR1AIP1	Homo sapiens torsin A interacting protein 1 (TOR1AIP1), mRNA.	327.09	162.42	2.01	1.00E-04	164.67
TULP4	Homo sapiens tubby like protein 4 (TULP4), transcript variant 2, mRNA.	269.50	133.28	2.02	0.003	136.22
C13orf23	Homo sapiens chromosome 13 open reading frame 23 (C13orf23), transcript variant 1, mRNA.	267.11	131.32	2.03	0.018	135.79
C13orf23	Homo sapiens chromosome 13 open reading frame 23 (C13orf23), transcript variant 1, mRNA.	270.96	132.94	2.04	0.006	138.02
SPIN3	Homo sapiens spindlin family, member 3 (SPIN3), mRNA.	214.40	105.10	2.04	4.00E-04	109.29
ERGIC3	Homo sapiens ERGIC and golgi 3 (ERGIC3), transcript variant 1, mRNA.	599.19	291.97	2.05	0.016	307.21
AKR1A1	Homo sapiens aldo-keto reductase family 1, member A1 (aldehyde reductase) (AKR1A1), transcript variant 1, mRNA.	887.22	431.33	2.06	0.000	455.89
HDDC3	Homo sapiens HD domain containing 3 (HDDC3), mRNA.	342.90	163.04	2.10	3.00E-04	179.86
ZNF160	Homo sapiens zinc finger protein 160 (ZNF160), transcript variant 2, mRNA.	208.38	99.01	2.10	0.000	109.37
PTPRE	Homo sapiens protein tyrosine phosphatase, receptor type, E (PTPRE), transcript variant 2, mRNA.	313.64	147.67	2.12	0.004	165.98
LOC88523	Homo sapiens CG016 (LOC88523), mRNA.	641.30	298.34	2.15	0.010	342.96
GLB1	Homo sapiens galactosidase, beta 1 (GLB1), transcript variant 179423, mRNA.	646.62	297.54	2.17	0.024	349.08
SDAD1	Homo sapiens SDA1 domain containing 1 (SDAD1), mRNA.	725.52	331.02	2.19	0.015	394.50
AGBL5	Homo sapiens ATP/GTP binding protein-like 5 (AGBL5), transcript variant 3, mRNA.	244.79	110.02	2.22	0.000	134.76
	Homo sapiens cDNA FLJ46527 fis, clone THYMU3034853	700.65	307.32	2.28	0.013	393.34
DHX29	Homo sapiens DEAH (Asp-Glu-Ala-His) box polypeptide 29 (DHX29), mRNA.	376.41	161.47	2.33	0.000	214.94
PSMB5	Homo sapiens proteasome (prosome, macropain) subunit, beta type, 5 (PSMB5), mRNA.	440.08	187.96	2.34	0.009	252.12
HAVCR2	Homo sapiens hepatitis A virus cellular receptor 2 (HAVCR2), mRNA.	288.43	121.52	2.37	0.008	166.91
TM9SF1	Homo sapiens transmembrane 9 superfamily member 1 (TM9SF1), transcript variant 1, mRNA.	253.47	105.56	2.40	0.027	147.91
FLJ14213	Homo sapiens protor-2 (FLJ14213), mRNA.	447.49	177.52	2.52	0.050	269.98
FBXO28	Homo sapiens F-box protein 28 (FBXO28), mRNA.	266.26	104.97	2.54	0.000	161.30
FAM69A	Homo sapiens family with sequence similarity 69, member A (FAM69A), mRNA.	375.80	105.31	3.57	1.00E-04	270.49
D4S234E	Homo sapiens DNA segment on chromosome 4 (unique) 234 expressed sequence (D4S234E), transcript variant 2, mRNA.	314.39	85.62	3.67	0.000	228.77
HBB	Homo sapiens hemoglobin, beta (HBB), mRNA.	1184.93	134.17	8.83	0.004	1050.77

Comparison $CD4^{+}CD25^{high}$ T cells of MF^{+} individuals versus EN

Symbol	Definition	mean_Treg_Mfpos	mean_Treg_EN	FC	pvalue	diff
LOC729708	PREDICTED: Homo sapiens similar to rcTPI1, transcript variant 1 (LOC729708), mRNA.	205.33	1117.91	-5.44	0.049	912.58
CASZ1	Homo sapiens castor zinc finger 1 (CASZ1), transcript variant 2, mRNA.	84.59	324.37	-3.83	0.035	239.78
NUSAP1	Homo sapiens nucleolar and spindle associated protein 1 (NUSAP1), transcript variant 2, mRNA.	151.71	533.66	-3.52	0.022	381.95
CCR3	Homo sapiens chemokine (C-C motif) receptor 3 (CCR3), transcript variant 2, mRNA.	107.61	321.38	-2.99	0.042	213.77
C14orf80	Homo sapiens chromosome 14 open reading frame 80 (C14orf80), mRNA.	117.71	343.55	-2.92	0.003	225.85
ARHGAP10	Homo sapiens Rho GTPase activating protein 10 (ARHGAP10), mRNA.	112.63	310.32	-2.76	0.019	197.69
C19orf12	Homo sapiens chromosome 19 open reading frame 12 (C19orf12), transcript variant 1, mRNA.	196.04	491.80	-2.51	0.039	295.76
PLIN2	Homo sapiens perilipin 2 (PLIN2), mRNA.	331.91	742.70	-2.24	0.003	410.79
WDR23	Homo sapiens WD repeat domain 23 (WDR23), transcript variant 1, mRNA.	416.77	934.72	-2.24	0.000	517.95
C20orf20	Homo sapiens chromosome 20 open reading frame 20 (C20orf20), mRNA.	376.94	820.99	-2.18	0.009	444.05
C3orf75	Homo sapiens chromosome 3 open reading frame 75 (C3orf75), mRNA.	141.79	307.72	-2.17	0.032	165.94
DPH3	Homo sapiens DPH3, KTI11 homolog (S. cerevisiae) (DPH3), transcript variant 2, mRNA.	118.62	252.77	-2.13	0.026	134.15
E4F1	Homo sapiens E4F transcription factor 1 (E4F1), mRNA.	319.10	670.87	-2.10	0.006	351.77
NDUFA6	Homo sapiens NADH dehydrogenase (ubiquinone) 1 alpha subcomplex, 6, 14kDa (NDUFA6), nuclear gene encoding mitochondrial protein, mRNA.	300.79	630.14	-2.09	9.00E-04	329.35
MED20	Homo sapiens mediator complex subunit 20 (MED20), mRNA.	128.04	266.14	-2.08	0.000	138.10
MRPL23	Homo sapiens mitochondrial ribosomal protein L23 (MRPL23), nuclear gene encoding mitochondrial protein, mRNA.	252.15	525.26	-2.08	0.002	273.11
VPS18	Homo sapiens vacuolar protein sorting 18 homolog (S. cerevisiae) (VPS18), mRNA.	97.02	202.05	-2.08	3.00E-04	105.03
B4GALT4	Homo sapiens UDP-Gal:betaGlcNAc beta 1,4- galactosyltransferase, polypeptide 4 (B4GALT4), transcript variant 2, mRNA.	104.36	208.99	-2.00	0.007	104.64
TFIP11	Homo sapiens tuftelin interacting protein 11 (TFIP11), transcript variant 2, mRNA.	165.54	330.18	-1.99	0.000	164.64
NASP	Homo sapiens nuclear autoantigenic sperm protein (histone-binding) (NASP), transcript variant 2, mRNA.	194.59	385.22	-1.98	0.043	190.62
TCP1	Homo sapiens t-complex 1 (TCP1), transcript variant 1, mRNA.	117.51	232.77	-1.98	0.000	115.26
DPH3	Homo sapiens DPH3, KTI11 homolog (S. cerevisiae) (DPH3), transcript variant 1, mRNA.	111.44	219.25	-1.97	0.017	107.81
PMM2	Homo sapiens phosphomannomutase 2 (PMM2), mRNA.	172.62	340.81	-1.97	0.041	168.19
RABL4	Homo sapiens RAB, member of RAS oncogene family-like 4 (RABL4), mRNA.	154.62	304.58	-1.97	0.029	149.96
C6orf125	Homo sapiens chromosome 6 open reading frame 125 (C6orf125), mRNA.	158.76	309.35	-1.95	4.00E-04	150.59
MED22	Homo sapiens mediator complex subunit 22 (MED22), transcript variant c, mRNA.	264.49	509.62	-1.93	0.025	245.13
PGM1	Homo sapiens phosphoglucomutase 1 (PGM1), mRNA.	524.53	1003.63	-1.91	0.000	479.11
LAIR2	Homo sapiens leukocyte-associated immunoglobulin-like receptor 2 (LAIR2), transcript variant 1, mRNA.	120.38	229.24	-1.90	0.022	108.86
MAD2L2	Homo sapiens MAD2 mitotic arrest deficient-like 2 (yeast) (MAD2L2), mRNA.	175.41	332.78	-1.90	0.004	157.37
TFIP11	Homo sapiens tuftelin interacting protein 11 (TFIP11), transcript variant 2, mRNA.	265.59	505.62	-1.90	0.000	240.02
C9orf119	Homo sapiens chromosome 9 open reading frame 119 (C9orf119), mRNA.	153.16	285.58	-1.86	0.007	132.42
EIF4A1	Homo sapiens eukaryotic translation initiation factor 4A, isoform 1 (EIF4A1), mRNA.	300.68	560.08	-1.86	0.003	259.40
DCPS	Homo sapiens decapping enzyme, scavenger (DCPS), mRNA.	144.34	262.91	-1.82	0.006	118.56
ERCC3	Homo sapiens excision repair cross-complementing rodent repair deficiency, complementation group 3 (xeroderma pigmentosum group B complementing) (ERCC3), mRNA.	256.63	467.88	-1.82	0.010	211.24
NDUFB11	Homo sapiens NADH dehydrogenase (ubiquinone) 1 beta subcomplex, 11, 17.3kDa (NDUFB11), mRNA.	544.28	991.59	-1.82	0.003	447.31
RALGDS	Homo sapiens ral guanine nucleotide dissociation stimulator (RALGDS), transcript variant 1, mRNA.	348.98	635.06	-1.82	0.000	286.09
PRPF38A	Homo sapiens PRP38 pre-mRNA processing factor 38 (yeast) domain containing A (PRPF38A), mRNA.	173.05	313.46	-1.81	0.035	140.41
DDX56	Homo sapiens DEAD (Asp-Glu-Ala-Asp) box polypeptide 56 (DDX56), mRNA.	233.17	420.06	-1.80	0.002	186.89
WDR36	Homo sapiens WD repeat domain 36 (WDR36), mRNA.	166.25	298.22	-1.79	0.000	131.96
PGLS	Homo sapiens 6-phosphogluconolactonase (PGLS), mRNA.	249.59	437.79	-1.75	0.044	188.19
C16orf63	Homo sapiens chromosome 16 open reading frame 63 (C16orf63), mRNA.	217.28	377.21	-1.74	0.025	159.94
ZFYVE20	Homo sapiens zinc finger, FYVE domain containing 20 (ZFYVE20), mRNA.	157.98	274.60	-1.74	0.000	116.62
NOL11	Homo sapiens nucleolar protein 11 (NOL11), mRNA.	437.53	756.41	-1.73	0.000	318.89
C16orf33	Homo sapiens chromosome 16 open reading frame 33 (C16orf33), mRNA.	181.19	311.20	-1.72	0.043	130.00
ECHDC2	Homo sapiens enoyl Coenzyme A hydratase domain containing 2 (ECHDC2), mRNA.	1156.02	1985.37	-1.72	0.000	829.35
CCS	Homo sapiens copper chaperone for superoxide dismutase (CCS), mRNA.	196.03	335.98	-1.71	0.005	139.95

STK39	Homo sapiens serine threonine kinase 39 (STE20/SPS1 homolog, yeast) (STK39), mRNA.	473.65	803.38	-1.70	0.018	329.73
IDH3G	Homo sapiens isocitrate dehydrogenase 3 (NAD+) gamma (IDH3G), nuclear gene encoding mitochondrial protein, transcript variant 2, mRNA.	248.57	419.37	-1.69	0.002	170.8
CHKB	Homo sapiens choline kinase beta (CHKB), transcript variant 1, mRNA.	562.71	936.93	-1.67	0.041	374.21
PMPCA	Homo sapiens peptidase (mitochondrial processing) alpha (PMPCA), nuclear gene encoding mitochondrial protein, mRNA.	358.60	593.32	-1.65	0.046	234.72
ATP6V0E2	Homo sapiens ATPase, H+ transporting V0 subunit e2 (ATP6V0E2), transcript variant 1, mRNA.	513.44	839.12	-1.63	0.047	325.68
CCDC23	Homo sapiens coiled-coil domain containing 23 (CCDC23), mRNA.	204.06	321.85	-1.58	0.002	117.78
RNF166	Homo sapiens ring finger protein 166 (RNF166), mRNA.	268.49	423.24	-1.58	0.010	154.76
ATP6V1E1	Homo sapiens ATPase, H+ transporting, lysosomal 31kDa, V1 subunit E1 (ATP6V1E1), transcript variant 3, mRNA.	1156.63	1810.84	-1.57	0.029	654.21
C3orf37	Homo sapiens chromosome 3 open reading frame 37 (C3orf37), transcript variant 2, mRNA.	366.05	571.88	-1.56	2.00E-04	205.84
C6orf153	Homo sapiens chromosome 6 open reading frame 153 (C6orf153), mRNA.	441.46	690.08	-1.56	0.026	248.62
DAZAP1	Homo sapiens DAZ associated protein 1 (DAZAP1), transcript variant 1, mRNA.	232.75	357.00	-1.53	0.041	124.25
ESD	Homo sapiens esterase D/formylglutathione hydrolase (ESD), mRNA.	472.70	314.39	1.50	0.013	158.30
STAT1	Homo sapiens signal transducer and activator of transcription 1, 91kDa (STAT1), transcript variant alpha, mRNA.	1948.62	1290.43	1.51	9.00E-04	658.19
AHNAK	Homo sapiens AHNAK nucleoprotein (AHNAK), transcript variant 1, mRNA.	2396.45	1573.23	1.52	0.029	823.22
EDEM1	Homo sapiens ER degradation enhancer, mannosidase alpha-like 1 (EDEM1), mRNA.	441.97	290.29	1.52	0.048	151.68
LOC728855	Homo sapiens hypothetical LOC728855 (LOC728855), non-coding RNA.	1305.32	860.91	1.52	0.001	444.41
ATM	Homo sapiens ataxia telangiectasia mutated (ATM), transcript variant 1, mRNA.	384.86	252.14	1.53	0.024	132.72
ERH	Homo sapiens enhancer of rudimentary homolog (Drosophila) (ERH), mRNA.	390.41	255.61	1.53	0.013	134.8
PCID2	Homo sapiens PCI domain containing 2 (PCID2), mRNA.	1384.23	904.68	1.53	0.000	479.55
SETD3	Homo sapiens SET domain containing 3 (SETD3), transcript variant 1, mRNA.	2584.25	1691.14	1.53	0.000	893.12
ARL2BP	Homo sapiens ADP-ribosylation factor-like 2 binding protein (ARL2BP), mRNA.	1346.08	875.39	1.54	0.014	470.69
BAG3	Homo sapiens BCL2-associated athanogene 3 (BAG3), mRNA.	438.71	284.19	1.54	0.033	154.53
CFL1	Homo sapiens cofilin 1 (non-muscle) (CFL1), mRNA.	2029.13	1321.30	1.54	0.000	707.83
SRP14	Homo sapiens signal recognition particle 14kDa (homologous Alu RNA binding protein) (SRP14), mRNA.	494.85	320.27	1.55	0.000	174.58
ACTB	Homo sapiens actin, beta (ACTB), mRNA.	737.59	471.36	1.56	0.000	266.23
ACTL6A	Homo sapiens actin-like 6A (ACTL6A), transcript variant 2, mRNA.	578.00	369.75	1.56	0.035	208.24
EEF1G	Homo sapiens eukaryotic translation elongation factor 1 gamma (EEF1G), mRNA. XM_935976 XM_935977 XM_935978 XM_935979	1686.19	1081.67	1.56	0.005	604.52
TPT1	Homo sapiens tumor protein, translationally-controlled 1 (TPT1), mRNA.	2987.72	1903.72	1.57	0.031	1084.00
BIRC3	Homo sapiens baculoviral IAP repeat-containing 3 (BIRC3), transcript variant 1, mRNA.	2115.91	1332.42	1.59	0.004	783.49
CBLL1	Homo sapiens Cas-Br-M (murine) ecotropic retroviral transforming sequence-like 1 (CBLL1), mRNA.	584.23	366.64	1.59	0.000	217.59
SERBP1	Homo sapiens SERPINE1 mRNA binding protein 1 (SERBP1), transcript variant 3, mRNA.	286.23	179.43	1.60	0.023	106.80
ATRIP	Homo sapiens ATR interacting protein (ATRIP), transcript variant 2, mRNA.	363.05	225.43	1.61	0.008	137.62
KDM3B	Homo sapiens lysine (K)-specific demethylase 3B (KDM3B), mRNA.	351.63	218.73	1.61	0.046	132.91
LOC644033	PREDICTED: Homo sapiens similar to similar to RPL23AP7 protein (LOC644033), mRNA.	613.32	377.84	1.62	0.000	235.47
VAMP4	Homo sapiens vesicle-associated membrane protein 4 (VAMP4), transcript variant 1, mRNA.	317.31	195.73	1.62	0.007	121.58
YY1	Homo sapiens YY1 transcription factor (YY1), mRNA.	489.69	302.14	1.62	0.003	187.55
DOCK10	Homo sapiens dedicator of cytokinesis 10 (DOCK10), mRNA.	1098.04	674.47	1.63	0.013	423.57
PHKB	Homo sapiens phosphorylase kinase, beta (PHKB), transcript variant 1, mRNA.	397.44	244.38	1.63	3.00E-04	153.06
SFRS1	Homo sapiens splicing factor, arginine/serine-rich 1 (SFRS1), transcript variant 2, mRNA.	1508.62	920.30	1.64	0.004	588.32
CYFIP2	Homo sapiens cytoplasmic FMR1 interacting protein 2 (CYFIP2), transcript variant 3, mRNA.	3762.35	2283.71	1.65	1.00E-04	1478.63
PARP9	Homo sapiens poly (ADP-ribose) polymerase family, member 9 (PARP9), mRNA.	559.37	338.08	1.65	0.030	221.29
AKR1A1	Homo sapiens aldo-keto reductase family 1, member A1 (aldehyde reductase) (AKR1A1), transcript variant 1, mRNA.	725.99	431.33	1.68	0.012	294.66
EIF2B1	Homo sapiens eukaryotic translation initiation factor 2B, subunit 1 alpha, 26kDa (EIF2B1), mRNA.	643.18	381.63	1.69	0.029	261.56
XBP1	Homo sapiens X-box binding protein 1 (XBP1), transcript variant 1, mRNA.	726.60	430.46	1.69	0.030	296.14
CAPRIN2	Homo sapiens caprin family member 2 (CAPRIN2), transcript variant 1, mRNA.	337.45	197.38	1.71	0.000	140.06
EIF1AY	Homo sapiens eukaryotic translation initiation factor 1A, Y-linked (EIF1AY), mRNA.	262.31	153.78	1.71	0.032	108.52
COPS5	Homo sapiens COP9 constitutive photomorphogenic homolog subunit 5 (Arabidopsis) (COPS5), mRNA.	1281.88	743.49	1.72	0.005	538.38
CYFIP2	Homo sapiens cytoplasmic FMR1 interacting protein 2 (CYFIP2), transcript variant 1, mRNA.	680.33	392.05	1.74	0.011	288.28
FAM107B	Homo sapiens family with sequence similarity 107, member B (FAM107B), mRNA.	2204.07	1259.4	1.75	0.012	944.68

ADAM17	Homo sapiens ADAM metallopeptidase domain 17 (ADAM17), mRNA.	432.84	244.35	1.77	0.023	188.50
DUSP6	Homo sapiens dual specificity phosphatase 6 (DUSP6), transcript variant 2, mRNA.	319.83	181.15	1.77	1.00E-04	138.68
PNKP	Homo sapiens polynucleotide kinase 3'-phosphatase (PNKP), mRNA.	370.73	206.21	1.80	0.016	164.52
TMEM126B	Homo sapiens transmembrane protein 126B (TMEM126B), mRNA.	473.28	262.8	1.80	0.000	210.48
COPS7A	Homo sapiens COP9 constitutive photomorphogenic homolog subunit 7A (Arabidopsis) (COPS7A), mRNA.	454.71	251.16	1.81	0.003	203.55
LOC200030	Homo sapiens neuroblastoma breakpoint family, member 11-like (LOC200030), mRNA.	1424.19	785.32	1.81	0.020	638.87
TBK1	Homo sapiens TANK-binding kinase 1 (TBK1), mRNA.	785.24	433.53	1.81	0.007	351.71
COPS3	Homo sapiens COP9 constitutive photomorphogenic homolog subunit 3 (Arabidopsis) (COPS3), mRNA.	775.11	424.61	1.83	0.000	350.50
ST3GAL5	Homo sapiens ST3 beta-galactoside alpha-2,3-sialyltransferase 5 (ST3GAL5), transcript variant 2, mRNA.	362.32	196.80	1.84	0.000	165.52
NAT5	Homo sapiens N-acetyltransferase 5 (GCN5-related, putative) (NAT5), transcript variant 3, mRNA.	1842.96	997.27	1.85	0.028	845.69
PITPNB	Homo sapiens phosphatidylinositol transfer protein, beta (PITPNB), mRNA.	287.3	155.51	1.85	0.000	131.79
SRP9	Homo sapiens signal recognition particle 9kDa (SRP9), mRNA.	1347.65	726.92	1.85	0.023	620.73
TERF2IP	Homo sapiens telomeric repeat binding factor 2, interacting protein (TERF2IP), mRNA.	1244.83	672.72	1.85	0.044	572.11
ACLY	Homo sapiens ATP citrate lyase (ACLY), transcript variant 2, mRNA.	906.35	487.06	1.86	0.001	419.29
CYP2E1	Homo sapiens cytochrome P450, family 2, subfamily E, polypeptide 1 (CYP2E1), mRNA.	261.82	141.01	1.86	0.004	120.81
LOC647150	PREDICTED: Homo sapiens misc_RNA (LOC647150), miscRNA.	256.94	138.12	1.86	0.026	118.82
CDC14A	Homo sapiens CDC14 cell division cycle 14 homolog A (S. cerevisiae) (CDC14A), transcript variant 3, mRNA.	218.32	116.86	1.87	0.000	101.46
PATL1	Homo sapiens protein associated with topoisomerase II homolog 1 (yeast) (PATL1), mRNA.	745.27	399.36	1.87	0.031	345.91
CMAS	Homo sapiens cytidine monophosphate N-acetylneuraminic acid synthetase (CMAS), mRNA.	331.84	175.22	1.89	0.000	156.63
PKIA	Homo sapiens protein kinase (cAMP-dependent, catalytic) inhibitor alpha (PKIA), transcript variant 7, mRNA.	277.79	147.10	1.89	0.016	130.69
ZBED5	Homo sapiens zinc finger, BED-type containing 5 (ZBED5), mRNA.	541.97	287.44	1.89	5.00E-04	254.53
TMED2	Homo sapiens transmembrane emp24 domain trafficking protein 2 (TMED2), mRNA.	1008.2	530.68	1.90	5.00E-04	477.52
VBP1	Homo sapiens von Hippel-Lindau binding protein 1 (VBP1), mRNA.	347.03	182.68	1.90	0.003	164.35
LOC653226	PREDICTED: Homo sapiens similar to Signal recognition particle 9 kDa protein (SRP9) (LOC653226), mRNA.	1249.96	649.79	1.92	0.014	600.17
DUSP18	Homo sapiens dual specificity phosphatase 18 (DUSP18), mRNA.	268.42	139.14	1.93	0.049	129.28
RABEP1	Homo sapiens rabaptin, RAB GTPase binding effector protein 1 (RABEP1), transcript variant 2, mRNA.	385.55	200.12	1.93	5.00E-04	185.42
ATM	Homo sapiens ataxia telangiectasia mutated (ATM), transcript variant 1, mRNA.	881.71	455.44	1.94	0.004	426.28
CD84	Homo sapiens CD84 molecule (CD84), mRNA.	261.99	134.77	1.94	0.000	127.22
WDR19	Homo sapiens WD repeat domain 19 (WDR19), mRNA.	245.72	126.52	1.94	0.000	119.20
ZFR	Homo sapiens zinc finger RNA binding protein (ZFR), mRNA.	411.21	209.74	1.96	7.00E-04	201.47
CPNE3	Homo sapiens copine III (CPNE3), mRNA.	546.61	277.73	1.97	0.004	268.89
PIAS4	Homo sapiens protein inhibitor of activated STAT, 4 (PIAS4), mRNA.	247.32	125.07	1.98	6.00E-04	122.25
LOC651894	PREDICTED: Homo sapiens similar to ribosomal protein S12 (LOC651894), mRNA.	932.50	468.03	1.99	0.016	464.47
SMG1	Homo sapiens PI-3-kinase-related kinase SMG-1 (SMG1), mRNA.	516.87	258.07	2.00	0.003	258.79
PAG1	Homo sapiens phosphoprotein associated with glycosphingolipid microdomains 1 (PAG1), mRNA.	1074.96	535.06	2.01	0.005	539.91
ACTR2	Homo sapiens ARP2 actin-related protein 2 homolog (yeast) (ACTR2), transcript variant 1, mRNA.	1473.36	729.32	2.02	0.025	744.04
KLRB1	Homo sapiens killer cell lectin-like receptor subfamily B, member 1 (KLRB1), mRNA.	3274.95	1621.33	2.02	0.003	1653.62
LOC399804	PREDICTED: Homo sapiens misc_RNA (LOC399804), miscRNA.	658.16	323.37	2.04	0.002	334.79
FLJ22662	Homo sapiens hypothetical protein FLJ22662 (FLJ22662), mRNA.	337.16	164.42	2.05	0.018	172.75
RAD21	Homo sapiens RAD21 homolog (S. pombe) (RAD21), mRNA.	438.97	213.61	2.05	0.032	225.35
ITGB1	Homo sapiens integrin, beta 1 (fibronectin receptor, beta polypeptide, antigen CD29 includes MDF2, MSK12) (ITGB1), transcript variant 1D, mRNA.	372.48	179.21	2.08	0.041	193.27
PLEKHA1	Homo sapiens pleckstrin homology domain containing, family A (phosphoinositide binding specific) member 1 (PLEKHA1), transcript variant 2, mRNA.	327.88	157.47	2.08	0.000	170.41
RAB12	Homo sapiens RAB12, member RAS oncogene family (RAB12), mRNA.	212.86	102.51	2.08	0.003	110.35
SKAP1	Homo sapiens src kinase associated phosphoprotein 1 (SKAP1), transcript variant 2, mRNA.	400.17	192.09	2.08	0.050	208.08
TOR1AIP1	Homo sapiens torsin A interacting protein 1 (TOR1AIP1), mRNA.	338.31	162.42	2.08	0.000	175.89
DUSP12	Homo sapiens dual specificity phosphatase 12 (DUSP12), mRNA.	699.08	334.30	2.09	8.00E-04	364.78
GNA13	Homo sapiens guanine nucleotide binding protein (G protein), alpha 13 (GNA13), mRNA.	726.58	345.62	2.10	0.014	380.95
SEC23IP	Homo sapiens SEC23 interacting protein (SEC23IP), mRNA.	257.07	122.39	2.10	0.000	134.67

GMFB	Homo sapiens glia maturation factor, beta (GMFB), mRNA.	803.55	381.72	2.11	0.000	421.83
MAP3K7	Homo sapiens mitogen-activated protein kinase kinase kinase 7 (MAP3K7), transcript variant B, mRNA.	1023.03	485.78	2.11	0.033	537.24
SDAD1	Homo sapiens SDA1 domain containing 1 (SDAD1), mRNA.	697.43	331.02	2.11	0.028	366.41
SLC11A2	Homo sapiens solute carrier family 11 (proton-coupled divalent metal ion transporters), member 2 (SLC11A2), mRNA.	488.83	232.00	2.11	0.034	256.84
GNPDA1	Homo sapiens glucosamine-6-phosphate deaminase 1 (GNPDA1), mRNA.	872.63	411.67	2.12	0.001	460.96
GSPT2	Homo sapiens G1 to S phase transition 2 (GSPT2), mRNA.	289.87	136.22	2.13	0.000	153.66
LOC650215	PREDICTED: Homo sapiens similar to Exportin-T (tRNA exportin) (Exportin(tRNA)) (LOC650215), mRNA.	465.14	218.08	2.13	0.028	247.05
C13orf23	Homo sapiens chromosome 13 open reading frame 23 (C13orf23), transcript variant 1, mRNA.	281.48	131.32	2.14	0.001	150.16
ATAD1	Homo sapiens ATPase family, AAA domain containing 1 (ATAD1), mRNA.	268.01	124.18	2.16	0.003	143.83
CTSK	Homo sapiens cathepsin K (CTSK), mRNA.	358.37	165.62	2.16	0.030	192.75
ZNF383	Homo sapiens zinc finger protein 383 (ZNF383), mRNA.	216.58	99.36	2.18	0.049	117.23
C14orf131	Homo sapiens chromosome 14 open reading frame 131 (C14orf131), mRNA.	747.81	339.31	2.20	0.000	408.50
CMAS	Homo sapiens cytidine monophosphate N-acetylneuraminic acid synthetase (CMAS), mRNA.	413.22	188.23	2.20	0.000	225.00
C13orf23	Homo sapiens chromosome 13 open reading frame 23 (C13orf23), transcript variant 1, mRNA.	294.49	132.94	2.22	0.002	161.55
CDK7	Homo sapiens cyclin-dependent kinase 7 (MO15 homolog, Xenopus laevis, cdk-activating kinase) (CDK7), mRNA.	654.80	294.32	2.22	4.00E-04	360.48
ZCCHC6	Homo sapiens zinc finger, CCHC domain containing 6 (ZCCHC6), mRNA.	184.07	82.39	2.23	0.027	101.67
FBXO11	Homo sapiens F-box protein 11 (FBXO11), transcript variant 1, mRNA.	831.65	368.60	2.26	0.005	463.05
WBSCR22	Homo sapiens Williams Beuren syndrome chromosome region 22 (WBSCR22), mRNA.	1435.84	631.05	2.28	0.016	804.80
CBX6	Homo sapiens chromobox homolog 6 (CBX6), mRNA.	306.03	132.57	2.31	0.000	173.45
SEMA4B	Homo sapiens sema domain, immunoglobulin domain (Ig), transmembrane domain (TM) and short cytoplasmic domain, (semaphorin) 4B (SEMA4B), transcript variant 2, mRNA.	280.11	121.42	2.31	0.001	158.70
LACTB	Homo sapiens lactamase, beta (LACTB), nuclear gene encoding mitochondrial protein, transcript variant 1, mRNA.	842.44	360.78	2.34	0.006	481.66
ARFGEF1	Homo sapiens ADP-ribosylation factor guanine nucleotide-exchange factor 1(brefeldin A-inhibited) (ARFGEF1), mRNA.	619.98	258.81	2.40	0.000	361.17
CMPK1	Homo sapiens cytidine monophosphate (UMP-CMP) kinase 1, cytosolic (CMPK1), mRNA.	841.68	350.41	2.40	0.043	491.28
ZYG11B	Homo sapiens zyg-11 homolog B (C. elegans) (ZYG11B), mRNA.	692.25	284.70	2.43	0.000	407.55
TOR1AIP1	Homo sapiens torsin A interacting protein 1 (TOR1AIP1), mRNA.	652.74	267.27	2.44	0.016	385.47
RCBTB2	Homo sapiens regulator of chromosome condensation (RCC1) and BTB (POZ) domain containing protein 2 (RCBTB2), mRNA.	393.09	159.58	2.46	0.000	233.51
TCTEX1D2	Homo sapiens Tctex1 domain containing 2 (TCTEX1D2), mRNA.	698.07	282.95	2.47	0.026	415.12
MYNN	Homo sapiens myoneurin (MYNN), mRNA.	340.64	137.46	2.48	1.00E-04	203.17
C1orf19	Homo sapiens chromosome 1 open reading frame 19 (C1orf19), mRNA.	588.53	234.98	2.50	0.027	353.55
STAMBPL1	Homo sapiens STAM binding protein-like 1 (STAMBPL1), mRNA.	766.15	304.92	2.51	0.021	461.23
DHX29	Homo sapiens DEAH (Asp-Glu-Ala-His) box polypeptide 29 (DHX29), mRNA.	286.14	113.53	2.52	2.00E-04	172.61
A2LD1	Homo sapiens AIG2-like domain 1 (A2LD1), mRNA.	288.90	114.23	2.53	0.000	174.67
IL18RAP	Homo sapiens interleukin 18 receptor accessory protein (IL18RAP), mRNA.	316.05	122.72	2.58	2.00E-04	193.33
CREG1	Homo sapiens cellular repressor of E1A-stimulated genes 1 (CREG1), mRNA.	608.53	233.89	2.6	0.001	374.64
CRYZ	Homo sapiens crystallin, zeta (quinone reductase) (CRYZ), mRNA.	373.00	142.02	2.63	0.009	230.99
PRKAR1A	Homo sapiens protein kinase, cAMP-dependent, regulatory, type I, alpha (tissue specific extinguisher 1) (PRKAR1A), transcript variant 3, mRNA.	918.57	345.24	2.66	0.000	573.32
DAAM1	Homo sapiens dishevelled associated activator of morphogenesis 1 (DAAM1), mRNA.	366.01	134.16	2.73	5.00E-04	231.84
TNFRSF19	Homo sapiens tumor necrosis factor receptor superfamily, member 19 (TNFRSF19), transcript variant 2, mRNA.	328.88	120.67	2.73	0.000	208.21
RSBN1	Homo sapiens round spermatid basic protein 1 (RSBN1), mRNA.	346.98	125.89	2.76	0.000	221.08
ATAD1	Homo sapiens ATPase family, AAA domain containing 1 (ATAD1), mRNA.	441.47	156.17	2.83	0.041	285.30
	Homo sapiens cDNA FLJ34428 fis, clone HLUNG2000761	668.08	235.74	2.83	0.007	432.35
NBPF20	Homo sapiens neuroblastoma breakpoint family, member 20 (NBPF20), mRNA.	421.89	146.49	2.88	0.000	275.40
C17orf97	Homo sapiens chromosome 17 open reading frame 97 (C17orf97), mRNA.	271.10	93.73	2.89	0.012	177.37
DHX29	Homo sapiens DEAH (Asp-Glu-Ala-His) box polypeptide 29 (DHX29), mRNA.	496.48	161.47	3.07	0.000	335.00
LYN	Homo sapiens v-yes-1 Yamaguchi sarcoma viral related oncogene homolog (LYN), mRNA.	641.83	174.12	3.69	0.049	467.71
LOC644936	Homo sapiens cytoplasmic beta-actin pseudogene (LOC644936), non-coding RNA.	476.94	124.04	3.85	0.017	352.9
MYOM2	Homo sapiens myomesin (M-protein) 2, 165kDa (MYOM2), mRNA.	1021.8	223.90	4.56	0.000	797.90
D4S234E	Homo sapiens DNA segment on chromosome 4 (unique) 234 expressed sequence (D4S234E), transcript variant 2, mRNA.	962.66	85.62	11.24	0.010	877.04

Comparison $CD4^+CD25^-$ T cells of infected individuals versus EN

Symbol	Definition	mean_CD4_inf	mean_CD4_healthy	FC	pvalue	diff
EIF4A2	Homo sapiens eukaryotic translation initiation factor 4A, isoform 2 (EIF4A2), mRNA.	346.93	2213.11	-6.38	3.00E-04	1866.19
LOC388796	Homo sapiens hypothetical LOC388796 (LOC388796), non-coding RNA.	213.35	517.01	-2.42	0.038	303.66
LOC286512	PREDICTED: Homo sapiens misc_RNA (LOC286512), miscRNA.	108.53	255.68	-2.36	0.000	147.16
ERP27	Homo sapiens endoplasmic reticulum protein 27 kDa (ERP27), mRNA.	372.85	808.21	-2.17	0.012	435.35
EXOSC7	Homo sapiens exosome component 7 (EXOSC7), mRNA.	352.77	757.97	-2.15	0.034	405.20
CLASP1	Homo sapiens cytoplasmic linker associated protein 1 (CLASP1), mRNA.	223.78	464.81	-2.08	4.00E-04	241.02
ITPRIP	Homo sapiens inositol 1,4,5-triphosphate receptor interacting protein (ITPRIP), mRNA.	245.00	507.09	-2.07	0.029	262.10
ENO2	Homo sapiens enolase 2 (gamma, neuronal) (ENO2), mRNA.	342.33	706.42	-2.06	0.000	364.09
SKP1	Homo sapiens S-phase kinase-associated protein 1 (SKP1), transcript variant 1, mRNA.	447.99	923.15	-2.06	8.00E-04	475.16
SGK1	Homo sapiens serum/glucocorticoid regulated kinase 1 (SGK1), transcript variant 1, mRNA.	156.16	305.55	-1.96	0.040	149.40
C16orf33	Homo sapiens chromosome 16 open reading frame 33 (C16orf33), mRNA.	166.94	321.21	-1.92	0.040	154.27
	Homo sapiens cDNA clone IMAGE:30332316	210.38	375.92	-1.79	0.021	165.55
LOC440354	Homo sapiens PI-3-kinase-related kinase SMG-1 pseudogene (LOC440354), non-coding RNA.	177.73	311.55	-1.75	0.023	133.82
TSC22D3	Homo sapiens TSC22 domain family, member 3 (TSC22D3), transcript variant 1, mRNA.	2241.24	3845.93	-1.72	0.042	1604.7
METT11D1	Homo sapiens methyltransferase 11 domain containing 1 (METT11D1), transcript variant 1, mRNA.	352.93	596.66	-1.69	0.046	243.73
SPATS2L	Homo sapiens spermatogenesis associated, serine-rich 2-like (SPATS2L), transcript variant 2, mRNA.	194.44	329.45	-1.69	0.003	135.01
VIPR1	Homo sapiens vasoactive intestinal peptide receptor 1 (VIPR1), mRNA.	226.86	380.15	-1.68	0.025	153.29
PRPS1	Homo sapiens phosphoribosyl pyrophosphate synthetase 1 (PRPS1), mRNA.	234.34	388.39	-1.66	0.001	154.05
RRBP1	Homo sapiens ribosome binding protein 1 homolog 180kDa (dog) (RRBP1), transcript variant 1, mRNA.	229.08	375.94	-1.64	0.035	146.85
DBNDD2	Homo sapiens dysbindin (dystrobrevin binding protein 1) domain containing 2 (DBNDD2), transcript variant 3, mRNA.	426.85	691.70	-1.62	7.00E-04	264.85
CRIPAK	Homo sapiens cysteine-rich PAK1 inhibitor (CRIPAK), mRNA.	502.24	804.64	-1.60	0.032	302.39
RNF135	Homo sapiens ring finger protein 135 (RNF135), transcript variant 2, mRNA.	167.97	268.47	-1.60	0.041	100.51
C8orf33	Homo sapiens chromosome 8 open reading frame 33 (C8orf33), mRNA.	237.55	378.77	-1.59	0.021	141.22
LOC731049	PREDICTED: Homo sapiens similar to Ubiquitin-conjugating enzyme E2S (Ubiquitin-conjugating enzyme E2-24 kDa) (Ubiquitin-protein ligase) (Ubiquitin carrier protein) (E2-EPF5) (LOC731049), mRNA.	359.35	567.10	-1.58	0.007	207.75
SPG7	Homo sapiens spastic paraplegia 7 (pure and complicated autosomal recessive) (SPG7), nuclear gene encoding mitochondrial protein, transcript variant 1, mRNA.	1283.53	1989.08	-1.55	0.000	705.55
LOC100130092	PREDICTED: Homo sapiens misc_RNA (LOC100130092), miscRNA.	272.38	420.02	-1.54	3.00E-04	147.63
SCAP	Homo sapiens SREBF chaperone (SCAP), mRNA.	740.76	1139.96	-1.54	1.00E-04	399.20
UBA52	Homo sapiens ubiquitin A-52 residue ribosomal protein fusion product 1 (UBA52), transcript variant 2, mRNA.	215.15	330.46	-1.54	0.041	115.31
ZSCAN18	Homo sapiens zinc finger and SCAN domain containing 18 (ZSCAN18), mRNA.	184.65	285.20	-1.54	0.012	100.55
TUBGCP2	Homo sapiens tubulin, gamma complex associated protein 2 (TUBGCP2), mRNA.	238.13	365.52	-1.53	0.000	127.39
PLEKHM2	Homo sapiens pleckstrin homology domain containing, family M (with RUN domain) member 2 (PLEKHM2), mRNA.	345.89	526.93	-1.52	0.046	181.04
ARHGAP9	Homo sapiens Rho GTPase activating protein 9 (ARHGAP9), transcript variant 3, mRNA.	434.96	655.12	-1.51	0.025	220.17
C9orf78	Homo sapiens chromosome 9 open reading frame 78 (C9orf78), mRNA.	1325.40	1999.78	-1.51	0.005	674.38
TRPC4AP	Homo sapiens transient receptor potential cation channel, subfamily C, member 4 associated protein (TRPC4AP), transcript variant 1, mRNA.	483.16	728.79	-1.51	0.07	245.62
CSK	Homo sapiens c-src tyrosine kinase (CSK), mRNA.	799.39	528.69	1.51	0.012	270.71
NCOA4	Homo sapiens nuclear receptor coactivator 4 (NCOA4), mRNA.	4186.65	2772.01	1.51	0.000	1414.63
DNMT1	Homo sapiens DNA (cytosine-5-)-methyltransferase 1 (DNMT1), mRNA.	2041.95	1345.03	1.52	0.027	696.93
FAM38A	Homo sapiens family with sequence similarity 38, member A (FAM38A), mRNA.	816.77	537.41	1.52	0.004	279.36
LAX1	Homo sapiens lymphocyte transmembrane adaptor 1 (LAX1), mRNA.	455.33	298.69	1.52	0.009	156.65
SUSD1	Homo sapiens sushi domain containing 1 (SUSD1), mRNA.	535.57	351.47	1.52	0.013	184.10
ROD1	Homo sapiens ROD1 regulator of differentiation 1 (S. pombe) (ROD1), mRNA.	1790.70	1171.73	1.53	0.010	618.97
TRIM44	Homo sapiens tripartite motif-containing 44 (TRIM44), mRNA.	349.94	228.38	1.53	0.028	121.56
VEGFB	Homo sapiens vascular endothelial growth factor B (VEGFB), mRNA.	627.49	409.39	1.53	0.022	218.10
	Homo sapiens cDNA clone IMAGE:5277162	465.63	301.43	1.54	0.042	164.20
LOC651894	PREDICTED: Homo sapiens similar to ribosomal protein S12 (LOC651894), mRNA.	785.97	509.54	1.54	0.036	276.43

POGK	Homo sapiens pogo transposable element with KRAB domain (POGK), mRNA.	723.20	470.79	1.54	0.022	252.42
PSMA4	Homo sapiens proteasome (prosome, macropain) subunit, alpha type, 4 (PSMA4), mRNA.	1893.54	1228	1.54	0.008	665.54
SH3BGRL	Homo sapiens SH3 domain binding glutamic acid-rich protein like (SH3BGRL), mRNA.	482.52	311.05	1.55	0.006	171.46
XRN1	Homo sapiens 5'-3' exoribonuclease 1 (XRN1), mRNA.	498.55	320.95	1.55	0.006	177.60
ALDH9A1	Homo sapiens aldehyde dehydrogenase 9 family, member A1 (ALDH9A1), mRNA.	4157.34	2645.26	1.57	0.000	1512.07
AP1S2	Homo sapiens adaptor-related protein complex 1, sigma 2 subunit (AP1S2), mRNA.	1701.82	1074.58	1.58	0.018	627.25
CASP3	Homo sapiens caspase 3, apoptosis-related cysteine peptidase (CASP3), transcript variant beta, mRNA.	468.82	297.18	1.58	0.004	171.63
PTPLB	Homo sapiens protein tyrosine phosphatase-like (proline instead of catalytic arginine), member b (PTPLB), mRNA.	334.78	211.51	1.58	0.014	123.28
DYRK1A	Homo sapiens dual-specificity tyrosine-(Y)-phosphorylation regulated kinase 1A (DYRK1A), transcript variant 5, mRNA.	501.12	315.97	1.59	0.013	185.15
CLINT1	Homo sapiens clathrin interactor 1 (CLINT1), mRNA.	444.25	277.31	1.60	0.036	166.94
CUL5	Homo sapiens cullin 5 (CUL5), mRNA.	345.42	215.47	1.60	0.046	129.94
CLIP1	Homo sapiens CAP-GLY domain containing linker protein 1 (CLIP1), transcript variant 1, mRNA.	396.78	246.16	1.61	0.005	150.62
ZNF337	Homo sapiens zinc finger protein 337 (ZNF337), mRNA.	539.23	334.80	1.61	0.017	204.43
SH3KBP1	Homo sapiens SH3-domain kinase binding protein 1 (SH3KBP1), transcript variant 1, mRNA.	1640.31	1012.12	1.62	0.037	628.19
C1orf131	Homo sapiens chromosome 1 open reading frame 131 (C1orf131), mRNA.	324.30	199.18	1.63	0.012	125.11
WASPIP	Homo sapiens Wiskott-Aldrich syndrome protein interacting protein (WASPIP), mRNA.	714.99	438.21	1.63	0.004	276.78
C5orf15	Homo sapiens chromosome 5 open reading frame 15 (C5orf15), mRNA.	946.06	576.73	1.64	0.000	369.32
C1orf24	Homo sapiens chromosome 1 open reading frame 24 (C1orf24), transcript variant 2, mRNA.	482.53	292.50	1.65	0.047	190.03
DNASE2	Homo sapiens deoxyribonuclease II, lysosomal (DNASE2), mRNA.	300.32	180.39	1.66	0.006	119.93
KLRB1	Homo sapiens killer cell lectin-like receptor subfamily B, member 1 (KLRB1), mRNA.	3555.44	2129.00	1.67	0.001	1426.44
ACSL5	Homo sapiens acyl-CoA synthetase long-chain family member 5 (ACSL5), transcript variant 2, mRNA.	313.07	184.78	1.69	0.002	128.29
BMI1	Homo sapiens BMI1 polycomb ring finger oncogene (BMI1), mRNA.	467.37	275.23	1.70	0.025	192.15
ST13	Homo sapiens suppression of tumorigenicity 13 (colon carcinoma) (Hsp70 interacting protein) (ST13), mRNA.	359.12	211.59	1.70	0.039	147.53
UBE2Q2	Homo sapiens ubiquitin-conjugating enzyme E2Q family member 2 (UBE2Q2), mRNA.	593.86	348.35	1.70	0.013	245.51
XBP1	Homo sapiens X-box binding protein 1 (XBP1), transcript variant 1, mRNA.	918.23	536.54	1.71	0.003	381.69
AGL	Homo sapiens amylo-1, 6-glucosidase, 4-alpha-glucanotransferase (AGL), transcript variant 5, mRNA.	337.24	193.21	1.75	0.042	144.03
ARL5A	Homo sapiens ADP-ribosylation factor-like 5A (ARL5A), transcript variant 3, mRNA.	780.10	446.17	1.75	0.050	333.93
ARL6IP1	Homo sapiens ADP-ribosylation factor-like 6 interacting protein 1 (ARL6IP1), mRNA.	1463.73	831.30	1.76	0.002	632.43
RAP2A	Homo sapiens RAP2A, member of RAS oncogene family (RAP2A), mRNA.	337.99	190.06	1.78	0.043	147.93
SRPK1	Homo sapiens SFRS protein kinase 1 (SRPK1), mRNA.	356.37	200.37	1.78	0.006	156.00
CDS2	Homo sapiens CDP-diacylglycerol synthase (phosphatidate cytidylyltransferase) 2 (CDS2), mRNA.	305.11	169.27	1.80	0.001	135.84
FANCE	Homo sapiens Fanconi anemia, complementation group E (FANCE), mRNA.	267.57	148.38	1.80	0.036	119.18
GEMIN4	Homo sapiens gem (nuclear organelle) associated protein 4 (GEMIN4), mRNA.	432.27	240.62	1.80	0.037	191.66
	Homo sapiens cDNA clone IMAGE:5261213	1001.42	553.52	1.81	0.046	447.89
PIP5K1C	Homo sapiens phosphatidylinositol-4-phosphate 5-kinase, type I, gamma (PIP5K1C), mRNA.	317.87	175.12	1.82	0.002	142.75
YWHAQ	Homo sapiens tyrosine 3-monooxygenase/tryptophan 5-monooxygenase activation protein, theta polypeptide (YWHAQ), mRNA.	3439.00	1892.13	1.82	5.00E-04	1546.87
MLKL	Homo sapiens mixed lineage kinase domain-like (MLKL), mRNA.	1774.43	971.05	1.83	0.007	803.39
STAT1	Homo sapiens signal transducer and activator of transcription 1, 91kDa (STAT1), transcript variant alpha, mRNA.	2181.94	1186.49	1.84	0.046	995.45
FGD2	Homo sapiens FYVE, RhoGEF and PH domain containing 2 (FGD2), mRNA.	329.39	177.66	1.85	0.000	151.73
HIGD1A	Homo sapiens HIG1 hypoxia inducible domain family, member 1A (HIGD1A), transcript variant 1, mRNA.	375.36	202.05	1.86	0.042	173.32
ZMYM1	Homo sapiens zinc finger, MYM-type 1 (ZMYM1), mRNA.	235.19	125.75	1.87	0.002	109.44
FOXN2	Homo sapiens forkhead box N2 (FOXN2), mRNA.	559.87	295.43	1.90	0.038	264.44
CDC2L5	Homo sapiens cell division cycle 2-like 5 (cholinesterase-related cell division controller) (CDC2L5), transcript variant 1, mRNA.	430.67	225.11	1.91	0.025	205.55
B4GALT7	Homo sapiens xylosylprotein beta 1,4-galactosyltransferase, polypeptide 7 (galactosyltransferase I) (B4GALT7), mRNA.	284.67	147.65	1.93	0.019	137.02
HEATR1	Homo sapiens HEAT repeat containing 1 (HEATR1), mRNA.	418.38	215.15	1.94	0.001	203.23
ZNF302	Homo sapiens zinc finger protein 302 (ZNF302), transcript variant 1, mRNA.	364.61	183.56	1.99	0.016	181.05
CHST7	Homo sapiens carbohydrate (N-acetylglucosamine 6-O) sulfotransferase 7 (CHST7), mRNA.	275.61	136.51	2.02	0.024	139.11
RFX7	Homo sapiens regulatory factor X, 7 (RFX7), mRNA.	519.42	255.03	2.04	4.00E-04	264.39
VPS4B	Homo sapiens vacuolar protein sorting 4 homolog B (S. cerevisiae) (VPS4B), mRNA.	690.37	337.34	2.05	0.034	353.03
ATP6AP2	Homo sapiens ATPase, H+ transporting, lysosomal accessory protein 2 (ATP6AP2), mRNA.	820.81	390.95	2.10	2.00E-04	429.86

TMEM209	Homo sapiens transmembrane protein 209 (TMEM209), mRNA.	290.13	137.86	2.10	0.017	152.27
IQGAP2	Homo sapiens IQ motif containing GTPase activating protein 2 (IQGAP2), mRNA.	702.85	332.08	2.12	0.017	370.76
TNFSF10	Homo sapiens tumor necrosis factor (ligand) superfamily, member 10 (TNFSF10), mRNA.	568.49	258.23	2.2	0.001	310.26
PTGDR	Homo sapiens prostaglandin D2 receptor (DP) (PTGDR), mRNA.	327.56	145.43	2.25	0.007	182.13
ZW10	Homo sapiens ZW10, kinetochore associated, homolog (Drosophila) (ZW10), mRNA.	386.47	152.43	2.54	0.001	234.04

Comparison $CD4^+CD25^-$ T cells of MF^- versus MF^+ individuals

Symbol	Definition	mean_CD4_Mfneg	mean_CD4_Mfpos	FC	pvalue	diff
SOD2	Homo sapiens superoxide dismutase 2, mitochondrial (SOD2), nuclear gene encoding mitochondrial protein, transcript variant 2, mRNA.	261.63	994.61	-3.80	0.000	732.98
LILRA3	Homo sapiens leukocyte immunoglobulin-like receptor, subfamily A (without TM domain), member 3 (LILRA3), mRNA.	523.26	1785.06	-3.41	0.006	1261.79
IL8	Homo sapiens interleukin 8 (IL8), mRNA.	100.25	297.87	-2.97	0.038	197.62
SFXN4	Homo sapiens sideroflexin 4 (SFXN4), mRNA.	148.17	395.57	-2.67	0.047	247.39
SDCCAG10	Homo sapiens serologically defined colon cancer antigen 10 (SDCCAG10), mRNA.	206.11	478.32	-2.32	2.00E-04	272.21
NFKBIA	Homo sapiens nuclear factor of kappa light polypeptide gene enhancer in B-cells inhibitor, alpha (NFKBIA), mRNA.	506.30	1145.58	-2.26	0.019	639.28
HSD17B12	Homo sapiens hydroxysteroid (17-beta) dehydrogenase 12 (HSD17B12), mRNA.	243.75	506.99	-2.08	2.00E-04	263.24
ZNF101	Homo sapiens zinc finger protein 101 (ZNF101), mRNA.	139.07	282.56	-2.03	0.039	143.48
PTS	Homo sapiens 6-pyruvoyltetrahydropterin synthase (PTS), mRNA.	278.76	562.36	-2.02	0.048	283.60
FECH	Homo sapiens ferrochelatase (protoporphyria) (FECH), nuclear gene encoding mitochondrial protein, transcript variant 2, mRNA.	141.80	284.39	-2.01	2.00E-04	142.59
KLF6	Homo sapiens Kruppel-like factor 6 (KLF6), transcript variant 2, mRNA.	1170.61	2313.46	-1.98	0.021	1142.85
FGL2	Homo sapiens fibrinogen-like 2 (FGL2), mRNA.	309.46	608.4	-1.97	0.043	298.94
GLCE	Homo sapiens glucuronic acid epimerase (GLCE), mRNA.	108.91	213.22	-1.96	4.00E-04	104.31
HPS4	Homo sapiens Hermansky-Pudlak syndrome 4 (HPS4), transcript variant 2, mRNA.	123.09	241.14	-1.96	0.012	118.05
SLC11A1	Homo sapiens solute carrier family 11 (proton-coupled divalent metal ion transporters), member 1 (SLC11A1), mRNA.	195.44	383.02	-1.96	0.000	187.58
C14orf109	Homo sapiens chromosome 14 open reading frame 109 (C14orf109), transcript variant 2, mRNA.	139.45	272.36	-1.95	2.00E-04	132.91
HSD17B12	Homo sapiens hydroxysteroid (17-beta) dehydrogenase 12 (HSD17B12), mRNA.	137.51	262.64	-1.91	0.023	125.14
KLF11	PREDICTED: Homo sapiens Kruppel-like factor 11 (KLF11), mRNA.	455.61	871.89	-1.91	0.000	416.27
ACVR1	Homo sapiens activin A receptor, type I (ACVR1), mRNA.	198.71	374.64	-1.89	0.017	175.93
GZMK	Homo sapiens granzyme K (granzyme 3; tryptase II) (GZMK), mRNA.	1122.7	2121.28	-1.89	0.040	998.57
NOD2	Homo sapiens nucleotide-binding oligomerization domain containing 2 (NOD2), mRNA.	153.14	288.38	-1.88	0.000	135.24
GBP1	Homo sapiens guanylate binding protein 1, interferon-inducible, 67kDa (GBP1), mRNA.	359.24	670.65	-1.87	0.000	311.41
CREG1	Homo sapiens cellular repressor of E1A-stimulated genes 1 (CREG1), mRNA.	165.38	306.63	-1.85	0.000	141.25
NFKBIZ	Homo sapiens nuclear factor of kappa light polypeptide gene enhancer in B-cells inhibitor, zeta (NFKBIZ), transcript variant 2, mRNA.	466.51	863.42	-1.85	0.033	396.91
PUM1	Homo sapiens pumilio homolog 1 (Drosophila) (PUM1), transcript variant 1, mRNA.	206.04	374.93	-1.82	0.000	168.89
MCEE	Homo sapiens methylmalonyl CoA epimerase (MCEE), mRNA.	154.45	279.69	-1.81	0.000	125.24
SRI	Homo sapiens sorcin (SRI), transcript variant 1, mRNA.	157.55	284.40	-1.81	0.044	126.84
COQ2	Homo sapiens coenzyme Q2 homolog, prenyltransferase (yeast) (COQ2), mRNA.	132.94	237.73	-1.79	0.037	104.8
LOC650215	PREDICTED: Homo sapiens similar to Exportin-T (tRNA exportin) (Exportin(tRNA)) (LOC650215), mRNA.	218.25	388.79	-1.78	0.029	170.55
PARP9	Homo sapiens poly (ADP-ribose) polymerase family, member 9 (PARP9), mRNA.	337.14	591.83	-1.76	0.001	254.69
SPCS3	Homo sapiens signal peptidase complex subunit 3 homolog (S. cerevisiae) (SPCS3), mRNA.	199.54	352.05	-1.76	3.00E-04	152.52
WARS	Homo sapiens tryptophanyl-tRNA synthetase (WARS), transcript variant 2, mRNA.	307.50	531.60	-1.73	0.020	224.1
GBP1	Homo sapiens guanylate binding protein 1, interferon-inducible, 67kDa (GBP1), mRNA.	441.73	758.77	-1.72	0.011	317.04
KLF4	Homo sapiens Kruppel-like factor 4 (gut) (KLF4), mRNA.	174.03	300.13	-1.72	0.009	126.1
MED4	Homo sapiens mediator complex subunit 4 (MED4), mRNA.	189.45	323.51	-1.71	0.014	134.06
CCNB1IP1	Homo sapiens cyclin B1 interacting protein 1 (CCNB1IP1), transcript variant 3, mRNA.	463.28	780.51	-1.68	0.002	317.24
WWP2	Homo sapiens WW domain containing E3 ubiquitin protein ligase 2 (WWP2), transcript variant 3, mRNA.	242.19	406.44	-1.68	0.000	164.25
KLF6	Homo sapiens Kruppel-like factor 6 (KLF6), transcript variant 1, mRNA.	179.70	297.07	-1.65	3.00E-04	117.38
LILRB2	Homo sapiens leukocyte immunoglobulin-like receptor, subfamily B (with TM and ITIM domains), member 2 (LILRB2), transcript variant 2, mRNA.	343.55	561.28	-1.63	0.003	217.73
CCNB1IP1	Homo sapiens cyclin B1 interacting protein 1 (CCNB1IP1), transcript variant 2, mRNA.	240.02	388.41	-1.62	0.013	148.39

LOC729217	PREDICTED: Homo sapiens misc_RNA (LOC729217), miscRNA.	220.37	354.84	-1.61	9.00E-04	134.46
ME2	Homo sapiens malic enzyme 2, NAD(+)-dependent, mitochondrial (ME2), nuclear gene encoding mitochondrial protein, mRNA.	200.48	315.03	-1.57	0.013	114.55
ECGF1	Homo sapiens endothelial cell growth factor 1 (platelet-derived) (ECGF1), mRNA.	969.73	1511.66	-1.56	0.018	541.93
PPA1	Homo sapiens pyrophosphatase (inorganic) 1 (PPA1), mRNA.	977.32	1528.2	-1.56	0.007	550.87
DNAJA2	Homo sapiens DnaJ (Hsp40) homolog, subfamily A, member 2 (DNAJA2), mRNA.	352.07	545.26	-1.55	2.00E-04	193.19
CCDC53	Homo sapiens coiled-coil domain containing 53 (CCDC53), mRNA.	223.56	343.71	-1.54	0.039	120.16
SUCLG2	Homo sapiens succinate-CoA ligase, GDP-forming, beta subunit (SUCLG2), mRNA.	208.16	321.08	-1.54	0.023	112.92
IFITM3	Homo sapiens interferon induced transmembrane protein 3 (1-8U) (IFITM3), mRNA.	388.29	592.77	-1.53	0.035	204.48
OAT	Homo sapiens ornithine aminotransferase (gyrate atrophy) (OAT), nuclear gene encoding mitochondrial protein, mRNA.	229.97	347.95	-1.51	0.019	117.98
YPEL5	Homo sapiens yippee-like 5 (Drosophila) (YPEL5), mRNA.	1224.68	1854.75	-1.51	0.047	630.07
ZNF721	Homo sapiens zinc finger protein 721 (ZNF721), mRNA.	450.46	299.84	1.50	0.029	150.62
RAP2A	Homo sapiens RAP2A, member of RAS oncogene family (RAP2A), mRNA.	408.03	267.95	1.52	0.049	140.08
LOC440348	Homo sapiens similar to nuclear pore complex interacting protein (LOC440348), mRNA.	372.89	243.45	1.53	0.000	129.43
ZNF142	Homo sapiens zinc finger protein 142 (ZNF142), transcript variant 2, mRNA.	445.72	291.29	1.53	0.000	154.43
SBK1	Homo sapiens SH3-binding domain kinase 1 (SBK1), mRNA.	1054.14	682.07	1.55	0.000	372.07
SLAMF6	Homo sapiens SLAM family member 6 (SLAMF6), mRNA.	3391.56	2188.44	1.55	0.0169	1203.12
CCDC28A	Homo sapiens coiled-coil domain containing 28A (CCDC28A), mRNA.	812.83	520.17	1.56	0.0429	292.66
KLHL8	Homo sapiens kelch-like 8 (Drosophila) (KLHL8), mRNA.	292.44	187.50	1.56	0.000	104.93
MBD6	Homo sapiens methyl-CpG binding domain protein 6 (MBD6), mRNA.	329.79	209.33	1.58	0.000	120.47
RBM33	Homo sapiens RNA binding motif protein 33 (RBM33), transcript variant 1, mRNA.	865.24	543.78	1.59	0.0103	321.46
IP6K1	Homo sapiens inositol hexakisphosphate kinase 1 (IP6K1), transcript variant 2, mRNA.	323.00	201.90	1.60	1.00E-04	121.1
MZF1	Homo sapiens myeloid zinc finger 1 (MZF1), transcript variant 2, mRNA.	454.58	284.14	1.60	0,0000	170.44
EDG4	Homo sapiens endothelial differentiation, lysophosphatidic acid G-protein-coupled receptor, 4 (EDG4), mRNA.	634.95	390.61	1.63	0.0197	244.33
FRAP1	Homo sapiens FK506 binding protein 12-rapamycin associated protein 1 (FRAP1), mRNA.	675.49	412.19	1.64	0.0043	263.29
MFSD6	Homo sapiens major facilitator superfamily domain containing 6 (MFSD6), mRNA.	256.64	154.80	1.66	0.0038	101.85
SNTB1	Homo sapiens syntrophin, beta 1 (dystrophin-associated protein A1, 59kDa, basic component 1) (SNTB1), mRNA.	287.49	171.96	1.67	0.000	115.54
TMEM115	Homo sapiens transmembrane protein 115 (TMEM115), mRNA.	296.93	174.90	1.70	0.0188	122.03
LRSAM1	Homo sapiens leucine rich repeat and sterile alpha motif containing 1 (LRSAM1), transcript variant 1, mRNA.	351.98	203.26	1.73	0.0014	148.72
SLC25A42	Homo sapiens solute carrier family 25, member 42 (SLC25A42), mRNA.	764.11	438.89	1.74	0.0075	325.22
SEC22A	Homo sapiens SEC22 vesicle trafficking protein homolog A (S. cerevisiae) (SEC22A), mRNA.	425.45	243.63	1.75	0.0301	181.82
SYTL3	Homo sapiens synaptotagmin-like 3 (SYTL3), mRNA.	661.50	378.09	1.75	0.000	283.42
ABCC5	Homo sapiens ATP-binding cassette, sub-family C (CFTR/MRP), member 5 (ABCC5), transcript variant 2, mRNA.	311.36	176.35	1.77	0.027	135.00
OSBP	Homo sapiens oxysterol binding protein (OSBP), mRNA.	658.43	368.91	1.78	0.015	289.53
ASTE1	Homo sapiens asteroid homolog 1 (Drosophila) (ASTE1), mRNA.	278.08	154.47	1.80	6.00E-04	123.61
NCRNA00092	Homo sapiens non-protein coding RNA 92 (NCRNA00092), non-coding RNA.	235.97	130.82	1.80	0.021	105.15
C9orf103	Homo sapiens chromosome 9 open reading frame 103 (C9orf103), mRNA.	388.28	214.65	1.81	0.016	173.64
MFSD6	Homo sapiens major facilitator superfamily domain containing 6 (MFSD6), mRNA.	468.71	258.31	1.81	0.034	210.40
DIDO1	Homo sapiens death inducer-obliterator 1 (DIDO1), transcript variant 3, mRNA.	297.44	162.50	1.83	0.024	134.94
LPAR5	Homo sapiens lysophosphatidic acid receptor 5 (LPAR5), mRNA.	240.27	130.80	1.84	0.005	109.47
POMGNT1	Homo sapiens protein O-linked mannose beta1,2-N-acetylglucosaminyltransferase (POMGNT1), mRNA.	474.14	257.29	1.84	0.003	216.84
LOC730432	PREDICTED: Homo sapiens similar to serine/threonine/tyrosine interacting protein, transcript variant 1 (LOC730432), mRNA.	652.13	350.57	1.86	0.009	301.56
ZNF493	Homo sapiens zinc finger protein 493 (ZNF493), transcript variant 3, mRNA.	315.36	168.56	1.87	0.004	146.81
WDR4	Homo sapiens WD repeat domain 4 (WDR4), transcript variant 2, mRNA.	295.85	156.65	1.89	0.000	139.20
RNF149	Homo sapiens ring finger protein 149 (RNF149), mRNA.	1127.05	565.71	1.99	0.004	561.34
PLEKHA9	Homo sapiens pleckstrin homology domain containing, family A (phosphoinositide binding specific) member 9 (PLEKHA9), mRNA.	489.71	244.19	2.01	0.006	245.52
PROK2	Homo sapiens prokineticin 2 (PROK2), mRNA.	446.87	211.13	2.12	0.031	235.74
TATDN3	Homo sapiens TatD DNase domain containing 3 (TATDN3), transcript variant 1, mRNA.	372.80	175.26	2.13	0.028	197.55
	PREDICTED: Homo sapiens hypothetical LOC400999 (LOC400999), mRNA	277.67	127.98	2.17	0.000	149.69
ADRB2	Homo sapiens adrenergic, beta-2-, receptor, surface (ADRB2), mRNA.	1433.37	589.94	2.43	0.000	843.43
LOC729708	PREDICTED: Homo sapiens similar to rcTPI1, transcript variant 1 (LOC729708), mRNA.	930.10	192.97	4.82	0.033	737.12

Comparison $CD4^{+}CD25^{-}$ T cells of MF^{-} individuals EN

Symbol	Definition	mean_CD4_Mfneg	mean_CD4_EN	FC	pvalue	diff
ERP27	Homo sapiens endoplasmic reticulum protein 27 kDa (ERP27), mRNA.	270.52	808.21	-2.99	2.00E-04	537.69
SGK1	Homo sapiens serum/glucocorticoid regulated kinase 1 (SGK1), transcript variant 1, mRNA.	124.24	305.55	-2.46	0.002	181.31
CPVL	Homo sapiens carboxypeptidase, vitellogenic-like (CPVL), transcript variant 1, mRNA.	273.63	638.42	-2.33	0.025	364.79
C16orf33	Homo sapiens chromosome 16 open reading frame 33 (C16orf33), mRNA.	144.65	321.21	-2.22	0.002	176.56
SMAGP	Homo sapiens small cell adhesion glycoprotein (SMAGP), transcript variant 2, mRNA.	99.59	216.48	-2.17	0.005	116.89
LOC440354	Homo sapiens PI-3-kinase-related kinase SMG-1 pseudogene (LOC440354), non-coding RNA.	144.03	311.55	-2.16	0.000	167.51
LOC286512	PREDICTED: Homo sapiens misc_RNA (LOC286512), miscRNA.	126.13	255.68	-2.03	0.018	129.55
ENO2	Homo sapiens enolase 2 (gamma, neuronal) (ENO2), mRNA.	352.04	706.42	-2.01	4.00E-04	354.38
HPS4	Homo sapiens Hermansky-Pudlak syndrome 4 (HPS4), transcript variant 2, mRNA.	123.09	246.49	-2,00	0.002	123.40
SGK1	Homo sapiens serum/glucocorticoid regulated kinase 1 (SGK1), transcript variant 1, mRNA.	114.84	227.37	-1.98	2.00E-04	112.53
DBNDD2	Homo sapiens dysbindin (dystrobrevin binding protein 1) domain containing 2 (DBNDD2), transcript variant 3, mRNA.	360.14	691.70	-1.92	0.024	331.56
CCNB1IP1	Homo sapiens cyclin B1 interacting protein 1 (CCNB1IP1), transcript variant 2, mRNA.	240.02	451.91	-1.88	0.014	211.89
SKP1	Homo sapiens S-phase kinase-associated protein 1 (SKP1), transcript variant 1, mRNA.	490.55	923.15	-1.88	0.003	432.59
VIPR1	Homo sapiens vasoactive intestinal peptide receptor 1 (VIPR1), mRNA.	206.11	380.15	-1.84	0.002	174.04
SPATS2L	Homo sapiens spermatogenesis associated, serine-rich 2-like (SPATS2L), transcript variant 2, mRNA.	180.43	329.45	-1.83	0.013	149.02
CLASP1	Homo sapiens cytoplasmic linker associated protein 1 (CLASP1), mRNA.	258.98	464.81	-1.79	0.004	205.83
UBQLN1	Homo sapiens ubiquilin 1 (UBQLN1), transcript variant 2, mRNA.	140.42	247.88	-1.77	0.039	107.46
ARHGAP9	Homo sapiens Rho GTPase activating protein 9 (ARHGAP9), transcript variant 3, mRNA.	373.11	655.12	-1.76	0.000	282.02
MED10	Homo sapiens mediator complex subunit 10 (MED10), mRNA.	433.77	763.83	-1.76	0.003	330.06
CCNB1IP1	Homo sapiens cyclin B1 interacting protein 1 (CCNB1IP1), transcript variant 3, mRNA.	463.28	797.04	-1.72	0.027	333.76
METT11D1	Homo sapiens methyltransferase 11 domain containing 1 (METT11D1), transcript variant 1, mRNA.	355.33	596.66	-1.68	0.041	241.34
ZSCAN18	Homo sapiens zinc finger and SCAN domain containing 18 (ZSCAN18), mRNA.	169.91	285.2	-1.68	0.010	115.29
LOC642333	PREDICTED: Homo sapiens similar to M-phase phosphoprotein, mpp8 (LOC642333), mRNA.	326.02	544.88	-1.67	0.003	218.87
LOC100128196	PREDICTED: Homo sapiens misc_RNA (LOC100128196), miscRNA.	244.63	406.86	-1.66	0.000	162.23
LOC100133185	PREDICTED: Homo sapiens misc_RNA (LOC100133185), miscRNA.	199.41	329.66	-1.65	0.000	130.25
CIRBP	Homo sapiens cold inducible RNA binding protein (CIRBP), mRNA.	2218.4	3636.87	-1.64	0.029	1418.46
BRI3	Homo sapiens brain protein I3 (BRI3), mRNA.	269.23	438.33	-1.63	2.00E-04	169.10
SFRS14	Homo sapiens splicing factor, arginine/serine-rich 14 (SFRS14), transcript variant 1, mRNA.	257.33	418.91	-1.63	0.008	161.58
TCEB3	Homo sapiens transcription elongation factor B (SIII), polypeptide 3 (110kDa, elongin A) (TCEB3), mRNA.	170.22	277.18	-1.63	0.001	106.96
PRPS1	Homo sapiens phosphoribosyl pyrophosphate synthetase 1 (PRPS1), mRNA.	239.95	388.39	-1.62	0.010	148.45
SCAP	Homo sapiens SREBF chaperone (SCAP), mRNA.	709.62	1139.96	-1.61	0.000	430.35
SNHG5	Homo sapiens small nucleolar RNA host gene (non-protein coding) 5 (SNHG5) on chromosome 6.	176.73	283.81	-1.61	0.003	107.08
SSBP1	Homo sapiens single-stranded DNA binding protein 1 (SSBP1), mRNA.	295.63	472.36	-1.6	0.000	176.73
GARS	Homo sapiens glycyl-tRNA synthetase (GARS), mRNA.	390.46	621.52	-1.59	0.020	231.06
PTPMT1	Homo sapiens protein tyrosine phosphatase, mitochondrial 1 (PTPMT1), nuclear gene encoding mitochondrial protein, mRNA.	251.13	394.93	-1.57	0.038	143.80
KIAA0391	Homo sapiens KIAA0391 (KIAA0391), mRNA.	301.01	469.99	-1.56	3.00E-04	168.98
CCDC53	Homo sapiens coiled-coil domain containing 53 (CCDC53), mRNA.	223.56	346.36	-1.55	0.000	122.80
LOC100130092	PREDICTED: Homo sapiens misc_RNA (LOC100130092), miscRNA.	270.28	420.02	-1.55	1.00E-04	149.74
SYF2	Homo sapiens SYF2 homolog, RNA splicing factor (S. cerevisiae) (SYF2), transcript variant 1, mRNA.	228.81	348.18	-1.52	0.016	119.37
DTD1	Homo sapiens D-tyrosyl-tRNA deacylase 1 homolog (S. cerevisiae) (DTD1), nuclear gene encoding mitochondrial protein, mRNA.	518.44	783.93	-1.51	4.00E-04	265.48
PTPLB	Homo sapiens protein tyrosine phosphatase-like (proline instead of catalytic arginine), member b (PTPLB), mRNA.	320.22	211.51	1.51	0.041	108.71
RNF34	Homo sapiens ring finger protein 34 (RNF34), transcript variant 2, mRNA.	923.36	612.38	1.51	0.008	310.98
UBP1	Homo sapiens upstream binding protein 1 (LBP-1a) (UBP1), mRNA.	755.68	500.26	1.51	0.009	255.42
ZGPAT	Homo sapiens zinc finger, CCCH-type with G patch domain (ZGPAT), transcript variant 1, mRNA.	668.75	443.73	1.51	0.000	225.02
ARHGEF6	Homo sapiens Rac/Cdc42 guanine nucleotide exchange factor (GEF) 6 (ARHGEF6), mRNA.	3414.4	2241.45	1.52	0.002	1172.95

CDC2L5	Homo sapiens cell division cycle 2-like 5 (cholinesterase-related cell division controller) (CDC2L5), transcript variant 2, mRNA.	326.31	213.99	1.52	2.00E-04	112.32
CCDC25	Homo sapiens coiled-coil domain containing 25 (CCDC25), mRNA.	649.56	422.85	1.54	0.004	226.71
CKAP5	Homo sapiens cytoskeleton associated protein 5 (CKAP5), transcript variant 1, mRNA.	905.28	587.59	1.54	1.00E-04	317.70
MRI1	Homo sapiens methylthioribose-1-phosphate isomerase homolog (S. cerevisiae) (MRI1), transcript variant 1, mRNA.	564.06	365.59	1.54	4.00E-04	198.47
TBP	Homo sapiens TATA box binding protein (TBP), mRNA.	377.26	244.64	1.54	0.000	132.62
C14orf135	Homo sapiens chromosome 14 open reading frame 135 (C14orf135), mRNA.	305.88	196.4	1.56	6.00E-04	109.47
AP1S2	Homo sapiens adaptor-related protein complex 1, sigma 2 subunit (AP1S2), mRNA.	1682.09	1074.58	1.57	0.034	607.52
ANGEL2	Homo sapiens angel homolog 2 (Drosophila) (ANGEL2), mRNA.	890.28	564.54	1.58	0.013	325.74
FAM38A	Homo sapiens family with sequence similarity 38, member A (FAM38A), mRNA.	847.71	537.41	1.58	0.002	310.30
ALDH9A1	Homo sapiens aldehyde dehydrogenase 9 family, member A1 (ALDH9A1), mRNA.	4193.07	2645.26	1.59	0.000	1547.8
CDS2	Homo sapiens CDP-diacylglycerol synthase (phosphatidate cytidylyltransferase) 2 (CDS2), mRNA.	273.79	169.27	1.62	0.040	104.52
KLRB1	Homo sapiens killer cell lectin-like receptor subfamily B, member 1 (KLRB1), mRNA.	3453.31	2129	1.62	0.003	1324.31
SH3KBP1	Homo sapiens SH3-domain kinase binding protein 1 (SH3KBP1), transcript variant 1, mRNA.	1636.06	1012.12	1.62	0.033	623.94
C5orf15	Homo sapiens chromosome 5 open reading frame 15 (C5orf15), mRNA.	940.75	576.73	1.63	0.005	364.01
RAB11A	Homo sapiens RAB11A, member RAS oncogene family (RAB11A), mRNA.	1494.19	916.21	1.63	0.000	577.97
ZNF721	Homo sapiens zinc finger protein 721 (ZNF721), mRNA.	450.46	273.78	1.65	0.004	176.68
CLIP1	Homo sapiens CAP-GLY domain containing linker protein 1 (CLIP1), transcript variant 1, mRNA.	411.43	246.16	1.67	0.011	165.27
FANCE	Homo sapiens Fanconi anemia, complementation group E (FANCE), mRNA.	248.43	148.38	1.67	0.026	100.05
ARHGAP30	Homo sapiens Rho GTPase activating protein 30 (ARHGAP30), transcript variant 1, mRNA.	1858.45	1102.01	1.69	0.020	756.44
POGK	Homo sapiens pogo transposable element with KRAB domain (POGK), mRNA.	793.91	470.79	1.69	0.000	323.13
KATNB1	Homo sapiens katanin p80 (WD repeat containing) subunit B 1 (KATNB1), mRNA.	277.06	162.93	1.7	5.00E-04	114.14
RAB40C	Homo sapiens RAB40C, member RAS oncogene family (RAB40C), mRNA.	716.94	418.11	1.71	0.0318	298.83
GFI1	Homo sapiens growth factor independent 1 transcription repressor (GFI1), mRNA.	739.52	425.69	1.74	0.000	313.82
C1orf131	Homo sapiens chromosome 1 open reading frame 131 (C1orf131), mRNA.	354.43	199.18	1.78	2.00E-04	155.25
ARL5A	Homo sapiens ADP-ribosylation factor-like 5A (ARL5A), transcript variant 3, mRNA.	466.45	261.28	1.79	0.0036	205.17
CASP3	Homo sapiens caspase 3, apoptosis-related cysteine peptidase (CASP3), transcript variant beta, mRNA.	533.35	297.18	1.79	1.00E-04	236.16
GEMIN4	Homo sapiens gem (nuclear organelle) associated protein 4 (GEMIN4), mRNA.	439.11	240.62	1.82	0.000	198.50
UBE2Q2	Homo sapiens ubiquitin-conjugating enzyme E2Q family member 2 (UBE2Q2), mRNA.	642.78	348.35	1.85	0.049	294.43
ZNF322A	Homo sapiens zinc finger protein 322A (ZNF322A), mRNA.	324.09	174.97	1.85	0.013	149.12
FGD2	Homo sapiens FYVE, RhoGEF and PH domain containing 2 (FGD2), mRNA.	333.36	177.66	1.88	0.000	155.70
	Homo sapiens cDNA clone IMAGE:5261213	1042.66	553.52	1.88	0.001	489.13
TNFSF10	Homo sapiens tumor necrosis factor (ligand) superfamily, member 10 (TNFSF10), mRNA.	486.50	258.23	1.88	0.019	228.26
ATP6AP2	Homo sapiens ATPase, H+ transporting, lysosomal accessory protein 2 (ATP6AP2), mRNA.	738.70	390.95	1.89	0.000	347.75
ZNF434	Homo sapiens zinc finger protein 434 (ZNF434), mRNA.	298.73	158.11	1.89	0.001	140.62
TOR1AIP1	Homo sapiens torsin A interacting protein 1 (TOR1AIP1), mRNA.	750.62	395.23	1.9	0.045	355.39
MYBL1	Homo sapiens v-myb myeloblastosis viral oncogene homolog (avian)-like 1 (MYBL1), mRNA.	330.65	172.33	1.92	0.015	158.32
MLKL	Homo sapiens mixed lineage kinase domain-like (MLKL), mRNA.	1884.5	971.05	1.94	0.006	913.46
PIP5K1C	Homo sapiens phosphatidylinositol-4-phosphate 5-kinase, type I, gamma (PIP5K1C), mRNA.	349.36	175.12	1.99	0.032	174.24
CLCN7	Homo sapiens chloride channel 7 (CLCN7), mRNA.	1009.75	499.35	2.02	0.029	510.4
LOC100132901	PREDICTED: Homo sapiens similar to KIAA1874 protein (LOC100132901), mRNA.	228.28	112.98	2.02	0.001	115.29
LPAR5	Homo sapiens lysophosphatidic acid receptor 5 (LPAR5), mRNA.	240.27	116.40	2.06	0.002	123.87
WDR4	Homo sapiens WD repeat domain 4 (WDR4), transcript variant 2, mRNA.	295.85	143.2	2.07	3.00E-04	152.65
ZW10	Homo sapiens ZW10, kinetochore associated, homolog (Drosophila) (ZW10), mRNA.	317.48	152.43	2.08	0.011	165.05
CDC2L5	Homo sapiens cell division cycle 2-like 5 (cholinesterase-related cell division controller) (CDC2L5), transcript variant 1, mRNA.	473.91	225.11	2.11	0.001	248.79
RAP2A	Homo sapiens RAP2A, member of RAS oncogene family (RAP2A), mRNA.	408.03	190.06	2.15	0.000	217.97
LOC730432	PREDICTED: Homo sapiens similar to serine/threonine/tyrosine interacting protein, transcript variant 1 (LOC730432), mRNA.	652.13	301.41	2.16	1.00E-04	350.72
ZNF493	Homo sapiens zinc finger protein 493 (ZNF493), transcript variant 3, mRNA.	315.36	145.24	2.17	0.013	170.13
TATDN3	Homo sapiens TatD DNase domain containing 3 (TATDN3), transcript variant 1, mRNA.	372.80	169.84	2.2	0.018	202.96
B4GALT7	Homo sapiens xylosylprotein beta 1,4-galactosyltransferase, polypeptide 7 (galactosyltransferase I) (B4GALT7), mRNA.	332.19	147.65	2.25	0.036	184.54

RFX7	Homo sapiens regulatory factor X, 7 (RFX7), mRNA.	594.94	255.03	2.33	0.011	339.91
LRSAM1	Homo sapiens leucine rich repeat and sterile alpha motif containing 1 (LRSAM1), transcript variant 1, mRNA.	351.98	142.92	2.46	1.00E-04	209.06
PTGDR	Homo sapiens prostaglandin D2 receptor (DP) (PTGDR), mRNA.	362.77	145.43	2.49	9.00E-04	217.34
WDR92	Homo sapiens WD repeat domain 92 (WDR92), mRNA.	214.21	84.72	2.53	2.00E-04	129.49
MXRA7	Homo sapiens matrix-remodelling associated 7 (MXRA7), transcript variant 1, mRNA.	376.40	137.14	2.74	0.015	239.26

Comparison $CD4^{+}CD25^{-}$ T cells of MF^{+} individuals EN

Symbol	Definition	mean_CD4_Mfpos	mean_CD4_EN	FC	pvalue	diff
EIF4A2	Homo sapiens eukaryotic translation initiation factor 4A, isoform 2 (EIF4A2), mRNA.	126.72	2213.11	-17.46	0.000	2086.39
LOC729708	PREDICTED: Homo sapiens similar to rcTPI1, transcript variant 1 (LOC729708), mRNA.	192.97	621.22	-3.22	0.000	428.24
LOC286512	PREDICTED: Homo sapiens misc_RNA (LOC286512), miscRNA.	90.92	255.68	-2.81	0.000	164.76
LOC388796	Homo sapiens hypothetical LOC388796 (LOC388796), non-coding RNA.	199.80	517.01	-2.59	0.012	317.21
CLASP1	Homo sapiens cytoplasmic linker associated protein 1 (CLASP1), mRNA.	188.59	464.81	-2.46	0.000	276.22
SKP1	Homo sapiens S-phase kinase-associated protein 1 (SKP1), transcript variant 1, mRNA.	405.42	923.15	-2.28	2.00E-04	517.73
RRBP1	Homo sapiens ribosome binding protein 1 homolog 180kDa (dog) (RRBP1), transcript variant 1, mRNA.	168.41	375.94	-2.23	0.000	207.53
C9orf102	Homo sapiens chromosome 9 open reading frame 102 (C9orf102), mRNA.	118.21	262.67	-2.22	0.003	144.46
ITPRIP	Homo sapiens inositol 1,4,5-triphosphate receptor interacting protein (ITPRIP), mRNA.	230.99	507.09	-2.20	0.009	276.11
BANP	Homo sapiens BTG3 associated nuclear protein (BANP), transcript variant 2, mRNA.	1132.63	2426.44	-2.14	0.046	1293.81
CCL4L1	Homo sapiens chemokine (C-C motif) ligand 4-like 1 (CCL4L1), mRNA.	157.41	336.32	-2.14	1.00E-04	178.91
ENO2	Homo sapiens enolase 2 (gamma, neuronal) (ENO2), mRNA.	332.61	706.42	-2.12	0.000	373.81
TPM2	Homo sapiens tropomyosin 2 (beta) (TPM2), transcript variant 2, mRNA.	253.82	528.87	-2.08	0.029	275.05
EXOSC7	Homo sapiens exosome component 7 (EXOSC7), mRNA.	367.35	757.97	-2.06	0.021	390.62
ZNF419	Homo sapiens zinc finger protein 419 (ZNF419), transcript variant 6, mRNA.	119.29	241.99	-2.03	0.003	122.70
ZNF792	Homo sapiens zinc finger protein 792 (ZNF792), mRNA.	156.03	313.44	-2.01	0.011	157.42
TPM2	Homo sapiens tropomyosin 2 (beta) (TPM2), transcript variant 2, mRNA.	219.84	439.07	-2.00	0.035	219.23
KLF2	Homo sapiens Kruppel-like factor 2 (lung) (KLF2), mRNA.	1845.82	3643.46	-1.97	0.003	1797.64
PASK	Homo sapiens PAS domain containing serine/threonine kinase (PASK), mRNA.	151.72	297.85	-1.96	0.032	146.13
	Homo sapiens cDNA clone IMAGE:30332316	198.33	375.92	-1.90	0.027	177.59
TMEM41B	Homo sapiens transmembrane protein 41B (TMEM41B), mRNA.	531.75	1001.39	-1.88	4.00E-04	469.64
C8orf33	Homo sapiens chromosome 8 open reading frame 33 (C8orf33), mRNA.	202.81	378.77	-1.87	1.00E-04	175.96
DDX24	Homo sapiens DEAD (Asp-Glu-Ala-Asp) box polypeptide 24 (DDX24), mRNA.	704.06	1293.38	-1.84	0.007	589.32
RNF135	Homo sapiens ring finger protein 135 (RNF135), transcript variant 2, mRNA.	149.53	268.47	-1.80	0.006	118.94
PLEKHM2	Homo sapiens pleckstrin homology domain containing, family M (with RUN domain) member 2 (PLEKHM2), mRNA.	295.41	526.93	-1.78	5.00E-04	231.52
TSC22D3	Homo sapiens TSC22 domain family, member 3 (TSC22D3), transcript variant 1, mRNA.	2185.19	3845.93	-1.76	0.041	1660.74
LOC731049	PREDICTED: Homo sapiens similar to Ubiquitin-conjugating enzyme E2S (Ubiquitin-conjugating enzyme E2-24 kDa) (Ubiquitin-protein ligase) (Ubiquitin carrier protein) (E2-EPF5) (LOC731049), mRNA.	324.97	567.1	-1.75	9.00E-04	242.13
POMGNT1	Homo sapiens protein O-linked mannose beta1,2-N-acetylglucosaminyltransferase (POMGNT1), mRNA.	257.29	444.65	-1.73	6.00E-04	187.36
CYTH1	Homo sapiens cytohesin 1 (CYTH1), transcript variant 2, mRNA.	955.19	1638.42	-1.72	0.030	683.23
POLR2C	Homo sapiens polymerase (RNA) II (DNA directed) polypeptide C, 33kDa (POLR2C), mRNA.	150.11	256.02	-1.71	0.002	105.91
METT11D1	Homo sapiens methyltransferase 11 domain containing 1 (METT11D1), transcript variant 1, mRNA.	350.54	596.66	-1.70	0.039	246.12
PRPS1	Homo sapiens phosphoribosyl pyrophosphate synthetase 1 (PRPS1), mRNA.	228.73	388.39	-1.70	7.00E-04	159.66
SPG7	Homo sapiens spastic paraplegia 7 (pure and complicated autosomal recessive) (SPG7), nuclear gene encoding mitochondrial protein, transcript variant 1, mRNA.	1171.66	1989.08	-1.70	0.000	817.42
CCDC93	Homo sapiens coiled-coil domain containing 93 (CCDC93), mRNA.	419.42	699.06	-1.67	0.028	279.64
ELMO1	Homo sapiens engulfment and cell motility 1 (ELMO1), transcript variant 1, mRNA.	148.50	248.59	-1.67	0.000	100.09
ADPRHL2	Homo sapiens ADP-ribosylhydrolase like 2 (ADPRHL2), mRNA.	264.24	437.94	-1.66	0.026	173.7
CLYBL	Homo sapiens citrate lyase beta like (CLYBL), mRNA.	224.65	371.57	-1.65	0.002	146.91
E4F1	Homo sapiens E4F transcription factor 1 (E4F1), mRNA.	446.72	738.18	-1.65	0.042	291.46

MCRS1	Homo sapiens microspherule protein 1 (MCRS1), transcript variant 1, mRNA.	284.00	468.14	-1.65	0.000	184.14
TMEM97	Homo sapiens transmembrane protein 97 (TMEM97), mRNA.	159.02	261.96	-1.65	1.00E-04	102.93
CHMP1A	Homo sapiens chromatin modifying protein 1A (CHMP1A), transcript variant 2, mRNA.	281.94	463.09	-1.64	0.001	181.16
EDG4	Homo sapiens endothelial differentiation, lysophosphatidic acid G-protein-coupled receptor, 4 (EDG4), mRNA.	390.61	640.58	-1.64	0.000	249.96
AK1	Homo sapiens adenylate kinase 1 (AK1), mRNA.	220.77	360.03	-1.63	0.000	139.26
SLC2A1	Homo sapiens solute carrier family 2 (facilitated glucose transporter), member 1 (SLC2A1), mRNA.	263.51	425.62	-1.62	0.008	162.11
SNRPN	Homo sapiens small nuclear ribonucleoprotein polypeptide N (SNRPN), transcript variant 2, mRNA.	377.04	612.37	-1.62	0.016	235.33
TUBGCP2	Homo sapiens tubulin, gamma complex associated protein 2 (TUBGCP2), mRNA.	225.20	365.52	-1.62	0.000	140.32
AMT	Homo sapiens aminomethyltransferase (AMT), mRNA.	265.40	427.26	-1.61	0.020	161.87
C9orf78	Homo sapiens chromosome 9 open reading frame 78 (C9orf78), mRNA.	1242.62	1999.78	-1.61	0.000	757.15
NDUFS3	Homo sapiens NADH dehydrogenase (ubiquinone) Fe-S protein 3, 30kDa (NADH-coenzyme Q reductase) (NDUFS3), mRNA.	738.99	1187.73	-1.61	0.000	448.74
SFRS14	Homo sapiens splicing factor, arginine/serine-rich 14 (SFRS14), transcript variant 2, mRNA.	922.01	1481.73	-1.61	0.000	559.72
C18orf8	Homo sapiens chromosome 18 open reading frame 8 (C18orf8), mRNA.	473.19	756.52	-1.60	0.005	283.33
TRPC4AP	Homo sapiens transient receptor potential cation channel, subfamily C, member 4 associated protein (TRPC4AP), transcript variant 1, mRNA.	455.83	728.79	-1.60	0.08	272.95
IP6K1	Homo sapiens inositol hexakisphosphate kinase 1 (IP6K1), transcript variant 2, mRNA.	201.90	320.25	-1.59	3.00E-04	118.35
TMEM219	Homo sapiens transmembrane protein 219 (TMEM219), transcript variant 1, mRNA.	419.07	666.29	-1.59	0.034	247.22
LOC652685	PREDICTED: Homo sapiens similar to PMS1 protein homolog 2 (DNA mismatch repair protein PMS2) (LOC652685), mRNA.	206.61	326.66	-1.58	0.017	120.05
SPATS2L	Homo sapiens spermatogenesis associated, serine-rich 2-like (SPATS2L), transcript variant 2, mRNA.	208.45	329.45	-1.58	0.004	120.99
MTRF1	Homo sapiens mitochondrial translational release factor 1 (MTRF1), nuclear gene encoding mitochondrial protein, mRNA.	185.83	289.16	-1.56	0.045	103.33
LOC387841	PREDICTED: Homo sapiens similar to ribosomal protein L13a, transcript variant 2 (LOC387841), mRNA.	1196.54	1857.12	-1.55	0.006	660.58
SLC25A28	Homo sapiens solute carrier family 25, member 28 (SLC25A28), mRNA.	761.89	1183.17	-1.55	0.038	421.29
KIAA0182	Homo sapiens KIAA0182 (KIAA0182), mRNA.	315.81	482.18	-1.53	0.030	166.37
LOC100130092	PREDICTED: Homo sapiens misc_RNA (LOC100130092), miscRNA.	274.49	420.02	-1.53	0.012	145.53
OXA1L	Homo sapiens oxidase (cytochrome c) assembly 1-like (OXA1L), mRNA.	433.56	658.64	-1.52	0.000	225.08
PSME3	Homo sapiens proteasome (prosome, macropain) activator subunit 3 (PA28 gamma; Ki) (PSME3), transcript variant 1, mRNA.	197.36	299.58	-1.52	0.000	102.22
STAU1	Homo sapiens staufen, RNA binding protein, homolog 1 (Drosophila) (STAU1), transcript variant T1, mRNA.	1224.09	1865.74	-1.52	0.011	641.65
TM9SF2	Homo sapiens transmembrane 9 superfamily member 2 (TM9SF2), mRNA.	977.59	650.89	1.50	6.00E-04	326.7
TTC37	Homo sapiens tetratricopeptide repeat domain 37 (TTC37), mRNA.	504.46	335.48	1.50	0.049	168.98
CAP1	Homo sapiens CAP, adenylate cyclase-associated protein 1 (yeast) (CAP1), mRNA.	5129.00	3399.89	1.51	8.00E-04	1729.1
LOC730288	PREDICTED: Homo sapiens similar to 40S ribosomal protein S28 (LOC730288), mRNA.	418.89	276.83	1.51	0.000	142.05
RHOT1	Homo sapiens ras homolog gene family, member T1 (RHOT1), transcript variant 2, mRNA.	537.23	355.86	1.51	0.011	181.36
PARP9	Homo sapiens poly (ADP-ribose) polymerase family, member 9 (PARP9), mRNA.	591.83	388.51	1.52	1.00E-04	203.31
NCOA4	Homo sapiens nuclear receptor coactivator 4 (NCOA4), mRNA.	4253.75	2772.01	1.53	0.000	1481.74
RASGRP1	Homo sapiens RAS guanyl releasing protein 1 (calcium and DAG-regulated) (RASGRP1), mRNA.	1090.09	711.62	1.53	3.00E-04	378.48
PCID2	Homo sapiens PCI domain containing 2 (PCID2), mRNA.	2071.8	1348.15	1.54	0.000	723.65
BMI1	Homo sapiens BMI1 polycomb ring finger oncogene (BMI1), mRNA.	425.29	275.23	1.55	1.00E-04	150.07
TSSC1	Homo sapiens tumor suppressing subtransferable candidate 1 (TSSC1), mRNA.	490.43	315.83	1.55	0.045	174.59
ALDH9A1	Homo sapiens aldehyde dehydrogenase 9 family, member A1 (ALDH9A1), mRNA.	4121.61	2645.26	1.56	0.022	1476.34
MBNL1	Homo sapiens muscleblind-like (Drosophila) (MBNL1), transcript variant 5, mRNA.	733.49	469.30	1.56	0.016	264.19
CSK	Homo sapiens c-src tyrosine kinase (CSK), mRNA.	829.13	528.69	1.57	0.011	300.45
DEK	Homo sapiens DEK oncogene (DNA binding) (DEK), mRNA.	935.21	594.98	1.57	5.00E-04	340.23
XRN1	Homo sapiens 5'-3' exoribonuclease 1 (XRN1), mRNA.	503.68	320.95	1.57	0.005	182.73
LOC341457	PREDICTED: Homo sapiens similar to peptidylprolyl isomerase A isoform 1 (LOC341457), mRNA.	298.78	189.28	1.58	0.000	109.50
LOC399748	PREDICTED: Homo sapiens misc_RNA (LOC399748), miscRNA.	1674.12	1061.76	1.58	0.046	612.36
ME2	Homo sapiens malic enzyme 2, NAD(+)-dependent, mitochondrial (ME2), nuclear gene encoding mitochondrial protein, mRNA.	335.57	212.46	1.58	0.000	123.11
PPP2R3C	Homo sapiens protein phosphatase 2 (formerly 2A), regulatory subunit B'', gamma (PPP2R3C), mRNA.	378.82	240.51	1.58	0.005	138.31
PGRMC1	Homo sapiens progesterone receptor membrane component 1 (PGRMC1), mRNA.	458.83	287.84	1.59	0.029	170.98
ATP2B4	Homo sapiens ATPase, Ca++ transporting, plasma membrane 4 (ATP2B4), transcript variant 1, mRNA.	1092.84	684.64	1.60	0.011	408.19
MAP3K7	Homo sapiens mitogen-activated protein kinase kinase kinase 7 (MAP3K7), transcript variant B, mRNA.	890.61	555.95	1.60	0.000	334.66
CREG1	Homo sapiens cellular repressor of E1A-stimulated genes 1 (CREG1), mRNA.	306.63	190.37	1.61	0.0224	116.26

SRP54	PREDICTED: Homo sapiens signal recognition particle 54kDa (SRP54), mRNA.	1087.87	676.56	1.61	0,0000	411.31
SRPK1	Homo sapiens SFRS protein kinase 1 (SRPK1), mRNA.	322.86	200.37	1.61	0.006	122.5
TRAM1	Homo sapiens translocation associated membrane protein 1 (TRAM1), mRNA.	3297.43	2052.29	1.61	2.00E-04	1245.14
SH3KBP1	Homo sapiens SH3-domain kinase binding protein 1 (SH3KBP1), transcript variant 1, mRNA.	1644.57	1012.12	1.62	0.032	632.45
WDR7	Homo sapiens WD repeat domain 7 (WDR7), transcript variant 1, mRNA.	300.88	186.3	1.62	1.00E-04	114.58
CUL5	Homo sapiens cullin 5 (CUL5), mRNA.	350.98	215.47	1.63	0.050	135.51
HMGN4	Homo sapiens high mobility group nucleosomal binding domain 4 (HMGN4), mRNA.	1535.30	943.24	1.63	0.000	592.06
LAX1	Homo sapiens lymphocyte transmembrane adaptor 1 (LAX1), mRNA.	487.84	298.69	1.63	0.000	189.15
ACOT7	Homo sapiens acyl-CoA thioesterase 7 (ACOT7), transcript variant hBACHb, mRNA.	479.34	292.33	1.64	0.004	187.02
CMPK1	Homo sapiens cytidine monophosphate (UMP-CMP) kinase 1, cytosolic (CMPK1), mRNA.	608.08	371.04	1.64	0.033	237.04
PIP5K1C	Homo sapiens phosphatidylinositol-4-phosphate 5-kinase, type I, gamma (PIP5K1C), mRNA.	286.38	175.12	1.64	0.002	111.25
C5orf15	Homo sapiens chromosome 5 open reading frame 15 (C5orf15), mRNA.	951.37	576.73	1.65	0.012	374.64
CKLF	Homo sapiens chemokine-like factor (CKLF), transcript variant 5, mRNA.	646.58	392.66	1.65	4.00E-04	253.92
PTPLB	Homo sapiens protein tyrosine phosphatase-like (proline instead of catalytic arginine), member b (PTPLB), mRNA.	349.35	211.51	1.65	0.034	137.84
ATXN1	Homo sapiens ataxin 1 (ATXN1), mRNA.	259.37	156.06	1.66	6.00E-04	103.32
DNASE2	Homo sapiens deoxyribonuclease II, lysosomal (DNASE2), mRNA.	299.59	180.39	1.66	0.002	119.20
EXOC2	Homo sapiens exocyst complex component 2 (EXOC2), mRNA.	383.61	230.87	1.66	0.000	152.74
C14orf109	Homo sapiens chromosome 14 open reading frame 109 (C14orf109), transcript variant 2, mRNA.	272.36	163.5	1.67	0.015	108.86
DOCK10	Homo sapiens dedicator of cytokinesis 10 (DOCK10), mRNA.	1740.06	1043.43	1.67	0.009	696.63
LOC644330	PREDICTED: Homo sapiens similar to tropomyosin 3 isoform 2 (LOC644330), mRNA.	423.24	252.89	1.67	0.011	170.35
PUM2	Homo sapiens pumilio homolog 2 (Drosophila) (PUM2), mRNA.	1200.63	720.41	1.67	0.012	480.22
SUSD1	Homo sapiens sushi domain containing 1 (SUSD1), mRNA.	585.39	351.47	1.67	0.011	233.92
DNMT1	Homo sapiens DNA (cytosine-5-)-methyltransferase 1 (DNMT1), mRNA.	2264.26	1345.03	1.68	0.000	919.23
LOC729148	PREDICTED: Homo sapiens similar to lethal (2) k00619 CG4775-PA (LOC729148), mRNA.	536.69	319.55	1.68	0.049	217.14
ABCB10	Homo sapiens ATP-binding cassette, sub-family B (MDR/TAP), member 10 (ABCB10), nuclear gene encoding mitochondrial protein, mRNA.	249.93	148.03	1.69	0.046	101.90
PPP2R5E	Homo sapiens protein phosphatase 2, regulatory subunit B', epsilon isoform (PPP2R5E), mRNA.	455.40	268.91	1.69	0.005	186.48
DYRK1A	Homo sapiens dual-specificity tyrosine-(Y)-phosphorylation regulated kinase 1A (DYRK1A), transcript variant 4, mRNA.	602.89	354.75	1.70	0.036	248.15
DYRK1A	Homo sapiens dual-specificity tyrosine-(Y)-phosphorylation regulated kinase 1A (DYRK1A), transcript variant 5, mRNA.	538.40	315.97	1.70	0.000	222.43
OAT	Homo sapiens ornithine aminotransferase (gyrate atrophy) (OAT), nuclear gene encoding mitochondrial protein, mRNA.	347.95	204.21	1.70	0.014	143.74
PSMA4	Homo sapiens proteasome (prosome, macropain) subunit, alpha type, 4 (PSMA4), mRNA.	2081.73	1228.00	1.70	0.000	853.73
ROD1	Homo sapiens ROD1 regulator of differentiation 1 (S. pombe) (ROD1), mRNA.	1987.19	1171.73	1.70	0.000	815.46
ZMYND11	Homo sapiens zinc finger, MYND domain containing 11 (ZMYND11), transcript variant 1, mRNA.	1181.10	696.80	1.70	0.030	484.30
CTSC	Homo sapiens cathepsin C (CTSC), transcript variant 1, mRNA.	523.02	304.98	1.71	0.050	218.04
VAMP4	Homo sapiens vesicle-associated membrane protein 4 (VAMP4), transcript variant 1, mRNA.	349.88	204.44	1.71	0.014	145.44
C1orf24	Homo sapiens chromosome 1 open reading frame 24 (C1orf24), transcript variant 2, mRNA.	503.04	292.50	1.72	0.000	210.54
KLRB1	Homo sapiens killer cell lectin-like receptor subfamily B, member 1 (KLRB1), mRNA.	3657.58	2129.00	1.72	0.033	1528.58
ME2	Homo sapiens malic enzyme 2, NAD(+)-dependent, mitochondrial (ME2), nuclear gene encoding mitochondrial protein, mRNA.	315.03	183.36	1.72	2.00E-04	131.67
IFI44L	Homo sapiens interferon-induced protein 44-like (IFI44L), mRNA.	239.60	137.87	1.74	0.011	101.73
RFX7	Homo sapiens regulatory factor X, 7 (RFX7), mRNA.	443.91	255.03	1.74	0.000	188.88
TMX1	Homo sapiens thioredoxin-related transmembrane protein 1 (TMX1), mRNA.	236.55	135.63	1.74	0.029	100.92
CLINT1	Homo sapiens clathrin interactor 1 (CLINT1), mRNA.	485.76	277.31	1.75	0.043	208.45
7-Mar	Homo sapiens membrane-associated ring finger (C3HC4) 7 (MARCH7), mRNA.	310.46	177.87	1.75	0.001	132.59
SH3BGRL	Homo sapiens SH3 domain binding glutamic acid-rich protein like (SH3BGRL), mRNA.	545.97	311.05	1.76	0.002	234.92
SRI	Homo sapiens sorcin (SRI), transcript variant 1, mRNA.	284.40	161.39	1.76	0.027	123.00
TRIM44	Homo sapiens tripartite motif-containing 44 (TRIM44), mRNA.	401.89	228.38	1.76	3.00E-04	173.5
XBP1	Homo sapiens X-box binding protein 1 (XBP1), transcript variant 1, mRNA.	942.25	536.54	1.76	0.003	405.71
WASPIP	Homo sapiens Wiskott-Aldrich syndrome protein interacting protein (WASPIP), mRNA.	785.62	438.21	1.79	0.000	347.41
LACTB	Homo sapiens lactamase, beta (LACTB), nuclear gene encoding mitochondrial protein, transcript variant 1, mRNA.	535.09	297.95	1.80	0.021	237.13
LOC100128510	PREDICTED: Homo sapiens hypothetical protein LOC100128510 (LOC100128510), mRNA.	254.45	141.17	1.80	0.004	113.28
	qk02b10.x1 NCI_CGAP_Kid3 Homo sapiens cDNA clone IMAGE:1867771 3, mRNA sequence	319.87	176.55	1.81	1.00E-04	143.32

PRKAR1A	Homo sapiens protein kinase, cAMP-dependent, regulatory, type I, alpha (tissue specific extinguisher 1) (PRKAR1A), transcript variant 3, mRNA.	679.88	374.70	1.81	0.015	305.18
GBP1	Homo sapiens guanylate binding protein 1, interferon-inducible, 67kDa (GBP1), mRNA.	670.65	369.39	1.82	0.000	301.26
IL15	Homo sapiens interleukin 15 (IL15), transcript variant 3, mRNA.	477.59	262.14	1.82	0.047	215.46
RECQL	Homo sapiens RecQ protein-like (DNA helicase Q1-like) (RECQL), transcript variant 1, mRNA.	266.29	146.07	1.82	1.00E-04	120.22
SCAMP1	Homo sapiens secretory carrier membrane protein 1 (SCAMP1), mRNA.	1007.63	553.17	1.82	0.002	454.46
FGD2	Homo sapiens FYVE, RhoGEF and PH domain containing 2 (FGD2), mRNA.	325.42	177.66	1.83	0.000	147.76
EMR2	Homo sapiens egf-like module containing, mucin-like, hormone receptor-like 2 (EMR2), transcript variant 2, mRNA.	398.79	216.31	1.84	0.000	182.48
SMG1	Homo sapiens PI-3-kinase-related kinase SMG-1 (SMG1), mRNA.	534.73	290.33	1.84	0.023	244.40
ST13	Homo sapiens suppression of tumorigenicity 13 (colon carcinoma) (Hsp70 interacting protein) (ST13), mRNA.	391.99	211.59	1.85	0.005	180.40
TMEM123	Homo sapiens transmembrane protein 123 (TMEM123), mRNA.	1749.82	948.28	1.85	0.0134	801.54
ARL5A	Homo sapiens ADP-ribosylation factor-like 5A (ARL5A), transcript variant 3, mRNA.	827.67	446.17	1.86	0.006	381.49
LAMP2	Homo sapiens lysosomal-associated membrane protein 2 (LAMP2), transcript variant LAMP2B, mRNA.	424.04	227.90	1.86	0.047	196.14
PHYH	Homo sapiens phytanoyl-CoA 2-hydroxylase (PHYH), transcript variant 2, mRNA.	339.60	182.56	1.86	0.002	157.04
ZCCHC7	Homo sapiens zinc finger, CCHC domain containing 7 (ZCCHC7), mRNA.	278.52	149.74	1.86	0.010	128.78
KIAA0528	Homo sapiens KIAA0528 (KIAA0528), mRNA.	486.84	259.25	1.88	4.00E-04	227.59
SLC25A43	Homo sapiens solute carrier family 25, member 43 (SLC25A43), mRNA.	248.95	132.69	1.88	0.036	116.26
ACSL5	Homo sapiens acyl-CoA synthetase long-chain family member 5 (ACSL5), transcript variant 2, mRNA.	348.95	184.78	1.89	0.021	164.17
YWHAQ	Homo sapiens tyrosine 3-monooxygenase/tryptophan 5-monooxygenase activation protein, theta polypeptide (YWHAQ), mRNA.	3647.07	1892.13	1.93	2.00E-04	1754.94
ARL6IP1	Homo sapiens ADP-ribosylation factor-like 6 interacting protein 1 (ARL6IP1), mRNA.	1608.58	831.30	1.94	0.000	777.27
HNRNPA0	Homo sapiens heterogeneous nuclear ribonucleoprotein A0 (HNRNPA0), mRNA.	472.05	240.29	1.96	0.027	231.76
ACTR2	Homo sapiens ARP2 actin-related protein 2 homolog (yeast) (ACTR2), transcript variant 1, mRNA.	1650.45	836.23	1.97	0.024	814.22
THUMPD1	Homo sapiens THUMP domain containing 1 (THUMPD1), mRNA.	613.84	309.83	1.98	0.007	304.02
CDS2	Homo sapiens CDP-diacylglycerol synthase (phosphatidate cytidylyltransferase) 2 (CDS2), mRNA.	336.43	169.27	1.99	4.00E-04	167.17
HEATR1	Homo sapiens HEAT repeat containing 1 (HEATR1), mRNA.	428.28	215.15	1.99	0.000	213.13
SH2D1A	Homo sapiens SH2 domain protein 1A, Duncan's disease (lymphoproliferative syndrome) (SH2D1A), mRNA.	1127.50	562.54	2.00	0.027	564.95
RALB	Homo sapiens v-ral simian leukemia viral oncogene homolog B (ras related; GTP binding protein) (RALB), mRNA.	688.16	340.20	2.02	0.001	347.96
MAP4K5	Homo sapiens mitogen-activated protein kinase kinase kinase kinase 5 (MAP4K5), transcript variant 2, mRNA.	359.90	177.11	2.03	0.044	182.79
CHST7	Homo sapiens carbohydrate (N-acetylglucosamine 6-O) sulfotransferase 7 (CHST7), mRNA.	277.83	136.51	2.04	8.00E-04	141.32
ZMYM1	Homo sapiens zinc finger, MYM-type 1 (ZMYM1), mRNA.	256.10	125.75	2.04	0.000	130.35
IQGAP2	Homo sapiens IQ motif containing GTPase activating protein 2 (IQGAP2), mRNA.	683.06	332.08	2.06	0.003	350.98
	Homo sapiens cDNA FLJ33738 fis, clone BRAWH2018527	197.27	95.12	2.07	0.032	102.15
TMEM156	Homo sapiens transmembrane protein 156 (TMEM156), mRNA.	1007.69	485.23	2.08	0.002	522.46
TMEM209	Homo sapiens transmembrane protein 209 (TMEM209), mRNA.	286.83	137.86	2.08	0.009	148.97
UCP2	Homo sapiens uncoupling protein 2 (mitochondrial, proton carrier) (UCP2), nuclear gene encoding mitochondrial protein, mRNA.	493.53	236.86	2.08	0.005	256.67
IL10RB	Homo sapiens interleukin 10 receptor, beta (IL10RB), mRNA.	1041.19	497.58	2.09	0.023	543.62
CEACAM1	Homo sapiens carcinoembryonic antigen-related cell adhesion molecule 1 (biliary glycoprotein) (CEACAM1), transcript variant 2, mRNA.	191.30	91.18	2.10	0.003	100.12
DHFRL1	Homo sapiens dihydrofolate reductase-like 1 (DHFRL1), mRNA.	190.31	90.21	2.11	0.000	100.10
STS-1	Homo sapiens Cbl-interacting protein Sts-1 (STS-1), mRNA.	497.62	234.7	2.12	0.003	262.92
NOD2	Homo sapiens nucleotide-binding oligomerization domain containing 2 (NOD2), mRNA.	288.38	134.35	2.15	0.008	154.03
HIGD1A	Homo sapiens HIG1 hypoxia inducible domain family, member 1A (HIGD1A), transcript variant 1, mRNA.	449.25	202.05	2.22	0.008	247.20
KYNU	Homo sapiens kynureninase (L-kynurenine hydrolase) (KYNU), transcript variant 1, mRNA.	358.89	156.57	2.29	0.007	202.33
ATP6AP2	Homo sapiens ATPase, H+ transporting, lysosomal accessory protein 2 (ATP6AP2), mRNA.	902.91	390.95	2.31	0.014	511.97
TNFSF10	Homo sapiens tumor necrosis factor (ligand) superfamily, member 10 (TNFSF10), mRNA.	650.48	258.23	2.52	0.000	392.25
SDCCAG10	Homo sapiens serologically defined colon cancer antigen 10 (SDCCAG10), mRNA.	478.32	187.66	2.55	3.00E-04	290.66
ZW10	Homo sapiens ZW10, kinetochore associated, homolog (Drosophila) (ZW10), mRNA.	455.47	152.43	2.99	8.00E-04	303.03
LILRA3	Homo sapiens leukocyte immunoglobulin-like receptor, subfamily A (without TM domain), member 3 (LILRA3), mRNA.	1785.06	327.48	5.45	0.000	1457.58

Comparison CD8$^+$ T cells of infected individuals versus EN

Symbol	Definition	mean_CD8_inf	mean_CD8_healthy	FC	pvalue	diff
SOD2	Homo sapiens superoxide dismutase 2, mitochondrial (SOD2), nuclear gene encoding mitochondrial protein, transcript variant 2, mRNA.	361.70	884.22	-2.44	0.000	522.53
LOC338758	PREDICTED: Homo sapiens hypothetical protein LOC338758 (LOC338758), mRNA.	280.00	668.89	-2.39	0.006	388.9
BTBD7	Homo sapiens BTB (POZ) domain containing 7 (BTBD7), transcript variant 2, mRNA.	163.16	360.10	-2.21	0.008	196.95
SGK	Homo sapiens serum/glucocorticoid regulated kinase (SGK), mRNA.	224.32	494.4	-2.20	7.00E-04	270.08
C7orf40	Homo sapiens chromosome 7 open reading frame 40 (C7orf40), non-coding RNA.	238.98	500.25	-2.09	0.004	261.27
KLF4	Homo sapiens Kruppel-like factor 4 (gut) (KLF4), mRNA.	120.15	249.90	-2.08	0,000	129.74
NFKBIZ	Homo sapiens nuclear factor of kappa light polypeptide gene enhancer in B-cells inhibitor, zeta (NFKBIZ), transcript variant 2, mRNA.	601.55	1189.31	-1.98	0.027	587.76
SERTAD3	Homo sapiens SERTA domain containing 3 (SERTAD3), transcript variant 1, mRNA.	140.78	266.87	-1.90	0.024	126.09
ACSL3	Homo sapiens acyl-CoA synthetase long-chain family member 3 (ACSL3), transcript variant 2, mRNA.	294.53	518.23	-1.76	0,000	223.71
	Homo sapiens cDNA clone IMAGE:30332316	202.03	343.18	-1.70	0.003	141.15
MYLIP	Homo sapiens myosin regulatory light chain interacting protein (MYLIP), mRNA.	1749.65	2935.22	-1.68	4.00E-04	1185.57
LRP5L	Homo sapiens low density lipoprotein receptor-related protein 5-like (LRP5L), mRNA.	263.56	428.72	-1.63	0.035	165.16
BCL6	Homo sapiens B-cell CLL/lymphoma 6 (zinc finger protein 51) (BCL6), transcript variant 1, mRNA.	529.75	859.96	-1.62	0.029	330.21
PHAX	Homo sapiens phosphorylated adaptor for RNA export (PHAX), mRNA.	225.61	354.27	-1.57	0.004	128.65
GSK3B	Homo sapiens glycogen synthase kinase 3 beta (GSK3B), mRNA.	393.89	602.69	-1.53	0.045	208.8
FBXO44	Homo sapiens F-box protein 44 (FBXO44), transcript variant 4, mRNA.	192.28	293.23	-1.52	0.004	100.95
CGRRF1	Homo sapiens cell growth regulator with ring finger domain 1 (CGRRF1), mRNA.	210.00	316.76	-1.51	0.025	106.76
LOC606724	Homo sapiens coronin, actin binding protein, 1A pseudogene (LOC606724), non-coding RNA.	1639.11	1082.57	1.51	0.007	556.53
SRP68	Homo sapiens signal recognition particle 68kDa (SRP68), mRNA.	661.14	433.38	1.53	0.002	227.76
WDR40A	Homo sapiens WD repeat domain 40A (WDR40A), mRNA.	329.84	215.38	1.53	0.011	114.45
POMGNT1	Homo sapiens protein O-linked mannose beta1,2-N-acetylglucosaminyltransferase (POMGNT1), mRNA.	350.44	227.96	1.54	0,000	122.47
C9orf69	Homo sapiens chromosome 9 open reading frame 69 (C9orf69), mRNA.	338.91	216.67	1.56	0,000	122.24
LOC730415	PREDICTED: Homo sapiens hypothetical LOC730415, transcript variant 2 (LOC730415), mRNA.	1647.72	1053.23	1.56	0.046	594.49
LRP10	Homo sapiens low density lipoprotein receptor-related protein 10 (LRP10), mRNA.	897.20	562.20	1.60	0.044	335.01
TMBIM4	Homo sapiens transmembrane BAX inhibitor motif containing 4 (TMBIM4), mRNA.	2526.66	1541.72	1.64	0.050	984.93
SRXN1	Homo sapiens sulfiredoxin 1 homolog (S. cerevisiae) (SRXN1), mRNA.	258.19	155.44	1.66	0.047	102.75
SGSH	Homo sapiens N-sulfoglucosamine sulfohydrolase (sulfamidase) (SGSH), mRNA.	655.14	385.11	1.70	0,000	270.02
NME1	Homo sapiens non-metastatic cells 1, protein (NM23A) expressed in (NME1), transcript variant 2, mRNA.	431.35	252.21	1.71	0.0230	179.14
RNF121	Homo sapiens ring finger protein 121 (RNF121), transcript variant 1, mRNA.	250.24	145.07	1.72	0.022	105.16
	Homo sapiens cDNA FLJ12874 fis, clone NT2RP2003769	449.14	238.55	1.88	0.017	210.59
PKP4	Homo sapiens plakophilin 4 (PKP4), transcript variant 1, mRNA.	237.86	126.45	1.88	0.016	111.41
UBL4A	Homo sapiens ubiquitin-like 4A (UBL4A), mRNA.	458.02	242.77	1.89	2.00E-04	215.25
ARL17P1	Homo sapiens ADP-ribosylation factor-like 17 pseudogene 1 (ARL17P1), mRNA.	273.87	138.25	1.98	0.020	135.62
WIBG	Homo sapiens within bgcn homolog (Drosophila) (WIBG), mRNA.	278.42	135.55	2.05	0.006	142.86
ACVR1	Homo sapiens activin A receptor, type I (ACVR1), mRNA.	285.08	136.16	2.09	0.025	148.93
RABEP1	Homo sapiens rabaptin, RAB GTPase binding effector protein 1 (RABEP1), transcript variant 2, mRNA.	453.53	215.90	2.10	0,000	237.63
METT10D	Homo sapiens methyltransferase 10 domain containing (METT10D), mRNA.	201.87	85.45	2.36	0.002	116.43
APPBP2	Homo sapiens amyloid beta precursor protein (cytoplasmic tail) binding protein 2 (APPBP2), mRNA.	203.09	85.38	2.38	0,000	117.72
ZNF232	Homo sapiens zinc finger protein 232 (ZNF232), mRNA.	245.29	103.27	2.38	1.00E-04	142.01
PTGDR	Homo sapiens prostaglandin D2 receptor (DP) (PTGDR), mRNA.	554.81	215.00	2.58	0.003	339.81
FANCD2	Homo sapiens Fanconi anemia, complementation group D2 (FANCD2), transcript variant 2, mRNA.	279.10	99.42	2.81	0.005	179.68

Comparison $CD8^+$ T cells of MF^+ versus MF^- individuals

Symbol	Definition	mean_CD8_Mfneg	mean_CD8_Mfpos	FC	pvalue	diff
MYOM2	Homo sapiens myomesin (M-protein) 2, 165kDa (MYOM2), mRNA.	97.84	3806.31	-38.9	0.042	3708.47
HAVCR2	Homo sapiens hepatitis A virus cellular receptor 2 (HAVCR2), mRNA.	340.25	1095.55	-3.22	0.000	755.30
VPS13C	Homo sapiens vacuolar protein sorting 13 homolog C (S. cerevisiae) (VPS13C), transcript variant 1B, mRNA.	103.33	294.16	-2.85	1.00E-04	190.83
CDC42SE1	Homo sapiens CDC42 small effector 1 (CDC42SE1), transcript variant 1, mRNA.	100.84	236.50	-2.35	0.000	135.66
MIER1	Homo sapiens mesoderm induction early response 1 homolog (Xenopus laevis) (MIER1), transcript variant 1, mRNA.	184.21	385.53	-2.09	0.035	201.32
COMMD7	Homo sapiens COMM domain containing 7 (COMMD7), transcript variant 2, mRNA.	563.70	1150.54	-2.04	0.000	586.84
LOC440093	Homo sapiens histone H3-like (LOC440093), mRNA.	604.94	1188.75	-1.97	0.000	583.81
RUSC1	Homo sapiens RUN and SH3 domain containing 1 (RUSC1), mRNA.	370.93	702.77	-1.89	0.010	331.84
CCDC53	Homo sapiens coiled-coil domain containing 53 (CCDC53), mRNA.	207.11	370.11	-1.79	1.00E-04	163,00
WIPI1	Homo sapiens WD repeat domain, phosphoinositide interacting 1 (WIPI1), mRNA.	183.00	321.58	-1.76	0.003	138.58
CCT2	Homo sapiens chaperonin containing TCP1, subunit 2 (beta) (CCT2), mRNA.	529.37	924.18	-1.75	0.006	394.81
STK17B	Homo sapiens serine/threonine kinase 17b (STK17B), mRNA.	234.60	409.55	-1.75	0.002	174.95
SAE1	Homo sapiens SUMO1 activating enzyme subunit 1 (SAE1), mRNA.	815.21	1417.47	-1.74	0.037	602.26
AGTPBP1	Homo sapiens ATP/GTP binding protein 1 (AGTPBP1), mRNA.	527.25	900.71	-1.71	0.000	373.46
C9orf114	Homo sapiens chromosome 9 open reading frame 114 (C9orf114), mRNA.	154.38	264.42	-1.71	0.028	110.04
ING2	Homo sapiens inhibitor of growth family, member 2 (ING2), mRNA.	140.92	240.94	-1.71	0.000	100.02
TFDP1	Homo sapiens transcription factor Dp-1 (TFDP1), mRNA.	343.59	586.31	-1.71	0.000	242.72
DDX3X	Homo sapiens DEAD (Asp-Glu-Ala-Asp) box polypeptide 3, X-linked (DDX3X), mRNA.	583.74	988.33	-1.69	0.008	404.59
ADNP2	Homo sapiens ADNP homeobox 2 (ADNP2), mRNA.	319.49	535.12	-1.67	0.007	215.63
RPAIN	Homo sapiens RPA interacting protein (RPAIN), mRNA.	268.13	447.34	-1.67	0.002	179.22
HPRT1	Homo sapiens hypoxanthine phosphoribosyltransferase 1 (Lesch-Nyhan syndrome) (HPRT1), mRNA.	365.19	604.52	-1.66	0.005	239.33
LOC100131531	PREDICTED: Homo sapiens similar to hCG1644658 (LOC100131531), mRNA.	483.58	796.32	-1.65	0.003	312.74
SHFM1	Homo sapiens split hand/foot malformation (ectrodactyly) type 1 (SHFM1), mRNA.	222.41	365.98	-1.65	0.018	143.58
LRPAP1	Homo sapiens low density lipoprotein receptor-related protein associated protein 1 (LRPAP1), mRNA.	263.14	430.91	-1.64	0.031	167.77
FASTKD5	Homo sapiens FAST kinase domains 5 (FASTKD5), mRNA.	291.27	476.19	-1.63	0.000	184.92
GSDMB	Homo sapiens gasdermin B (GSDMB), transcript variant 2, mRNA.	307.92	497.54	-1.62	0.006	189.62
NHP2	Homo sapiens NHP2 ribonucleoprotein homolog (yeast) (NHP2), transcript variant 1, mRNA.	254.47	411.78	-1.62	0.024	157.30
C5orf21	Homo sapiens chromosome 5 open reading frame 21 (C5orf21), mRNA.	252.51	396.11	-1.57	0.047	143.60
AZIN1	Homo sapiens antizyme inhibitor 1 (AZIN1), transcript variant 1, mRNA.	635.96	989.35	-1.56	0.046	353.40
CXCR4	Homo sapiens chemokine (C-X-C motif) receptor 4 (CXCR4), transcript variant 1, mRNA.	447.63	683.04	-1.53	0.003	235.41
PSMB9	Homo sapiens proteasome (prosome, macropain) subunit, beta type, 9 (large multifunctional peptidase 2) (PSMB9), transcript variant 1, mRNA.	497.57	746.84	-1.50	0.044	249.28
ACADM	Homo sapiens acyl-Coenzyme A dehydrogenase, C-4 to C-12 straight chain (ACADM), nuclear gene encoding mitochondrial protein, mRNA.	338.73	222.53	1.52	0.003	116.20
NOP2	Homo sapiens NOP2 nucleolar protein homolog (yeast) (NOP2), transcript variant 2, mRNA.	651.85	427.72	1.52	0.000	224.13
ASB1	Homo sapiens ankyrin repeat and SOCS box-containing 1 (ASB1), mRNA.	640.02	419.01	1.53	0.042	221.01
TUBA4A	Homo sapiens tubulin, alpha 4a (TUBA4A), mRNA.	1615.24	1052.71	1.53	0.000	562.53
C6orf170	Homo sapiens chromosome 6 open reading frame 170 (C6orf170), mRNA.	390.55	251.19	1.55	0.012	139.37
FRYL	Homo sapiens FRY-like (FRYL), mRNA.	1254.74	810.78	1.55	0.010	443.97
ZNF75D	Homo sapiens zinc finger protein 75D (ZNF75D), mRNA.	301.76	193.37	1.56	0.000	108.39
INTS8	Homo sapiens integrator complex subunit 8 (INTS8), mRNA.	325.25	207.28	1.57	0.001	117.96
ZNF33B	Homo sapiens zinc finger protein 33B (ZNF33B), mRNA.	322.64	203.72	1.58	0.030	118.92
ZNF395	Homo sapiens zinc finger protein 395 (ZNF395), mRNA.	453.54	285.05	1.59	0.000	168.49
MRPS31	Homo sapiens mitochondrial ribosomal protein S31 (MRPS31), nuclear gene encoding mitochondrial protein, mRNA.	745.56	462.52	1.61	0.003	283.04
LHPP	Homo sapiens phospholysine phosphohistidine inorganic pyrophosphate phosphatase (LHPP), mRNA.	291.37	180.26	1.62	1.00E-04	111.11
GIMAP5	Homo sapiens GTPase, IMAP family member 5 (GIMAP5), mRNA.	2073.99	1272.79	1.63	0.029	801.20
POLR3F	Homo sapiens polymerase (RNA) III (DNA directed) polypeptide F, 39 kDa (POLR3F), mRNA.	347.89	211.47	1.65	0.000	136.42
ZMYM6	Homo sapiens zinc finger, MYM-type 6 (ZMYM6), mRNA.	359.76	217.67	1.65	0.000	142.08
GALT	Homo sapiens galactose-1-phosphate uridylyltransferase (GALT), mRNA.	461.12	275.63	1.67	0.005	185.49
SERGEF	Homo sapiens secretion regulating guanine nucleotide exchange factor (SERGEF), mRNA.	559.03	335.40	1.67	0.001	223.64

C12orf52	Homo sapiens chromosome 12 open reading frame 52 (C12orf52), mRNA.	276.31	164.70	1.68	0.000	111.60
GCLC	Homo sapiens glutamate-cysteine ligase, catalytic subunit (GCLC), mRNA.	301.25	179.69	1.68	0.000	121.56
	full-length cDNA clone CS0DF005YI08 of Fetal brain of Homo sapiens (human)	325.61	193.78	1.68	1.00E-04	131.83
KLHDC3	Homo sapiens kelch domain containing 3 (KLHDC3), mRNA.	551.83	329.41	1.68	3.00E-04	222.43
TMUB2	Homo sapiens transmembrane and ubiquitin-like domain containing 2 (TMUB2), transcript variant 1, mRNA.	321.10	189.52	1.69	0.000	131.59
PDE4B	Homo sapiens phosphodiesterase 4B, cAMP-specific (phosphodiesterase E4 dunce homolog, Drosophila) (PDE4B), transcript variant a, mRNA.	720.05	422.45	1.70	0.001	297.60
MRPL35	Homo sapiens mitochondrial ribosomal protein L35 (MRPL35), nuclear gene encoding mitochondrial protein, transcript variant 1, mRNA.	373.23	214.63	1.74	0.000	158.60
IFIH1	Homo sapiens interferon induced with helicase C domain 1 (IFIH1), mRNA.	344.35	194.44	1.77	6.00E-04	149.91
DEGS1	Homo sapiens degenerative spermatocyte homolog 1, lipid desaturase (Drosophila) (DEGS1), transcript variant 1, mRNA.	728.54	410.24	1.78	1.00E-04	318.30
DDX19A	Homo sapiens DEAD (Asp-Glu-Ala-As) box polypeptide 19A (DDX19A), mRNA.	449.50	251.46	1.79	4.00E-04	198.04
TBL1X	Homo sapiens transducin (beta)-like 1X-linked (TBL1X), mRNA.	416.48	227.17	1.83	0.008	189.31
VAV3	Homo sapiens vav 3 guanine nucleotide exchange factor (VAV3), transcript variant 1, mRNA.	354.17	192.19	1.84	0.010	161.98
CYTSA	Homo sapiens cytospin A (CYTSA), mRNA.	904.41	488.36	1.85	0.023	416.05
TM7SF2	Homo sapiens transmembrane 7 superfamily member 2 (TM7SF2), mRNA.	260.06	138.27	1.88	0.043	121.79
SENP5	Homo sapiens SUMO1/sentrin specific peptidase 5 (SENP5), mRNA.	358.17	189.97	1.89	0.025	168.21
C17orf44	Homo sapiens chromosome 17 open reading frame 44 (C17orf44), mRNA.	338.32	178.35	1.90	0.000	159.97
ASTE1	Homo sapiens asteroid homolog 1 (Drosophila) (ASTE1), mRNA.	227.61	117.12	1.94	0.014	110.50
USP7	Homo sapiens ubiquitin specific peptidase 7 (herpes virus-associated) (USP7), mRNA.	907.59	458.78	1.98	0.025	448.81
KLHL3	Homo sapiens kelch-like 3 (Drosophila) (KLHL3), mRNA.	348.51	174.85	1.99	0.033	173.66
SLC26A11	PREDICTED: Homo sapiens solute carrier family 26, member 11 (SLC26A11), mRNA.	439.78	217.69	2.02	0.000	222.09
ADRB2	Homo sapiens adrenergic, beta-2-, receptor, surface (ADRB2), mRNA.	1887.73	925.7	2.04	0.000	962.03
NCF2	Homo sapiens neutrophil cytosolic factor 2 (65kDa, chronic granulomatous disease, autosomal 2) (NCF2), mRNA.	307.95	149.47	2.06	0.024	158.49
CHST7	Homo sapiens carbohydrate (N-acetylglucosamine 6-O) sulfotransferase 7 (CHST7), mRNA.	312.63	150.87	2.07	0.036	161.75
DHFRL1	Homo sapiens dihydrofolate reductase-like 1 (DHFRL1), mRNA.	200.70	95.02	2.11	0.016	105.68
ZBTB48	Homo sapiens zinc finger and BTB domain containing 48 (ZBTB48), mRNA.	365.21	164.51	2.22	1.00E-04	200.70
WHSC1L1	Homo sapiens Wolf-Hirschhorn syndrome candidate 1-like 1 (WHSC1L1), transcript variant short, mRNA.	196.78	86.23	2.28	0.000	110.55
WDR36	Homo sapiens WD repeat domain 36 (WDR36), mRNA.	302.97	120.75	2.51	7.00E-04	182.22
EIF2B4	Homo sapiens eukaryotic translation initiation factor 2B, subunit 4 delta, 67kDa (EIF2B4), transcript variant 3, mRNA.	851.89	328.27	2.60	0.024	523.62
C3orf19	Homo sapiens chromosome 3 open reading frame 19 (C3orf19), mRNA.	495.51	151.67	3.27	0.000	343.84
LOC729708	PREDICTED: Homo sapiens similar to rcTPI1, transcript variant 1 (LOC729708), mRNA.	898.41	216.65	4.15	0.000	681.76

Comparison CD8^{+} T cells of MF^{-} individuals versus EN

7	Definition	mean_CD8_Mfneg	mean_CD8_EN	FC	pvalue	diff
FOS	Homo sapiens v-fos FBJ murine osteosarcoma viral oncogene homolog (FOS), mRNA.	349.32	1608.68	-4.61	0.003	1259.35
PPP1R15A	Homo sapiens protein phosphatase 1, regulatory (inhibitor) subunit 15A (PPP1R15A), mRNA.	382.73	1625.30	-4.25	0.044	1242.57
DUSP1	Homo sapiens dual specificity phosphatase 1 (DUSP1), mRNA.	1319.64	5150.74	-3.90	0.034	3831.09
SGK	Homo sapiens serum/glucocorticoid regulated kinase (SGK), mRNA.	137.71	494.40	-3.59	0.000	356.68
LOC338758	PREDICTED: Homo sapiens hypothetical protein LOC338758 (LOC338758), mRNA.	191.42	668.89	-3.49	0.000	477.47
NFKBIZ	Homo sapiens nuclear factor of kappa light polypeptide gene enhancer in B-cells inhibitor, zeta (NFKBIZ), transcript variant 2, mRNA.	423.81	1189.31	-2.81	3.00E-04	765.51
TIPARP	Homo sapiens TCDD-inducible poly(ADP-ribose) polymerase (TIPARP), mRNA.	472.43	1270.95	-2.69	0.014	798.52
BTBD7	Homo sapiens BTB (POZ) domain containing 7 (BTBD7), transcript variant 2, mRNA.	148.37	360.10	-2.43	7.00E-04	211.73
KLF4	Homo sapiens Kruppel-like factor 4 (gut) (KLF4), mRNA.	104.36	249.90	-2.39	0.000	145.54
SGK1	Homo sapiens serum/glucocorticoid regulated kinase 1 (SGK1), transcript variant 1, mRNA.	110.71	240.41	-2.17	0.000	129.70
SERTAD3	Homo sapiens SERTA domain containing 3 (SERTAD3), transcript variant 1, mRNA.	125.44	266.87	-2.13	0.004	141.43
TMEM170A	Homo sapiens transmembrane protein 170A (TMEM170A), mRNA.	139.62	293.19	-2.10	0.000	153.57
TSC22D3	Homo sapiens TSC22 domain family, member 3 (TSC22D3), transcript variant 2, mRNA.	744.39	1540.5	-2.07	0.022	796.11
SOD2	Homo sapiens superoxide dismutase 2, mitochondrial (SOD2), nuclear gene encoding mitochondrial protein, transcript variant 2, mRNA.	428.65	884.22	-2.06	0.000	455.57
EIF2C2	Homo sapiens eukaryotic translation initiation factor 2C, 2 (EIF2C2), mRNA.	169.02	339.18	-2.01	0.014	170.16

SGK1	Homo sapiens serum/glucocorticoid regulated kinase 1 (SGK1), transcript variant 1, mRNA.	111.64	224.81	-2.01	0.037	113.17
TARSL2	Homo sapiens threonyl-tRNA synthetase-like 2 (TARSL2), mRNA.	122.47	244.50	-2.00	0.010	122.03
GATS	Homo sapiens opposite strand transcription unit to STAG3 (GATS), mRNA.	165.00	322.29	-1.95	0.041	157.29
CGRRF1	Homo sapiens cell growth regulator with ring finger domain 1 (CGRRF1), mRNA.	164.56	316.76	-1.92	1.00E-04	152.20
ZFAND5	Homo sapiens zinc finger, AN1-type domain 5 (ZFAND5), mRNA.	537.57	1014.89	-1.89	0.000	477.32
CYCSL1	Homo sapiens cytochrome c, somatic-like 1 (CYCSL1) on chromosome 6.	171.50	317.51	-1.85	0.018	146.01
PCCB	Homo sapiens propionyl Coenzyme A carboxylase, beta polypeptide (PCCB), nuclear gene encoding mitochondrial protein, mRNA.	261.68	483.32	-1.85	0.012	221.64
LOC440093	Homo sapiens histone H3-like (LOC440093), mRNA.	604.94	1100.74	-1.82	0.000	495.80
LRPAP1	Homo sapiens low density lipoprotein receptor-related protein associated protein 1 (LRPAP1), mRNA.	263.14	479.84	-1.82	0.042	216.70
BCL6	Homo sapiens B-cell CLL/lymphoma 6 (zinc finger protein 51) (BCL6), transcript variant 1, mRNA.	477.19	859.96	-1.80	0.034	382.77
CHUK	Homo sapiens conserved helix-loop-helix ubiquitous kinase (CHUK), mRNA.	279.12	502.22	-1.80	0.002	223.10
LRP5L	Homo sapiens low density lipoprotein receptor-related protein 5-like (LRP5L), mRNA.	242.82	428.72	-1.77	0.037	185.9
ING2	Homo sapiens inhibitor of growth family, member 2 (ING2), mRNA.	140.92	248.38	-1.76	0.035	107.46
MED30	Homo sapiens mediator complex subunit 30 (MED30), mRNA.	174.34	295.76	-1.70	0.008	121.42
CCT2	Homo sapiens chaperonin containing TCP1, subunit 2 (beta) (CCT2), mRNA.	529.37	884.04	-1.67	0.002	354.67
ACSL3	Homo sapiens acyl-CoA synthetase long-chain family member 3 (ACSL3), transcript variant 2, mRNA.	314.66	518.23	-1.65	0.000	203.57
CGGBP1	Homo sapiens CGG triplet repeat binding protein 1 (CGGBP1), transcript variant 2, mRNA.	501.34	817.47	-1.63	0.049	316.13
MAP3K5	Homo sapiens mitogen-activated protein kinase kinase kinase 5 (MAP3K5), mRNA.	178.72	290.30	-1.62	0.003	111.58
NDUFA6	Homo sapiens NADH dehydrogenase (ubiquinone) 1 alpha subcomplex, 6, 14kDa (NDUFA6), nuclear gene encoding mitochondrial protein, mRNA.	322.21	522.76	-1.62	0.026	200.55
UBE2J1	Homo sapiens ubiquitin-conjugating enzyme E2, J1 (UBC6 homolog, yeast) (UBE2J1), mRNA.	412.89	666.74	-1.61	4.00E-04	253.85
VAMP3	Homo sapiens vesicle-associated membrane protein 3 (cellubrevin) (VAMP3), mRNA.	306.54	483.98	-1.58	0.017	177.43
ARHGAP19	Homo sapiens Rho GTPase activating protein 19 (ARHGAP19), mRNA.	267.56	418.84	-1.57	0.000	151.28
EIF2A	Homo sapiens eukaryotic translation initiation factor 2A, 65kDa (EIF2A), mRNA.	497.41	773.65	-1.56	9.00E-04	276.24
BCCIP	Homo sapiens BRCA2 and CDKN1A interacting protein (BCCIP), transcript variant B, mRNA.	396.66	602.13	-1.52	0.030	205.47
MRFAP1	Homo sapiens Mof4 family associated protein 1 (MRFAP1), mRNA.	972.90	1479.89	-1.52	0.024	506.99
ODC1	Homo sapiens ornithine decarboxylase 1 (ODC1), mRNA.	738.79	1121.6	-1.52	0.013	382.81
FASTKD5	Homo sapiens FAST kinase domains 5 (FASTKD5), mRNA.	291.27	439.00	-1.51	0.000	147.73
KLHDC3	Homo sapiens kelch domain containing 3 (KLHDC3), mRNA.	551.83	361.17	1.53	0.026	190.66
PTP4A2	Homo sapiens protein tyrosine phosphatase type IVA, member 2 (PTP4A2), transcript variant 2, mRNA. XM_944930 XM_944934	3019.32	1967.91	1.53	0.035	1051.41
C9orf69	Homo sapiens chromosome 9 open reading frame 69 (C9orf69), mRNA.	335.20	216.67	1.55	0.000	118.53
RPS6KA1	Homo sapiens ribosomal protein S6 kinase, 90kDa, polypeptide 1 (RPS6KA1), transcript variant 1, mRNA.	854.60	552.26	1.55	0.000	302.34
POGK	Homo sapiens pogo transposable element with KRAB domain (POGK), mRNA.	848.49	544.15	1.56	0.038	304.34
LOC606724	Homo sapiens coronin, actin binding protein, 1A pseudogene (LOC606724), non-coding RNA.	1696.37	1082.57	1.57	0.007	613.79
TMEM203	Homo sapiens transmembrane protein 203 (TMEM203), mRNA.	919.25	578.01	1.59	0.025	341.24
MRP63	Homo sapiens mitochondrial ribosomal protein 63 (MRP63), nuclear gene encoding mitochondrial protein, mRNA.	270.51	168.94	1.60	0.001	101.57
RUFY3	Homo sapiens RUN and FYVE domain containing 3 (RUFY3), transcript variant 1, mRNA.	327.65	205.08	1.60	0.023	122.57
PRPF31	Homo sapiens PRP31 pre-mRNA processing factor 31 homolog (S. cerevisiae) (PRPF31), mRNA.	644.07	400.03	1.61	0.000	244.04
TMBIM4	Homo sapiens transmembrane BAX inhibitor motif containing 4 (TMBIM4), mRNA.	2478.92	1541.72	1.61	0.048	937.20
CALHM2	Homo sapiens calcium homeostasis modulator 2 (CALHM2), mRNA.	374.61	231.76	1.62	0.017	142.85
LRP10	Homo sapiens low density lipoprotein receptor-related protein 10 (LRP10), mRNA.	916.97	562.20	1.63	0.002	354.77
VKORC1	Homo sapiens vitamin K epoxide reductase complex, subunit 1 (VKORC1), transcript variant 1, mRNA.	1378.8	829.06	1.66	0.017	549.74
WDR40A	Homo sapiens WD repeat domain 40A (WDR40A), mRNA.	359.35	215.38	1.67	0.000	143.97
TM7SF2	Homo sapiens transmembrane 7 superfamily member 2 (TM7SF2), mRNA.	260.06	147.71	1.76	0.004	112.35
C3orf19	Homo sapiens chromosome 3 open reading frame 19 (C3orf19), mRNA.	495.51	273.14	1.81	0.002	222.37
FRYL	Homo sapiens FRY-like (FRYL), mRNA.	1254.74	691.90	1.81	2.00E-04	562.84
NCF2	Homo sapiens neutrophil cytosolic factor 2 (65kDa, chronic granulomatous disease, autosomal 2) (NCF2), mRNA.	307.95	167.77	1.84	0.049	140.18
PRKAA1	Homo sapiens protein kinase, AMP-activated, alpha 1 catalytic subunit (PRKAA1), transcript variant 1, mRNA.	298.88	162.59	1.84	1.00E-04	136.29
SGSH	Homo sapiens N-sulfoglucosamine sulfohydrolase (sulfamidase) (SGSH), mRNA.	715.43	385.11	1.86	0.000	330.32
UBL4A	Homo sapiens ubiquitin-like 4A (UBL4A), mRNA.	454.95	242.77	1.87	0.001	212.19

ZNF75D	Homo sapiens zinc finger protein 75D (ZNF75D), mRNA.	301.76	159.24	1.89	0.000	142.52
TFB1M	Homo sapiens transcription factor B1, mitochondrial (TFB1M), mRNA.	347.58	181.28	1.92	0.005	166.3
ADRB2	Homo sapiens adrenergic, beta-2-, receptor, surface (ADRB2), mRNA.	1887.73	960.35	1.97	0.023	927.38
RABEP1	Homo sapiens rabaptin, RAB GTPase binding effector protein 1 (RABEP1), transcript variant 2, mRNA.	430.89	215.90	2.00	1.00E-04	214.98
SHMT1	Homo sapiens serine hydroxymethyltransferase 1 (soluble) (SHMT1), transcript variant 1, mRNA.	273.36	134.14	2.04	2.00E-04	139.22
PKP4	Homo sapiens plakophilin 4 (PKP4), transcript variant 1, mRNA.	263.00	126.45	2.08	0.019	136.55
PRAGMIN	Homo sapiens homolog of rat pragma of Rnd2 (PRAGMIN), mRNA.	285.24	131.07	2.18	2.00E-04	154.17
WIBG	Homo sapiens within bgcn homolog (Drosophila) (WIBG), mRNA.	295.41	135.55	2.18	0.014	159.86
APPBP2	Homo sapiens amyloid beta precursor protein (cytoplasmic tail) binding protein 2 (APPBP2), mRNA.	191.40	85.38	2.24	0.000	106.02
LMNB2	Homo sapiens lamin B2 (LMNB2), mRNA.	496.34	210.12	2.36	2.00E-04	286.22
ZNF232	Homo sapiens zinc finger protein 232 (ZNF232), mRNA.	248.51	103.27	2.41	0.013	145.23
METT10D	Homo sapiens methyltransferase 10 domain containing (METT10D), mRNA.	239.22	85.45	2.80	0.000	153.77
FANCD2	Homo sapiens Fanconi anemia, complementation group D2 (FANCD2), transcript variant 2, mRNA.	285.13	99.42	2.87	0.033	185.70
VAV3	Homo sapiens vav 3 guanine nucleotide exchange factor (VAV3), transcript variant 1, mRNA.	626.60	90.29	6.94	1.00E-04	536.31

Comparison CD8$^+$ T cells of MF$^+$ individuals versus EN

Symbol	Definition	mean_CD8_Mfpos	mean_CD8_EN	FC	pvalue	diff
SOD2	Homo sapiens superoxide dismutase 2, mitochondrial (SOD2), nuclear gene encoding mitochondrial protein, transcript variant 2, mRNA.	294.74	884.22	-3.0	0.000	589.48
ETF1	Homo sapiens eukaryotic translation termination factor 1 (ETF1), mRNA.	525.62	1436.46	-2.73	0.024	910.84
FLJ10986	Homo sapiens hypothetical protein FLJ10986 (FLJ10986), mRNA.	82.92	220.40	-2.66	0.000	137.49
PYHIN1	Homo sapiens pyrin and HIN domain family, member 1 (PYHIN1), transcript variant b2, mRNA.	152.93	368.55	-2.41	0.020	215.62
	CR743533 Soares_testis_NHT Homo sapiens cDNA clone IMAGp971L1944 ; IMAGE:727458 5, mRNA sequence	120.28	284.3	-2.36	0.038	164.02
SPHK2	Homo sapiens sphingosine kinase 2 (SPHK2), mRNA.	186.57	427.48	-2.29	1.00E-04	240.91
C7orf40	Homo sapiens chromosome 7 open reading frame 40 (C7orf40), non-coding RNA.	224.47	500.25	-2.23	0.001	275.78
ZCWPW1	Homo sapiens zinc finger, CW type with PWWP domain 1 (ZCWPW1), mRNA.	135.01	300.95	-2.23	0.009	165.94
	Homo sapiens clone TESTIS-609 mRNA sequence	101.02	215.32	-2.13	0.001	114.30
SLC37A4	Homo sapiens solute carrier family 37 (glucose-6-phosphate transporter), member 4 (SLC37A4), mRNA.	174.34	369.38	-2.12	5.00E-04	195.05
RAB11FIP1	Homo sapiens RAB11 family interacting protein 1 (class I) (RAB11FIP1), transcript variant 3, mRNA.	216.36	440.96	-2.04	0.000	224.59
AZI1	Homo sapiens 5-azacytidine induced 1 (AZI1), transcript variant 1, mRNA.	165.28	332.67	-2.01	0.003	167.40
HBP1	Homo sapiens HMG-box transcription factor 1 (HBP1), mRNA.	246.88	495.07	-2.01	0.004	248.20
EEF2K	Homo sapiens eukaryotic elongation factor-2 kinase (EEF2K), mRNA.	134.83	265.51	-1.97	0.000	130.68
LOC652685	PREDICTED: Homo sapiens similar to PMS1 protein homolog 2 (DNA mismatch repair protein PMS2) (LOC652685), mRNA.	179.28	352.58	-1.97	0.000	173.31
HIBADH	Homo sapiens 3-hydroxyisobutyrate dehydrogenase (HIBADH), mRNA.	220.26	422.93	-1.92	0.038	202.67
ACSL3	Homo sapiens acyl-CoA synthetase long-chain family member 3 (ACSL3), transcript variant 2, mRNA.	274.39	518.23	-1.89	0.000	243.85
PPOX	Homo sapiens protoporphyrinogen oxidase (PPOX), nuclear gene encoding mitochondrial protein, mRNA.	164.21	310.27	-1.89	0.017	146.06
AUTS2	Homo sapiens autism susceptibility candidate 2 (AUTS2), mRNA.	337.51	633.78	-1.88	0.020	296.27
KLF4	Homo sapiens Kruppel-like factor 4 (gut) (KLF4), mRNA.	135.95	249.9	-1.84	0.003	113.95
CRIPAK	Homo sapiens cysteine-rich PAK1 inhibitor (CRIPAK), mRNA.	410.02	723.99	-1.77	0.033	313.97
RMND5A	Homo sapiens required for meiotic nuclear division 5 homolog A (S. cerevisiae) (RMND5A), mRNA.	177.87	315.42	-1.77	0.035	137.56
TMUB2	Homo sapiens transmembrane and ubiquitin-like domain containing 2 (TMUB2), transcript variant 1, mRNA.	189.52	335.37	-1.77	0.000	145.85
SERTAD3	Homo sapiens SERTA domain containing 3 (SERTAD3), transcript variant 1, mRNA.	156.13	266.87	-1.71	0.050	110.74
MYLIP	Homo sapiens myosin regulatory light chain interacting protein (MYLIP), mRNA.	1727.68	2935.22	-1.70	0.023	1207.53
HBP1	Homo sapiens HMG-box transcription factor 1 (HBP1), mRNA.	166.46	280.92	-1.69	2.00E-04	114.46
DCTN5	Homo sapiens dynactin 5 (p25) (DCTN5), mRNA.	455.95	756.54	-1.66	0.002	300.58
ZNF211	Homo sapiens zinc finger protein 211 (ZNF211), transcript variant 1, mRNA.	219.27	362.78	-1.65	0.032	143.52
NARF	Homo sapiens nuclear prelamin A recognition factor (NARF), transcript variant 3, mRNA.	455.31	743.36	-1.63	0.007	288.05
	Homo sapiens cDNA clone IMAGE:30332316	211.51	343.18	-1.62	4.00E-04	131.67
FBXO44	Homo sapiens F-box protein 44 (FBXO44), transcript variant 4, mRNA.	182.37	293.23	-1.61	0.045	110.86

FN3KRP	Homo sapiens fructosamine-3-kinase-related protein (FN3KRP), mRNA.	424.16	672.65	-1.59	0.000	248.49
KIF22	Homo sapiens kinesin family member 22 (KIF22), mRNA.	365.59	581.24	-1.59	0.006	215.65
PHAX	Homo sapiens phosphorylated adaptor for RNA export (PHAX), mRNA.	223.77	354.27	-1.58	0.017	130.50
ALG8	Homo sapiens asparagine-linked glycosylation 8, alpha-1,3-glucosyltransferase homolog (S. cerevisiae) (ALG8), transcript variant 1, mRNA.	192.45	300.70	-1.56	0.000	108.26
LSM1	Homo sapiens LSM1 homolog, U6 small nuclear RNA associated (S. cerevisiae) (LSM1), mRNA.	1106.08	1710.97	-1.55	0.001	604.88
CNNM3	Homo sapiens cyclin M3 (CNNM3), transcript variant 1, mRNA.	293.57	448.57	-1.53	0.002	155,00
SGSH	Homo sapiens N-sulfoglucosamine sulfohydrolase (sulfamidase) (SGSH), mRNA.	594.84	385.11	1.54	0.001	209.73
C9orf69	Homo sapiens chromosome 9 open reading frame 69 (C9orf69), mRNA.	342.63	216.67	1.58	0.039	125.95
RFX5	Homo sapiens regulatory factor X, 5 (influences HLA class II expression) (RFX5), transcript variant 2, mRNA.	990.73	617.09	1.61	0.023	373.64
FBXO11	Homo sapiens F-box protein 11 (FBXO11), transcript variant 1, mRNA.	702.60	434.36	1.62	0.015	268.24
LRRFIP2	Homo sapiens leucine rich repeat (in FLII) interacting protein 2 (LRRFIP2), transcript variant 2, mRNA.	290.62	177.43	1.64	0.025	113.19
SRXN1	Homo sapiens sulfiredoxin 1 homolog (S. cerevisiae) (SRXN1), mRNA.	255.57	155.44	1.64	0.003	100.13
POMGNT1	Homo sapiens protein O-linked mannose beta1,2-N-acetylglucosaminyltransferase (POMGNT1), mRNA.	376.80	227.96	1.65	0.000	148.83
ACTB	Homo sapiens actin, beta (ACTB), mRNA.	534.58	319.71	1.67	0.012	214.87
LAMP2	Homo sapiens lysosomal-associated membrane protein 2 (LAMP2), transcript variant LAMP2B, mRNA.	335.13	196.86	1.70	0.035	138.27
RAB11A	Homo sapiens RAB11A, member RAS oncogene family (RAB11A), mRNA.	1383.15	803.49	1.72	0.002	579.66
GSDMB	Homo sapiens gasdermin B (GSDMB), transcript variant 2, mRNA.	497.54	283.14	1.76	0.000	214.4
LAMP2	Homo sapiens lysosomal-associated membrane protein 2 (LAMP2), transcript variant LAMP2B, mRNA.	387.28	220.47	1.76	0.014	166.81
CDC42SE1	Homo sapiens CDC42 small effector 1 (CDC42SE1), transcript variant 1, mRNA.	236.50	129.34	1.83	0.000	107.15
RNF121	Homo sapiens ring finger protein 121 (RNF121), transcript variant 1, mRNA.	272.74	145.07	1.88	0.002	127.67
ZNF83	Homo sapiens zinc finger protein 83 (ZNF83), mRNA.	254.95	134.7	1.89	0.013	120.25
UBL4A	Homo sapiens ubiquitin-like 4A (UBL4A), mRNA.	461.08	242.77	1.90	0.002	218.32
WIPI1	Homo sapiens WD repeat domain, phosphoinositide interacting 1 (WIPI1), mRNA.	321.58	167.7	1.92	0.003	153.88
AHCTF1	Homo sapiens AT hook containing transcription factor 1 (AHCTF1), mRNA.	443.59	229.34	1.93	0.015	214.25
ARFIP1	Homo sapiens ADP-ribosylation factor interacting protein 1 (ARFIP1), transcript variant 2, mRNA.	254.04	131.68	1.93	0.010	122.36
NME1	Homo sapiens non-metastatic cells 1, protein (NM23A) expressed in (NME1), transcript variant 2, mRNA.	506.07	252.21	2.01	0.000	253.86
	Homo sapiens cDNA FLJ12874 fis, clone NT2RP2003769	487.59	238.55	2.04	0.045	249.04
NDUFB5	Homo sapiens NADH dehydrogenase (ubiquinone) 1 beta subcomplex, 5, 16kDa (NDUFB5), nuclear gene encoding mitochondrial protein, mRNA.	718.51	332.16	2.16	0.027	386.35
ARL17P1	Homo sapiens ADP-ribosylation factor-like 17 pseudogene 1 (ARL17P1), mRNA.	304.28	138.25	2.20	0.014	166.04
RABEP1	Homo sapiens rabaptin, RAB GTPase binding effector protein 1 (RABEP1), transcript variant 2, mRNA.	476.17	215.90	2.21	0.035	260.27
RCOR3	Homo sapiens REST corepressor 3 (RCOR3), mRNA.	667.98	295.89	2.26	1.00E-04	372.08
RHBDD1	Homo sapiens rhomboid domain containing 1 (RHBDD1), mRNA.	221.47	95.85	2.31	0.014	125.62
ZNF232	Homo sapiens zinc finger protein 232 (ZNF232), mRNA.	242.07	103.27	2.34	0.028	138.79
APPBP2	Homo sapiens amyloid beta precursor protein (cytoplasmic tail) binding protein 2 (APPBP2), mRNA.	214.79	85.38	2.52	0.001	129.42
PTGDR	Homo sapiens prostaglandin D2 receptor (DP) (PTGDR), mRNA.	572.73	215,00	2.66	0.006	357.73
VPS13C	Homo sapiens vacuolar protein sorting 13 homolog C (S. cerevisiae) (VPS13C), transcript variant 1B, mRNA.	294.16	106.22	2.77	1.00E-04	187.94
HAVCR2	Homo sapiens hepatitis A virus cellular receptor 2 (HAVCR2), mRNA.	1095.55	391.70	2.80	9.00E-04	703.85

Erklärung

An Eides statt versichere ich, dass die vorgelegte Arbeit – abgesehen von den ausdrücklich bezeichneten Hilfsmitteln – persönlich, selbständig und ohne Benutzung anderer als der angegebenen Hilfsmittel angefertigt wurde, die aus anderen Quellen direkt oder indirekt übernommenen Daten und Konzepte unter Angabe der Quelle kenntlich gemacht sind, die vorgelegte Arbeit oder ähnliche Arbeiten nicht bereits anderweitig als Dissertation eingereicht worden ist bzw. sind, sowie eine Erklärung über frühere Promotionsversuche und deren Resultate, für die inhaltlich-materielle Erstellung der vorgelegten Arbeit keine fremde Hilfe, insbesondere keine entgeltliche Hilfe von Vermittlungs- bzw. Beratungsdiensten (Promotionsberater oder andere Personen) in Anspruch genommen wurde sowie keinerlei Dritte vom Doktoranden unmittelbar oder mittelbar geldwerte Leistungen für Tätigkeiten erhalten haben, die im Zusammenhang mit dem Inhalt der vorgelegten Arbeit stehen.

Bonn,